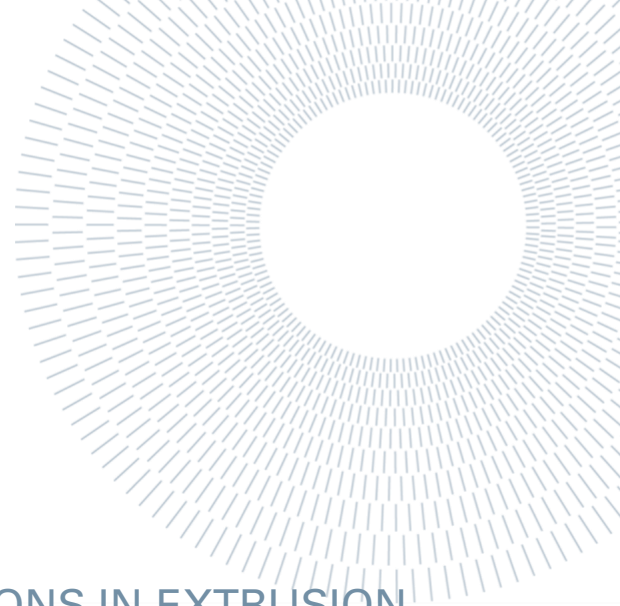




**POLITECNICO
MILANO 1863**

**SCUOLA DI INGEGNERIA INDUSTRIALE
E DELL'INFORMAZIONE**



EXECUTIVE SUMMARY OF THE THESIS

IMPROVEMENT OF THERMAL CONDITIONS IN EXTRUSION ADDITIVE MANUFACTURING OF ULTEM

TESI MAGISTRALE IN MECHANICAL ENGINEERING – INGEGNERIA MECCANICA

AUTHOR: MATTEO FABRIZIO

ADVISOR: PROF. MATTEO STRANO

ACADEMIC YEAR: 2020-2021

1 Introduction

The Additive Manufacturing industry has grown a lot in the past years and will continue to do so in the following, due to the high extent of complexity and customization which can be achieved. In the AM industry the most commercially diffused technology is Extrusion AM, which can be performed with material in form of filament or pellets. The latter offers wider possibilities in terms of materials printable and cheaper feedstock. In the last years AM with high performance thermoplastics has developed, to increase mechanical and thermal resistance of the produced parts thanks to the material's properties. Many papers have been published on filament EAM with PEI but no scientific researches are present in the field of pellet EAM of PEI, which would reduce dramatically the cost of the printed objects.

For these reasons, this thesis was carried out in this field, focusing on the thermal AM-process parameters of the machine, which strictly affect the properties and quality of the produced parts.

This work is divided in two main parts. In the first one the EFeSTO machine will be presented along with the improvements made on the specific machine. In the second part the experimental campaign carried out on the improved machine

will be presented, to highlight how thermal parameters affect quality and properties of the printed objects.

The material chosen for the experimental campaign is PEI, polyetherimide, in pellet form, commercially called ULTEM by its producer Sabic. PEI is a high strength amorphous polymer, characterized by high temperature and chemical resistance.

In each chapter, for further details, pictures and explanations please refer to the main thesis.

2 Scientific Background

2.1 Extrusion Additive Manufacturing

Different types of additive manufacturing exist depending on the type of thermal energy provided, with lasers or resistances, and type of material to be produced.

Among them, the most commercially diffused is extrusion additive manufacturing (EAM), also called FDM, in which the material is heated through resistances and deposited layer by layer. EAM can be performed with material in form of wire or pellets, both having advantages and disadvantages.

The main principle behind this technology is to heat the material over its glass transition temperature and extrude it through a nozzle which is moved in space through motors driven by a PLC.

The STL geometry is sliced by a software and paths in space for the nozzle are defined, which are then executed by the PLC coordinating all the different axes.

EAM can be mainly performed with polymers, but also with metals, alloys and ceramics with a thermoplastic binder, which need to be debinded and sintered after printing. In the last years the tendency to adopt high performances polymers such as PEEK and PEI in EAM has developed both from a commercial and scientific point of view. Among the researches published, K. P. Motaparti et al. [1] studied the relation between build direction, raster angle of the filling and air gap with compression properties at different temperatures on Ultem 9085 parts, produced by filament AM. E. L. Gilmer et al. [2] studied how the molecular diffusion and degree of healing are affected by the temperature field, to predict the tear resistance of the components produced with PEI filament material. They also tried to predict the warping tendency by analyzing the thermal stresses buildup in the first layer. Some commercial machines have adopted new features to make high temperature polymers printing possible, such as heated chambers and preheaters to increase layer bonding. In the research field some particular methods have been adopted such as the one used by P. Han et al. [3]. They used a 10,6 μm wavelength localized laser to improve the interface strength in Ultem 1010 objects produced with filament FDM, studying the tensile strength with varying laser power between 0.3 to 2 W.

2.2 Thermal problems in EAM

Being EAM a thermal technology, many problems are present related to an excess or shortage of heat flux through the piece.

Among the problems related to excess of heat flux it is possible to highlight:

- **Overheating:** this problem results in the geometry of the printed object not being respected even if the path of the nozzle is correct, due to poor substrate stability which tends to be dragged by the nozzle and fall due to gravity.
- **Impossibility of making overhangs:** even this problem is given by the low extrudate stiffness which is not able to maintain its shape when deposited in overhang condition, it tends to fall due to gravity.
- **Impossibility of making bridges:** to make bridge features the just extruded material must possess

a sufficient degree of stiffness to sustain its own weight with support only on the two sides.

- **Heat Creep:** the heat creep problem consists in heat going up through the extrusion head in places where it's not supposed to be, it can result in clogs or damages of the machine.

The ones related to a lack of heat flux are:

- **Warping:** the warping problem is usually caused by non-uniform cooling of the object, often occurs when the bed temperature is too low for the printed material. When the first layers cool down they tend to shrink while the upper layers, still hot, are expanded. Being the layers bonded together some thermal stresses arise. If the adhesion force between the first layer and the build surface is not enough the stresses will generate deformations, corners will tend to curl and warping occurs.
- **Delamination and poor layers bonding:** the delamination problem occurs when the temperature of the previous layer is too low when depositing the next one and bonding and diffusion cannot occur, resulting in detached layers. This phenomenon is mainly driven by the glass transition temperature of the material, if the extrudate temperature gets below it, when depositing the next layer, the diffusion phenomenon cannot occur properly and intralayer strength decreases dramatically [4].

3 EFeSTO

The machine on which the improvements and experimental campaign are carried out is a prototype from Politecnico di Milano. This machine features an injection molding head fixed in space and a parallel kinematic build plate to which all the three DOF in space are assigned. The injection molding unit is a modified machine which features two chambers with pistons pushing the material. The pistons are driven by brushless motors and the two distinct chambers are devoted respectively to the plasticization and extrusion of the material. In the first chamber the material is fed in form of pellets from the hopper and the plasticization piston pushes it through some metal spheres, used to increase shear stresses, to plasticize and inject it in the extrusion chamber in form of viscous fluid. The second chamber and piston have the role of keeping the material in the viscous fluid state and push it out of the nozzle with a precise volumetric flow rate.

The extrusion unit has three resistances and thermocouples to heat the material and reduce its viscosity [5]. They are located in the plasticization chamber, extrusion chamber and nozzle zone. A fourth thermocouple is present in the thermal cutoff zone, to check that the temperature doesn't exceed a certain value, to protect the heat sensitive components.

Since the head was originally designed for injection molding the material must be in a low viscosity state for a flawless working of the machine. In injection molding indeed the low viscosity of the material permits a fast filling of the mold and a reduction of the pressure needed to inject the material in the mold. This unit, having a consistent volume of plasticized material in the extrusion chamber, has to deal with the viscous problem, including elastic effects and thermal degradation of the material.

The injection unit features a pneumatic closure of the nozzle, to stop the flow through the orifice when needed, and a water-cooling circuit, used to protect the heat sensitive zones from heat creep.

As this thesis started many problems were present on the machine, both from the thermal point of view and from the nominal working point of view. Among the thermal problems the cooling system was very undersized and did not guarantee enough heat extraction for the unit to work for long time.

The machine was also missing the layer fan, useful to control the convection behavior of the extruded material. The machine was completely open, without any mean to keep the printing area at constant thermal conditions, resulting in difficulties to print high temperature materials.

The heated bed on the machine was not working in closed loop, so it was not possible to set and maintain a constant temperature of the build surface. The resistance used to heat the build surface was undersized and the bed could not go at temperatures higher than 75 °C.

Among the other problems, the nozzle diameter was unknown and its geometry was not designed for the pneumatic closure of the nozzle, which was not configured for that reason.

Some parameters on the PLC were not adequate for the flawless working of the machine, mainly the maximum temperature reachable and the "loop disconnection judgment time", resulting in frequent errors.

4 Improvements on the machine

To solve the beforementioned problems and improve the EFeSTO machine many technological improvements have been carried out. These improvements have a focus on the process, to be able to print with higher quality, strength and reliability of the process, making the machine more competitive with the commercial ones and under some aspects better and more innovative than the ones available on the market. The improvements will also enable the EFeSTO machine to print high temperature polymers such as ULTEM.

4.1 Cooling system

To improve the cooling system, a new pump capable of providing up to 10,5 l/min was chosen, with fans on the sides to cool the pump in continuous use. The original 4 mm tubes were changed with 10 mm hoses to reduce pressure losses. The tank was upgraded to a 50 liters one to have higher thermal inertia. Water-cooled heatsinks (Figure 1) were mounted on the extruder and plasticizer brushless motors, with thermal paste, to enhance cooling on the critical motors.



Figure 1: Heatsinks on the motors

4.2 PLC tuning

The "loop disconnection judgment time" was raised until no more errors occurred during heating, this timer prevents damages due to disconnection or short circuit of the heaters and thermocouples, by verifying that with the heater at full power the temperature raises of at least 2 °C in the set time. The maximum temperature reachable has been raised to 410 °C, which does not represent an issue for the machine for two reasons: firstly, according to the producer of the injection unit, the maximum temperature reachable by the extruder is 420 °C. Secondly, the new cooling circuit successfully prevents overheating of sensitive parts of the head.

4.3 Heated bed

A new 200 W resistance with embedded thermistor was installed with a SSR to couple it with a microcontroller running the opensource software Marlin. The resistance works on 220 AC line, while the board at 12 V DC, the SSR allows the board to

control the switching of the AC line with PWM based on PID control on the temperature error. A thermistor was also inserted in the water tank to check the water temperature during working. To easily control the bed temperature a display with additive manufactured enclosure, shown in Figure 2, was used.



Figure 2: Display to control bed temperature and fan

4.4 Pneumatic closure of the nozzle

The pneumatic shutter was enabled by attaching the pneumatic switch to the compressed air in the lab and the switch to the actuator with tubes for compressed air. The geometry of the pin which strikes on the internal surface of the nozzle has been taken into account for the nozzle design.

4.5 Layer fan

To cool the layers while they are deposited, a 5015 fan (Figure 3) has been installed, controlled in open loop with PWM by the board which controls the bed. To convey the air close to the nozzle a tube has been used. The tube is made by copper because it passes below IR lights, therefore, a plastic material would not have been suited for the case.



Figure 3: Layer fan and copper tube

4.6 IR preheater

A reflector with three IR lamps (Figure 4) has been installed in the proximity of the nozzle, to preheat the substrate before the next layer is deposited. The total IR power is 900 W, more than enough for heating the piece and controlling the air temperature around the object. The power of the IR preheater can be partialized thanks to a knob which controls a TRIAC via PWM, all embedded in a control unit which can drive up to 3 kW in continuous use.



Figure 4: IR preheater and layer fan tip

4.7 Nozzle

Two new nozzles have been designed and produced with orifice size of 0,6 mm and 0,4 mm. The nozzles (Figure 5) feature a 2 mm channel to streamline the flow and increase the nozzle length, useful for compatibility with the preheater. The internal geometry has been designed to be compatible with the pneumatic shutter pin. Tight geometrical tolerances have been used to ensure circularity (0,02 mm) of the orifice and concentricity (0,05 mm) of the different sections.



Figure 5: Produced nozzle

5 Experimental campaign

In this section the experimental campaign will be presented, highlighting the relation between thermal variables, quality and strength of the produced parts. The experimental campaign will be carried out with ULTEM material, which, due to its high temperature resistance and high glass transition temperature (215°C), requires high extrusion temperatures, bed temperature and, for big pieces, a controlled environment to avoid poor layer bonding.

5.1 Preliminary trials on ULTEM

As the material was delivered, some extrusions of the material in air were performed, varying the extrusion temperature until the extrudate aspect and properties were adequate. After that, some simple geometries were printed (namely cubes and flat blocks) to find default parameters to begin the experimental campaign. The parameters obtained from the first trials are reported in Table 1.

Parameter	Value
Plasticization Temperature	355 °C
Body Temperature	380 °C
Nozzle Temperature	385 °C
Bed Temperature	150 °C
Flow	1.1
1° Layer Speed	10 mm/s
Other Layers Speed	25 mm/s
1° Layer Height	0,4 mm
Other Layers Height	0,25 mm
Infrared Power 1° Layer	25%
Infrared Other Layers	0%
Fan Speed	0%
Line Width	0,6 mm
Number of Perimeters	3

Table 1: Basic printing parameters

5.2 DOE

In the design of the experiments, it was decided to keep all the printing parameter constant and for each geometry vary only the most significant variable.

The models designed for the experimental campaign are multiple: an “overhang test” part with different angles, a cube engraved to test the quality of the print, a “bridge test” part, a cylinder for compression tests, a tensile specimen, a “staircase effect” part and a “warping test” part.

The variables related to each specimen are reported in Tables 2, 3 and 4.

Layer fan	0%	25%	50%
Overhang	1	2	3
Cube engraved	1	2	3
Bridge	1	2	3
Staircase	1	2	3

Table 2: Layer fan related trials

For the compression specimen a factorial approach linking fan and body temperature has been chosen, with nozzle temperature always 5 °C higher than the body one. The fan speed used are 0%, 25%, 50%, while the body temperatures 370 °C, 375 °C, 380 °C, 385 °C. In total, 12 trials were printed. For the trials completed 3 specimens will be printed for testing.

Tensile specimen	1	2	3
IR power	0%	25%	50%

Table 3: Tensile specimens trials

Warping test	1	2	3
Bed Temp. °C	120	150	180

Table 4: Warping test trials

5.3 Results

The results can be summarized as follows.

5.3.1 Layer fan

The best condition has been found at 25% layer fan power (Figure 6), which permits to print adequately the overhang test, bridge test, engraved cube and staircase effect test. Other conditions result in slight/strong overheating, for lower fan speeds, or delamination, for too high fan power.

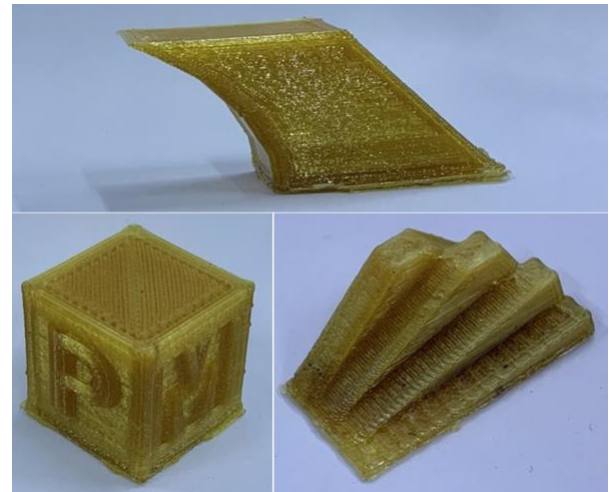


Figure 6: 25% fan specimens

5.3.2 IR power

The condition at 50% IR power results in overheating and material degradation. Up to 25% power no significant modifications on the geometry and aspect of the objects is present. Since the specimens are small the positive effects of IR lights are limited [6], probably because the substrate layer does not go below the glass transition temperature in normal extrusion conditions, resulting in good bonding between layers even with 0% IR power.

It has been found that IR lights reduces dramatically the warping tendency if used during the first layer, by keeping the deposited filament at a uniform temperature.

5.3.3 Body and Nozzle temperatures

The best conditions have been found for a nozzle temperature of 380-385 °C, with body temperature always 5 °C lower. For lower temperatures machine overload is present due to a too high material viscosity, while for higher temperatures the material degrades inside the machine.

5.3.4 Bed Temperature

The bed temperature affects mainly the adhesion and warping tendency. The best condition has been found at about 180 °C, since this temperature is close enough to PEI glass transition temperature. For lower temperatures the warping tendency increases decreasing the bed temperature.

5.3.5 Process window

From the factorial approach adopted in the printing of compression specimens a process window can be identified, presented in Figure 7, relating fan speed and nozzle temperature (body temperature 5°C lower).

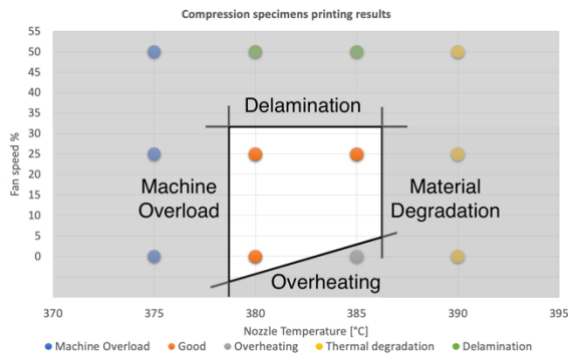


Figure 7: Temperature-Fan process window

5.3.6 Effect of geometry

The geometry of the sample affects the building process behavior from a thermal point of view. For smaller layer area the heat exchanged by convection and conduction will be lower, since the time to perform a layer will be lower, and thus the tendency to overheating will increase.

5.3.7 Comparison with ABS results

The layer fan needs to be adjusted depending on the geometry and material to be printed. In ABS printing it is noticeable that, for the same geometry, a higher fan speed for respect to ULTEM is needed to achieve the same quality. This is due to the lower extrusion and glass transition temperatures and lower conductivity of ABS. The gradient between the extrusion temperature and ambient is lower in ABS extrusion, thus less heat will be extracted by convection, assuming a constant convection coefficient. It will be more difficult for ABS to reach a temperature close to its glass transition temperature, at which the material has some stiffness but is also able to bond well with the substrate.

5.3.8 Compression testing

The mechanical results in compression are satisfactory (Figure 8), with a yielding compression stress of about 109 MPa, showing how ULTEM can be used as Rapid Tooling material, thanks to its high resistance in compression and in high temperature environments. The thermal conditions in the process window do not influence the results in a significant manner, since the process window is really small.

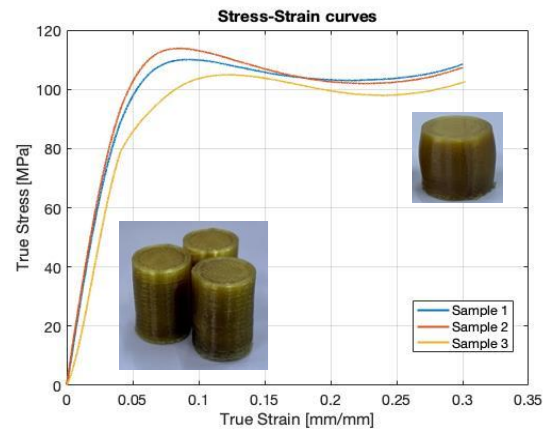


Figure 8: Stress-Strain curves Nozzle T. 380°C - Fan 25%

5.3.9 Tensile testing

The tensile testing results (Figure 9) are adequate for additive manufactured PEI, with an average UTS of about 88 MPa and an Elastic Modulus of about 3400 MPa. The different IR conditions do not affect in a significant manner the result. The IR 50% condition confirmed material degradation also upon testing, with higher dispersion and lower strength. The sample n. 3 with IR 25% showed characteristics really close to the ones present in the material datasheet for injection molded samples. Further studies should verify the repeatability of this condition. The dispersion of the results is large due to the small population present in the campaign (3 for each condition) and to the many uncontrollable defects additive manufacturing can produce in the samples, such as porosities.

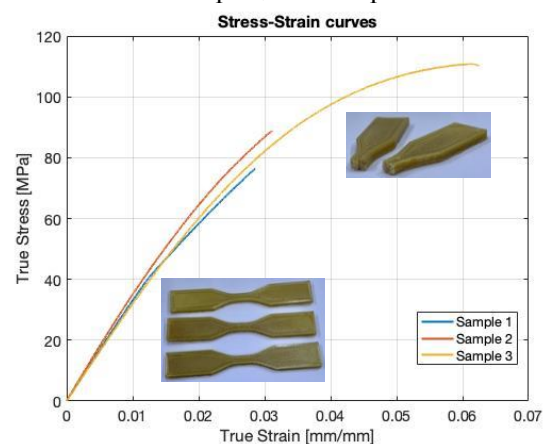


Figure 9: Stress-Strain curves for IR 25%

5.4 Conclusion

This thesis was aimed at improving the EFeSTO machine to print properly and test the printability of high strength thermoplastics in pellet form such as PEI.

The most significant conclusions obtained are summarized as follows.

- Many problems present on the machine were solved with the improvements carried out.
- The improvements affected reliability, functionality and thermal conditions in the machine.
- The machine is now able to print even high temperature materials such as PEI pellets with good quality and mechanical properties.
- The experimental campaign showed the importance of the improvements done and how the thermal condition in EAM affect the printed object quality.
- The thermal conditions should be controlled considering geometry and material to be produced.
- The best results in terms of quality and strength of the PEI objects can be achieved with 380-385 °C nozzle temperature, 180 °C bed temperature, 25% layer fan speed and IR at 25% during the first layer.

Therefore it is possible to regard the objectives of this work achieved.

6 Bibliography

- [1] Krishna P. Motaparti, Gregory Taylor, Ming C. Leu, K. Chandrashekhara, James Castle, Mike Matlack, Effects of build parameters on compression properties for ULTEM 9085 parts by fused deposition modeling.
- [2] Eric L. Gilmer, David Anderegg, John M. Gardner, Godfrey Sauti, Emilie J. Siochi, Steven H. McKnight, David A. Dillard, Claire McLroy, Michael J. Bortner, Temperature, diffusion, and stress modeling in filament extrusion additive manufacturing of polyetherimide: An examination of the influence of processing parameters and importance of modeling assumptions, *Additive Manufacturing*, Volume 48, Part A, 2021.
- [3] Pu Han, Alireza Tofangchi, Anagh Deshpande, Sihan Zhang, Keng Hsu, An approach to improve interface healing in FFF-3D printed Ultem 1010 using laser pre-deposition heating, *Procedia Manufacturing*, Volume 34, 2019, Pages 672-677.
- [4] N. Turner, B., Strong, R. and A. Gold, S. (2014), "A review of melt extrusion additive manufacturing processes: I. Process design and modeling", *Rapid Prototyping Journal*, Vol. 20 No. 3, pp. 192-204.
- [5] Thesis: Alessandro Marseglia, Prof. Ing. Hermes Giberti, Progetto e Sviluppo di una Testa di Iniezione MIM applicata ad una Stampante 3D, 2016.
- [6] Andrzej Nycz, Vidya Kishore, John Lindahl, Chad Duty, Charles Carnal, Vlastimil Kunc, Controlling substrate temperature with infrared heating to improve mechanical properties of large-scale printed parts, *Additive Manufacturing*, Volume 33, 2020.



POLITECNICO
MILANO 1863

SCUOLA DI INGEGNERIA INDUSTRIALE
E DELL'INFORMAZIONE

IMPROVEMENT OF THERMAL CONDITIONS IN EXTRUSION ADDITIVE MANUFACTURING OF ULTEM

TESI DI LAUREA MAGISTRALE IN
MECHANICAL ENGINEERING - INGEGNERIA MECCANICA

Author: **Matteo Fabrizio**

Student ID:	945600
Advisor:	Prof. Matteo Strano
Academic Year:	2020-21

Ringraziamenti

Giunto alla fine di questo percorso non posso fare a meno di fermarmi a pensare a quello che è stato e quello che sarà.

In primo luogo vorrei ringraziare il mio relatore Matteo Strano per avermi seguito e aiutato nella realizzazione di questa tesi, dimostrando disponibilità, professionalità e grandi doti ingegneristiche. È stato un piacere averlo conosciuto anche al di fuori delle aule didattiche.

Un sentito ringraziamento a Daniele Farioli, ottimo ingegnere e grande persona, per avermi guidato in questi mesi con le sue fondamentali indicazioni e per aver creduto sempre nelle mie capacità, spronandomi a migliorare.

Grazie a Jurgen, collega e amico con la battuta sempre pronta, per aver reso questi mesi di lavoro più leggeri con il suo supporto e la sua simpatia.

Vorrei ringraziare tutti i miei amici: da quelli che porto nel cuore dall'infanzia a quelli che ho incontrato durante il cammino. Tutti voi, così diversi ma così importanti, ognuno per ragioni uniche, mi avete dato ricordi indimenticabili e altri me ne darete.

Non sono il tipo di persona che mostra in maniera esplicita l'affetto nei confronti dei propri familiari, ma colgo l'occasione per esprimere tutta la mia gratitudine a loro, a mia sorella Giovanna, a mio fratello Niccolò e in particolare a mia mamma. Tutto il mio amore va a lei, che con i suoi sacrifici, il suo sostegno e la sua costante presenza è stata la prima a credere in me e mi ha insegnato ad essere un uomo migliore.

Grazie ai miei nonni Giancarlo e Giovanna per essere stati sempre al mio fianco in questo percorso e nella vita. I loro preziosi consigli e il loro affetto mi hanno reso la persona che sono.

Un pensiero speciale va a Leo, che mi è stato vicino in questi ultimi anni, regalandomi sorrisi e gioie che non avrei provato altrimenti. La sua presenza mi ha aiutato a superare le sfide e le difficoltà.

Infine un grazie di cuore a Giorgia, la mia ragazza e la mia migliore amica, per avermi supportato e sopportato in questi anni, per aver creduto in me e avermi regalato la sua presenza e amore. È difficile spiegare a parole quanto sia importante per me ma sono sicuro che, senza l'affetto e la forza che mi dà ogni giorno, non sarei mai arrivato fin qua.

Abstract

The Additive Manufacturing technology has grown significantly in the past few years thanks to the improved quality of manufactured parts, decrease in the investment costs, high flexibility and possibility to produce complex shapes. Among them Extrusion Additive manufacturing is one of the most flexible, efficient, reliable and safe thanks to the absence of lasers. The Additive Manufacturing technology uses thermal energy to bond the different layers and roads of materials, in EAM this energy is used to rise the temperature of the material over its glass transition temperature. The thermal energy is responsible for diffusion and bonding of the extruded roads of material, but if not properly controlled might generate thermal problems in the process, depending on material and geometry. Due to the importance of heat in EAM, this thesis will be focused on the thermal part of the process, considering some fixed kinematics and technological variables to simplify the problem. Pellet Extrusion Additive Manufacturing is gaining interest in the field due to the possibility of using all the polymers available on the market and not only the ones available in form of filaments for FDM. This technology also lowers the cost of production due to the cheaper feedstock with respect to filaments, which are produced starting from pellets.

ULTEM is the commercial name given by Sabic to PEI, polyetherimide polymer. PEI is a high strength amorphous thermoplastic used in automotive and aerospace fields, with good high-temperature resistance due to an exceptionally high glass transition temperature of 215 °C. Thanks to its outstanding mechanical and thermal properties it is also employed as material for Rapid Tools in injection molding. PEI components are usually produced with injection molding but in the last years some researches and articles have been published in the field of Filament Additive Manufacturing with this material. Commercial machines able to Additive manufacture PEI in filament form exist but they are all high-cost machines,

with heated and enclosed build volume and embedded filament dryer. To my knowledge and researches, no scientific publications are present instead on the Extrusion Additive Manufacturing of PEI components directly from pellets, which would reduce the cost and time for production significantly. For this reasons this work will focus on the innovative and interesting field of ULTEM Extrusion Additive Manufacturing directly from pellets, which has not been studied so far.

This thesis is divided in two main parts. In the first one the purpose is to improve an EAM machine to be able to print with a higher quality, strength and higher reliability of the process. The improvements are also aimed at enabling this machine to print high temperature polymers. The machine, called EFeSTO (Extrusion of Feedstock for Sintered Tiny Objects), has an injection molding head fixed in space and a parallel kinematic bed which moves in X, Y and Z. The injection molding head is fed with feedstock in pellet form, this gives great freedom in terms of material which can be printed: thermoplastics, including PLA, ABS and Nylon, but also metals and ceramics with a binder which need to be debinded and sintered after printing.

In the second section an experimental campaign, with the definition of a DOE, will be carried out to study the effects of thermal variables on the desired characteristics and to find an optimum process window, by printing different specimens with ULTEM 1000 pellets.

This work was able to meet the expected outputs under many aspects. Firstly the improvements carried out are able to enhance quality and strength of the printed objects, increase the reliability of the process and enable high-temperature printing. The printing phase of ULTEM in pellet form gave the desired results: the machine was able to produce the designed components without issues, a process window for the material has been defined and the quality and mechanical properties of the produced parts were satisfactory.

Key words: extrusion additive manufacturing, thermal improvements, EFeSTO, pellet, ULTEM.

Sommario in Italiano

Il settore dell'Additive Manufacturing è cresciuto in modo significativo negli ultimi anni grazie alla migliore qualità delle parti prodotte, alla diminuzione dell'investimento necessario, all'elevata flessibilità e alla possibilità di produrre forme complesse. Tra le varie tecnologie la produzione additiva tramite estrusione è una delle più flessibili, efficienti, affidabili e sicure grazie all'assenza di laser. Le tecnologie di produzione additiva utilizzano l'energia termica per legare i diversi strati e filamenti di materiale, in EAM questa energia viene utilizzata per aumentare la temperatura del materiale oltre la sua temperatura di transizione vetrosa. L'energia termica è responsabile della diffusione e dell'unione dei filamenti di materiale estruso, ma se non adeguatamente controllata potrebbe generare problemi termici nel processo, a seconda del materiale e della geometria. Data l'importanza del calore in EAM, questa tesi sarà focalizzata sulla parte termica del processo, considerando alcune variabili cinematiche e tecnologiche fisse per semplificare il problema. La produzione additiva con pellet sta guadagnando interesse nel settore grazie alla possibilità di utilizzare tutti i polimeri disponibili sul mercato e non solo quelli disponibili sotto forma di filamenti per FDM. Questa tecnologia abbassa anche il costo di produzione grazie al materiale più economico rispetto ai filamenti, che vengono prodotti a partire dai pellet.

ULTEM è il nome commerciale dato da Sabic al PEI, polieterimmide. Il PEI è un polimero termoplastico amorfo ad alta resistenza utilizzato nel settore automobilistico e aerospaziale, con una buona resistenza alle alte temperature grazie ad una temperatura di transizione vetrosa eccezionalmente elevata di 215 °C. Grazie alle sue eccezionali proprietà

meccaniche e termiche viene impiegato anche come materiale per stampi rapidi nello stampaggio ad iniezione. I componenti in PEI sono solitamente prodotti con stampaggio ad iniezione ma negli ultimi anni sono state pubblicate alcune ricerche e articoli nel campo della produzione additiva a filamento con questo materiale. Esistono macchine commerciali in grado di stampare il PEI sotto forma di filamento, ma sono tutte macchine ad alto costo, con area di stampa riscaldata e chiusa e con essiccatore di filamento incorporato. Dalle mie ricerche, non sono invece presenti pubblicazioni scientifiche sulla produzione additiva tramite estrusione di componenti in PEI direttamente dai pellet, che ridurrebbe significativamente i costi e i tempi di produzione.

Per questo motivo il mio lavoro si concentrerà sull'innovativo e interessante campo della produzione additiva tramite estrusione di ULTEM direttamente dai pellet, che finora non è stato studiato.

Questa tesi è divisa in due parti principali. Nella prima lo scopo è quello di migliorare una macchina EAM per poter stampare con una maggiore qualità, resistenza dei componenti e maggiore affidabilità del processo. I miglioramenti mirano anche a consentire a questa macchina di stampare polimeri ad alta temperatura. La macchina, denominata EFeSTO (Extrusion of Feedstock for Sintered Tiny Objects), ha una testa di stampaggio ad iniezione fissa nello spazio e un piano a cinematica parallela che si muove in X, Y e Z. La testa di stampaggio ad iniezione è alimentata con materiale sotto forma di pellet, questo offre grande libertà in termini del materiale che può essere stampato: termoplastici, inclusi PLA, ABS e Nylon, ma anche metalli e ceramiche con un legante che devono essere puliti e sinterizzati dopo la stampa.

Nella seconda sezione verrà condotta una campagna sperimentale, con la definizione di un piano sperimentale, per studiare gli effetti delle variabili termiche sulle caratteristiche desiderate e per trovare una finestra di processo ottimale, stampando diversi campioni con pellet di ULTEM 1000.

Questo lavoro è stato in grado di soddisfare i risultati attesi sotto molti aspetti. In primo luogo i miglioramenti apportati sono in grado di migliorare la qualità e la resistenza degli oggetti stampati, aumentare l'affidabilità del processo e consentire la stampa ad alta temperatura. La fase di stampa di pellet di ULTEM ha dato i risultati desiderati: la macchina è stata in grado di produrre i componenti progettati senza problemi, è stata definita una finestra di processo per il materiale e la qualità e le proprietà meccaniche delle parti prodotte sono state soddisfacenti.

Parole chiave: Stampa 3D, estrusione, miglioramenti termici, EFeSTO, pellet, ULTEM.

Table of Contents

1	INTRODUCTION	1
2	STATE OF THE ART	4
2.1	ADDITIVE MANUFACTURING.....	4
2.1.1	<i>The process and workflow</i>	6
2.1.2	<i>Additive and traditional manufacturing</i>	8
2.1.3	<i>Different types of additive manufacturing.....</i>	11
2.2	INJECTION MOLDING	16
2.2.1	<i>Process and machine</i>	16
2.2.2	<i>Process parameters and defects</i>	19
2.2.3	<i>Thermal flow in injection molding.....</i>	20
2.2.4	<i>The mold: materials and Rapid Tooling.....</i>	23
2.3	EXTRUSION.....	26
2.3.1	<i>Metal extrusion.....</i>	26
2.3.2	<i>Plastic extrusion.....</i>	28
2.3.3	<i>Elasticity in plastic extrusion</i>	33
2.4	VISCOSITY AND POLYMER RHEOLOGY	35
2.5	THERMAL PROBLEMS IN EAM	44
2.5.1	<i>Thermal parameters of interest in additive manufacturing</i>	44
2.5.2	<i>Material thermal history.....</i>	49
2.5.3	<i>Thermal related problems.....</i>	54
2.5.4	<i>High temperature materials thermal problems</i>	66
2.5.5	<i>Thermal achievements in additive manufacturing</i>	67
3	EFESTO.....	77
3.1	EXTRUSION GROUP	78
3.2	KINEMATIC SYSTEM.....	82
3.3	CONTROL OF THE MACHINE.....	85
3.4	EX-ANTE PROBLEMS OF THE EFESTO MACHINE	91
3.5	THERMAL PROBLEM ON THE EFESTO MACHINE	97
3.6	LIMITS OF THE MACHINE.....	100
4	IMPROVEMENTS ON THE MACHINE.....	102
4.1	GENERAL IMPROVEMENTS	102
4.2	COOLING CIRCUIT.....	103

4.3	PLC TUNING.....	110
4.4	HEATED BED.....	111
4.5	PNEUMATIC CLOSURE OF THE NOZZLE.....	116
4.6	LAYER FAN.....	117
4.7	INFRARED PREHEATING FOR HIGH TEMPERATURE THERMOPLASTICS.....	120
4.8	NOZZLE.....	124
4.9	SUMMARY OF THE MODIFICATIONS	127
5	EXPERIMENTAL CAMPAIGN	128
5.1	ULTEM	129
5.2	DRYER	131
5.3	MATERIALS FOR IMPROVING BED ADHESION	132
5.4	MODELS DESIGNED FOR THE CAMPAIGN	134
5.5	ABS TRIALS WITH THE IMPROVED EFESTO MACHINE.....	140
5.6	PRELIMINARY ULTEM TRIALS	146
5.7	DESIGN OF EXPERIMENTS	151
5.8	RESULTS	155
5.8.1	<i>Overhang Test</i>	155
5.8.2	<i>Engraved Cube</i>	159
5.8.3	<i>Bridge Test</i>	162
5.8.4	<i>Compression Specimen</i>	165
5.8.5	<i>Mechanical compression testing</i>	173
5.8.6	<i>Tensile Specimen</i>	179
5.8.7	<i>Mechanical tensile testing</i>	181
5.8.8	<i>Warping Test</i>	188
5.8.9	<i>Staircase Effect Test</i>	192
5.8.10	<i>Considerations on the results obtained</i>	194
5.8.11	<i>Comparison with ABS results</i>	195
6	CONCLUSIONS	203
	APPENDIX A	205
	APPENDIX B	206
	APPENDIX C.....	211
	REFERENCES.....	215

LIST OF FIGURES

FIGURE 1: DIFFERENT PROCESSES SCHEMATIC9

FIGURE 2: ASTM AM CLASSIFICATION [4]12

FIGURE 3: VAT PHOTOPOLYMERIZATION [5]12

FIGURE 4: POWDER BED TECHNOLOGY [5].....13

FIGURE 5: MATERIAL JETTING TECHNOLOGY [5]13

FIGURE 6: BINDER JETTING TECHNOLOGY [5]14

FIGURE 7: DIRECT ENERGY DEPOSITION TECHNOLOGY [5]14

FIGURE 8: MATERIAL EXTRUSION TECHNOLOGY [5].....15

FIGURE 9: INJECTION MOLDING MACHINE [6]18

FIGURE 10: RUNNERS, GATES AND SPRUE [6]19

FIGURE 11: PRESSURE AND TEMPERATURE BEHAVIOR IN TIME [8]19

FIGURE 12: INJECTION MOLDING PROCESS WINDOW [8].....20

FIGURE 13: INJECTION MOLDING PRESSURE-TEMPERATURE BEHAVIOR [10]21

FIGURE 14: FOUNTAIN FLOW FILLING [10]22

FIGURE 15: RAPID TOOL FOR INJECTION MOLDING MADE WITH ULTEM25

FIGURE 16: DIRECT AND INDIRECT METAL EXTRUSION [12]27

FIGURE 17: METAL EXTRUSION PRODUCTS [14].....27

FIGURE 18: PLASTIC EXTRUSION MACHINE [15].....28

FIGURE 19: VENT PORT AND SCREW SCHEMATIC [16].....29

FIGURE 20: SCREW AND DIE CHARACTERISTIC CURVES [17].....30

FIGURE 21: SCREW AND DIE CHARACTERISTIC CURVE FOR NON-NEWTONIAN FLUIDS [17].....31

FIGURE 22: PRESSURE BEHAVIOR IN DIFFERENT STAGES [17].....32

FIGURE 23: TYPICAL SCREW DESIGN33

FIGURE 24: DIE SWELL EFFECT [19].....34

FIGURE 25: MELT FRACTURE [19]35

FIGURE 26: AMORPHOUS AND SEMI-CRYSTALLINE MATERIALS.....36

FIGURE 27: FREE VOLUME BEHAVIOR IN TEMPERATURE [20].....37

FIGURE 28: VISCOUS FLOW SCHEMATIC37

FIGURE 29: DIFFERENT VISCOSITY BEHAVIORS [21]39

FIGURE 30: PSEUDOPLASTIC BEHAVIOR FOR SHEAR STRESS AND VISCOSITY39

FIGURE 31: VISCOSITY REGIONS FOR PSEUDOPLASTIC MATERIALS [21]40

FIGURE 32: POWER LAW MODEL [21].....41

FIGURE 33: FLOW IN A DUCT FOR NEWTONIAN FLUIDS.....41

FIGURE 34: CROSS-WLF MODEL [21]43

FIGURE 35: CAPILLARY RHEOMETER SCHEMATIC44

FIGURE 36: CONDUCTIVITY OF DIFFERENT MATERIALS.....45

FIGURE 37: CONDUCTIVITY-TEMPERATURE BEHAVIOR.....46

FIGURE 38: TEMPERATURE BEHAVIOR IN INJECTION MOLDING [8]49

FIGURE 39: TEMPERATURE PROFILE THROUGH FDM NOZZLE [23].....50

FIGURE 40: TEMPERATURE GRADIENTS DURING BUILDING.....	51
FIGURE 41: TEMPERATURE BEHAVIOR OF FIRST LAYER WHILE BUILDING THE OBJECT [23].....	52
FIGURE 42: DIFFERENT CONDITIONS IN FDM AM [25]	54
FIGURE 43: SHRINKING FORCES IN CORNERS	56
FIGURE 44: FEM MODEL OF A 3D PRINTED TENSILE SPECIMEN [26]	56
FIGURE 45: PRINTS WITH DIFFERENT BUILD SURFACE TEMPERATURES [27].....	57
FIGURE 46: NECK FORMATION AND DIFFUSION BETWEEN BEADS [28]	58
FIGURE 47: TEMPERATURE PROFILE IN TIME OF LAYERS AND WELD ZONES [32]	60
FIGURE 48: OVERHEATING EFFECTS [34]	62
FIGURE 49: OVERHANG BEHAVIOR [35].....	63
FIGURE 50: BRIDGE STRUCTURES [36]	63
FIGURE 51: PPSU VISCOSITY CURVES [37]	66
FIGURE 52: INVERTED PRINTER DESIGN [42]	71
FIGURE 53: SCHEMATIC OF LASER PREHEATING [43].....	71
FIGURE 54: SCHEMATIC OF INFRARED PREHEATING [44].....	72
FIGURE 55: TEMPERATURE PROFILE WITH INFRARED PREHEATING [44].....	73
FIGURE 56: TENSILE STRENGTH OF COOLED SPECIMENS WITH AND WITHOUT PREHEATING [45]	74
FIGURE 57: TENSILE STRENGTH OF UNCOOLED SPECIMENS WITH AND WITHOUT PREHEATING [45]	74
FIGURE 58: SCHEMATIC OF MICROWAVE HEATING [46]	75
FIGURE 59: PREHEATER METAL BLOCK [47].....	75
FIGURE 60: RENDERING OF THE EFeSTO MACHINE [52]	77
FIGURE 61: UAI BABYPLAST MACHINE [49].....	78
FIGURE 62: EXTRUSION UNIT WITH MOTORS [52].....	80
FIGURE 63: PNEUMATIC CLOSURE OF THE NOZZLE [49]	81
FIGURE 64: SCHEMATIC OF THE LINEAR DELTA SYSTEM [48].....	82
FIGURE 65: SCHEMATIC OF THE OPTIMIZATION VARIABLES OF THE PKM [52]	83
FIGURE 66: DYNAMIC MODEL OF THE PKM [52].....	84
FIGURE 67: MOTOR AND SERVO DRIVE [49].....	86
FIGURE 68: ELECTRIC SCHEME OF THE MACHINE [49]	88
FIGURE 69: HMI TEMPERATURE CONTROL.....	89
FIGURE 70: G-CODE INTERPRETER FOR CAM INSTRUCTIONS.....	90
FIGURE 71: SOFTWARE FOR THE SERIAL COMMUNICATION	91
FIGURE 72: PIECES PRINTED BEFORE THE IMPROVEMENTS	92
FIGURE 73: EXPOSED CABLE.....	92
FIGURE 74: CABLES ARRANGEMENT	93
FIGURE 75: ORIGINAL COOLING CIRCUIT	94
FIGURE 76: FLOW RATE OF THE ORIGINAL COOLING CIRCUIT	95
FIGURE 77: SCHEMATIC OF THE SHUTTER [49].....	96
FIGURE 78: EFeSTO CHAMBERS SECTION [49]	98
FIGURE 79: ORDERED CABLES	102

FIGURE 80: SERVO DRIVER BATTERY.....	103
FIGURE 81: TUBE USED FOR WATER CIRCULATION.....	104
FIGURE 82: OLD PNEUMATIC CONNECTORS.....	104
FIGURE 83: NEW G1/8 BRASS CONNECTORS.....	105
FIGURE 84: WATER TANK.....	105
FIGURE 85: PUMP CHARACTERISTIC CURVE.....	106
FIGURE 86: NEW PUMP.....	107
FIGURE 87: DIMENSIONS OF THE PUMP.....	107
FIGURE 88: PUMP STRUCTURE WITH FANS.....	108
FIGURE 89: MOTORS WATER-COOLED HEATSINK.....	108
FIGURE 90: THERMAL PASTE USED.....	109
FIGURE 91: HEATSINKS MOUNTED ON THE MOTORS.....	109
FIGURE 92: TANK TEMPERATURE READING.....	110
FIGURE 93: CLEANED BUILD SURFACE.....	112
FIGURE 94: NEW RESISTANCE WITH THERMISTOR.....	112
FIGURE 95: SOLID STATE RELAY (SSR).....	113
FIGURE 96: ELECTRIC REPRESENTATION OF A TRIAC.....	114
FIGURE 97: BIGTREE TECH SKR 1.4.....	115
FIGURE 98: DISPLAY TO CONTROL BED AND FAN.....	115
FIGURE 99: SCHEMATIC OF THE SHUTTER CONTROL [49].....	117
FIGURE 100: DIMENSIONS AND APPEARANCE OF A 5015 FAN.....	118
FIGURE 101: FAN AND CONNECTION WITH COPPER TUBE.....	119
FIGURE 102: COPPER FAN DUCT.....	119
FIGURE 103: MODEL OF THE INFRARED HEATER.....	120
FIGURE 104: IR LAMP.....	121
FIGURE 105: LIGHTS CONTROLLER.....	122
FIGURE 106: TRIAC BEHAVIOR RESPECT TO CASE TEMPERATURE [57].....	122
FIGURE 107: IR HEATER SIDE VIEW.....	123
FIGURE 108: IR HEATER FRONT VIEW.....	123
FIGURE 109: TECHNICAL DRAWING OF THE NOZZLE.....	125
FIGURE 110: NOZZLE TIP VIEW.....	126
FIGURE 111: NOZZLE BACK VIEW.....	126
FIGURE 112: EFeSTO MACHINE WHILE PRINTING THE 1ST LAYER OF A SAMPLE.....	128
FIGURE 113: PEI MOLECULAR STRUCTURE [58].....	129
FIGURE 114: ULTEM PELLETS.....	130
FIGURE 115: ARID DRIER BY 3Devo.....	132
FIGURE 116: DIMAFIX CHARACTERISTIC CURVE.....	133
FIGURE 117: MAGIGOO HT ADHESIVE.....	134
FIGURE 118: SIMPLE CUBE MODEL.....	135
FIGURE 119: FLAT BLOCK MODEL.....	135

FIGURE 120: TENSILE SPECIMEN MODEL	136
FIGURE 121: COMPRESSION SPECIMEN MODEL	136
FIGURE 122: OVERHANG TEST MODEL	137
FIGURE 123: BRIDGE TEST MODEL	137
FIGURE 124: BRIDGE FEATURE SLICED	138
FIGURE 125: ENGRAVED CUBE MODEL	138
FIGURE 126: STAIRCASE EFFECT MODEL	139
FIGURE 127: WARPING TEST MODEL	139
FIGURE 128: OVERHEATED ABS ENGRAVED CUBE	141
FIGURE 129: OVERHEATED ABS CUBE	142
FIGURE 130: OVERHEATED ABS STAIRCASE TEST	142
FIGURE 131: ABS OVERHANG TEST WITH 100% FAN SPEED	143
FIGURE 132: ABS ENGRAVED CUBE WITH 100% FAN SPEED	143
FIGURE 133: ABS STAIRCASE EFFECT TEST WITH 100% FAN SPEED	144
FIGURE 134: ABS TENSILE SPECIMEN	144
FIGURE 135: ABS COMPRESSION SPECIMEN	145
FIGURE 136: OVERHANG TEST 0% FAN	156
FIGURE 137: OVERHANG TEST 25% FAN	157
FIGURE 138: OVERHANG TEST 50% FAN	158
FIGURE 139: ENGRAVED CUBE 0% FAN	159
FIGURE 140: ENGRAVED CUBE 25% FAN	160
FIGURE 141: ENGRAVED CUBE 50% FAN	161
FIGURE 142: BRIDGE TEST 0% FAN	162
FIGURE 143: BRIDGE TEST 25% FAN	163
FIGURE 144: BRIDGE TEST 50% FAN	164
FIGURE 145: BRIDGE TEST 50% FAN CLOSE UP	165
FIGURE 146: COMPRESSION SPECIMEN N. 1	166
FIGURE 147: COMPRESSION SPECIMEN N. 2	167
FIGURE 148: COMPRESSION SPECIMEN N. 3	167
FIGURE 149: COMPRESSION SPECIMEN N. 4	168
FIGURE 150: COMPRESSION SPECIMEN N. 5	168
FIGURE 151: COMPRESSION SPECIMEN N. 6	169
FIGURE 152: COMPRESSION SPECIMEN N. 7	169
FIGURE 153: COMPRESSION SPECIMEN N. 8	170
FIGURE 154: COMPRESSION SPECIMEN N. 10	170
FIGURE 155: COMPRESSION SPECIMEN N. 11	171
FIGURE 156: TEMPERATURE-FAN PROCESS WINDOW FOR CYLINDER SPECIMEN	173
FIGURE 157: COMPRESSION TEST MACHINE	173
FIGURE 158: COMPRESSION SPECIMENS AFTER TESTING	174
FIGURE 159: STRESS-STRAIN CURVES NOZZLE T. 380°C - FAN 0%	175

FIGURE 160: STRESS-STRAIN CURVES NOZZLE T. 380°C - FAN 25%.....	176
FIGURE 161: STRESS-STRAIN CURVES NOZZLE T. 385°C - FAN 25%.....	176
FIGURE 162: COMPRESSION ELASTIC MODULUS COMPARISON	177
FIGURE 163: YIELDING COMPRESSION STRESS COMPARISON	178
FIGURE 164: TENSILE SPECIMEN GEOMETRY	179
FIGURE 165: TENSILE SPECIMENS IR 0%	179
FIGURE 166: TENSILE SPECIMENS IR 25%	180
FIGURE 167: TENSILE SPECIMENS IR 50%	181
FIGURE 168: TENSILE TEST MACHINE	182
FIGURE 169: TENSILE SPECIMEN FRACTURE	182
FIGURE 170: STRESS-STRAIN CURVES FOR IR 0%.....	184
FIGURE 171: STRESS-STRAIN CURVES FOR IR 25%.....	184
FIGURE 172: STRESS-STRAIN CURVES FOR IR 50%.....	185
FIGURE 173: TENSILE ELASTIC MODULUS COMPARISON	186
FIGURE 174: PEAK TENSILE STRESS COMPARISON	186
FIGURE 175: STRAIN AT BREAK COMPARISON	187
FIGURE 176: WARPING TEST N. 1	189
FIGURE 177: WARPING TEST N. 2	190
FIGURE 178: WARPING TEST N. 3	191
FIGURE 179: WARPING TESTS COMPARISON	192
FIGURE 180: STAIRCASE EFFECT TEST 0% FAN	192
FIGURE 181: STAIRCASE EFFECT TEST 25% FAN	193
FIGURE 182: TEMPERATURE BEHAVIOR IN TIME.....	199
FIGURE 183: T* FOR DIFFERENT MATERIALS AND EXTRUSION CONDITIONS	201
FIGURE 184: OVERHEATING AND DELAMINATION TENDENCY ABS AND ULTEM	202

LIST OF TABLES

TABLE 1: DIFFUSIVITY FOR DIFFERENT MATERIALS	47
TABLE 2: SUMMARY OF EAM THERMAL PROBLEMS	65
TABLE 3: ELECTRICAL COMPONENTS OF THE EFESTO MACHINE	89
TABLE 4: SUMMARY OF THE IMPROVEMENTS.....	127
TABLE 5: DESIGNED MODELS PURPOSE AND RELATED VARIABLES.....	140
TABLE 6: PRELIMINARY TRIALS PARAMETERS	147
TABLE 7: PRELIMINARY TRIALS ASPECT	149
TABLE 8: DEFAULT PRINTING PARAMETERS.....	151
TABLE 9: OVERHANG TEST TRIALS	152
TABLE 10: ENGRAVED CUBE TRIALS	152
TABLE 11: BRIDGE TEST TRIALS	153
TABLE 12: COMPRESSION SPECIMENS TRIALS.....	153
TABLE 13: TENSILE SPECIMENS TRIALS.....	153
TABLE 14: WARPING TEST TRIALS	154
TABLE 15: STAIRCASE TEST TRIALS.....	154
TABLE 16: OVERHANG TEST RESULTS.....	158
TABLE 17: ENGRAVED CUBE RESULTS	161
TABLE 18: BRIDGE TEST RESULTS.....	165
TABLE 19: COMPRESSION SPECIMENS PRINTING PHASE RESULTS.....	172
TABLE 20: COMPRESSION TEST RAW DATA	174
TABLE 21: MEAN AND STANDARD DEVIATION OF THE PARAMETERS OF INTEREST	177
TABLE 22: TENSILE SPECIMENS PRINTING PHASE RESULTS.....	181
TABLE 23: TENSILE TEST RAW DATA	183
TABLE 24: MEAN AND STANDARD DEVIATION OF THE PROPERTIES OF INTEREST.....	185
TABLE 25: WARPING TEST RESULTS.....	191
TABLE 26: STAIRCASE TEST RESULT.....	194
TABLE 27: ABS-ULTEM PROPERTIES OF INTEREST	196

LIST OF ABBREVIATIONS

ABS = ACRYLONITRILE BUTADIENE STYRENE

AC = ALTERNATING CURRENT

AM = ADDITIVE MANUFACTURING

ASTM = AMERICAN SOCIETY FOR TESTING AND MATERIALS INTERNATIONAL

BAAM= BIG AREA ADDITIVE MANUFACTURING

CAD= COMPUTER AIDED DESIGN

CAM = COMPUTER AIDED MANUFACTURING

CDLP = CONTINUOUS DIGITAL LIGHT PROCESSING

CFD= COMPUTER FLUID DYNAMIC

CLIP = CONTINUOUS LIQUID INTERFACE PRODUCTION

CNC = COMPUTER NUMERIC CONTROL

CNT= CARBON NANOTUBE

CTE= COEFFICIENT OF THERMAL EXPANSION

DED = DIRECT ENERGY DEPOSITION

DLP = DIGITAL LIGHT PROCESSING

DMLS = DIRECT METAL LASER SINTERING

DOD = DROP ON DEMAND

DOE = DESIGN OF EXPERIMENTS

DOF = DEGREE OF FREEDOM

DPP = DAYLIGHT POLYMER PRINTING

EAM = EXTRUSION ADDITIVE MANUFACTURING

EBAM = ELECTRON BEAM ADDITIVE MANUFACTURING

EBM = ELECTRON BEAM MELTING

ECM= ELECTROCHEMICAL MACHINING

EDM= ELECTRICAL DISCHARGE MACHINING

EEPROM = ELECTRONICALLY ERASABLE PROGRAMMABLE READ-ONLY MEMORY

EFeSTO = EXTRUSION OF FEEDSTOCK FOR SINTERED TINY OBJECTS

FDM = FUSED DEPOSITION MODELING

FEM= FINITE ELEMENT METHOD

FDM= FUSED DEPOSITION MODELING

HIPS = HIGH-IMPACT POLYSTYRENE

HMI = HUMAN MACHINE INTERFACE

IR = INFRA RED

ISO = INTERNATIONAL ORGANIZATION FOR STANDARDIZATION

LDW = LASER DEPOSITION WELDING

XVIII

LED = LIGHT EMITTING DIODE
LOM = LAMINATED OBJECT MANUFACTURING
MIM= METAL INJECTION MOLDING
MIT = MASSACHUSETTS INSTITUTE OF TECHNOLOGY
MJF = MULTI JET FUSION
NTC = NEGATIVE TEMPERATURE COEFFICIENT
PA = POLYAMIDES
PBF = POWER BED FUSION
PBI= PLOYBENZIMIDAZOLE
PC = PERSONAL COMPUTER
PEEK = POLYETHER ETHER KETONE
PEKK = POLYETHER KETONE KETONE
PEI = POLYETHERIMIDE
PID= PROPORTIONAL INTEGRAL DERIVATIVE
PLA = POLYLACTIC ACID
PLC= PROGRAMMABLE LOGIC CONTROLLER
PPSU= POLYPROPYLENE SULFONE
PTFE=POLYTETRAFLUOROETHYLENE
PVC=POLYVINIL CHLORIDE
PWM= PULSE WIDTH MODULATION
RT= RAPID TOOLING
SCR = SILICON CONTROLLED RECTIFIER
SFC = SEQUENTIAL FUNCTION CHART
SLA = STEREO LITHOGRAPHY
SLM = SELECTIVE LASER MELTING
SLS = SELECTIVE LASER SINTERING
SSR = SOLID STATE RELAY
STL= STANDARD TRIANGULATION LANGUAGE
TRIAC = TRIODE FOR ALTERNATING CURRENT
USB = UNIVERSAL SERIAL BUS
UTS = ULTIMATE TENSILE STRENGTH
WLF= WILLIAMS LANDEL FERRY

1 Introduction

The Extrusion Additive Manufacturing (EAM) can be regarded as a thermal technology since it uses heat to enhance bonding and diffusion between different deposited roads of material. The thermal problem is therefore of primary importance in this production method to ensure proper building of the parts and no problems during production, related both to excess or lack of heat flux. EAM can be performed with the material in form of filaments or pellets. Filament EAM is a more established and reliable technology, on which many papers and publications can be found, while pellets EAM is less developed but has many advantages. First of all the cost of raw material is decreased dramatically since usually the production of filaments from pellets is expensive, due to the tight tolerances required by the extruders. Using directly pellets for EAM also enables the possibility of performing Additive Manufacturing with all the polymers available on the market, not only the ones produced in filament form by other companies. The following thesis will first focus on the main thermal problems in additive manufacturing, in particular for EAM with thermoplastics, but which are present in pretty much all materials. Secondly, the improvements on the already built EFeSTO machine, which is a pellet Additive Manufacturing machine, will be explained. These improvements will enable the machine to print more sophisticated and difficult materials and in general increase the quality of the produced parts and the reliability of the process. The improvements carried out will be verified with an experimental campaign, focused on the thermal aspects of the process, with ULTEM 1000 material.

ULTEM is the commercial name given by Sabic to PEI, polyetherimide polymer. PEI is a high strength amorphous thermoplastic used in automotive and aerospace fields, with good high-temperature resistance due to an exceptionally high glass transition temperature of 215 °C. Thanks

to its outstanding mechanical and thermal properties it is also employed as material for Rapid Tools in injection molding. PEI components are usually produced with injection molding but in the last years some researches and articles have been published in the field of Filament Additive Manufacturing with this material. Commercial machines able to Additive manufacture PEI in filament form exist but they are all high-cost machines, with heated and enclosed build volume and embedded filament dryer. To my knowledge and researches, no scientific publications are present instead on the Extrusion Additive Manufacturing of PEI components directly from pellets, which would reduce the cost and time for production significantly. In the first section an overview of the scientific literature of the field will be carried out, mainly regarding additive manufacturing, injection molding, extrusion, thermal evolution of the printed component and thermal problems in Additive Manufacturing.

In the second section an overview of the EFeSTO machine is carried out, including characteristics, limits and problems of the machine with care and attention on the thermal side of the printer used, regarding both the cold end and the hot part of the machine.

In the third section the improvement made on the machine are presented, including modifications on the cooling system, the bed on which the object is built, the addition of an infrared lamp close to the nozzle to heat the substrate layer on which the machine will lay the next layer and the design of a new nozzle with a more precise hole and coherence of the material flux, which will be designed keeping in mind the pneumatic closure of the nozzle. The pneumatic closure will be configured to close the flow of the material when not printing and prevent oozing of the material before and after the printing phase, but also during the recharge of the chambers. The last improvement will consist in adding a layer fan close to the nozzle in order to cool the layer when needed, for example to print complex

geometries in overhang or when the substrate needs to be more solidified to prevent deposition on a loose substrate.

In the fourth section an experimental campaign will be carried out to find an experimental optimum process window from a thermal point of view for the ULTEM polymer and to study the relation between thermal process variables, quality and strength of the produced components.

2 State of the art

In this section a review of additive manufacturing technology is carried out, mainly focusing on EAM, then some keys ideas are presented about injection molding and plastic extrusion, two processes which share the viscous flow of polymer and nozzle behavior with pellets EAM machines. A brief explanation of polymer rheology is illustrated to understand the flow behavior inside these processes. At the end of the section the attention will be shifted on thermal characteristics, problems and solutions for EAM additive manufacturing.

2.1 Additive Manufacturing

Additive manufacturing is a production process which consist in the generation of an object by superposition of different layers of material. Defined by ASTM as “process of joining materials to make objects from three-dimensional (3D) model data, usually layer upon layer, as opposed to subtractive manufacturing methodologies”.

This technology has been developed at MIT at the beginning of the 80s. It was then commercialized by 3D system in 1987. From there, the development of this system has continued and in the last year has increased exponentially thanks to the falling of the patent for 3D printers; many companies started producing their own printers, prices of components dropped dramatically and a lot of open-source project started. In the last 20 years this technology has moved also from industry to private customers which can have a desktop 3D printer in their house and so start a decentralized and personalized production of objects. AM market will continue to grow in the following years thanks to a decrease in the price of machines and its versatility. This technology can make parts which were impossible or really difficult to be made in the past. Geometry of the piece is only one of the aspects in which additive manufacturing has advantages

over other production methods, also the time that elapses between the project and the actual piece is decreased a lot, giving faster prototypes or final pieces which can then be iterated in a faster manner.

Through the years AM has expanded in many sectors and disciplines, moving away from the research field it was at the beginning of the 90s. Nowadays many companies have entered the field producing objects of different kinds, from tooth braces to components for jet turbines.

The techniques used to do so are many. Among them it is possible to find SLA, SLS, LOM, FDM, EBM, LENS and DED (see list of abbreviations).

There are many reasons for which AM is gaining popularity in the last years.

Additive manufacturing technology well fits in the field of industry 4.0, which is gaining interest in the last years. Industry 4.0 considers production methods which are strictly correlated with internet and digital information, used to simplify and speed up the work and for a more reliable production. AM is indeed a completely digital technology, really versatile and fast to implement, with not so many parameters to be set for the specific work and with a universal tool: the nozzle.

It is regarded in Industry 4.0 since it starts from a digital model in STL format, which is then sliced to give a path for each layer to be followed by the deposition head, everything is controlled in a digital manner from a PLC and once the job is started the human operator can leave, since more sophisticated machines are also able to detect errors and sometimes compensate for them.

Additive manufacturing is also regarded when considering circular economy since it guarantees the possibility of recycling the printed object at the end of their life when using thermoplastics, reducing the environmental impact of production. In this case pieces needs to be grinded, sieved, dried and, depending on the machine, extruded in form of filament or kept as pellets.

Another aspect for which AM is gaining importance is that it produces way less scrap material for each job for respect to classical manufacturing: when milling the piece is obtained by removing chips of material from a block which often cannot be recycled due to contamination with cooling liquid, in AM instead the nozzle deposits the material only where needed thus saving material.

Moreover, a reason for the popularity of AM in the last years is the freedom which gives to the producer: depending on the machine many materials can be printed, ranging from thermoplastics to metals and including ceramics, clay, concrete, edible materials and biocompatible ones. Really complex geometries can be obtained with no specific tools, only by giving to the nozzle a predefined path in space and time. This feature reduces even more the costs for producing small batches or personalized components for respect to injection molding, machining and other production methods.

2.1.1 The process and workflow

Additive manufacturing technologies differ in material used and type of energy provided but are similar in process characteristics and production workflow. The production workflow can be divided in:

- Product planning, with analysis of feasibility, objectives and constrains to be respected, mechanical studies to choose material and technology to be used.
- CAD design, which involves the drawing and development of the desired object with a 3D CAD software, with attention on the technology chosen limitations, to facilitate the building. The object will be then exported as a mesh, usually STL, which is a grid of triangles in space that covers the surface of the part.
- Slicing. With the help of a slicer software the STL is sliced in layers and for each layer a path for the printhead is defined. Many settings can be chosen according to the technology used but some decisions

are taken automatically by the software. The software exports a G-Code which is a text file with coordinates, speeds and desired flow rate for each point of the process, given a resolution chosen in the slicer software.

- Production. The G-Code is usually sent directly to the printer which starts building the object in an autonomous way, the operator presence is needed only to stop the machine in case of errors or to change material. After minutes, hours or days depending on the dimension, complexity and settings the part is ready to be removed from the build surface and for post-processing.
- Post-processing. Depending on the technology used the post processing might consist in removing the supports and flaws, debinding and sintering, hot isostatic pressing, curing or even machining of some desired characteristics.

This process can easily be iterated after the component trial, to improve the design or modify some features or dimensions, at a lower cost for respect to iterating a machining or injection molding process. This technology was called in origin rapid prototyping since it is the most convenient one for making first prototypes of an object to be manufactured. Nowadays it is also used to make rapid tools for injection molding, sheet working and other manufacturing technologies, since the properties of the additive manufactured component have improved a lot. This technology can also be used to make finished parts, mainly small batches or customized production.

In the last years it is gaining popularity also the automated design of an object given the desired properties, constrains and loads to be applied to the part, this generative design can save a lot of material for respect to traditional design by giving strength and stiffness only where needed.

The characteristics of the process which are in common between different additive manufacturing technologies are the layer by layer construction, in

which material or energy is deposited only where it is written in the G-Code, the bonding energy, which in most of the technologies is thermal energy, the kinematics characteristics, which for most of the machines result in stepper motors moving some linear carriages, forming cartesian or delta kinematics, and the digital and automatic nature of the process, common to all additive manufacturing technologies.

2.1.2 Additive and traditional manufacturing

Traditional manufacturing considers many production methods, including casting, forging, machining, injection molding and many others well studied and established technologies. On the other hand, Additive Manufacturing is considered in the field of advanced manufacturing processes, which includes laser, plasma, waterjet, EDM, ECM and ultrasonic processes, as it is a more recent technology, provides high accuracy, there is no physical tool-piece contact and is suited for customized production of small batches. These new production methods are often controlled by a digital microprocessor, which defines the parameter of production in a digital manner, giving a higher degree of automation, as opposed to the possibility of full mechanical machines in traditional manufacturing.

With Additive Manufacturing the cost vs number of pieces curve is way flatter than with traditional manufacturing, due to lower cost of setup and of tooling which have to be amortized on the number of pieces.

As pointed out by T Pereira in [1] a production method can be classified based on Complexity, Customization and Volume of production. For mass production of simple pieces traditional manufacturing is still more reliable and cheaper, while AM is often preferred for low volume production of complex parts and customized ones. In AM the complexity of an object is not a big problem due to its universal tool and the deposition of material only where needed, supports may be added for features which does not

have any material under the deposition layer (overhangs or bridges) or in case of a 6dof printer also the printing orientation can be modified, while in conventional machining the features are constrained by the possibility of inserting the cutting tool, in machining, or, in injection molding, by the viscosity of the material and removal from the mold (Figure 1).

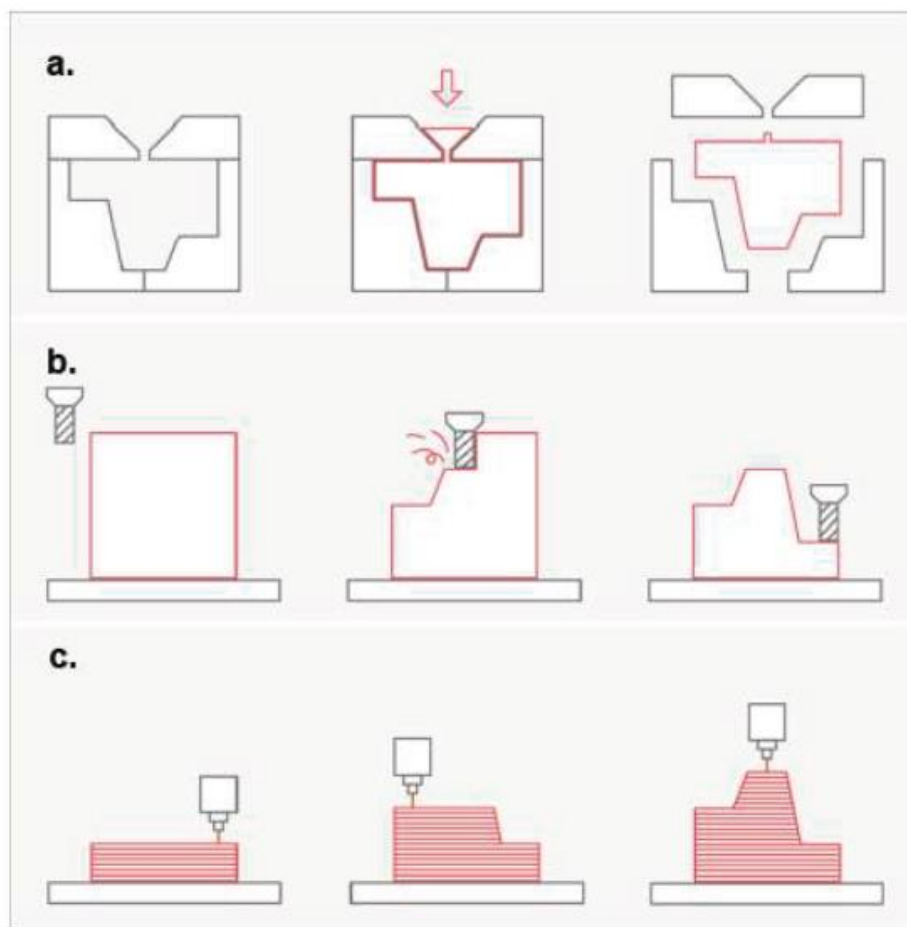


Figure 1: Different processes schematic

Notes: a. formative manufacturing, b. subtractive manufacturing, c. additive manufacturing

Customization is another advantage of 3D printing since it is possible to make small variation of the same object basically for free due to the additive and digital nature of the technology, while with conventional

manufacturing each change in the project requires time and money. One big concern is instead the quality because usually Additive Manufacturing cannot guarantee the same quality reached by machining or molding, due to the layer construction but also due to unpredictable and casual variations made by the printer at a microscopic level. Some really precise additive technologies exist, but often for a better quality require more printing time, due to smaller layer thickness, which sometimes make it unfeasible from an economic point of view.

For respect to traditional production AM can also work 24/7 without an operator always present, due to the digital nature of the process, this can help to relieve long printing times of some big, complex and high quality parts, but in some cases traditional manufacturing is still preferred. With AM the rules of the Design For Manufacturing or Assembly are not so important and this gives the designer more freedom and the possibility of making objects in one part that with classical manufacturing would require an assembly. Some design rules exist also for Additive production, mainly related to the problems of this technology such as overhangs, warping and “stair-stepping” effect [2]. With the additive technology it is also possible to produce small mechanisms or moving assemblies in one part which would require more parts and joints with traditional manufacturing. Overall, the two types of manufacturing have two separated application fields, with traditional manufacturing for mass production of standard pieces and additive for complex and customized objects, even if in some cases a more in dept cost/quality analysis has to be carried out to choose the preferable one. One big concern of additive manufacturing from a microscopical point of view is the presence of porosities between roads, since the material is deposited in adjacent beads and between them some air is usually present, improvements on this aspect has been continuously made, for example by using negative inter-roads spacing, as pointed out by Wang et al. [3], to

improve strength, or by using hot isostatic pressing on the printed part to provide isotropic properties and higher density.

For mass production additive manufacturing can be used in the first stages of the project of an object as rapid prototyping, in order to reduce the time between ideas and real-life object and make easier the iterations in the design. Additive manufacturing can also enhance the possibility of delocalized manufacturing, with production of parts closer to the customer or directly by the customer, selling and sending only digital CAD files and thus saving in warehouses, logistics and transport costs. There is also the possibility of hybrid manufacturing in which, on the same machine, additive and subtractive manufacturing are carried out: the piece is built with an additive technology while finishing to remove layer roughness or particular features are carried out with CNC milling.

2.1.3 Different types of additive manufacturing

The additive technology consists in construction of an object layer by layer, adding material to the substrate only where needed. Even if this basic principle is always valid there exist different types of additive manufacturing, depending on the type of the material, on the form of energy provided for bonding and on many other aspects.

The different additive manufacturing technology are similar in the building technique and in the workflow of production adopted, starting from a digital CAD, then sliced, built and post-processed.

Among them it is possible to find vat photopolymerization, powder bed fusion, material jetting, binder jetting, laminated object manufacturing, direct energy deposition and material extrusion. One first classification by ASTM regarding processes, materials and finished parts is presented in Figure 2.

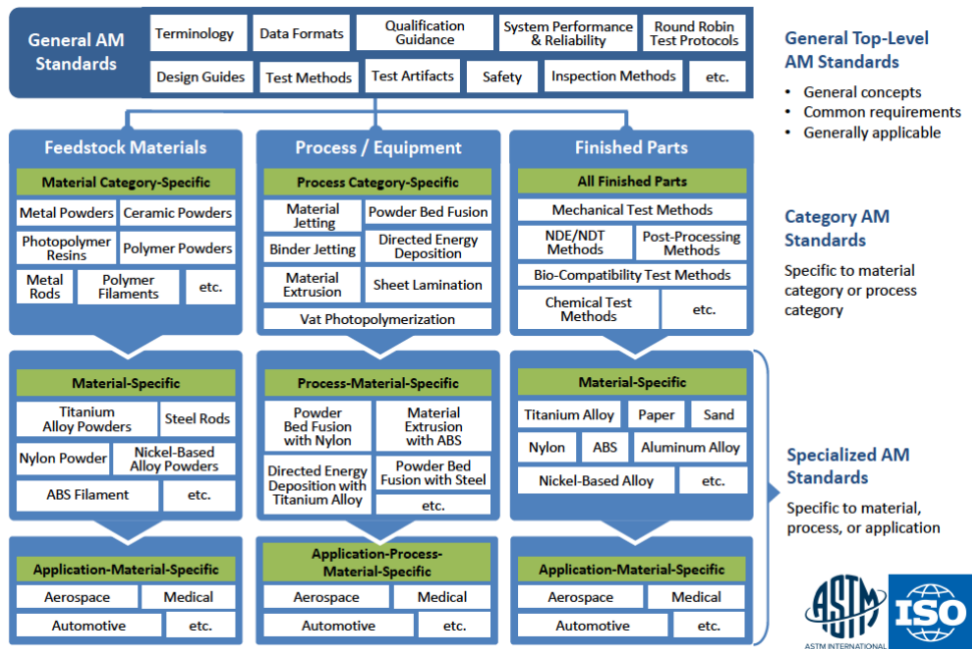


Figure 2: ASTM AM classification [4]

- Vat photopolymerization (Figure 3) is divided in SLA, DLP, DPP and CLIP, this process can be adopted only with some resins that react with light by giving fine details and acceptable mechanical properties, the part is built at the interface between the last layer and the surface of the resin tank. DLP is faster than SLA since in the latter a laser beam controlled by mirrors moves on the printing surface to scan the layer, while in DLP all the layer is scanned simultaneously by projecting the whole shape on the vat [5].

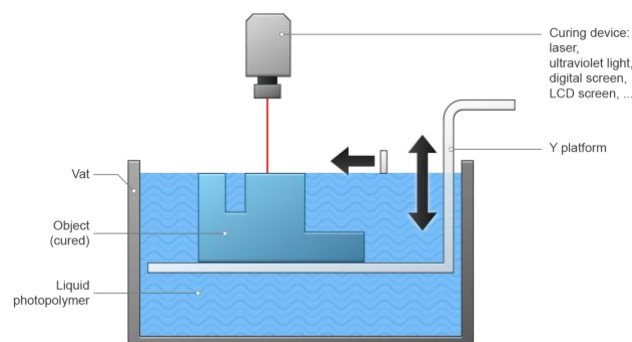


Figure 3: VAT photopolymerization [5]

- Powder bed fusion technologies (Figure 4) on the other hand use a heat source, usually lasers or electron beam to build, layer by layer, complex geometrical structures from powder material, it is divided in DMLS, SLS, SLM, MJF and EBM depending on material used and level of energy necessary for the bonding. Selective laser sintering is used with thermoplastics or metal with binders, while Melting technologies use a full metal powder to build the object.

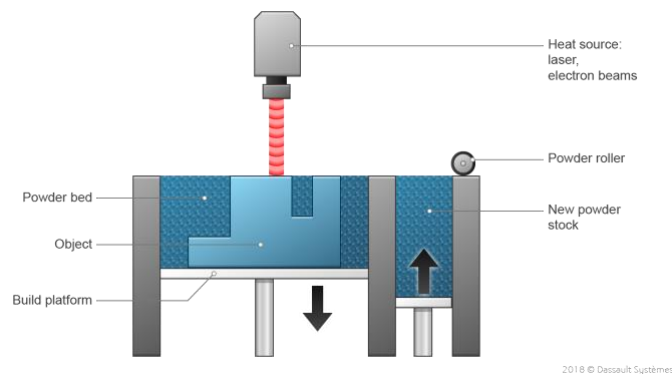


Figure 4: Powder bed technology [5]

- Material jetting (Figure 5) deposits tiny droplets of material on the previous layer which are directly cured and solidified using UV light, it is a really precise technology but it is expensive and UV cured photopolymers can become brittle over time. Many materials, including waxes, metals and photopolymers, can be deposited on the same part. It is the most similar process to 2D printing.

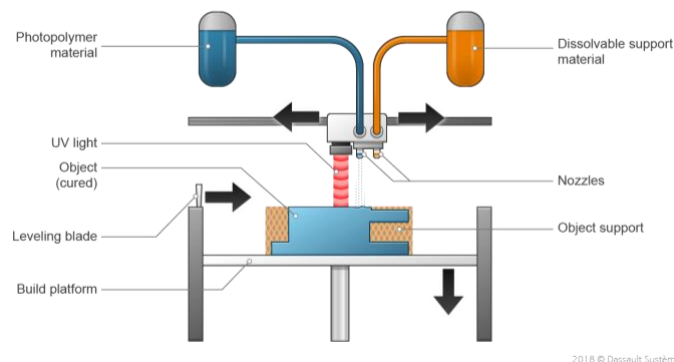


Figure 5: Material jetting technology [5]

- Binder jetting (Figure 6) instead does not involve any heat source but has the same printhead with tiny nozzles as for material jetting. A binder is deposited on metal or ceramic powder in specific points to build the part. Since this process does not involve heat the objects are built with no residual stresses in them but often need to be sintered in a second moment.

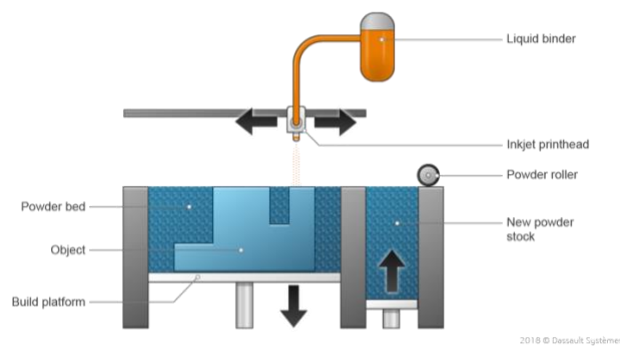


Figure 6: Binder jetting technology [5]

- Direct energy deposition (Figure 7) is becoming really popular in the last years, it directly melts the material as it is deposited on the substrate in form of wire or powder, the materials used can be metals, alloys, ceramics or composites, it can provide high mass flow rate of printing material and so is considered a pretty fast technology. It encompasses LENS, EBAM, LDW, classified depending on the state of material and source of energy provided, which can be laser or electron beam. These technologies usually need an enclosed chamber filled with inert gases to prevent oxidation.

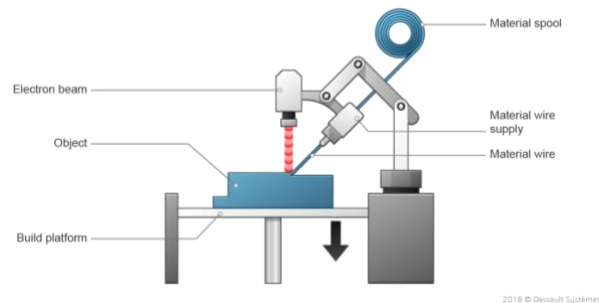


Figure 7: Direct energy deposition technology [5]

- Material extrusion (Figure 8) is the most widespread technology from a commercial point of view. It consists in the deposition of material, which can be thermoplastics, concrete, edibles materials or ceramic/metal with binder. The extrusion happens through a nozzle after it has been heated close to the nozzle itself to improve bonding and diffusion and to facilitate extrusion by reducing the viscosity. This technology is also known as Fused Deposition Modeling (FDM) and it can be performed starting from material in filament spools, with rack and pinion extruders, or from pellets, extruded through pistons or screw extruders. Comparing it to the beforementioned technologies FDM is characterized by greater anisotropy and dimensional accuracy limitations, the latter can be easily improved with more precise machines which can decrease the layer height significantly, but this would imply an increase in time and cost both of the machine and of the part. The kinematics of the machine can assume different configurations, with motion assigned to the build plate, to the nozzle or partially to one and the other. It usually involves a three axis kinematics in cartesian, delta or polar systems, but some state-of-the-art machines can involve up to 5 or 6 axes, increasing thus the deposition possibilities but also the programming complexity.

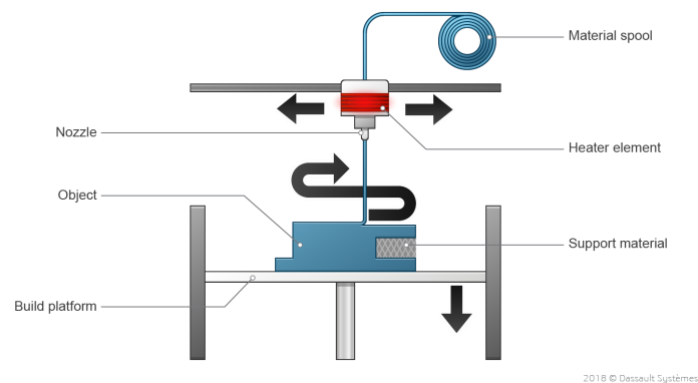


Figure 8: Material extrusion technology [5]

2.2 Injection molding

Injection molding is a traditional manufacturing process used to produce pieces made of plastic or metal, in the latter case it is called metal injection molding (MIM) or powder injection molding since the metal is in powder form bonded to a plastic matrix which will be removed during debinding and sintering. The basic principle is to push the material, which has been softened by thermal energy, into a mold and then let it solidify in the mold by keeping some pressure on it. There exist different types of machines for injection molding, the main two categories are screw ones and pistons ones, which differ on the mechanism used to push the material in the mold. In injection molding the material has to be really soft, and this softening is achieved by increasing the temperature, in order to have a better control of filling by the pressure and a faster filling of the mold. This process is used for mass production of plastic components, since it can be easily automated and can guarantee a high productivity due to fast cycles. It can also be used to make complex parts being aware of the need to open the mold after the process, so severe undercuts cannot be produced with this technique.

Due to the high productivity, variety of materials which can be manufactured and high-quality regarding reproducibility of parts, tight tolerances and good surface roughness, which is strictly related to the one of the molds, this process is widely used in industry to manufacture goods of different shapes and sizes, and about 35 wt% of polymer components are produced with this method.

2.2.1 Process and machine

The process is divided in clamping, injection, dwelling (packing), cooling, opening of the mold and removal of the piece.

- In clamping the mold is closed with mechanical actuators.
- During injection the injection unit approaches the mold and the screw starts pushing the material inside it. The pressure has to be

sufficient to guarantee the filling of the mold before the material solidify to avoid defects.

- During dwelling or packing the plastic is held in the mold under pressure to compensate for shrinkage of the piece in the mold and reduce porosity of the piece, this stage ends when the material in the runner and in the gate is solidified, since the pressure from the screw cannot affect anymore the material inside the mold.
- Cooling starts when the material exits the nozzle of the machine, the temperature of the molten polymer decreases with time due to heat extraction from the mold, the duration of this stage is strictly related to material thermal properties, mold conductivity and starting temperature.
- Opening and removal of the piece is done before the piece reaches ambient temperature but when it is cool enough to have some stiffness, the mold opens and the ejector pins push the piece out of the mobile half of the mold. Care has to be adopted in not deforming the part during extraction. The final shape and dimensions are obtained after the material has completely cooled to ambient temperature out of the mold.

The injection molding machine can have several layouts different in complexity and maximum pressure reachable, the drive unit can be hydraulic or electrical. Nowadays in industry the most common configuration is to have a rotating screw which both plasticize the material and pushes it into the mold. Every machine is anyway characterized by an injection unit and a mold unit.

The screw driven injection unit is characterized by a hopper, in which raw material is stored, a heated barrel, with more than one PID control of the temperatures for different zones, a screw driven by an electric motor, and a convergent-divergent nozzle.

The mold unit is composed by a fixed mold, a mobile mold, extractor pins and mechanical actuators to close the mold.

The screw or piston has to feed the material to the mold, it is usually controlled in speed in the first part of the process and in pressure once a critical pressure is exceeded.

In screw machines the screw itself has the double function of pushing the soft material into the mold and at the same time plasticize new material coming from the hopper during its movement.

In Figure 9 the typical layout for an in-line screw injection molding machine is presented.

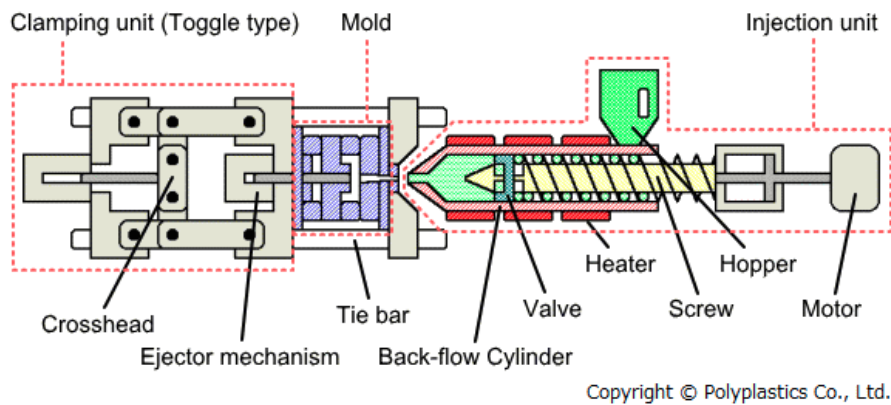


Figure 9: Injection molding machine [6]

As pointed out by P. D. Kale et al. [7] also the runner system is of primary importance for a consistent and efficient process, the runner (Figure 10) is the part of the machine which connects the sprue to the mold, used to deliver the material to the pieces, and it can be heated or not. In the heated configuration it guarantees faster cycle time, less waste, less friction and higher quality but it is more complicated and expensive and not suitable for some thermally sensitive materials.

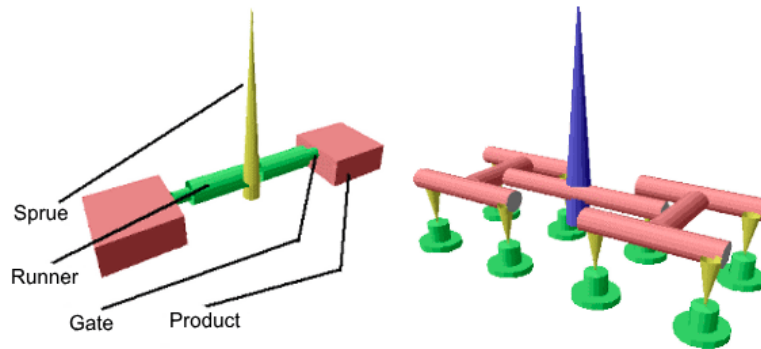


Figure 10: Runners, Gates and Sprue [6]

2.2.2 Process parameters and defects

The main process parameters are related to speed, pressure, time, temperature and stroke, among them it is possible to account for injection velocity, holding pressure, time for injection and for cooling, temperatures in the barrel, inside the mold and of the cooling water. In Figure 11 the typical behavior for pressure and temperature in time is reported:

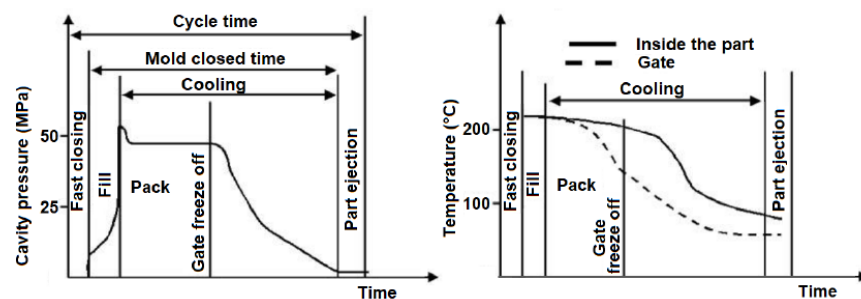


Figure 11: Pressure and Temperature behavior in time [8]

Temperature and pressure are among the most important parameters and can define a process window for defect free injection molding [8] as pointed out in Figure 12.

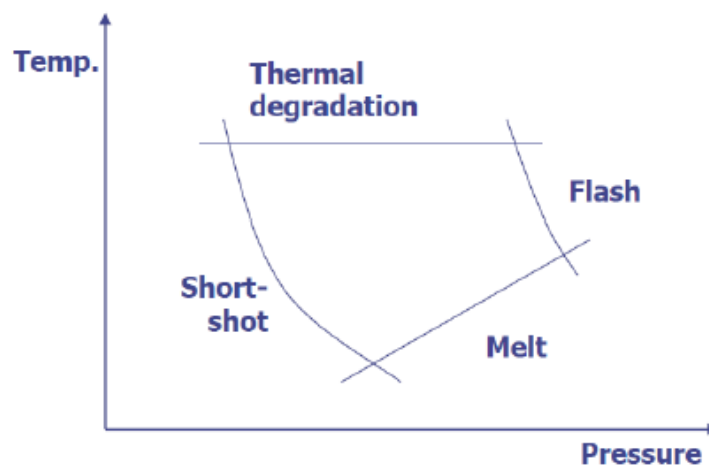


Figure 12: Injection molding process window [8]

The process parameters affect each other and an improper selection of parameters can lead to burn marks, warping, air pockets, delamination and weld lines. For this reason an optimal process window for the parameters has to be found for each specific machine, material and component to be produced. G. Singh [9], after a wide literature review, concluded that most studied defect are Shrinkage, Warping, Sink Marks and Weld Lines, correlated by many authors to different process parameters. In the last years the process parameters selection has to take care not only of the quality of the product but also of reducing as much as possible resource consumption and emission in the whole life cycle of an object, also involving the recycling of the latter at the end of its life.

2.2.3 Thermal flow in injection molding

In injection molding the polymer is heated and melted in the barrel, due to the simultaneous effect of temperature, pressure and viscous friction heating, it starts from solid granulates and proceeding in the chamber its viscosity drops tending to a fluid state. In the injection unit the material state is controlled and kept to a relatively low viscosity with the

temperature imposed by the heating elements, the process is not easy to be modeled due to gradients of temperature, non-Newtonian properties of the polymers, viscous effects and different properties of the material throughout the barrel. Some empirical model has been developed to link the process parameters to the characteristics of the material at the tip of the nozzle, where attention has to be focused.

In the molding unit instead simultaneous flow and cooling of the polymer happens during filling, packing and discharge [10]. The general behavior of pressure and temperature during injection cycle can be plotted as in Figure 13 since both pressure and temperature depend on time.

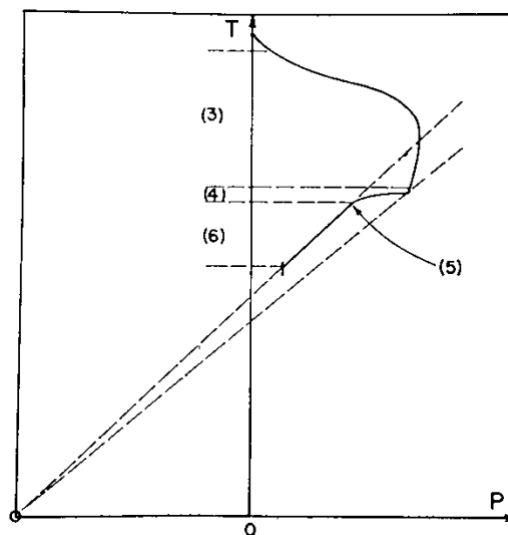


Figure 13: Injection molding pressure-temperature behavior [10]

During filling, the cooling effect is quite low due to the impulsive nature of this phase, even if some degree of cooling happens in this phase too as the material exits the nozzle and gets in touch with the mold walls. An analytical model of this phase is really complex to fit due to non-Newtonian flow properties which depend on pressure gradients and temperature gradients in the process, complicated even more by the geometry of the mold [10]. The flow of the material follows circular lines due to friction with

the mold walls and no constrains in the center, with increasing radius as the material proceeds in the mold, called fountain flow (Figure 14).

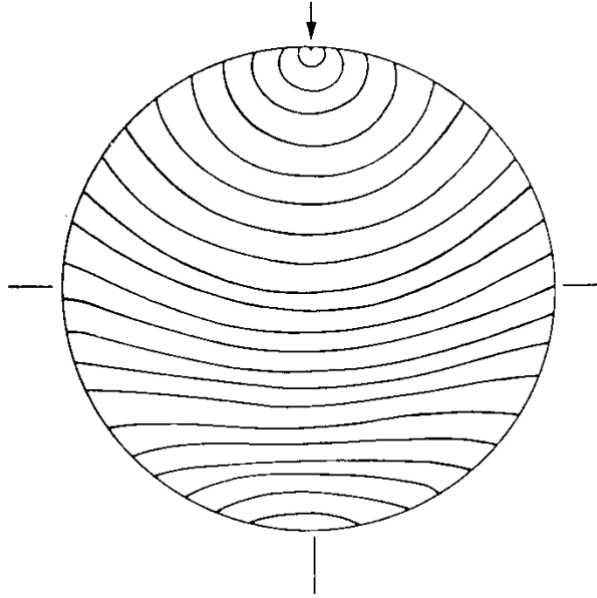


Figure 14: Fountain flow filling [10]

When the mold is full of material the pressure inside it is still quite low and increases as packing proceeds. During packing the cooling effects are more remarkable and some shrinkage occurs, to compensate for it the injection unit keep a predetermined level of pressure on the material so that the latter continues to flow in the mold. During this phase the temperature of the material decreases and might result in weld lines if the temperature of the material gets too low when two or more flows of material join in complex geometry molds. The flow of hot polymer is accompanied by a partial uncoiling of the chainlike molecules and orientation in the direction of the flow, this phenomenon is evident in the first thin layer which solidifies during filling, resulting in anisotropy and possible residual strains, which give a larger amount of shrinkage of this layer. In some cases this frozen orientation might occur also in the material which solidifies during packing for strong gradients, when the mold temperature is really low. In the

packing phase two opposite phenomenon occur, pressure is increased on the one hand by polymer being pressed from the ram or screw, up until the pressure exerted by the injection unit, on the other hand the pressure tends to decrease due to the cooling and solidification of plastic, so the pressure inside the cavity will rapidly rise until a maximum and then slowly decrease due to the cooling of the polymer [10].

It has to be considered that not all the pressure generated by the motor or hydraulic unit will be delivered to the polymer in the mold due to pressure losses. One first loss happens as the mechanical unit presses on the granular zone, since friction between pellets and with barrel walls occurs, this lowers the pressure at the nozzle of the injection unit. In addition, pressure losses occur also due to viscous friction heating of the material and in the travel of the polymer through the barrel, runners, gate and channels of the mold. Even this aspect is complex to be handled analytically but can be addressed with FEM models.

The discharge phase is quite rapid and happens as soon as the pressure on the mold is reduced due to the return of the ram to its initial position, some backflow might occur until the reversed pressure across the gate reduces and the temperature becomes cool enough so that the polymer in the gate solidifies and seal the mold. After this phase the cooling with frozen gate takes place, which is ruled by Fourier's law of conduction due to the heat extracted from the walls of the mold. Once the piece is cool enough the mold is opened and the piece extracted.

2.2.4 The mold: materials and Rapid Tooling

The mold has the primary function of containing the injected material under pressure, remove heat from its walls to let the piece cool and give shape to the object. It is usually composed by a fixed part, a moving side, extractor pins to remove the piece, channels, runners and gate to deliver the material

to the part and eventually channels for water cooling of the mold, for a faster cooling cycle.

The mold is usually made of hardened steel, tool steel, aluminum or other hard metals, chosen according to some criteria such as:

- Ease of machining;
- High yield point, hardness and elastic modulus;
- High thermal, corrosion and wear resistance;
- Low coefficient of thermal expansion;
- High thermal diffusivity to extract heat as fast as possible.

The mold is usually produced with CNC machining, even if for finer details also EDM can be used, then is usually subjected to thermal treatments and in case to superficial treatments to improve performances during repeated cycles.

The surface roughness of the mold directly affects the one of the piece to be produced, so it is defined depending on the desired finish and tolerances of the latter.

The mold has to be designed with small holes (about 0,3 mm) to let the air come out of it in order to avoid burn marks due to overheating of compressed air in the mold [11].

The material of the mold has to be chosen depending on the number of parts to be produced, steel being the material which lasts longer. In case of small batches also resin and high strength polymers can be used to produce the molds, this case it is regarded in the field of Rapid Tooling, in which the cost and time to produce the mold are reduced, but so is the duration and resistance of the mold itself, due to lower strength of the material used.

Rapid tooling is divided in direct and indirect RT. In direct rapid tooling the tool is directly produced by CNC machining on resins, cheaper and faster than on metals, or by additive manufacturing with thermoplastics, metals or ceramics. The strength of these molds is usually lower than their traditional manufactured hard metal equivalent due to higher porosity and

material properties. They usually withstand lower number of cycles but at low injection temperature and pressure the resistance in terms of production capacity is pretty similar. In indirect rapid tooling instead the additive manufacturing technique is used to create a model for the mold which is then produced with silicon, epoxy resin, ceramics or low melting point metals. In the last years due to the advancement of AM, direct rapid tooling is often preferred since the lead time is faster because there is one productive step less.

For small batches RT is gaining popularity in industry due to the possibility of making small modification of the design at low cost and to the faster lead time from project to mold. Also, the cost of rapid tooling is significantly lower than the one for tools made of tool steel or hardened steel. Nevertheless some drawbacks are present due to the process characteristics, such as lower resistance due to porosity which can result in flash, anisotropy, worse roughness due to the layer-by-layer technique and lower resistance at higher temperatures and pressure due to the materials mechanical properties.

One of the polymers preferred for RT is PEI, thanks to its high compressive resistance and high temperature resistance. It has a high glass transition temperature which permits repeated injection molding cycles without damages to the mold. In Figure 15 a PEI mold made with AM is shown.

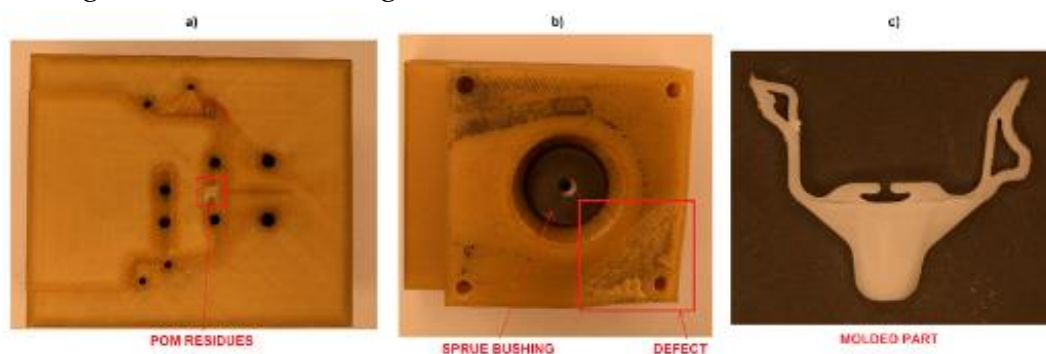


Figure 15: Rapid Tool for Injection Molding made with ULTEM

Molds in ULTEM material can be produced with additive manufacturing, which gives great freedom in terms of geometry of the object to be molded and also in the possibility of conformal cooling, with cooling channels inside the mold placed in critical positions to maximize the heat extraction.

2.3 Extrusion

The extrusion process is a manufacturing technology in which the material is shaped by forcing it out from a die with an opening. It can be performed on metal billets, preheated or in cold form, or with plastics, in which the plastic is heated inside the machine, to reduce viscosity and due to the brittle nature of polymers at ambient temperature.

2.3.1 Metal extrusion

In metal extrusion the billet is usually preheated to reduce the force needed for extrusion, not inside the machine but before inserting the material in the latter. Hot extrusion guarantees low surface quality due to scales on extrudate and lower strength of components since strain hardening cannot occur. Cold extrusion involves the production of elongated grains in the direction of extrusion and strain hardening of the material. The material undergoes plastic deformation, mainly driven by compressive and shear stresses, and acquires the shape of the die, by going out from the hole in it. Mainly two types of extrusion are used in the manufacturing industry: direct extrusion, in which the die is fixed in space and the force is provided with a ram, and indirect extrusion, in which the dies itself moves inside the channel to compress the material and force it out of the opening (Figure 16) [12]. In indirect extrusion the material moves in opposite direction for respect to the die movement and the force needed is lower than in direct one, due to absence of friction between the billet and the container, but the support of the extrudate is more difficult and the machines are usually more complicated.

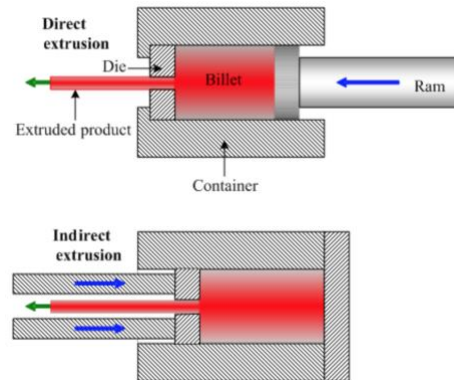


Figure 16: Direct and indirect metal extrusion [12]

X. Duan et al. [13] studied the microstructure evolution of hot extruded aluminum in order to predict the properties of extruded structural parts with a FEM model, concluding that it is strongly related to the ram speed profile: under constant speed profile the grain size and temperature increase by increasing ram displacement, not giving a uniform distribution of the microstructure, while with an isothermal extrusion process a uniform distribution of the microstructure can be achieved.

Metal extrusion is usually performed on aluminum or copper due to lower force and temperature needed for respect to steel but can also be performed on the latter with adequate machines. It is used to produce structural frame such as T-slot aluminum extrusions (Figure 17), often employed to build desktop FDM machine's frames, and also aluminum cans, heatsinks, pipes and tubes [14].



Figure 17: Metal extrusion products [14]

2.3.2 Plastic extrusion

Plastic extrusion on the other hand includes in the machine the heating elements and control of temperature, so the plastic is fed to the machine in cold solid form and it is softened inside the extrusion machine to reduce its viscosity and facilitate the process, cold plastic extrusion is not possible due to the poor ductility of the material at room temperature. Prior to extrusion the material has to be dried to reduce the moisture percentage inside the plastic, humidity worsens the aspect and properties of the extruded plastics and has to be avoided. The machine (Figure 18) is usually composed by a hopper, where raw material is placed in form of flakes, a heated barrel with one or more screw, for continuous extrusion, or a piston, for intermittent one, a feedpipe and a die [15].

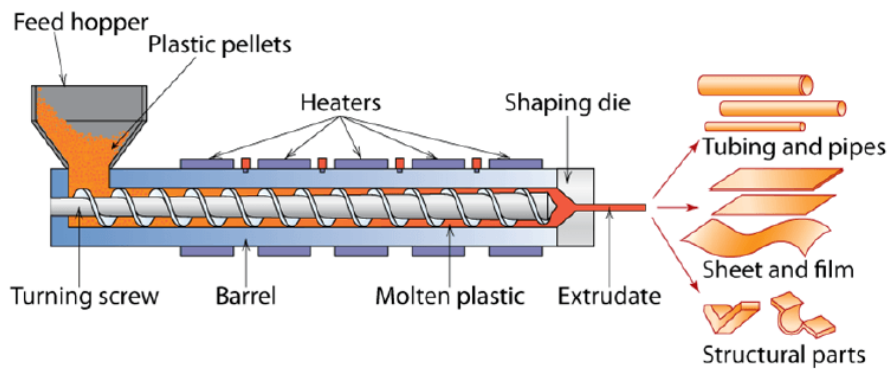


Figure 18: Plastic extrusion machine [15]

The heated barrel usually has different heat zones (three or more) to have a temperature gradient and allow a gradual melting, with a temperature close to the ambient one near the hopper and an increasing temperature as the plastic proceeds in the barrel. More complex extruders can also have a vent port (Figure 19) to remove air or to add fillers and additives. In the design of this type of extruders caution has to be used in having no positive pressure in correspondence of the vent port to avoid vent flow, a condition in which not only volatiles are going out of the vent port but also some polymer, as pointed out in [16].

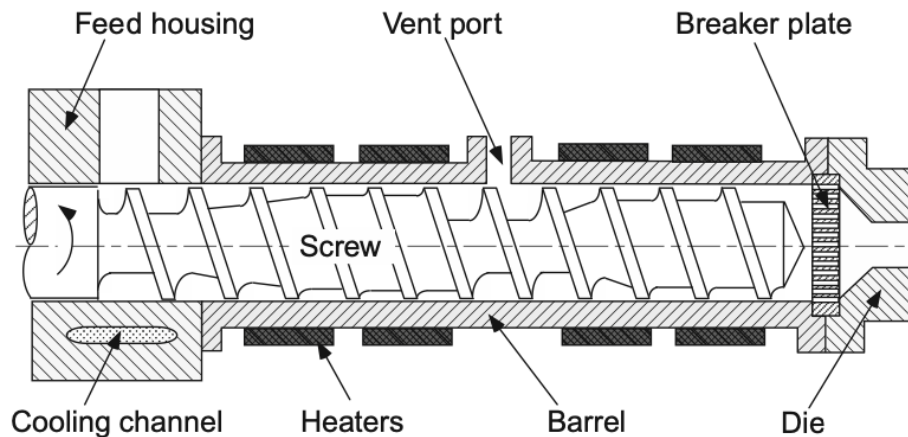


Figure 19: Vent port and screw schematic [16]

As the material is heated it is also pushed and compressed towards the die, the frictional heating on the material also contributes on reducing the viscosity of the material in addition to heat from the resistances on the barrel. The material exits through the die and is then cooled in water or with cooling rolls; as soon as the material exits the die it has also to be supported to prevent unwanted deformations of the desired profile. Plastic extrusion is used to produce plastic piping in PVC, window profiles, blinds but also to produce filament for pinion and rack FDM additive manufacturing machines.

Screw extruders are the most used in industry and manufacturing and are divided in plasticating extruders, in which the material is fed in flakes and about halfway in the length of the screw it becomes a highly viscous fluid, and melt extruders, which work as pumps with fluid all the way along the screw. Quite accurate analytical models have been developed to deal with the melt fraction of the material considering viscous, thermal and non-Newtonian properties of the polymer, resulting in differential equations for flow, drag and power [17]. For a complete description of plasticating extruders studies on the solids transport and energy relations at the feed end must be implemented.

These differential equations must be integrated to relate the overall output, pressure, temperature and design of the machine with specific boundary conditions obtaining different way of using the extruders, such as isothermal or adiabatic conditions. In isothermal condition the temperature is kept constant by extracting all the heat generated by viscous friction heating, in reality a condition close to isothermal is obtainable only at low screw speeds. With a constant screw channel and isothermal operation the pressure gradient must be constant, resulting in straight lines with negative slope as shown in Figure 20.

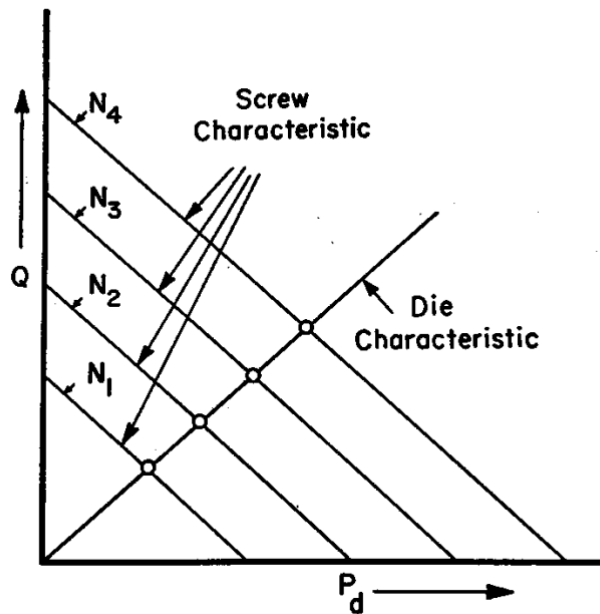


Figure 20: Screw and die characteristic curves [17]

The flow rate Q is decreasing for increasing variation of pressure P across the extruder and parallel increasing lines can be obtained by increasing the speed of the screw. The operating point can be obtained by intersecting the screw line with the die characteristic equation. Since the temperature is constant also the viscosity will be constant throughout the barrel, considering Newtonian melts.

In adiabatic conditions the extruder is considered to be perfectly isolated and the pressure and thermal energy on the material is obtained only from the action of the screw on the polymer. In this condition the temperature of the extrudate increases along the length of the screw, accompanied by a decrease in viscosity. Also in adiabatic condition it is possible to obtain a relation for Q , P and the screw rotational speed N , but in this case a law relating the viscosity with temperature has to be defined in order to integrate flow, drag and power equations along the screw length.

Considering non-Newtonian viscous properties of the melt the screw characteristic equation in isothermal condition is no more a straight line and the dependence of viscosity from the shear rate as to be taken into account with the power law. It can be shown, mainly qualitatively, that for increasing resistance and pressure at the die, the driving force for backflow increases, reducing the viscosity of the fluid, thus the curves will become steeper for increasing pressures, while the free discharge flow, with no restrictions after the screw, is pretty much unchanged for respect to Newtonian melts, as shown in Figure 21 with Newtonian melt dashed lines and non-Newtonian melts continuous lines.

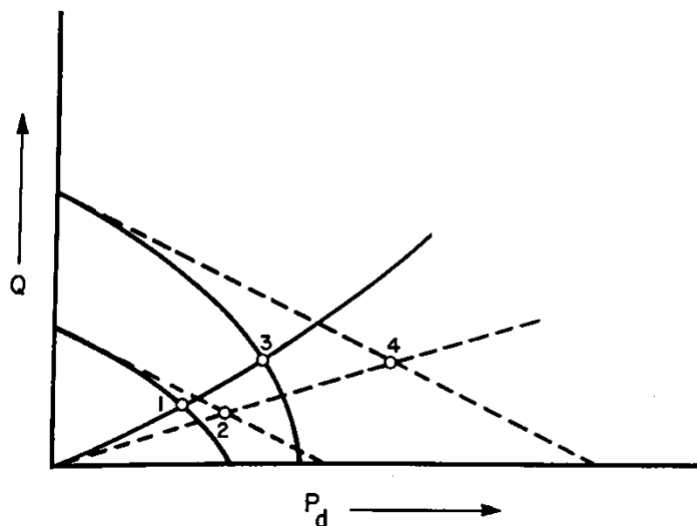


Figure 21: Screw and die characteristic curve for non-Newtonian fluids [17]

It can also be noticed that increasing the rotational speed the curves are no more parallel due to higher back flows for higher speeds at same pressure, which makes the higher speed curves steepen more rapidly.

Plasticating extruders have to deal with solid state flakes at the beginning of the screw and viscous melts at the end of the latter, they are usually divided in five sections: feed zone, melting and transition zone, metering or pumping zone, torpedo zone and filtering zone. In Figure 22 the behavior of pressure in different zones is represented.

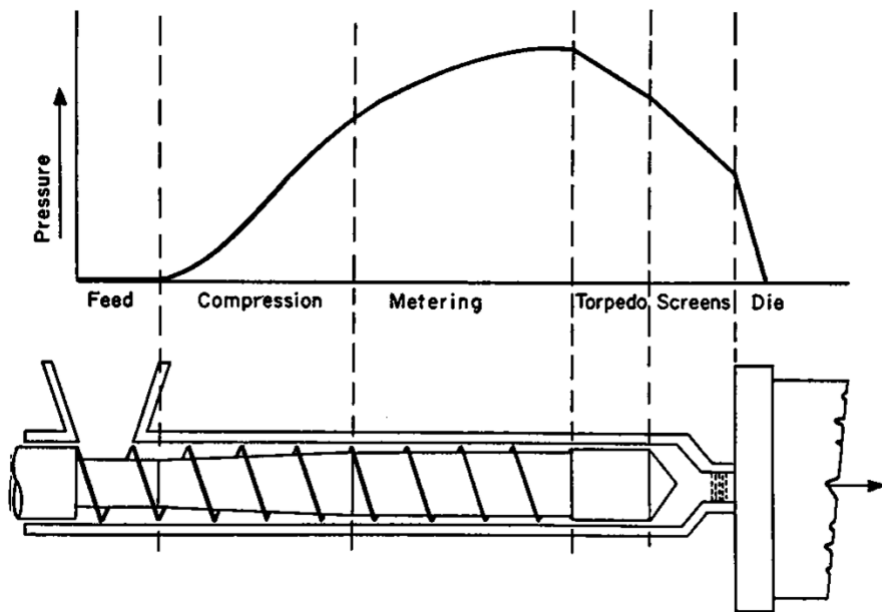


Figure 22: Pressure behavior in different stages [17]

The process can be governed by thermal energy providing heat or by mechanical energy by the rotation of the screw depending on the material. In nylon processing for example the energy is mainly thermally provided, because it is hard to shear the individual flakes, since they are hard, tough and rigid at ambient temperature. On the other hand for soft materials, like polyethylene, which can be deformed quite easily at ambient temperature, the heat is mainly generated internally through mechanical working, similarly to an adiabatic condition. The screw design (Figure 23) can be

different depending on the main type of energy used to reduce viscosity, giving higher efficiency of the process for optimized screws [17].

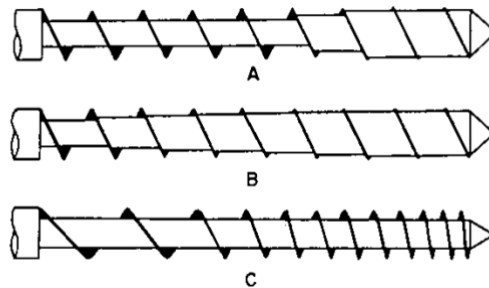


Figure 23: Typical screw design

Notes: A. Nylon type, B. Polyethylene type, C. rubber type [17]

2.3.3 Elasticity in plastic extrusion

The previous considerations on extrusion did not consider the elastic behavior of viscous polymer to simplify the study, while in real extrusion some elastic effects are present, which mainly result in pressure losses through the die, in the “post extrusion swell” effect and in some extrudate defects caused by the elastic nature of the fluid [18].

Theoretical and analytical approach to these problems is very complex and these effects differ on many aspects from the trials which can be performed in laboratory due to higher shear rate in extrusion process and not constant shear history for long time in dies, as would be in instruments such as the Weissenberg rheogoniometer. Therefore only a qualitative study on these aspects will be presented, highlighting the effects they give on the extrudate and the causes of these results.

The long chain molecules are distorted when subjected to shear forces during extrusion. These stresses tend to stretch the molecules inside the extruder and die but when the stresses cease the molecules tend to coil up

again at the exit of the die. This un-coiling and re-coiling of molecules give the so-called elastic effects [19].

Die swell effect is such that the extrudate at the exit of the die increases in size and expands due to elastic effects, other than for simple extrusion this phenomenon is important also in FDM Additive Manufacturing since it happens at the exit of the nozzle. The ratio of the extrudate diameter to the die diameter is known as die swell ratio, and its value usually is between 1,02 and 1,2 depending on processing conditions. Die swell is mainly caused by normal stress for respect to the flow which generate strain when the latter is no more constricted. This effect is governed by temperature, decreasing for an increasing temperature at constant extrusion rate, by the shear rate, increasing up to a maximum and then decreasing for increasing shear rate, but is also influenced by die geometry, polymer composition and melt index of the polymer. In Figure 24 the typical behavior of die swell is presented.

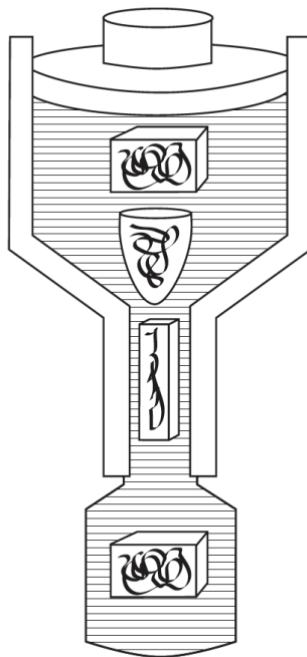


Figure 24: Die swell effect [19]

The pressure losses through the die are affected by the beforementioned parameters and are increased for respect to theoretical ones and the ones obtained in laboratory due to elastic effects in short dies where the flow is accelerates in a short time and length typical of material extrusion. Defects due to elastic effects can be generated at the entering of the die, in the die land region or at the exit region which might result in melt fracture, sharksink or spiral phenomenon. Melt fracture usually occurs when extrusion is carried out at high rates and consist in a distortion of the extrudate. It happens when the shear rate exceeds the critical shear rate at a given temperature. In Figure 25 the aspect of melt fracture is shown.

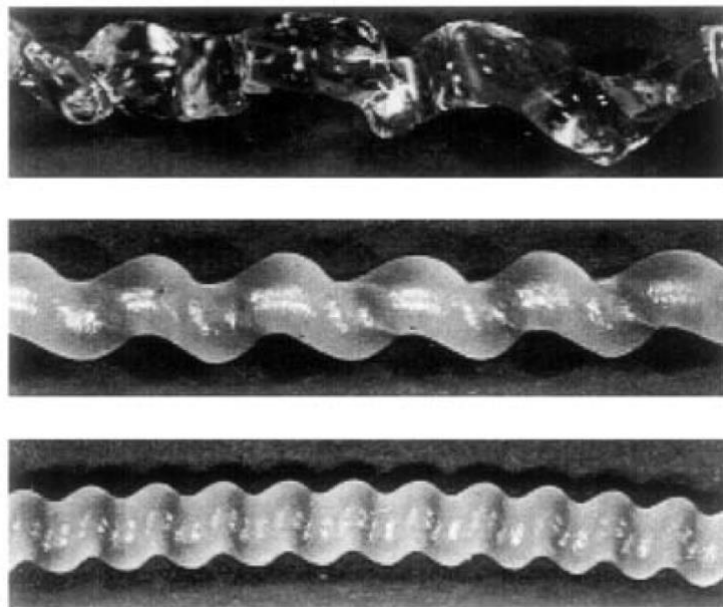


Figure 25: Melt fracture [19]

2.4 Viscosity and polymer rheology

Polymeric materials are made by many chains obtained from monomers by polymerization reactions, they can assume states of complete disorder, called amorphous, or partially ordered state, called semi-crystalline state,

in which some crystalline domains are present in the amorphous general structure (Figure 26).

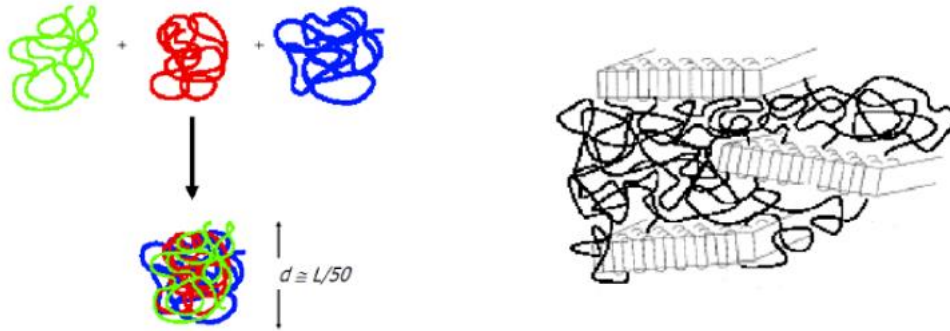


Figure 26: Amorphous and semi-crystalline materials

In amorphous state the polymers are in random coils, in which the covalent bonds among them allow molecular rotations. The total volume of a polymer can be divided in free volume, the one available for chain mobility, and occupied volume, the one of the actual molecules. For an amorphous polymer the glass transition temperature T_g is an important characteristic since for temperatures lower than T_g the material behaves like a solid and the free volume is constant, while for temperatures higher than T_g the material behaves similarly to a liquid, since the free volume increases linearly with temperature and the energy barrier for covalent bonds is lower, allowing continuous rotation. For temperatures higher than T_g the chain mobility increases dramatically [20] (Figure 27).

The glass transition temperature is not a constant value but depends on the thermal history of the polymer, for higher temperature increase rates T_g moves to higher values. Below T_g the thermodynamic state is not in equilibrium but it is more static, while above T_g rapid molecular rearrangements are possible approaching a thermodynamic equilibrium state.

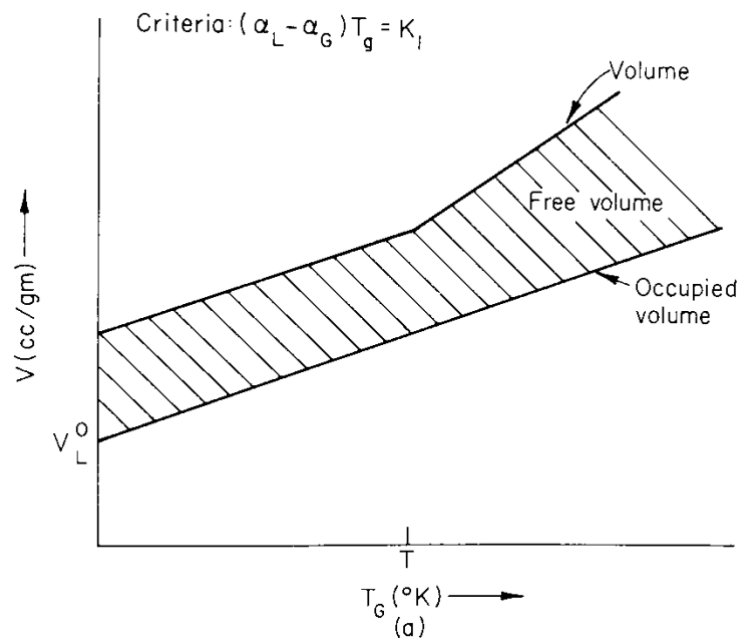


Figure 27: Free volume behavior in temperature [20]

Viscosity is a property which represents internal friction and thus energy dissipation in a material, it is due to the presence of interaction forces between molecules which are entangled. To understand the behavior of a viscous material Newton's law for viscous fluid is presented:

$$\tau_{xy} = -\mu \frac{dv_x}{dy}$$

$$\tau = \frac{F_{\text{tangential}}}{A}$$

$$\gamma = \frac{dx}{dy}$$

$$\dot{\gamma} = \frac{dv_x}{dy}$$

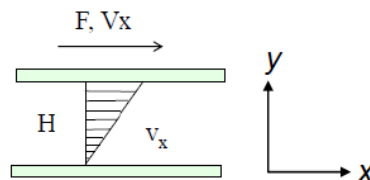


Figure 28: Viscous flow schematic

Being τ_{xy} the tangential shear stress, $F_{tangential}$ the tangential force acting on the area A , γ the shear strain and $\dot{\gamma}$ the shear strain rate.

So

$$\tau = -\mu\dot{\gamma}$$

In general

$$\tau = f(\dot{\gamma})$$

For a Newtonian fluid $\tau \propto \dot{\gamma}$ and $\mu = \eta = \text{constant}$, being η the apparent viscosity of the fluid.

All the work of deformation is converted in heat and can be considered energy dissipated, which will result in a rise of temperature of the material and reduction of its viscosity:

$$\frac{dW}{dV} = \frac{\tau^2}{\mu} = \mu\dot{\gamma}^2$$

In general the apparent viscosity depends on the shear strain rate, and its unit is $[Pa \cdot s]$, while the unit of $\dot{\gamma}$ is $[s^{-1}]$. For a polymeric viscous material over T_g the viscosity η is in the order of $10^2 - 10^4 Pa \cdot s$.

For a non-Newtonian fluid $\tau = \eta(\dot{\gamma})\dot{\gamma}$ and so the apparent viscosity can be considered as $\eta(\dot{\gamma}) = \frac{\tau}{\dot{\gamma}}$.

Different fluid behavior can be noticed in the relation of shear stress and shear strain rate, such as Newtonian, Dilatant, for which viscosity increases with shear rate, or Pseudoplastic, for which viscosity decrease with shear rate, as shown in Figure 29 [21].

Thermoplastics and fused polymers usually show a pseudoplastic behavior. For small $\dot{\gamma}$ all the three behaviors show a linear relation between $\dot{\gamma}$ and τ , and can therefore be regarded as Newtonian.

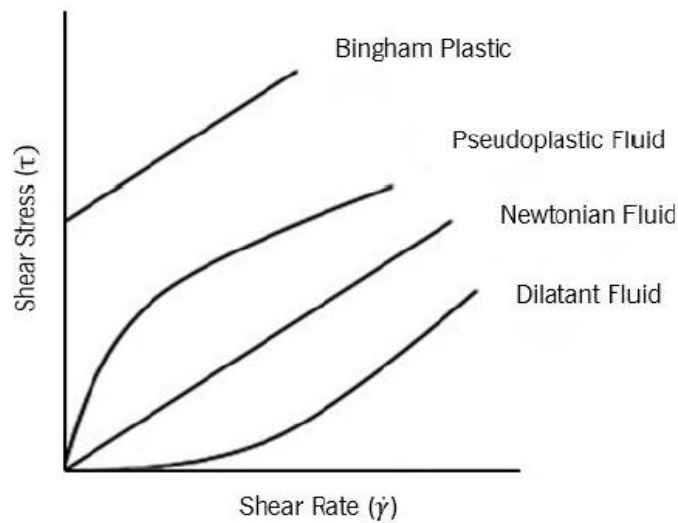


Figure 29: Different viscosity behaviors [21]

For a pseudoplastic material the relation of shear stress and viscosity with respect to shear strain rate is represented in Figure 30.

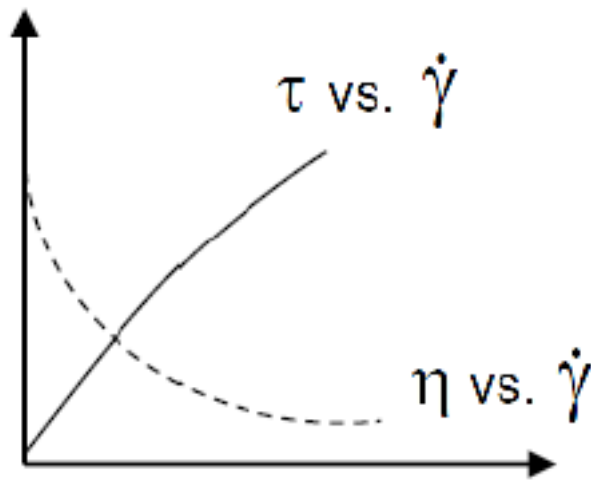


Figure 30: Pseudoplastic behavior for shear stress and viscosity

In log-log plot three different zones can be identified, upper Newtonian at low shear rates, with constant “zero-shear strain rate viscosity”, shear thinning region, with a linear decreasing trend, and lower Newtonian, with constant “infinite-shear strain rate viscosity” (Figure 31).

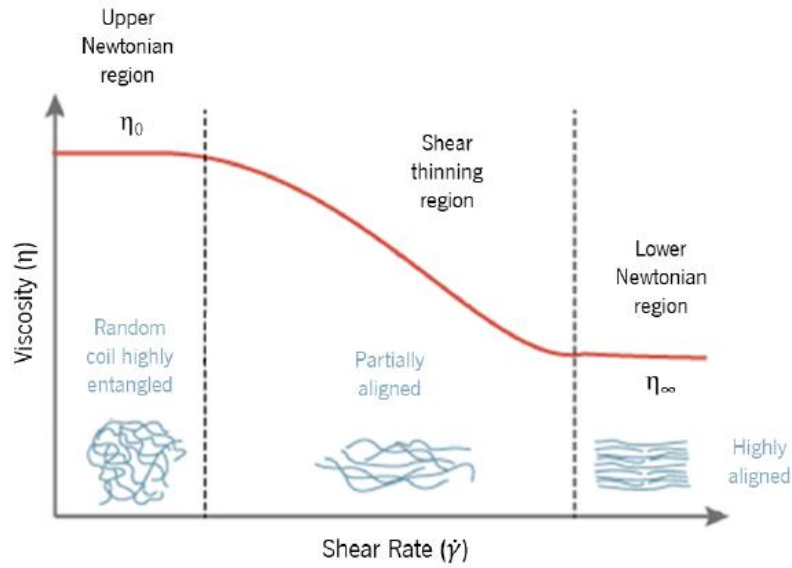


Figure 31: Viscosity regions for pseudoplastic materials [21]

In Figure 31 it is also possible to notice that the behavior of viscosity is due to higher breakage of entanglements at higher shear strain rates giving a decrease of physical interaction between chains and so of the viscosity itself. During extrusion and injection molding processes the shear strain rates are such to be in the shear thinning region, having thus a linear relation between the logarithms of viscosity and strain rate.

One simple model which can fit the Pseudoplastic and Dilatant behaviors in the shear thinning or thickening region is the Power Law model which is written as:

$$\tau = m\dot{\gamma}^n$$

$$\eta(\dot{\gamma}) = \frac{\tau}{\dot{\gamma}} = \frac{m\dot{\gamma}^n}{\dot{\gamma}} = m\dot{\gamma}^{n-1}$$

With m and n constant depending on the material under analysis. In Figure 32 it can be noticed the power law representation with a dashed line versus the real behavior (red) for a pseudoplastic material.

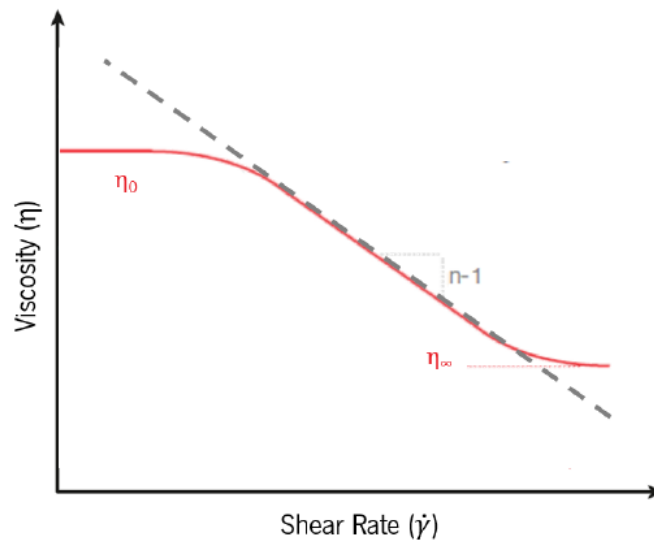


Figure 32: Power law model [21]

Considering the flow of a viscous fluid in a circular duct, for low Reynolds numbers, with a laminar flow the shear strain rate at the wall can be approximated as $\dot{\gamma}_{wall} = \frac{4Q}{\pi R^3}$, being Q the flow rate and R the radius of the duct. This approximation can be useful when dealing with extruders with pistons since the chamber, which is usually circular, does not have the screw inside but only the material. In Figure 33 the profiles of velocity and shear strain rate for the flow in a duct considering a Newtonian fluid are represented.

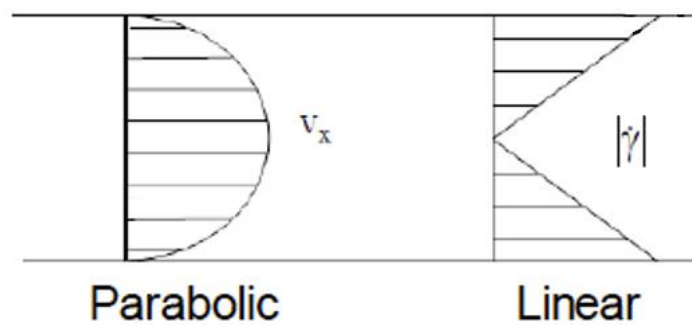


Figure 33: Flow in a duct for Newtonian fluids

Different models other than the power law can be used to represent the constitutive relation between the viscosity and the shear strain rate, including effect of temperature, pressure and other quantities.

Among them the Carreau-Winter model can also cover the Newtonian plateau other than the shear thinning region, it is formulated as:

$$\eta = \frac{\eta_0}{(1 + \lambda\dot{\gamma})^m}$$

With η_0 zero-shear viscosity, λ transition time and m viscosity exponent.

The WLF model includes the effect of temperature, in particular considering how far the polymer is from T_g . it can be written in the form:

$$\ln \frac{\eta}{\eta_g} = - \frac{c_1(T - T_g)}{c_2 + (T - T_g)}$$

With η_g viscosity at T_g , T temperature of the polymer and c_1 and c_2 constants depending on the material.

One of the most complete models is the Cross-WLF model, which includes effects of temperature and might also include the effect of pressure. This model can fit the whole shear stress-shear strain rate curve:

$$\eta = \frac{\eta_0}{1 + \left(\frac{\eta_0\dot{\gamma}}{\tau^*}\right)^{1-n}}$$

$$\eta_0 = D_1 \cdot e^{-\frac{c_1(T-T_g)}{c_2+(T-T_g)}}$$

With η_0 zero shear viscosity depending on temperature T , $\dot{\gamma}$ the shear strain rate, τ^* the critical stress level for the transition in shear thinning region, n the power law index in high shear strain rate regime, T_g the glass transition temperature and D_1 , c_1 and c_2 constants obtained by fitting experimental data. One representation of the model (red dashed line) versus real viscosity curve (blue line) is presented in Figure 34.

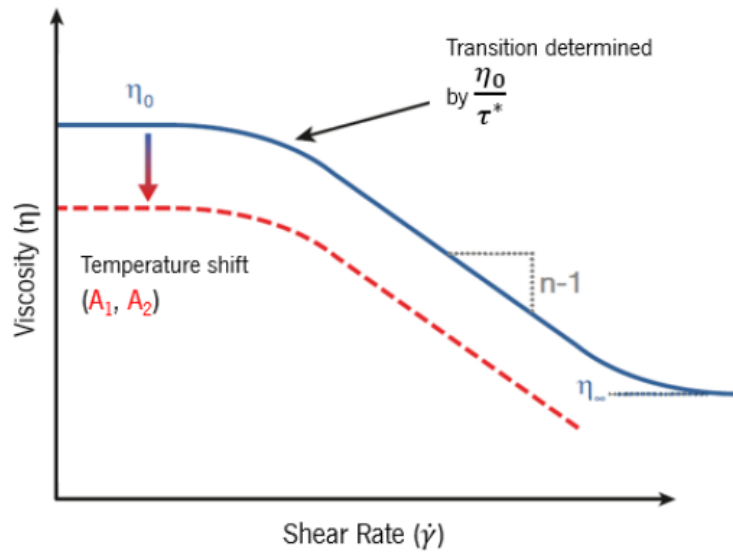


Figure 34: Cross-WLF model [21]

Different instruments can be used to measure viscosity, mainly depending on the strain shear rate level one might be better than the other. Among them the capillary rheometer is one of the most diffused, which consist in an instrument to measure the difference of pressure due to the passage in a capillary at a given temperature and flow rate, in commercial instruments two capillary rheometers are employed one with a shorter or without the capillary to estimate the real variation of pressure at the entrance of the capillary as shown in Figure 35.

With this instrument the viscosity can be estimated by estimating the difference in pressure drop and building the Bagley diagram.

For very low shear strain rates the Weissenberg rheogoniometer can be employed, mainly used to characterize the Newtonian plateau and the transition zone, depending on the material.

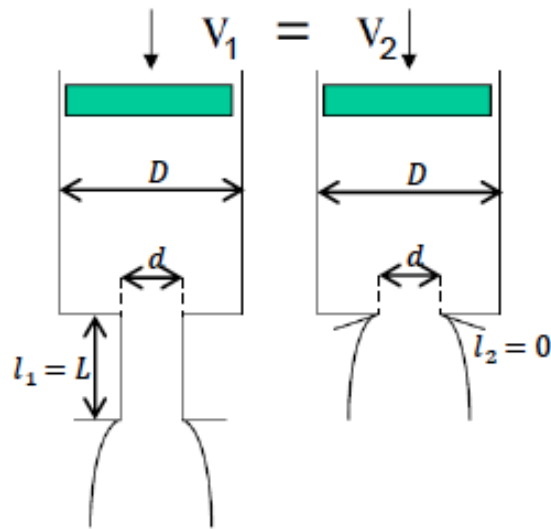


Figure 35: Capillary rheometer schematic

2.5 Thermal problems in EAM

Additive manufacturing can be considered as a thermal technology since the energy for bonding and diffusion is usually provided as thermal energy. Due to the nature of the process many characteristic problems occur in additive manufacturing, mainly related to temperature gradient in the piece and strong differences of temperature with the ambient surrounding the object while it is being built.

2.5.1 Thermal parameters of interest in additive manufacturing

To model or at least to understand qualitatively the behavior of temperature gradients and thermal behavior of an additive manufactured object there are some parameters which are more important than others. Among them it is possible to highlight the conductivity and diffusivity of the material, the convection coefficient, the coefficient of thermal expansion and the relation of viscosity with temperature.

The thermal conductivity is measured in $[\frac{W}{mK}]$ and can be formulated as

$$k = -\frac{q_x''}{\frac{\partial T}{\partial x}}$$

With k being the thermal conductivity, q_x'' the heat flux for unit of area in direction x and $\frac{\partial T}{\partial x}$ the partial derivative of the temperature for respect to direction x .

It represents how much heat flux will flow for an infinitesimal difference of temperature. In Figure 36 the conductivities of different materials are presented.

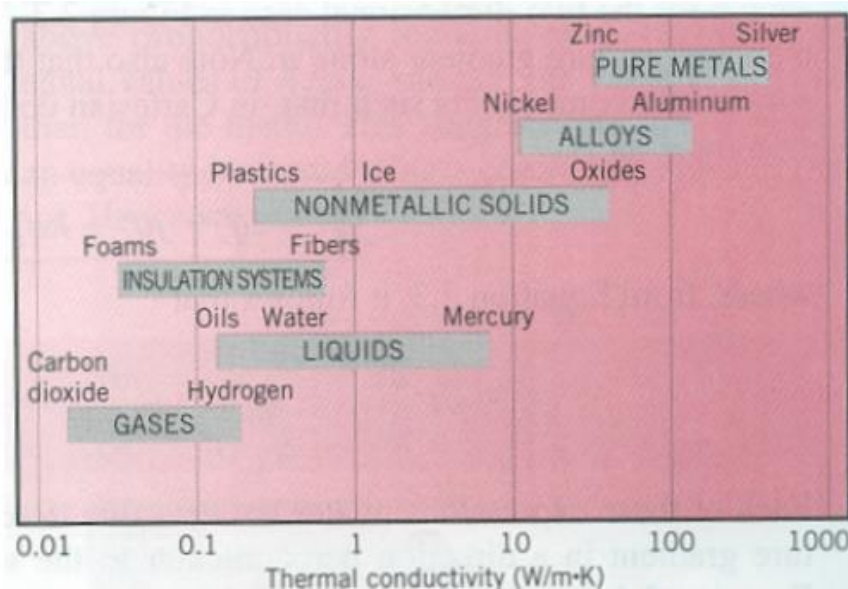


Figure 36: Conductivity of different materials

The thermal conductivity is not a constant value but it also depends on the temperature level of the material as highlighted in Figure 37, different materials will have a different behavior varying the temperature.

For an anisotropic material thermal conductivity might vary also depending on the direction of heat flux considered, at a constant temperature.

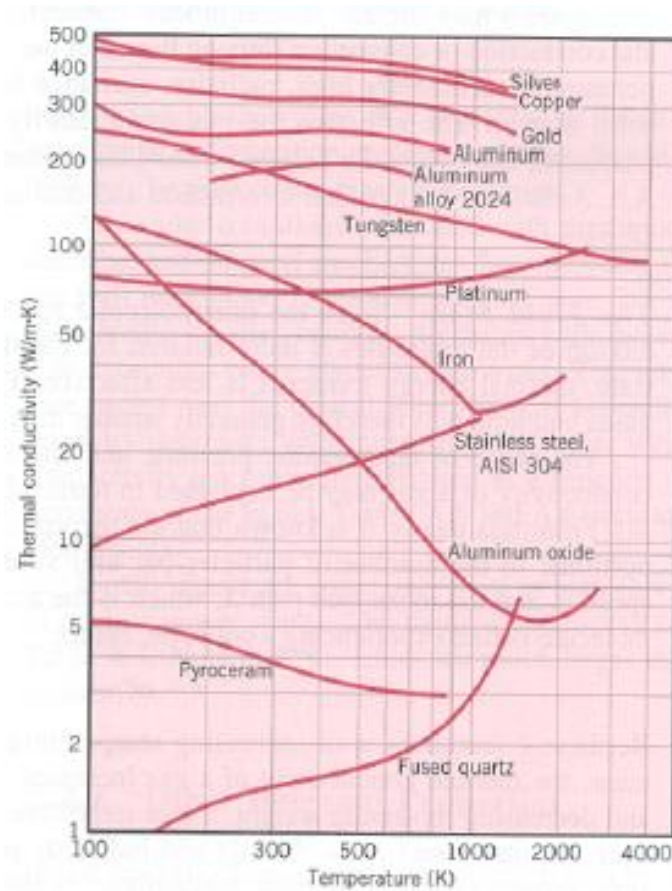


Figure 37: Conductivity-temperature behavior

For an additive manufactured object anisotropic properties in conductivity are developed also due to the building method, Elkholy et al. [22] studied the relation between raster width, raster angle and layer height on the conductivity anisotropy of the built specimen, concluding that raster width is the most influent in determining anisotropy of the conductivity, due to higher porosity for higher raster width. Also the infill percentage results in a drop of conductivity in z reducing the fill percentage due to more voids inside the piece.

The thermal diffusivity takes into account conductivity, specific heat and density of the material for a more compact definition of the Fourier's law for heat transfer and is formulated as:

$$\alpha = \frac{k}{\rho c_p}$$

It is measured in $[\frac{m^2}{s}]$, with α thermal diffusivity, k conductivity, ρ density of the material and c_p specific heat. It relates the variation of temperature in time with the second derivative of temperature in space.

In Table 1 values of diffusivity for some common materials are presented.

Material	Thermal diffusivity
	m^2/s
Aluminium	8.418×10^{-5}
Carbon steel (1%)	1.172×10^{-5}
Copper	1.1234×10^{-4}
Pure silver (99.9%)	1.6563×10^{-4}
Aluminium oxide (polycrystalline)	1.20×10^{-5}
Common brick	5.2×10^{-7}
Pyrolytic graphite, parallel to layers	1.22×10^{-3}
Pyrolytic graphite, normal to layers	3.6×10^{-6}
Window glass	3.4×10^{-7}
Nylon	9×10^{-8}
Sandstone	1.12×10^{-6} to 1.19×10^{-6}
Wood (Yellow Pine)	8.2×10^{-8}
Air (1 atm, 300 K)	2.2160×10^{-5}
Water vapour (1 atm, 400 K)	2.338×10^{-5}
Engine oil (saturated liquid, 100 °C)	7.38×10^{-8}

Table 1: Diffusivity for different materials

Considering a constant conductivity, for an isotropic and solid material the Fourier's law can be expressed as:

$$\frac{\partial^2 T}{\partial x^2} + \frac{\partial^2 T}{\partial y^2} + \frac{\partial^2 T}{\partial z^2} = \frac{1}{\alpha} \frac{\partial T}{\partial t}$$

The convection coefficient is instead important to deal with heat flux when a fluid is involved in the heat transport, this transport might occur by natural convection, due to difference of density, or by forced convection,

when external events increase the flow rate of the fluid. It is used in the Newton's law of conduction which can be formulated as:

$$q'' = h(T_s - T_\infty)$$

With q'' being the heat flux per unit of area, h the convection coefficient and T_s and T_∞ the temperatures respectively of the surface and of the fluid. The Newton's law can be used as a boundary condition for the Fourier's law if one side of the solid is in contact with a fluid.

Other boundaries conditions can be constant temperature on the surface, constant heat flux on the surface or adiabatic surface, so no heat flux on the surface on which the boundary condition is acting.

The coefficient of thermal expansion (CTE) is instead used to relate variations in dimensions with variations in temperature. The linear CTE is used for variation in length only on one dimension and this variation can be simply modeled as:

$$\Delta L = L\alpha_l\Delta T$$

With ΔL variation of length, L initial length, α_l linear coefficient of thermal expansion and ΔT variation of temperature.

For volumetric expansion and contraction instead the volume coefficient of thermal expansion is used and the relation can be written as:

$$\Delta V = V\alpha_v\Delta T$$

With ΔV variation of volume, V initial volume, α_v volume coefficient of thermal expansion and ΔT variation of temperature. Usually for isotropic materials α_v can be considered as $3\alpha_l$, but it has to be pointed out that many materials follow an anisotropic expansion following some crystallographic preferential directions.

These relations are useful in additive manufacturing since the material is deposited at a given temperature and then cools down with the temperature gradients following Fourier's law with Newton's law at one and more boundary. During cooling the material contracts and some thermal stresses rise due to this shrinkage, the thermal shrinkage in first

approximation can be modeled using the volume coefficient of thermal expansion.

2.5.2 Material thermal history

In FDM additive manufacturing the production process is very different for respect to injection molding even if many objects can be produced by both technologies with similar characteristics.

In injection molding all the material which is injected in the mold will be subjected to the same thermal history with same timings, with the only difference being related to geometrical characteristics which influence heat extraction from the mold. A piece with thin and thick walls will experience a faster cooling in the thinner walls due to a greater area of contact with the mold which will result in faster heat extraction from the wall. In Figure 38 the temperature behavior in time is presented, it must be pointed out that this behavior is followed similarly by all the volume of material which makes the piece.

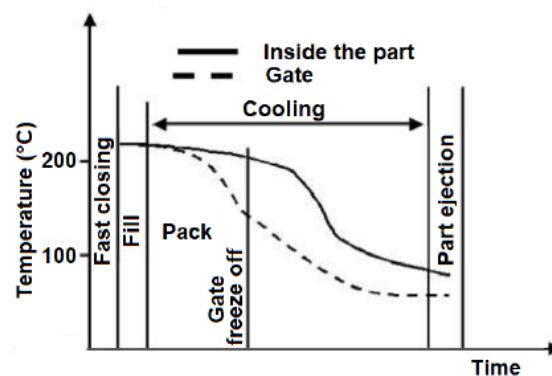


Figure 38: Temperature behavior in injection molding [8]

On the other hand, in FDM the timings of the thermal process will change for each infinitesimal material volume and many variables influence the thermal conditions of the extrudate. This is due to the process characteristics of building pieces layer by layer, in which each layer is undergoing a similar thermal history in the machine but once extruded the

cooling rate vary a lot depending on the layer position in the piece. The process cannot be considered isothermal and often fast solidification leads to limited chain diffusion between layers. B. D. Vogt et al. [23] studied with thermocouples both the temperature profile in the extruder head of a filament FDM machine and in the object which is being built, concluding that after extrusion the process is extremely non-isothermal. In Figure 39 the temperature profile measured with a thermocouple embedded in the filament as it passes through the heated nozzle at different speeds is presented.

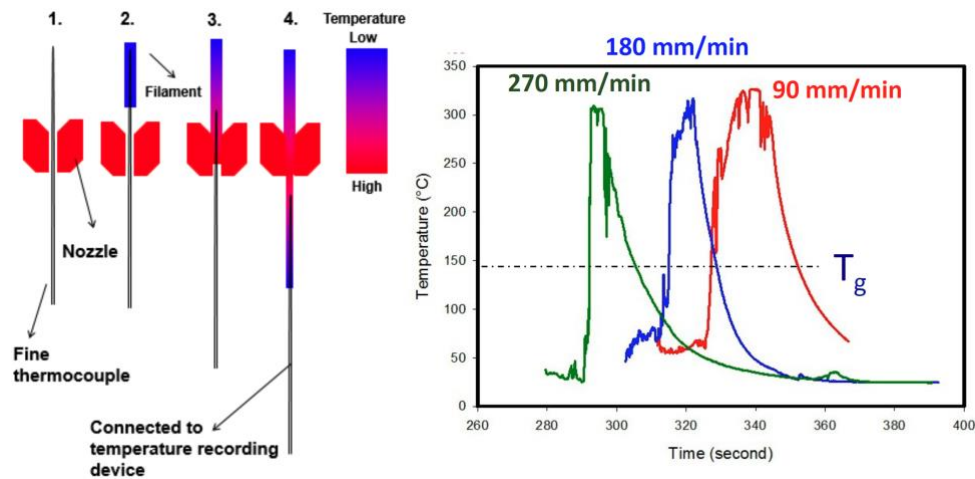


Figure 39: Temperature profile through FDM nozzle [23]

Considering a simple filament FDM machine with heated build surface and nozzle at two different temperatures, without heated chamber, it is possible to make some considerations. Inside the machine the filament is pushed toward the melt zone close to the nozzle. The length of the melt zone is variable depending on the heater installed, once it reaches this zone its viscosity drops due to increase in temperature meeting the straight walls of the nozzle. Once the material is over its glass transition temperature it undergoes deformation forced by the shape of the nozzle and exits from the hole in it, which usually is 0.4mm. Afterwards it undergoes the “die-swell effect” and slightly increases its section due to elastic recovery. Starting

from the first layer the material gets heated and melted inside the machine and once extruded will be in contact with the heated bed, so its temperature will reduce approaching that of the bed. While the first layer is cooling to the bed temperature another layer of material is deposited upon it which will heat back the first layer and eventually cool due to convection with ambient and conduction with the substrate. As the process goes on the first layer will be at a temperature close to the bed's one, while growing in height the layers will tend to get closer to ambient temperature. This process is affected in the other direction by the top layers which will still be at higher temperature, since the nozzle is at high temperature and the material just extruded will have a temperature close to it until it cools down always due to conduction and convection. So, in a tall piece the temperature gradient at each instant will be double, one negative one from the bed temperature to the ambient temperature and the other from ambient temperature to a temperature close to the nozzle one, as shown in Figure 40.

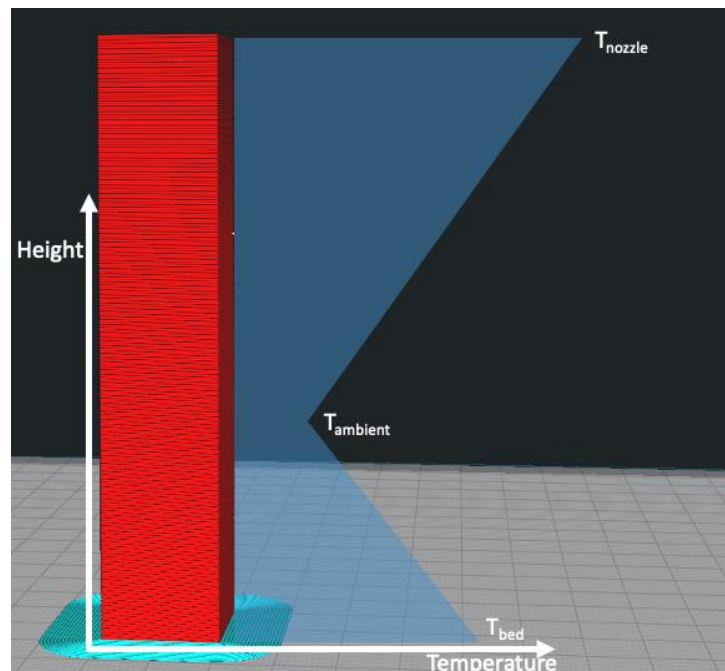


Figure 40: Temperature gradients during building

The steepness of both gradients will depend on the conductivity of the material and convection coefficient with the air surrounding the piece. It has to be noted that the bed actively heats the piece from the base while the top layers are just passive ones, once deposited the heat flux from the nozzle is minimal due to the low area of contact. In Figure 41 it is shown the results obtained by B. D. Vogt et al. [23] with a thermocouple embedded in the first layer at one specific point, it can be noticed that as the first layer is deposited the temperature rises getting close to the extrusion temperature (300°C), as time goes on the temperature approaches the one of the bed (180°C), then when each new layer is deposited upon it the temperature in the first layer increases to some extent, but the increase is less remarkable as the deposited layer is farther from the thermocouple.

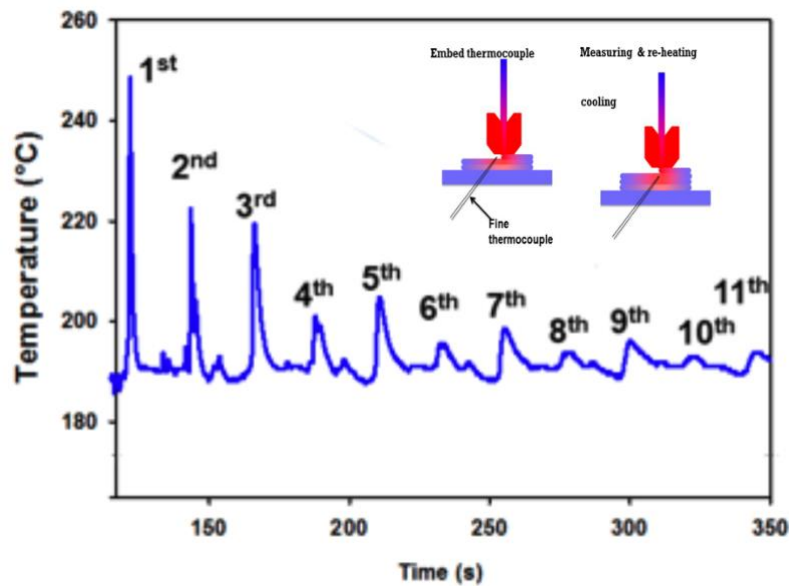


Figure 41: Temperature behavior of first layer while building the object [23]

In Figure 41 the layer temperature always cools down to the bed one since the thermocouple is almost in contact to the bed which tries to maintain a constant temperature, for layers distant from the bed the cooling effect will likely tend to the ambient temperature since the bed heat is decreased by convection losses as the height increases.

The power of the bed resistance plays an important role in how this gradient is shaped, since a more powerful bed can provide more heat to the piece giving thus a less steep gradient in the piece. It can be considered that the bed provides a boundary condition of fixed temperature constant in time to the Fourier's equation, while the top layer a condition of constant temperature varying in each infinitesimal time in position. The process is not simple to be modeled since each new layer increases the volume of material and moves the top boundary condition, never reaching a steady state while printing. To reduce the gradients it is possible to bring the ambient temperature close to the bed one, reducing thus the thermal stresses in the piece. Obviously, the bed itself provides some heat by convection to the air over it but often the power is not enough to give considerable heating of the air, especially as the height increases. The extrusion temperature is to be set carefully to achieve good bonding and diffusion between the substrate layer and the next one, the substrate layer has to be cool enough to sustain the next layer without deforming but hot enough to bond well with the next and hotter layer deposited above. Therefore the extrusion temperature has to be decided also considering the ambient temperature and the cooling rate of the piece, not just by being above the glass transition temperature. S. F. Costa et al. [24] studied how thermal condition affect heat transfer to define a numerical model and concluded that radiation is not influent between adjacent filaments and with air gaps and can also be neglected with ambient if the convection coefficient is sufficiently large. According to their study convection with ambient and conduction with adjacent filaments and with machine supports are the most affecting mechanisms. They also studied deformation of the deposited filaments due to their weight during assembly considering its influence minimal from a thermal point of view and for the dimensional accuracy of the part.

2.5.3 Thermal related problems

In FDM heat is of primary importance to achieve strong bonds between roads and layers, but the heat flux has not to be exaggerated in order not to encounter problems. Among the thermal related problems, it is possible to identify some of them related to poor heat flux throughout the piece and other ones which concern too much heat flux, it is thus possible to identify a process window to achieve pieces which can be regarded as good ones, which obviously depends on the material used. Poor bed adhesion and poor intralayer adhesion are due to a low temperature of the bed and of the nozzle, while the impossibility of making bridges, overhangs and the generation of deformed pieces are often due to too high extrusion temperature and thus too high heat flux through the piece. In Figure 42 it is presented a classification of the different conditions desirable and to be avoided in FDM additive manufacturing as pointed out by C. Duty at al. [25], including the extrusion consistency, the stability of the bead geometry, the functionality of the bead geometry and the component functionality.

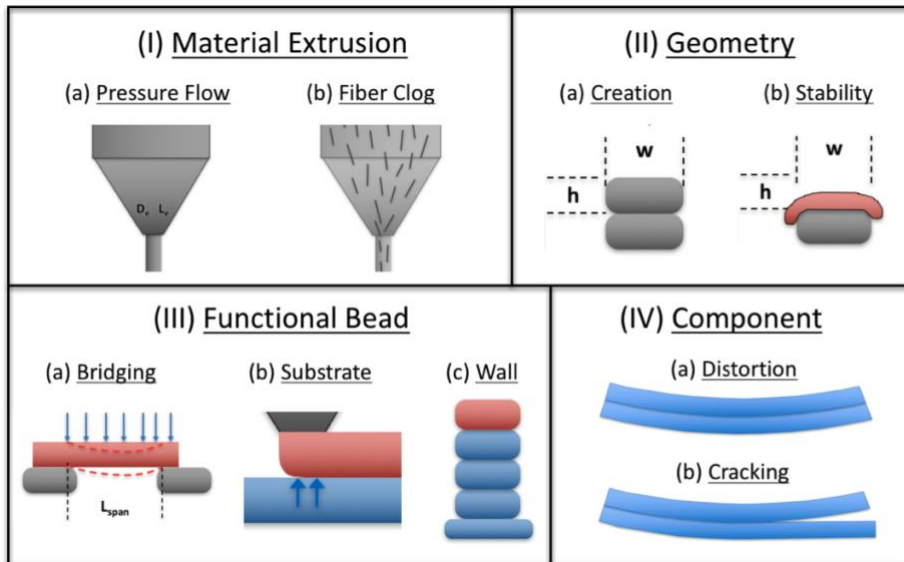


Figure 42: Different conditions in FDM AM [25]

Warping of the piece is related to high thermal gradients in the piece which result in different shrinkage rates and will give thermal stresses, exceeding a threshold this will result in thermal strains which will modify the geometry of the piece and give a failed print. Often the warping problem is present on the surface of contact between the first layer and the bed, since between two different materials the bonding strength is usually lower and thus will be the first point in which thermal stresses can generate deformations of the piece, resulting usually in poor bed adhesion and deformation of the corners.

Warping and distortion happens when the bonding between different layers of the part is adequate while the adhesion to the bed is not so strong and the rise of thermal stresses gives deformations on cooling of the whole piece.

The thermal stresses occur due to uneven cooling of the piece, in which usually the first layer has a faster cooling rate than the ones above it. During cooling each layer tend to shrink, but they are bonded one to the other resulting in tension stresses on the first layer since it would like to be smaller than the hotter layer above it. As the printed layers cool down each one of the will try to shrink exerting some tension on the first one, that is why usually the warping phenomenon increases as print proceeds, since more material will try to shrink pulling the layers below it. In corners this phenomenon is increased due to tensions in both sides of the corner, which will result in the corners being pulled up and inwards, as shown in Figure 43.

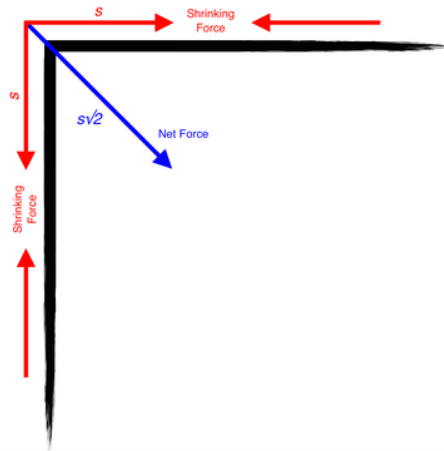


Figure 43: Shrinking forces in corners

Source: markforged.com

El Moumen et al. [26] developed a FEM model of a tensile specimen printed in PA12 investigating the temperature field and residual stresses, comparing the results with experiments, noticing how higher stresses are present in the first layer due to thermal gradients and stress concentration is highest in corners of the piece. In Figure 44 a frame from the simulation is reported, it has been generated in the cooling time of the piece, while all the material was approaching the bed temperature of 55°C.

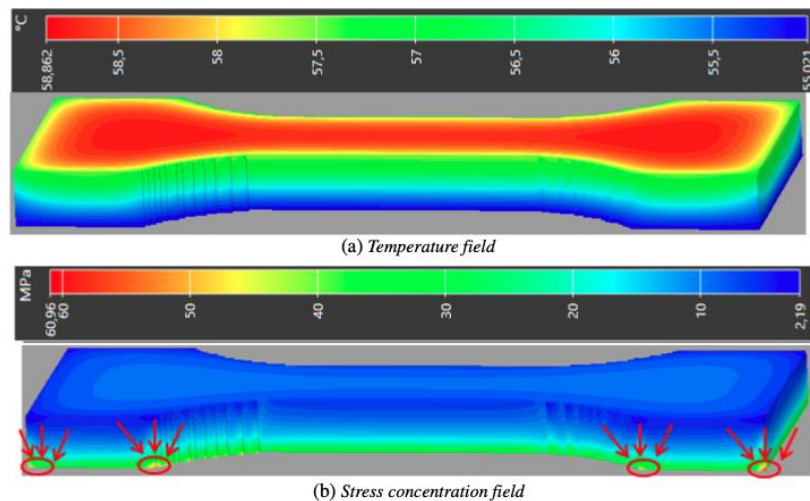


Figure 44: FEM model of a 3D printed tensile specimen [26]

Choi et al. [27] have pointed out how raising the bed temperature reduces the warping tendency of ABS specimens by printing some hexahedral specimen at different bed temperatures. In Figure 45 the results of their research are presented, increasing bed temperature from 40 to 110°C from case 1 to case 5.

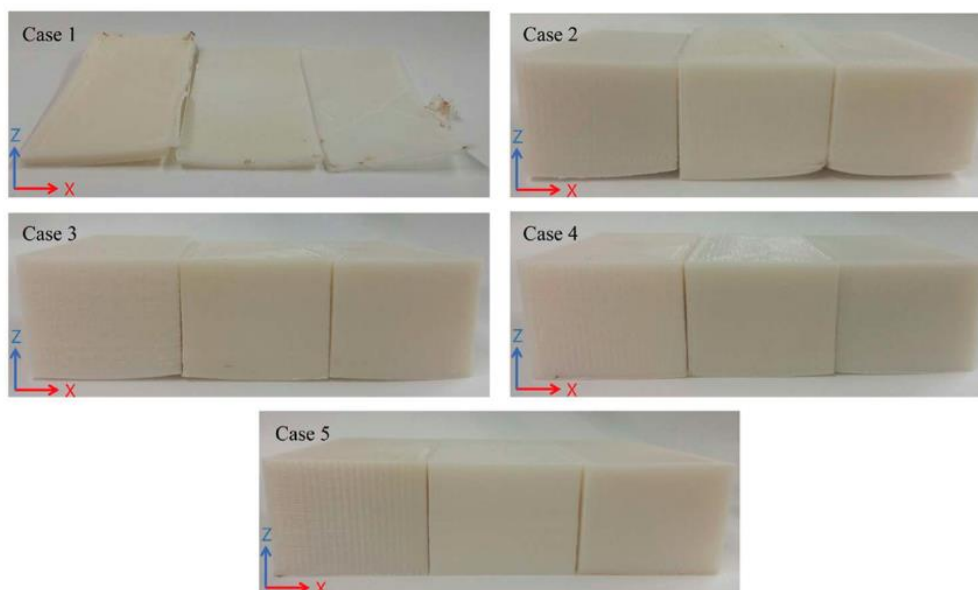


Figure 45: Prints with different build surface temperatures [27]

Poor bed adhesion due to low bed temperature can result also in detached pieces due to big temperature gradients between the build surface and the first deposited layer. To improve the situation in addition to heating the bed, which helps by maintaining a soft material close to the build surface, it is possible to use adhesive sprays to increase the bonding between the first layer and the bed.

Another condition to be avoided is low diffusion and bonding between layers, usually governed by the nozzle temperature and the surrounding air temperature. This condition can result in poor mechanical strength or even cracking due to thermal stresses in the deposited layers while cooling. This problem is mainly present between different layers because the cooling

time between one layer and the other deposited upon it is usually considerable since the machine has to finish the whole layer and then move up to deposit the one over it. For really low heat flux also the bonding between adjacent beads in the same layer might not be strong enough to sustain service conditions, this problem is usually marginal unless the printed object is very big. N. Turner et al. in their review of melt additive manufacturing [28] collected simple models to deal with many aspects of the FDM technique including die-swell, bead cooling, road deposition, spreading and bonding, highlighting how the bonding and neck formation between two roads can be modeled based on Newtonian sintering as presented in Figure 46. This sintering effect, with consequent diffusion of material chains across the interface and randomization, happens at a temperature well above the glass transition temperature. Of course, some degree of diffusivity is present even just above T_g , but for an actual neck formation the temperature needs to be way higher than the glass transition temperature, at least 100°C above it.

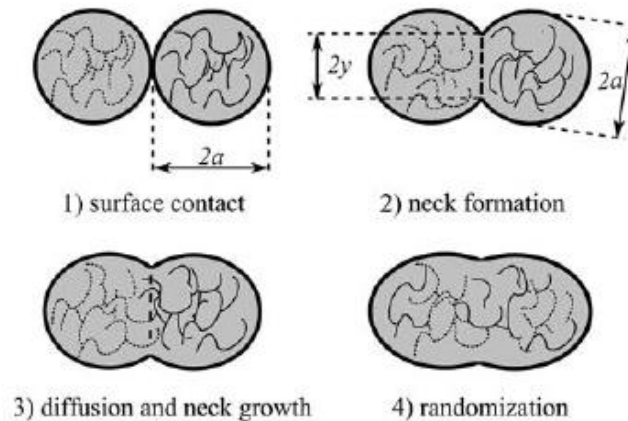


Figure 46: Neck formation and diffusion between beads [28]

Notes: 1) initial contact between roads of radius a . 2) neck formation. 3) inter-diffusion of polymer chains and neck growth. 4) randomization of chains between adjacent roads. In figure neck length $2y$, the closer to $2a$, the better bond quality

Y. Yan et al. [29] developed a model for relating in a simpler way the process parameter to the bonding strength and mechanical properties by introducing the bonding potential, which is a function depending on the temperature of the nozzle, that of the environment, the h/w ratio of the roads, with h height and w width, the size of the section, convection coefficient and conduction one. They highlighted how the environment temperature has more effect than the nozzle temperature in the bonding strength. They also pointed out that to obtain high bonding quality a tiny h/w ratio should be maintained, with big size of the cross section. They understood that a low convection coefficient in the forming room should be maintained and a material with low conductivity will guarantee less heat dispersion. The strength of the bonding is mainly affected by thermal parameters and properties but can also be increased by reducing the hatch spacing between roads, so decreasing the distance between the center of two extrusion roads to have an overlap. Geometrical and thermal characteristic participate in defining the mechanical strength of the piece, other than the material's actual mechanical properties. Many studies have been carried out relating the geometrical parameters of the printed objects and the mechanical properties, among them K. P. Motaparti et al. [30] studied the relation between build direction, raster angle of the filling and air gap with compression properties at different temperatures on Ultem 9085 parts. The printing speed is affecting quality and strength of the components, usually lower feed speeds guarantee higher mechanical strength by having more time for diffusion to occur, even if at really low speed the time to finish a layer would be so high that the lower layer might be too cool once the head deposits the next one above it and thus not guarantee an adequate bonding between the two.

Wang et al. [31] related the air gap size between two roads and the build plate temperature with the interfacial strength in roads of PLA extruded

material concluding that negative air gap is more effective for higher plate temperatures since more diffusion can occur.

J. E. Seppala et al. [32] tried to understand the development of weld strength in FDM additive manufacturing, integrating thermal history, molecular mobility and mechanical properties testing of the weld zone. They did so by using IR thermography, rheology and analyzing mode III of fracture. Attention was focused in studying the weld zone temperature in time as presented in Figure 47.

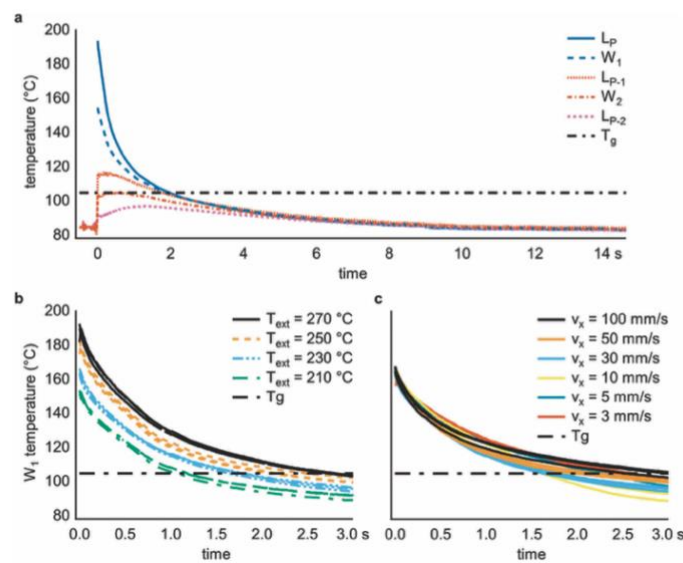


Figure 47: Temperature profile in time of layers and weld zones [32]

Notes: a) $T_{extrusion}$ 210°C, speed 50 mm/s. L_P print layer temperature, L_{P-1} first sublayer temperature, L_{P-2} second sublayer temperature, W_1 estimate of weld temperature between print layer and first sublayer, W_2 estimate of weld temperature between first and second sublayers. Dashed line glass transition temperature for ABS. b) Weld temperature profile estimates at different extrusion temperatures. c) Weld temperature profile estimates at different print speeds

C. Yang et al. [33] studied the mechanical properties of PEEK material by printing tensile tests with varying thermal conditions, such as ambient temperature, nozzle temperature and post extrusion thermal treatments, concluding that the nozzle temperature is a complicated factor since affects the crystal melting process, crystallization process, interface strength and

deterioration phenomenon, but in general increasing the nozzle temperature between 380-480 °C the tensile strength increases. The ambient temperature has a monotonic effect on tensile strength and crystallinity of the material, both increasing for increasing ambient temperature in the range 25-200 °C. The most suitable thermal treatments according to their paper is instead an annealing one at 200 °C, compared with tempering at 250 °C, air cooling, furnace cooling or quenching.

Nozzle temperatures too high can instead result in an excess of heat flux through the piece, which might give bad bead geometry stability, thus the impossibility of maintaining a semi rectangular bead, which will tend to melt and drop due to gravity, poor substrate support, which once the next layer is deposited on it will tend to collapse, poor bridging capabilities and impossibility of making overhangs, so not being able to make prints having raster angle different from a completely vertical surface without supports.

An excess of heat flux might affect the possibility of reproducing the geometry designed in the cad software, even if the machine is tuned and the nozzle is following the right geometrical path. This is due to the beforementioned poor bead geometry and stability in time; indeed the previous deposited layer needs to maintain its dimensions both in width and height for the next layer to be deposited upon it with some pressure from the nozzle and needs to be cool enough to have some mechanical stability for the next filament path to be deposited upon it. If the heat flux is too much the cooling time between one layer and the other might be not enough to guarantee this strength. This will result in the previous layer being deformed and dragged by the nozzle depositing the next one and in the worst cases might even get burnt due to the addition of heat by the next layer.

In Figure 48 two typical results of overheating are presented.

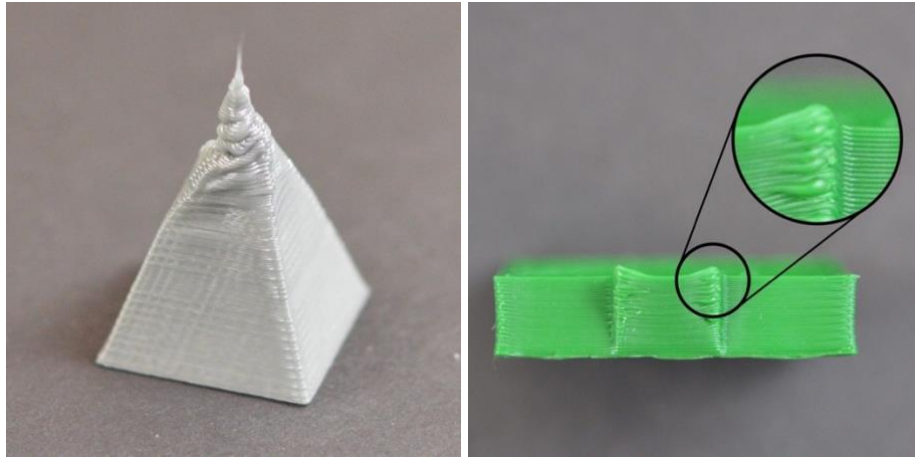


Figure 48: Overheating effects [34]

Overhangs are particular features that can be produced with a properly tuned additive manufacturing machine, they consist in the deposition of the next layer partially out of the geometry of the previous one in order to build an angle in the vertical direction without supports below it. The difficulty is that the layer has only a partial contact with the previous one and so needs to be strong enough to sustain its weight without collapsing, this is practically made by depositing the layer at the right temperature, which should be high enough to guarantee a bonding with the previous layer but cool enough to immediately after deposition reach a high viscosity state with some degree of toughness.

Different overhangs angles might require different cooling rates, for small angles like 15° or 30° from the vertical plane the right extrusion temperature might be enough to produce the structure, for higher angles a layer fan is required while for really high angles like 80° or 85° supports are mandatory [35]. In Figure 49 different overhangs angle are presented with a graphical explanation of the behavior.

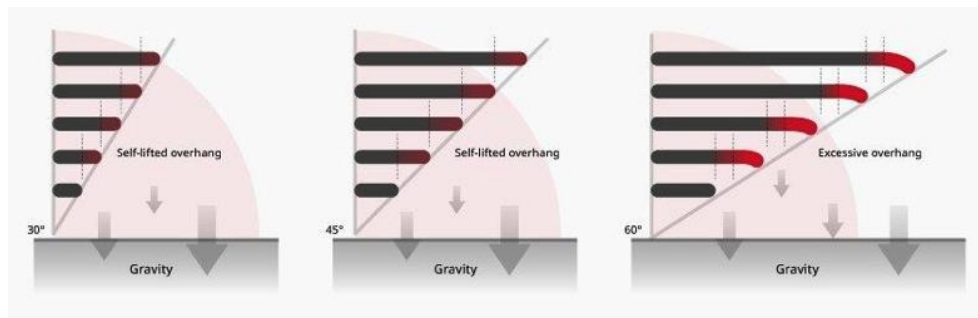


Figure 49: Overhang behavior [35]

Bridges are even more complicated to be performed with additive manufacturing, they consist in depositing a line of material with support only at the two ends, by stretching the filament to some degree and cooling it immediately with some additional air flux.

One of the main characteristics of bridges is the bridge length, indeed for increasing length the gravity force pulling the filament down increases. The deposited line behaves as a pinned solid beam subjected to gravitational force, with maximum deflection at the center and deflection increasing for increasing length, since the diameter is constant. Therefore, the probability of failing a bridge feature increases with increasing length.

In Figure 50 a bridge structure is presented, with the external walls in overhang at a constant angle and different bridge lengths, the upper one is produced with optimized settings.

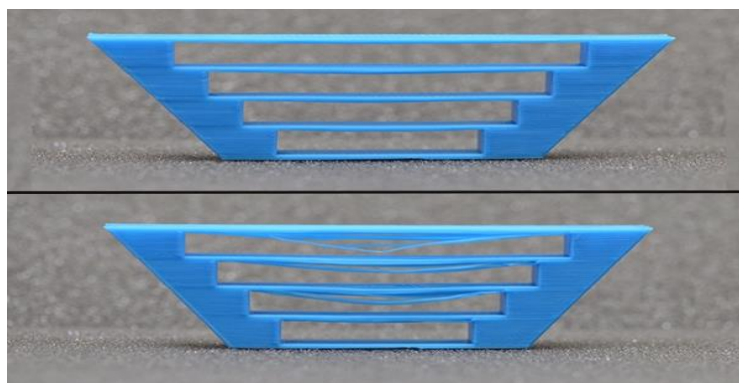


Figure 50: Bridge structures [36]

It is really difficult to find an extrusion temperature which guarantees printability of the material and bridging capabilities, so a layer fan is strictly required to produce these geometrical features. The layer fan will blow cool air on the line of material as it is extruded in midair and thus help solidify it and build the structure. In many commercial slicers for FDM additive manufacturing machines there are many settings to facilitate the building of bridges, such as automatic detection of bridge geometry and dedicated setting which gets activated when bridge features are detected. Among them there is the possibility of reducing the extruded flow rate of material for respect to the nominal one to stretch the filament in horizontal direction and to activate the layer fan at maximum speed in the bridge area while having another nominal speed throughout the rest of the print. It is understandable that for additive manufacturing of complex geometries of thermoplastics a layer fan is mandatory, to control better the heat flux and removal of heat through the printing process. An excess of air flow rate might result in cracking and poor layer adhesion due to a too fast cooling of the substrate, so the power should be carefully chosen depending on the material and extrusion temperature.

Another problem related to an excess of heat flux is the so called "heat creep", which consists in heat going in parts of the machine where it is not supposed to be, resulting in clogs. It is mainly present in filament FDM machines where the temperature rises also in parts which are supposed to be cool, such as gears pushing the filament or just over the melt zone, increasing the pressure losses to be overcome by the extruder and resulting in lost steps or filament grinding. Usually if this problem is present the job must be stopped and the machine cooled since the extrusion will not be regular or will completely stop.

In Table 2 the summary of the thermal problems which can be encountered in EAM is presented.

Problem	Explanation
Warping	Usually caused by non-uniform cooling of the object, often occurs when the bed temperature is too low for the printed material. When the first layers cool down they tend to shrink, the upper layers still hot are expanded and being the layers bonded together some thermal stresses arise. If the adhesion force between the first layer and the build surface is not enough the stresses will generate deformations, corners will tend to curl and warping occurs.
Delamination	Occurs when the temperature of the previous layer is too low when depositing the next one and bonding and diffusion cannot occur, resulting in detached layers. This phenomenon is mainly driven by the glass transition temperature of the material, if the extrudate temperature gets close or below it the diffusion phenomenon cannot occur properly and intralayer strength decreases dramatically
Overheating	Results in the geometry of the printed object not being respected even if the path of the nozzle is correct, due to poor substrate stability which tends to be dragged by the nozzle and fall due to gravity.
Impossibility of making overhangs	Is given by the low extrudate stiffness which is not able to maintain its shape when deposited in overhang condition, it tends to fall due to gravity.
Impossibility of making bridges	To make bridge features the just extruded material must possess a sufficient degree of stiffness to sustain its own weight with support only on the two sides.
Heat creep	Consists in heat going up through the extrusion head in places where it's not supposed to be, it can result in clogs or damages of the machine.

Table 2: Summary of EAM thermal problems

2.5.4 High temperature materials thermal problems

High temperature thermoplastics nowadays are increasing their applications number due to wider application sectors, lower costs and greater performances for respect to the past. These thermoplastics usually have high mechanical strength, are resistant to extreme temperatures and many chemicals and are lightweight for respect to metals, among them it is possible to highlight PEEK, PEI, PPSU, PTFE and PBI. They can often be used in substitution to aluminum or for rapid tooling in injection molding, due to their high strength and high temperature resistance. The problems highlighted in the previous paragraph are still important and present also for this kind of plastics, but also others arise. In particular they usually need to be extruded at really high temperatures, about 350-450°C and this feature can stress most of the commercial additive manufacturing FDM machines, since most of them are not designed to go at such high temperatures. Their viscosity vs strain rate curve is similar in shape to other thermoplastics but shifted upward for lower extrusion temperatures. In Figure 51 the viscosity-strain rate diagram for PPSU is shown, showing a high viscosity at 355°C, temperature at which most thermoplastics have a viscosity similar to oils [37].

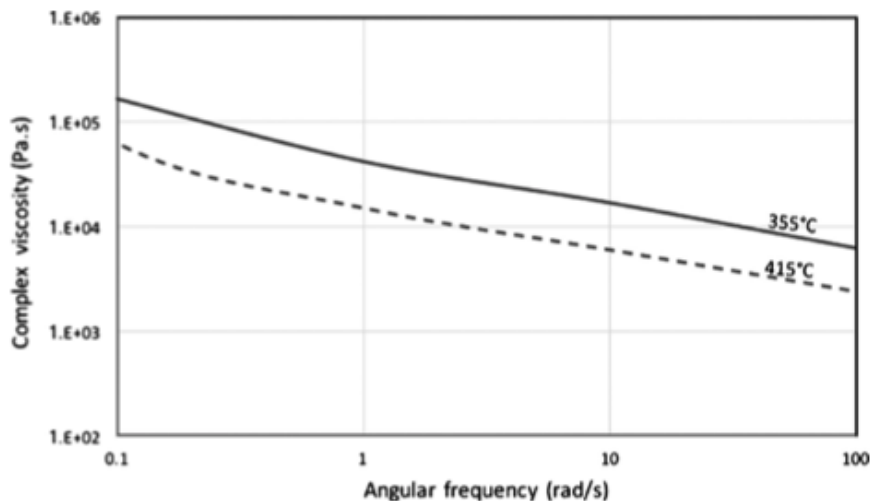


Figure 51: PPSU viscosity curves [37]

Even for these thermoplastics the higher the temperature the lower the viscosity as predicted with Cross-WLF model, but a value of viscosity which permits extrusion is obtainable at high absolute temperature, being their glass transition temperature often over 200°C.

Due to high extrusion temperature the heat flux with ambient will be way greater than other plastics assuming a constant ambient temperature and convection coefficient, thus their temperature will quickly drop below the temperature needed for good bonding and diffusion or even below their glass transition temperature. This involves the need for solutions which were not so important for other thermoplastics such as printing in a controlled environment, with a temperature of the chamber really high. For ABS printing for example a controlled environment is suggested but not completely mandatory and good properties and strength of objects can be achieved also with a heated bed and a tuned extrusion temperature. The temperature so high in the enclosed environment might stress every electrical component present in the chamber and even reduce life of belts and bearings of the machine.

The residual thermal stresses in these high temperature plastics after extrusion are higher than with other plastics due to higher thermal gradients. Also, the low conductivity of these material is a characteristic which might give problems when extruding them, since heat will less likely go through the material while heating them and thus a lower printing speed is usually needed. Lower conductivity is instead good in service and post extrusion since the extruded filaments will keep the heat inside them.

2.5.5 Thermal achievements in additive manufacturing

To solve the beforementioned problems many authors have tried different techniques, some of them not so helpful but others have even entered the commercial field since the improvement on quality is remarkable.

As mentioned before the heated bed is an important feature that nowadays is present in most of the commercial additive manufacturing machines, it increases both the adhesion with the build surface but also the diffusivity among layers, especially in the ones close to it.

The heated build surface is usually characterized by a resistance and a thermocouple or thermistor, with PID control strategy to reach and keep the desired temperature throughout the printing time. The power of the resistance directly influences the time needed to reach a certain temperature and the maximum temperature which can be reached, assuming all the components to be well designed. The maximum temperature reachable in first approximation is indeed that temperature for which the thermal losses due to convection with ambient equal the power of the resistance, for higher temperature the heat flux defined by Newton's law will be higher considering a constant ambient temperature and thus a higher resistance power will be needed.

A fan close to the nozzle is also common in most commercial FDM machines to cool the layers as they are deposited, thus increasing quality of the print, giving the possibility of producing greater overhangs and bridges. These fans are usually small and lightweight to be installed close to the heated end and not increase the moment of inertia of the nozzle area in moving printheads. The power of the fan can usually be controlled with Pulse Width Modulation (PWM) which guarantees the possibility of different air flow rate in different parts of the print.

More sophisticated additive manufacturing machines also have an enclosed print volume, which might be heated through the bed or with additional resistances and fans. The heated chamber reduces dramatically thermal gradients in the printed object, leading to lower tendency for distortion and cracking. Even in case of heated chamber a thermistor is needed with an associated PID control, in order to keep the desired temperature during the print. Often a fan with a filter to extract air is present to reduce the

temperature if it exceeds the desired one. The closed environment also increases the safety of the operators by keeping the vapors produced by thermoplastic extrusion inside the chamber, filtering the air coming out of it, and by not allowing to touch any hot and moving part of the machine while it is working. The design of an enclosed printer has to be carried out with care being sure not to exceed the maximum allowable temperature of any component inside the closed environment, this is done by choosing high temperature parts or by placing any sensitive component, such as electronics, out of the chamber.

As mentioned before, to print high temperature thermoplastics even more care has to be used when designing a printer. Some important features these machines should have are: high extruder temperature, capable of reaching temperature higher than 350 °C, high bed temperature to ensure adhesion and overall print quality, closed and heated chamber to prevent shrinkage and warping, which should be able to reach at least the glass transition temperature of the material. In some cases also a controlled cooling of the chamber might be required for best mechanical properties [38].

Some manufacturers produce printers with these characteristics, the price of these machines is obviously very high due to design and research costs but also due to high quality components, it can reach up to 200.000€. Among the manufacturers it is worth mentioning Roboze, an Italian company which produces industrial grade additive manufacturing machines for all kind of materials including high temperature ones, ARGO 350 is capable of 450 °C extruder temperature, 180 °C build plate and chamber temperature [39]. Another Italian company which produces machines capable of printing PEEK and PEI is WASP, which among its printers for clay and concrete has just introduced the Delta WASP 4070 TECH, capable of reaching an extruder temperature of about 500 °C, a build surface and chamber temperature of 300 °C and has a filament drier included in the

machine [40]. The drying process becomes even more important for these high temperature polymers.

Another key player in the production of additive manufacturing machines for high temperatures polymers is Stratasys, which has been in the market of additive manufacturing for more than 30 years and now is suppliers of many companies with their state-of-the-art technology. Their machine Fortus 450mc can reach an extruder temperature of 450 °C and a bed and chamber temperature of about 350 °C, thus being able to print PEEK and PEI as well as many other thermoplastics [41].

The scientific research is still ongoing on the high temperature material production with FDM additive manufacturing and on the improvement of properties of the printed objects.

Among them C. Zawaski et al. [42] developed an inverted printer design with a chamber able to reach 200 °C with heated walls and bed in order to reduce the machine cost and allow the democratization of high strength material production with FDM. They carried out CFD simulations to define the geometry of the chamber and tested the performance of the latter noticing an increase in tensile strength of the parts of about 48%. The inverted design was chosen to be able to put all the mechanical and electrical components out of the heated environment.

In Figure 52 the schematic design and a picture of the built machine is presented.

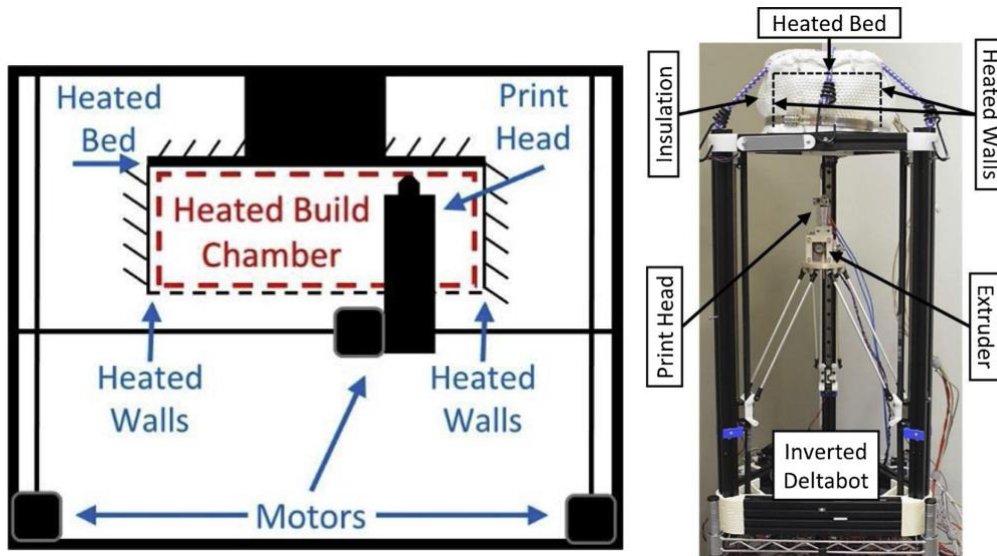


Figure 52: Inverted printer design [42]

P. Han et al. [43] used a $10.6 \mu\text{m}$ wavelength localized laser to improve the interface strength in Ultem 1010 object produced with filament FDM, studying the tensile strength with varying laser power between 0.3 to 2 W. in Figure 53 the schematic of their machine setup is shown.

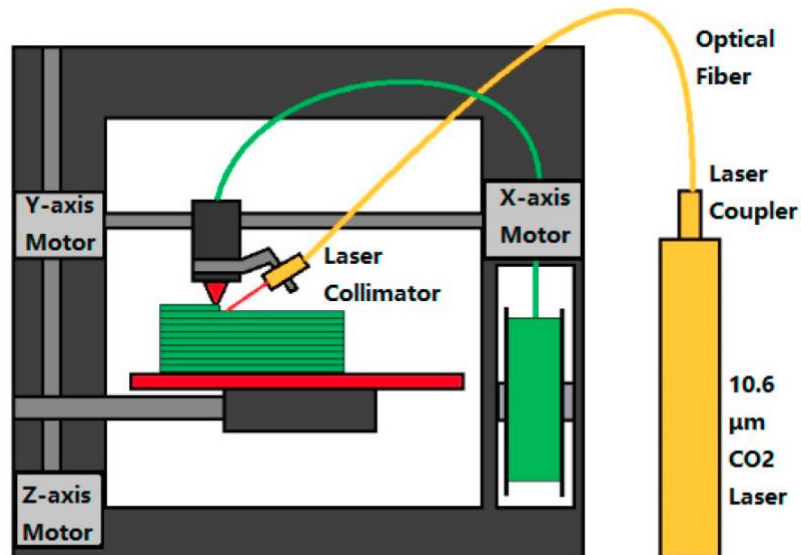


Figure 53: Schematic of laser preheating [43]

They noticed how the tensile strength increases with laser power up to 1.6 W and this result is due to an higher entanglement of polymer chains at layer interface with laser pre deposition heating.

V. Kishore et al. [44] developed an heating system for the substrate using infrared lamps and pyrometers in Big Area Additive Manufacturing to evaluate the substrate temperature difference upon IR heating. In Figure 54 the schematic of their design is presented.

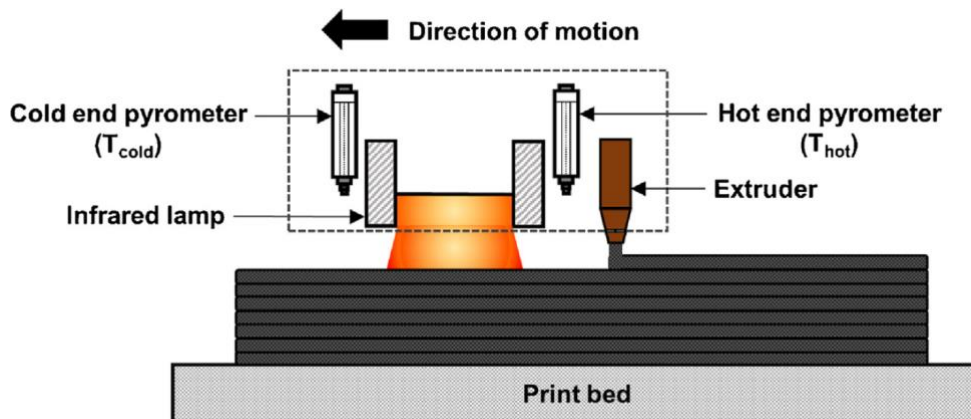


Figure 54: Schematic of infrared preheating [44]

The heating system is designed to heat the substrate only when the extruder is moving from right to left in the picture, using the parts of the object printed in the other direction as reference with same printing parameters but lamps off. Three conditions were tested varying the standoff distance of IR lamps for respect to the substrate

They observed an increase in fracture energy for the heated substrate until the degradation of substrate surface due to high intensities, which also depends on the feed rate of the printhead, since for higher velocity the time in which the IR light heats the substrate decreases.

A qualitative diagram of the time-temperature profile for each layer is shown in Figure 55.

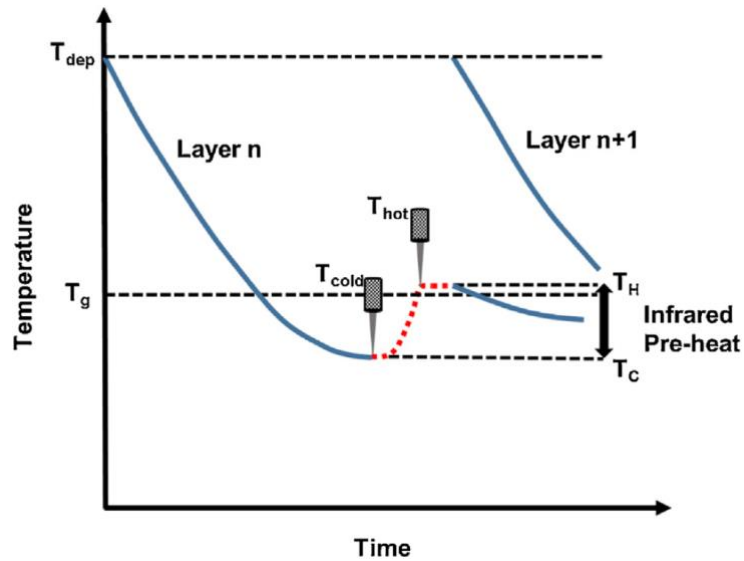


Figure 55: Temperature profile with infrared preheating [44]

A. Nycz et al. [45] continued Kishore research by adding an array of vortex chillers on both sides of the IR lamp to simulate the cooling present in large layers typical of Big Area Additive Manufacturing. Tensile specimens with ABS were printed to evaluate the effects on tensile strength of pre deposition temperature of the substrate. They showed that IR preheating did not have a significant impact on strength if the initial substrate temperature did not fall below the material's glass transition temperature while it has considerable impact if the substrate temperature has cooled below T_g . In Figures 56 and 57 the results for cooled and uncooled substrate are presented.

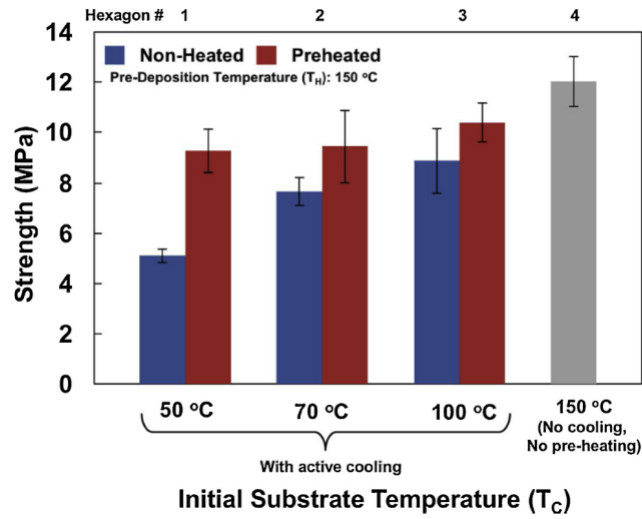


Figure 56: Tensile strength of cooled specimens with and without preheating [45]

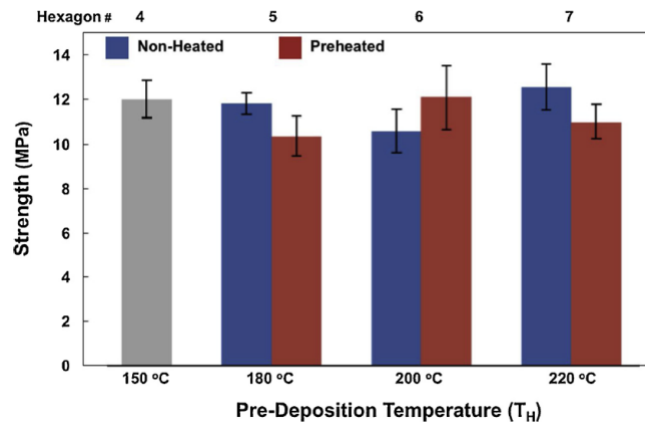


Figure 57: Tensile strength of uncooled specimens with and without preheating [45]

C. B. Sweeney et al. [46] patented a technology to preheat the substrate of Carbon Nanotubes (CNT) filled polymer composites with 2.45 GHz microwaves to increase inter-bead diffusion bonding in FDM. The CNTs are microwave absorbing materials which are incorporated in the volume of the polymer, their reaction with microwaves helps increase the overall strength of the final part and increase the isotropic mechanical properties of FDM built parts. In Figure 58 the schematic of the machine design is shown.

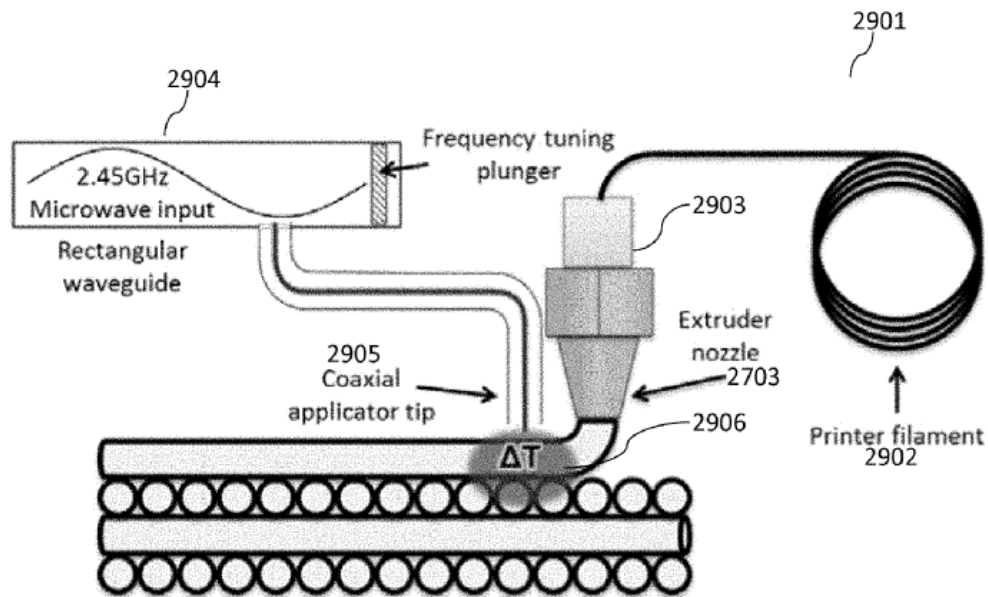


Figure 58: Schematic of microwave heating [46]

D. Ravoori et al. [47] developed a metal heater block for filament FDM machines with a preheater made of metal used to heat the substrate pre or post deposition. In Figure 59 the schematic and assembly of nozzle and heater block is presented.

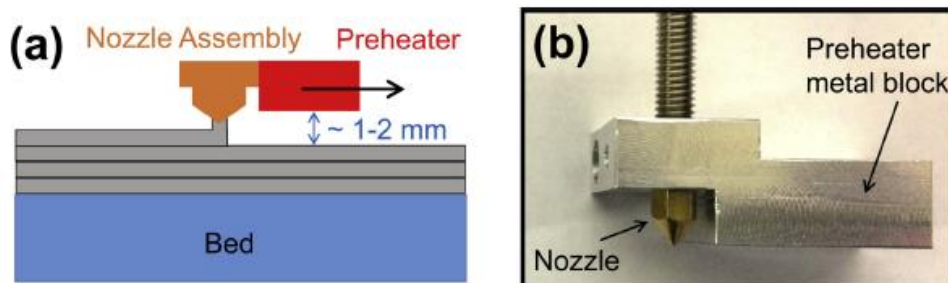


Figure 59: Preheater metal block [47]

Notes: a) schematic not in scale. b) picture of the metal block

They developed a finite element model and compared the result with the experimental campaign, showing some level of accordance between the two. They also studied the impact of their design in filament-to-filament bonding, noticing a greater necking and less void area with the use of the

pre-heater. To conclude their study, they also evaluated the tensile stress with and without the preheater noticing an increase of about 60% with substrate heating due to increased bonding and diffusion.

3 EFeSTO

The machine on which the improvements and study are carried out is an innovative machine developed at Politecnico di Milano since 2014. This machine is very different from the ones available on the market since it mounts a modified Metal Injection Molding deposition head combined with a parallel kinematic build plate. It has been developed by professors, theses and PhD students with many contributions in order to build an additive manufacturing machine capable of printing different materials with great precision. Among the printable materials there are metals and ceramics with a binder but also thermoplastics. The extrusion head is relatively powerful and heavy so it is fixed in space while all the three axes (X, Y and Z) are given to the build plate, avoiding vibrations that can occur during rapid change of direction, caused by high inertia forces of the extrusion system. The table is moved with parallel kinematics, which guarantees a high position accuracy of the tool center point [48]. In Figure 60 a render of the machine is presented.

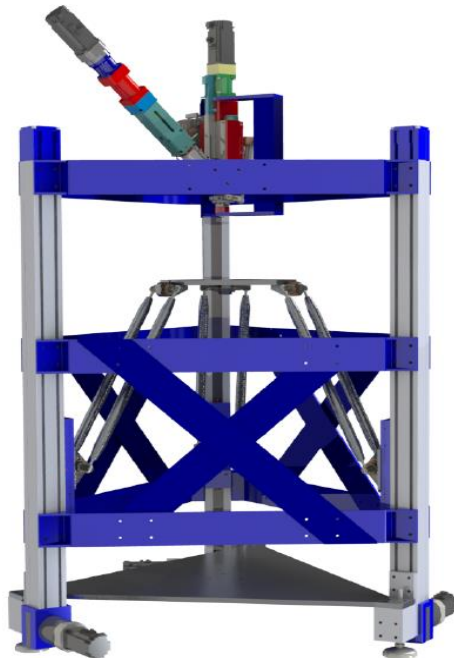


Figure 60: Rendering of the EFeSTO machine [52]

3.1 Extrusion group

The extrusion group is one of a kind, it has been developed by prof. H. Giberti and A. Marseglia [49] starting from a MIM machine called UAI Babyplast (Figure 61), commercialized by Rambaldi + Co.I.T. company. The original machine is intended to perform injection of viscous materials in small molds, it features two different chambers with pistons driving the material.



Figure 61: UAI Babyplast machine [49]

The two chambers mechanism is useful to decouple the plasticization and extrusion phases, since plasticization needs to be done at constant speed and pressure while extrusion with varying speed depending on the mold geometry. The plasticization chamber receives the material in form of flakes or pellets from the hopper by gravity and pushes it through some metal spheres to increase the shear stress, after which it enters in the extrusion chamber. The extrusion chamber has the role of keeping the viscous fluid at a given temperature and, thanks to the piston's movement, push it out of

the nozzle. To simplify the plasticization phase also in the loader (the plasticization chamber) there is a resistance with a thermocouple and PID control to maintain the desired temperature, since for higher temperature the viscosity decreases.

The pistons in origin were hydraulic actuated, in order to produce great forces and thus pressures on the material, for a fast injection in the mold. High pressures are needed in injection molding to fill the mold before the material starts solidifying and then to counterbalance backpressures and shrinkage of the piece in the mold. The hydraulic system is bulky, needs of cooling of the oil, maintenance of the hydraulic circuit, might leak oil in case of damages or improper use and, most importantly, cannot easily and precisely be controlled in position. Thus, the hydraulic system was eliminated and brushless motors were used to drive the pistons (Figure 62), which can guarantee a more reliable and precise control in speed and position, important in additive manufacturing for the coordination with the three axes in space. The pistons are connected to the motors with ball screws to have the most precise positioning possible, those transform the rotating movement of the motor in translation of the pistons. On the plasticization side a planetary reduction stage, a Wittenstein SP+ 60S, is present to increase the torque produced by the motor, since in this phase higher pressures are needed.

The plasticizer has a piston with diameter 20 mm and with the reducer can give to the material a pressure up to 26 MPa. The volume of the extrusion chamber is 9000 mm³, the extruder piston has diameter 14mm and it is capable of giving to the material a pressure up to 24 MPa.

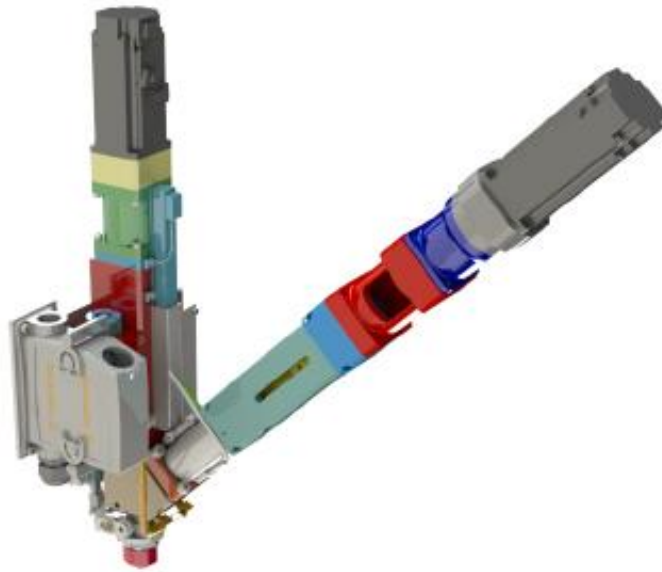


Figure 62: Extrusion Unit with motors [52]

The extrusion unit is equipped with four thermocouples type J, capable of measuring temperatures up to $750\text{ }^{\circ}\text{C}$, with a sensitivity of $51,7\ \mu\text{V}/^{\circ}\text{C}$. One is present in the nozzle, with a resistance, to heat the zone, with power 150 W , one in the extruder body, with a 500 W resistance, and one on the loader, with a 1000 W resistance to increase the temperature of the zone. The fourth thermocouple is present in the thermal cutoff zone, and it is used to control that the temperature in that zone does not exceed $60\text{ }^{\circ}\text{C}$, to protect the piston of the loader, motors and electronics. All the resistances are fed with 230 V alternated current.

The nozzle of the machine has also been modified and, after a comparison among different nozzles [50], the convergent-parallel wall geometry has been chosen as it is the one which allows better control of the extruded wire to achieve better precision of the machine, with a swelling coefficient of $1,05\text{-}1,15$. The parallel wall design is also aimed at stabilizing the direction of the viscous flow.

The extruder piston absolute position is known with a potentiometer connected through a screw to the piston, while the plasticizer piston has a proximity sensor at the end of the stroke at the motor side. Those sensors are useful to identify the home position of the extrusion unit, position from which the job can be started.

The extrusion unit was also equipped with a pneumatic closure of the nozzle, shown in Figure 63, in order to prevent the flow of material out of the nozzle while charging the extrusion chamber.

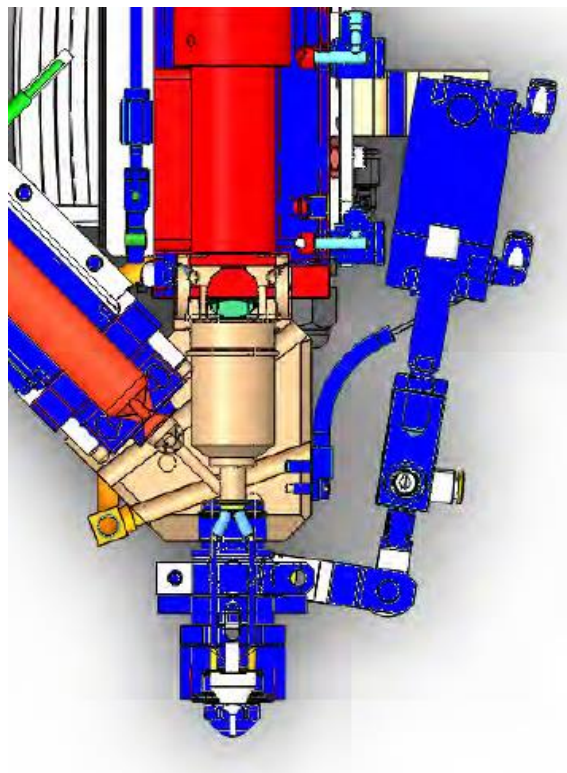


Figure 63: Pneumatic closure of the nozzle [49]

A water-cooling system is also present, which has channels in the extruder body, in the thermal cutoff section on the plasticizer unit and also in the shutter pneumatic actuator, since the actuator is directly connected to the nozzle zone, which can get really hot.

3.2 Kinematic system

The kinematic system consists in a parallel kinematic machine (PKM) which drives the build surface in space through the linear movement of three sliders (Figure 64).

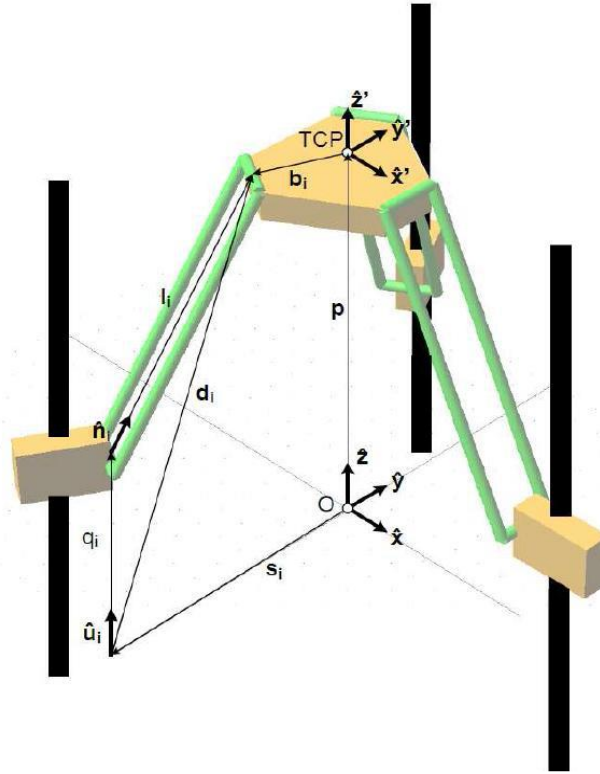


Figure 64: Schematic of the Linear Delta system [48]

The motion of the build surface is constrained to be parallel to the floor since parallelograms, which restrict some movements of the platform, are present in the kinematic system. The system is composed three units spaced 120° each other, each one of those is composed by a stepper motor, the same one used for the extrusion unit, a reducer, namely a Bonfiglioli TR 080, a linear guide present in the commercial market, the ELM 80 SP by Rollon, a slider which moves linearly on the guide, two arms for each slider, that guarantee rotations on more than one axis and connect the sliders to the build surface. The sliders position is known thanks to magnetic sensor on the rail and,

thanks to the direct kinematic, the position of the build surface is also known. To define the geometry of the kinematic system an optimization algorithm has been used [51][52], both from a dimensionless point of view to study the reciprocal effect of the parameters and from a dimensional point of view, to effectively choose the value of the parameters. In particular from the iterations the diameter of the machine in the build surface plane (D), the angular spacing between the guides and length of the arms (l) was retrieved, by imposing a workspace of 400 mm diameter in the build plane (Figure 65). The resulting dimensions are $D=913$ mm, $l=598$ mm and the angular spacing between the guides of 120° , for symmetry.

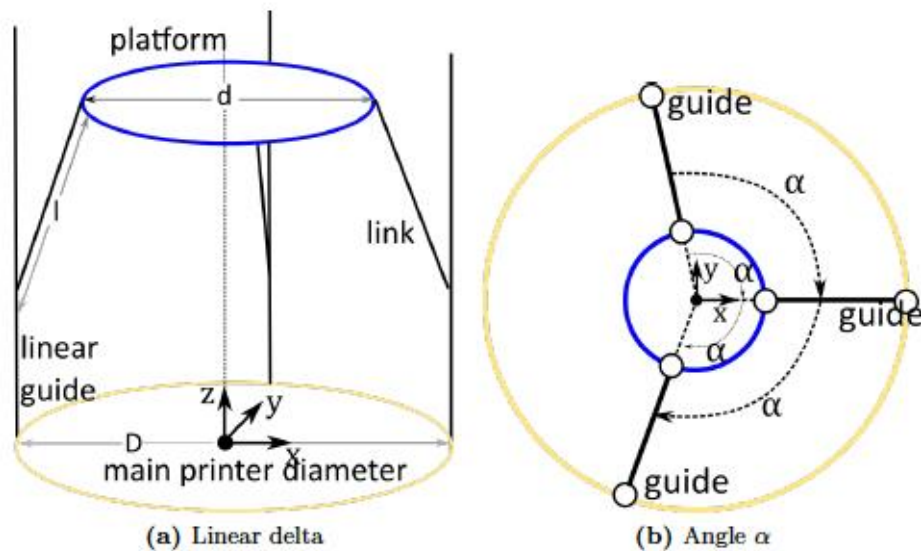


Figure 65: Schematic of the optimization variables of the PKM [52]

Thanks to the parallel kinematic design the z axis is not actually constrained, but the possible stroke in that direction depends on the length of the linear guide, since for a z movement the three sliders have to move synchronously in one direction. The arm length and diameter at which the sliders are placed instead is related to the maximum possible workspace in x - y dimensions. After the definition of the geometrical characteristics of the delta structure a dynamic model has been developed, presented in Figure

66, to size the actual mechanical components according to the maximum loads expected [52]. The structure has been developed in order to have really low deformations under the working loads, thus having high accuracy and precision. After the mechanical design the actual coverable workspace is 250 mm.

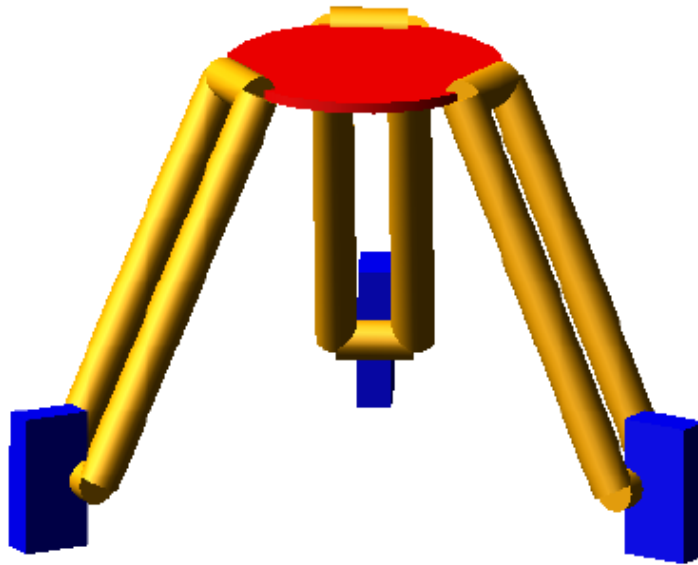


Figure 66: Dynamic model of the PKM [52]

The sliders use proximity sensors at the base of the frame to retrieve the home position, these are connected directly to the servo drivers as a digital input.

The inverse kinematic has also been developed, it relates the position of the tool center point with the position of the sliders, being thus important when sending G-codes to the machine, since those are usually composed by series of coordinates in a cartesian space to be followed by the tool. The study on the kinematic and deposition trajectories has been carried out by prof H. Giberti and Marco Parabiaghi [53].

Before starting a new job, the build surface has to be raised close to the nozzle at a defined height, since in the home position it is at the bottom of

its stroke. The position for printing mainly depends on the length of the nozzle and by changing nozzle it has to be modified.

A future improvement of the kinematic system would be to add two rotational degrees of freedom to the build surface in order to reduce the staircase effect and be able to print according to the model angle.

3.3 Control of the machine

All of the drives and control modules are produced by Mitsubishi, to have better integration and communication between different parts of the system.

The control of the machine is carried out through brushless motors, as said before the motor chosen are the same for all the axes, namely Mitsubishi HG-KR43B, those motors are capable of 1,3Nm of nominal torque and a peak torque of 4,5 Nm, even if it is lowered by software to 3 Nm. The motors have an embedded encoder and electromagnetic brake for emergency situations. The motors are connected to the servo drivers, model MR-J4-40B-RJ, which give the pulses for the motor to rotate, these drivers are really advanced and can detect errors such as overtemperature of the motor or of the driver itself, collisions of the load of the motor and thus high torque needed and many others. In Figure 67 the motor and servo driver of the machine are presented.

The drivers are controlled by the Motion Control unit, a Mitsubishi Q172DSCPU, which is responsible of getting the motion laws from the PLC and transferring the information to the servo drivers with the right timings. The motion control unit and the servo drivers are connected thanks to optic fiber cables in series, only the first servo driver is actually connected to the motion control unit and the others are connected to the previous one. The protocol used for this communication is SSCNETIII/H.



Figure 67: Motor and Servo drive [49]

A PID control is present in the servo drives to adjust the position and speed of the motor based on the error on position or speed, the gains for this control can be obtained by manual tuning, auto tuning or one-touch tuning. On the machine the auto tuning mode is activated, which automatically calculates the gains based on the ratio between load and motor inertia every 60 minutes, by saving them on the EEPROM of the servo drives themselves. The PLC is programmed with Ladder Diagram language, a low-level language used to activate switches and run programs on the motion control unit. The PLC is responsible of the overall control of the different modules of the machine, the communication with the PC, the communication with the human machine interface (HMI) and the storing of motion laws and programs on its memory.

The motion control unit is programmed using the Sequential Function Chart (SFC), and through this language many operations can be performed,

with the possibility of waiting for the first operation to finish before starting the second or of running more than one operation in parallel. It can handle the motor starting, the safety stop with electromagnetic brakes but also the execution of the motion laws.

The temperature control unit is a Mitsubishi Q64TCTTN, it is a very complex controller which can guarantee more functions than the ones needed for the EFeSTO purposes. In the machine it is used to control the three resistances based on the temperature readings from the thermocouples. The resistances are controlled just by setting on and off the relative switch based on a PID control, which guarantees the most precise and constant control of the temperature at the specified value. The module has an Auto-Tune features, which defines the gains of the PID control by analyzing the overshoots and undershoots for respect to the set value. Also this module is controlled by the PLC, with instructions coming from the PC or from the Human machine Interface.

In Figure 68 the complete electric scheme of the machine is presented, for simplicity only one servo drive and motor are depicted since the connections are the same for each one of them.

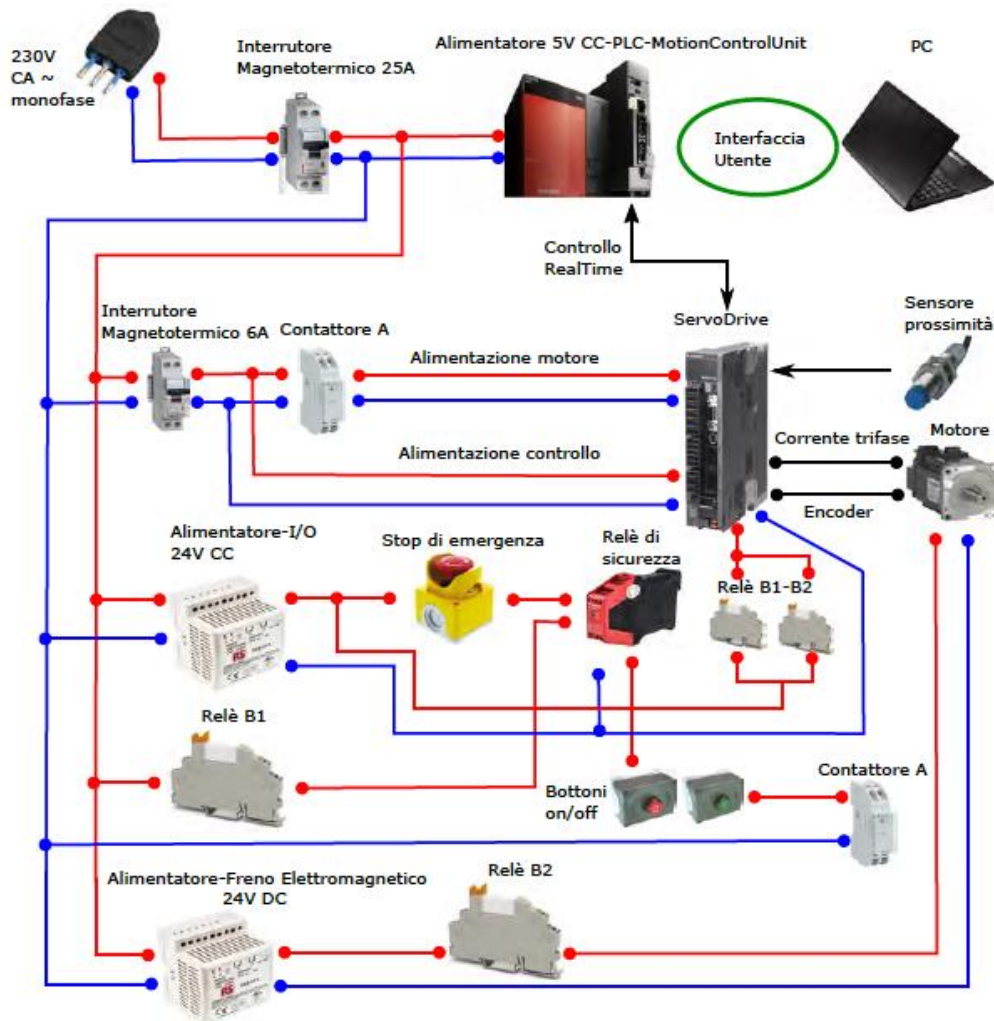


Figure 68: Electric scheme of the machine [49]

The HMI (Figure 69) is a display with a visual interface loaded on it, it permits the execution of simple operations without using the PC serial communication. On the HMI it is possible to activate motors, heaters and temperature control, preheat the various zones, bring to the home position the delta structure, the extruder and the loader. It is also possible to control in torque or position the extruder and loader to load material in the machine or to purge and clean the chambers. The delta structure can be controlled in

position from the HMI, defining the position of the tool center point and the speed to reach that position.



Figure 69: HMI temperature control

Another section permits to visualize the position of the motors with high precision and to see if all the motors are working properly.

In Table 3 the components used to control the machine are summarized.

Component	Model
PLC	Q03UDVCPU
Motion Control Unit	Q172DSCPU
Temperature Control Unit	Q64TCTTN
Servo Drives	MR-J4-40B-RJ
Motors	HG-KR43B
HMI	GS2107-WTBD

Table 3: Electrical components of the EFeSTO machine

For the actual printing phase the PC is strictly mandatory, both for the slicing of the STL file but also for the communication with the machine. First

of all, the cad needs to be sliced, then the G-code is given to a Matlab compiled program for Windows which handles the conversion of the G-code in CAM instructions for the machine (Figure 70), including limitations set for velocity and acceleration both of the sliders and of the workspace, this software also gives plots of the object and of the different axes position in time.

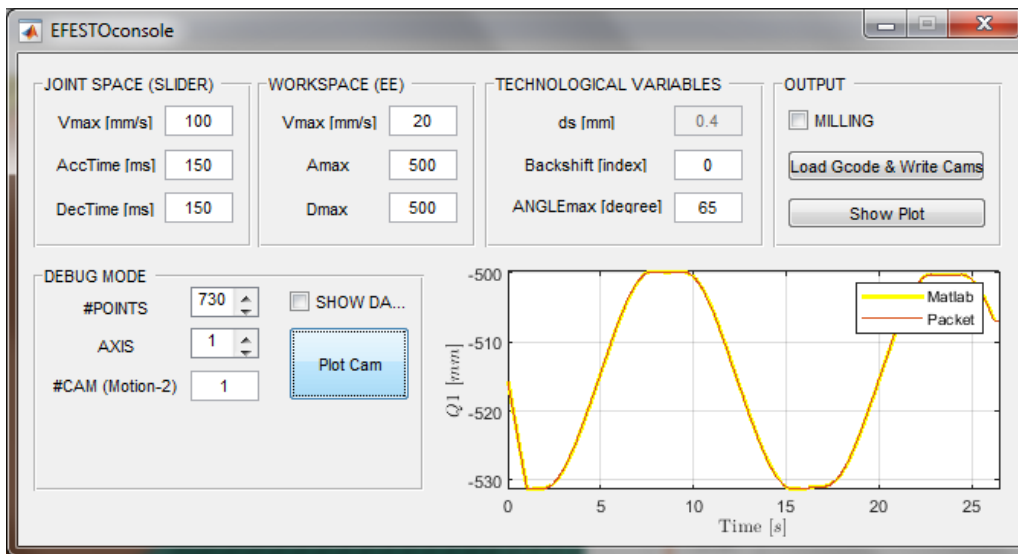


Figure 70: G-code interpreter for CAM instructions

A third software written in C# is then responsible of taking the .txt file generated by the Matlab software and send packets of data to the machine, with an online USB serial communication with the PLC. From this software it is also possible to kill or pause the job once started. The interface of this software is shown in Figure 71.

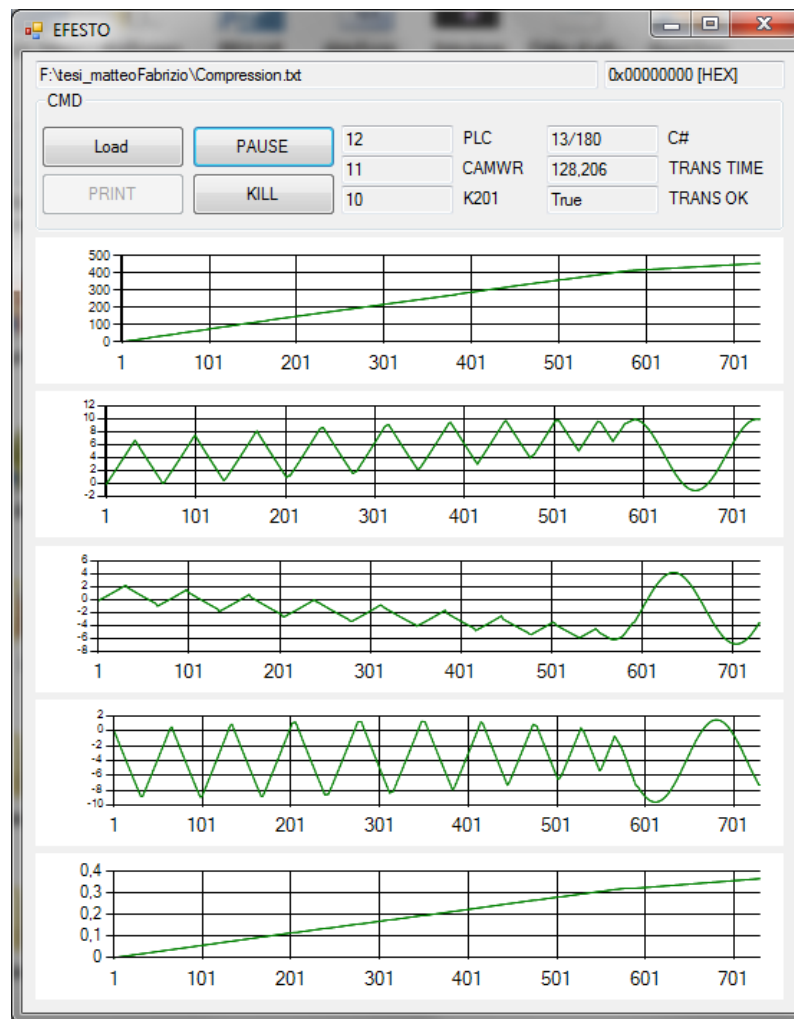


Figure 71: Software for the serial communication

3.4 EX-ANTE problems of the EFeSTO machine

One of the goals of this thesis was to solve the many problems which affected the EFeSTO machine, that are here summarized. These problems did not guarantee a proper working of EFeSTO as an additive manufacturing machine. Indeed the machine was not able to make any piece with quality comparable to the one of commercial machines (Figure 72), being able to print only tensile tests or simple geometries with a really bad quality.

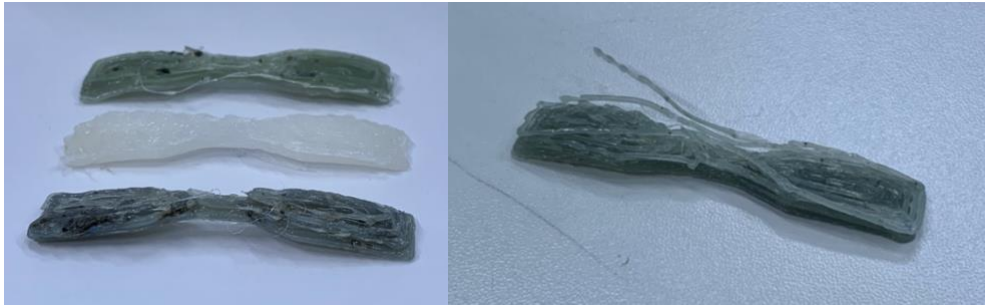


Figure 72: Pieces printed before the improvements

First of all the cables of the motors and temperature control were laying on the floor around the machine with no order. It was difficult even to walk past the machine since there were cables on the floor which were just laying around in a chaotic manner (Figures 73 and 74).

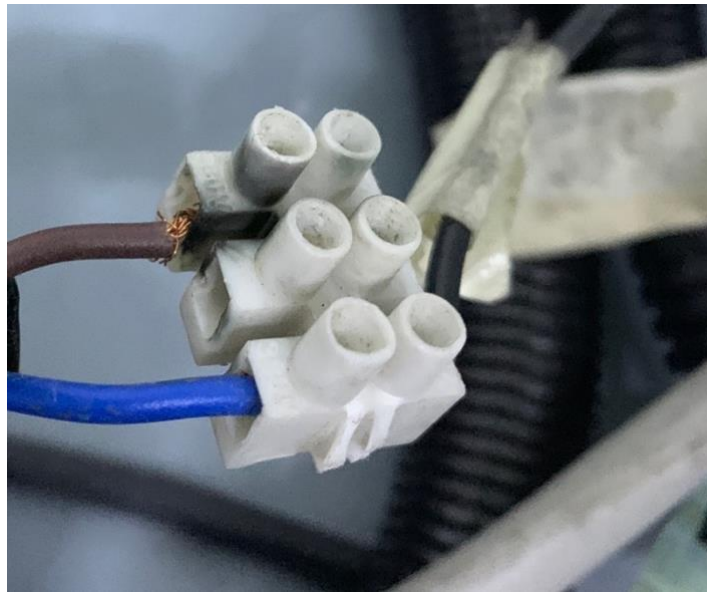


Figure 73: Exposed cable



Figure 74: Cables arrangement

The machine behaved also in a particular and strange manner since at the start of the day or when an error occurred due to overpressure or temperature, it needed to be powered on and off many times, until luckily all the drivers allowed the start of the machine and it started working. This problem was also annoying when the machine was in temperature because, in the time the machine allowed the restart of the motors, the plasticizer, extruder and nozzle would have cooled significantly. Sometimes it took more than 20 resets to get the machine working.

The cooling system was undersized, it used a low power pump to circulate the water in the machine, giving really low flow rate through the machine. This was even worsened by the tubes and connectors used in the circuit. Pneumatics joints with 90° curves were used and the tubes were 4 mm in internal diameter (Figure 75), which caused really high pressure losses throughout the circuit. The pneumatic connectors guaranteed easy removal of the tubes from the machine, but this is not needed since the circuit needs to be always connected and working.



Figure 75: Original cooling circuit

The tank for the water was positioned on top of the machine since the pump did not have enough head to bring the water from the floor to the highest part of the machine, at about 2 m. The tank itself was really small, no more than 10 liters of water were present in it and needed to be changed frequently.

The low cooling rate, shown in Figure 76, resulted in the control temperature reaching 60 °C in a small time interval even when printing at low temperatures, such as 230 °C.

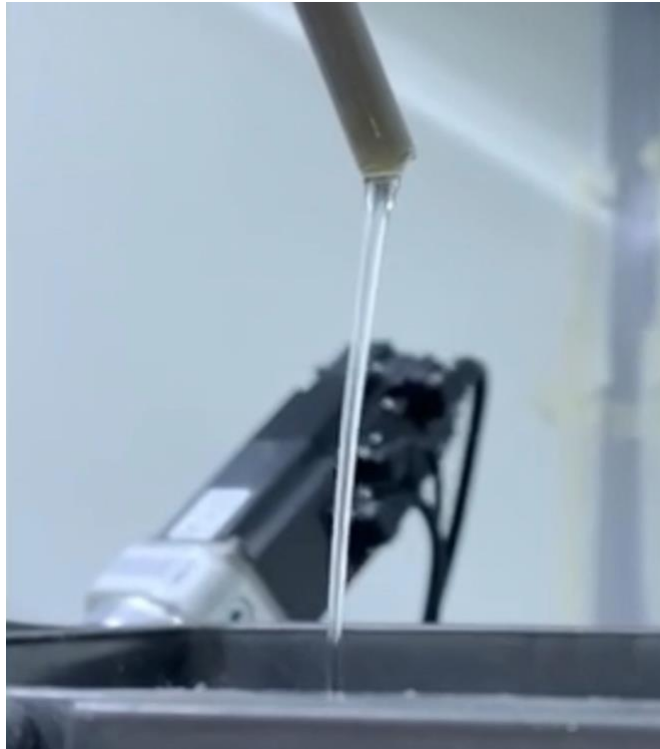


Figure 76: Flow rate of the original cooling circuit

The machine was limited by software to reach at maximum 230°C in all the different locations, this was wise having that low cooling rate, in order not to overheat the sensitive parts, but the temperature reached was not enough for many materials to be printed.

Another problem was that the machine would give thermal errors if it was directly set to go to 220 °C from ambient temperature, since the actual heating time was too low with respect to the “loop disconnection detection judgment time” [54] set from the software, and for the machine it was perceived as the heaters being disconnected, losing too much power or thermocouple malfunctioning, resulting in errors and need for a reset. The temperature control unit is indeed equipped with timers to detect thermal runaways, so that if the temperature does not rise of at least 2°C with the heater at maximum power in a predefined time interval it would block the system to prevent damages. This “loop disconnection detection judgment

time” was set too low for respect to the actual heating time in normal working conditions.

Another problem was that the heated bed was no more controlled in closed loop but the resistance was just connected to the 12 V power supply and it was running at maximum power for all the time. Even if it was set to maximum power it was not able to go at temperatures higher than 75°C, measured with an external sensor, since the resistance did not have enough power to go to higher temperatures. This problem did not allow a good bed adhesion and often resulted in warped pieces since the gradients in the object with the bed surface at these temperatures are too high. Not knowing the temperature of the bed is also a problem from a process point of view, since different materials need different bed temperatures for a proper adhesion to the build surface. It is even dangerous to run the resistance at maximum power in open loop for undefined time, since this component is designed to be controlled in temperature.

The pneumatic closure of the nozzle (Figure 77) was not configured. From a software point of view the machine tried to switch the commutator for the compressed air, but it was not attached to any compressed air tube and source, not being thus able to close the flow to the nozzle when needed.

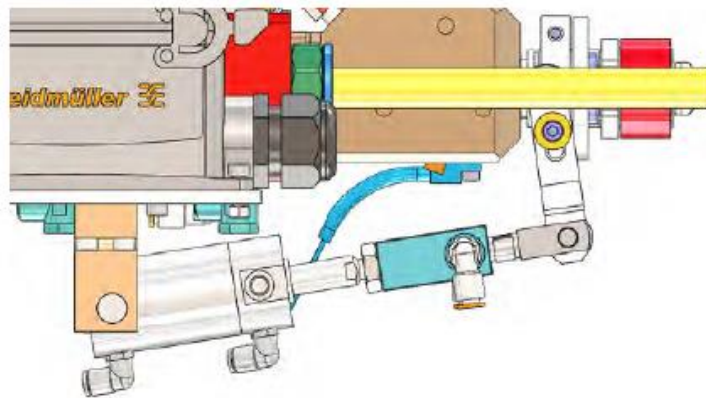


Figure 77: Schematic of the shutter [49]

The nozzle was of an undefined diameter, probably between 0.8 and 0.9 mm, consumed by years of extrusion and with a geometry which was not proper for the pneumatic closure to close the flow on it.

3.5 Thermal problem on the EFeSTO machine

All the problems explained in Paragraph 2.5.3 are still preset also in the building of objects with the EFeSTO machine, since these are common problems post extrusion of the EAM technique. In this section the attention will be focused on the main thermal problems for this specific machine, in particular prior to extrusion.

The extrusion unit was in origin designed to work as an injection molding unit, so with a viscosity of the material really low to have faster filling of the mold. This condition is achieved by raising the temperature of the extrusion chamber and nozzle. In additive manufacturing on the other hand the material has not to be too soft to prevent all the problems related to overheating and poor bead stability.

Thus, a compromise between the flawless working of the machine and the extrudate characteristics has to be found, this is achieved by regulating the temperatures of the chambers in order to get a viscosity which guarantees the possibility of extruding the material without overloading the motors and which is suitable, after exiting the nozzle and cooling to some extent, to perform FDM additive manufacturing. These temperatures have to be found experimentally by trial and error, since the geometry of the machine, thermal and viscosity characteristics of the specific material affect its behavior with EFeSTO and no technical datasheets can be used as given, but just as starting point.

Another important problem is thermal degradation of the material, which is a time and temperature related problem. The material, already plasticized, has to wait in the extrusion chamber (Figure 78) for some time.

During printing the piston moves really slow and it might take also half an hour to empty the chamber. This might result in problems, since the first material exiting from the nozzle, at a given temperature, could have good properties and good shape, while at the end, since the material has waited in the chamber for some time, the material might result degraded and the whole print has to be considered failed.

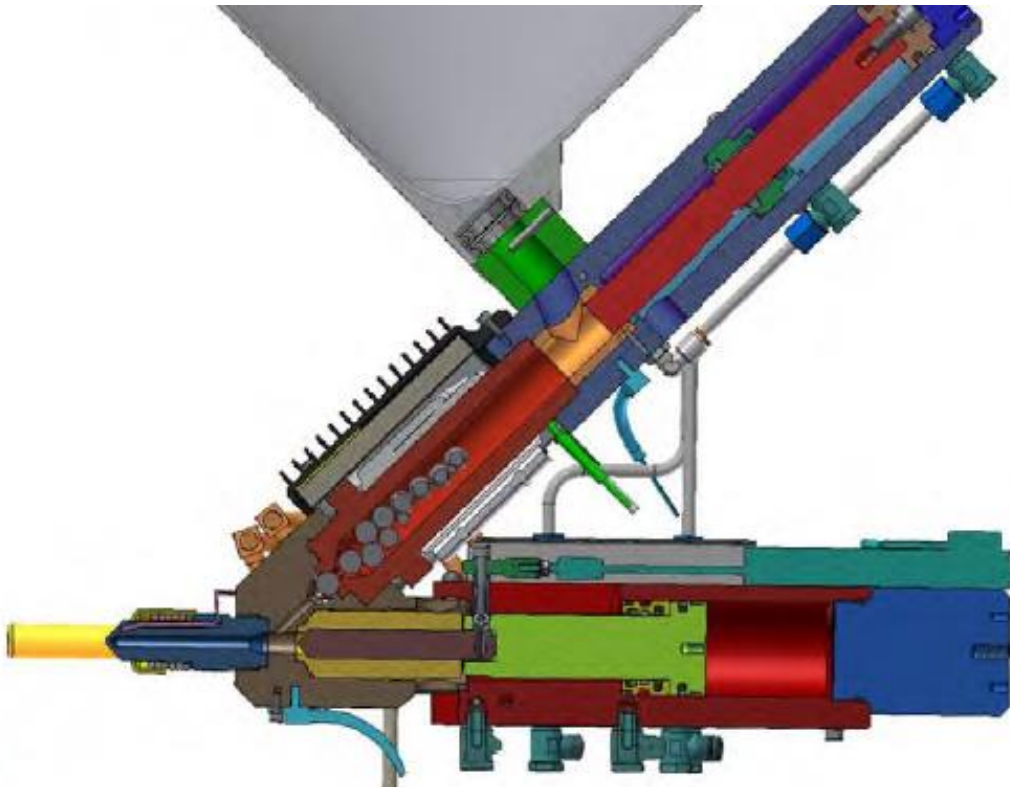


Figure 78: EFeSTO chambers section [49]

Also considering this problem the temperature of the extrusion chamber has to be set carefully, starting with the one which guarantees extrudability and not the overload of the motors and evaluating the results increasing temperatures.

In the most severe cases the degradation of the material might result in highly increased pressure needed for extrusion, which often cannot be guaranteed by the motors, or even in clogs.

The temperature of the body section and of the nozzle has therefore to be selected carefully, since a low temperature of extrusion might result in too high viscosity in the extruder and overload of the motors. A too high temperature in the extruder might result in thermal degradation of the material and too soft extrudate condition, not adequate to perform additive manufacturing. To solve these problems the decision I took is to set a temperature in the extruder chamber that would let the machine extrude the material without overload of the motors, but not so high to result in thermal degradation. After extrusion, with the improvements presented in Chapter 4, it is possible to control the state of the material depending on the geometry to be build, cooling it more rapidly with the fan or increasing the heat flux throughout the piece with IR preheating.

Another important aspect which was underestimated in the configuration I found the machine is the cooling of the parts which are sensitive to heat and the ones which needs to be cool. In particular the motors need to work at a proper temperature, not even close to the one needed for the plasticization and extrusion of the material. The motors themselves produce heat due to joule losses while working since some current is passing in the windings to produce the torque needed. This, in addition to the heat coming from the chambers, might increase their temperature reducing their efficiency or even damaging them, so a proper cooling is important. The bearings, ball screw and pistons also need to be at a controlled temperature to work properly, an improper heating of the pistons would result in blockage in the cylinder sleeve with consequent damage of the machine. Another part which needs to be cooler with respect to the chamber's temperature is the hopper and hopper channel, in order to prevent partial softening of the material in this section which would result in improper feeding to the plasticizer or clogs. The cooling system is therefore really important to separate the zones which need to be at higher temperatures from the ones which need to be at ambient one, to do so a proper flow rate of relatively

cool water is necessary. The channels are already designed in critical positions and with adequate section and length to cool the machine, but the tubes and pump in the initial configuration were not able to guarantee the necessary cooling action.

3.6 Limits of the machine

The machine is a completely different approach to FDM additive manufacturing, both from the extruder point of view and from the kinematics point of view. The extruder gives great freedom in the material which can be used, since all the possible mixture of metals, ceramics and thermoplastics can be printed. This choice also reduces the cost of the material, since pellets are way cheaper than filaments due to the absence of one productive step, the extrusion of filament starting from pellets.

The kinematics is also innovative since in most printers the DOF in space are assigned partly to the hot end and partly to the build plate. In delta printers all the DOF are assigned to the nozzle unit, but it is extremely rare that those are assigned to the build surface.

Nevertheless, being this machine still a prototype some limits are present. It has to be pointed out that due to the two chambers configuration pieces to be produced will come with better properties and quality if their volume is such to be built with just one chamber. The machine has a feature for which, if the material in extruder chamber is about to finish, the job will be paused, the piece moved away from it, the shutter closed and the chamber recharged. This feature is still under development and has to be refined, since once the shutter re-opens and the job is restarting the material takes some time to fill the channels close to the nozzle and a part of the layer will thus be missing. Even if this feature would be fixed, with the material coming out of the nozzle as soon as the extrusion head approaches back to the piece, the interruption of the print for recharging would let the already

extruded piece cool and thus the layer adhesion in the junction layer after recharging would be poor.

Another limit is the impossibility to perform retractions, which in filament FDM consist in the extruder pulling away the filament from the nozzle really fast when a travel move is about to start. With EFeSTO instead the material above the nozzle is already a viscous fluid and the retraction of the extruder piston would only result in a reduction of pressure on the material, but the latter would anyway ooze due to gravity. The possibility of closing the pneumatic shutter at every travel move would still give not satisfying results since the material present in the channels below the closure and orifice could anyway drop. Once the shutter is opened back there would be the problem of making the flow of material reach the orifice, resulting in an incomplete extrusion in the first moments after the shutter opens.

4 Improvements on the machine

In this section the improvements made on the EFeSTO machine are presented, mainly addressing the thermal issues of this additive manufacturing machine but also the ones needed for a proper working of the machine.

4.1 General improvements

First of all, I began by ordering the cables to have a cleaner workspace and the cables positioned according to their function, all the cables of the steppers passing in one tube and the ones for the temperature control in another one (Figure 79). I removed a broken cable which was just laying around and removed all the exposed connectors. To order the cable some clips made with a desktop additive manufacturing machines were designed, both for attaching the cables to the sides of the linear rails and to the base of the machine.



Figure 79: Ordered cables

For the heated bed cables and many other small cables laying around with different purposes I used a spiral cable wrap, which guarantees higher order without the need of disconnecting the cables to install or remove the wrap.

After a long troubleshooting reading the error codes on the servo drives and comparing them with the Mitsubishi error code guide [55], I managed to understand that the batteries which were used by the drives to keep the absolute position of the encoder were completely discharged. Thus the servo drives, every time the machine was switched off, lost their absolute position and would restart with an error, not allowing a proper start of the machine. This was the reason for the many resets needed for the machine to start. I changed all the 5 batteries of the stepper drivers with original batteries from Mitsubishi, model MR-BAT6V1, presented in Figure 80. Now the machine initializes as designed at first trial, without losing anymore the position of the motors.



Figure 80: Servo driver battery

4.2 Cooling circuit

As mentioned in the previous paragraph the cooling circuit was inadequate for the heat flow coming from the different chambers and lead to an overheat of the sensitive parts. I designed a new circuit, keeping the

channels present in the machine but providing more pressure and flow rate in order to remove more heat.

To do so I removed all the pneumatic joints (Figure 82) and substituted them with brass joints (Figure 83) which allow coupling with standard water hoses, I used a 10 mm internal diameter hose (Figure 81) to deliver water to the different parts of the machine.



Figure 81: Tube used for water circulation

These modifications allowed to remove unnecessary pressure losses through the circuit. I used Teflon tape on the threads to prevent any leakage and metal screw fasteners to set the tubes on the brass joints.



Figure 82: Old pneumatic connectors



Figure 83: New G1/8 brass connectors

The water tank was changed with a 50 liters tank placed on the floor, shown in Figure 84, which allows a much safer operation since the probability of tipping over and spilling water are minimized.



Figure 84: Water tank

The greater volume of water also gives higher thermal inertia to the circuit, since more water at ambient temperature is present and to rise the temperature of the whole tank more heat extracted is required. To have an idea of the water temperature an insulated thermistor with direct digital reading was put in the tank.

The pump was obviously changed, I choose a Seaflo 12V pump which guarantees 10,5 liters per minute of flow rate or a maximum pressure up to 3,45 bar. In Figure 85 the pump characteristic curve is presented, showing the relation between flow rate and pressure which the pump can provide.

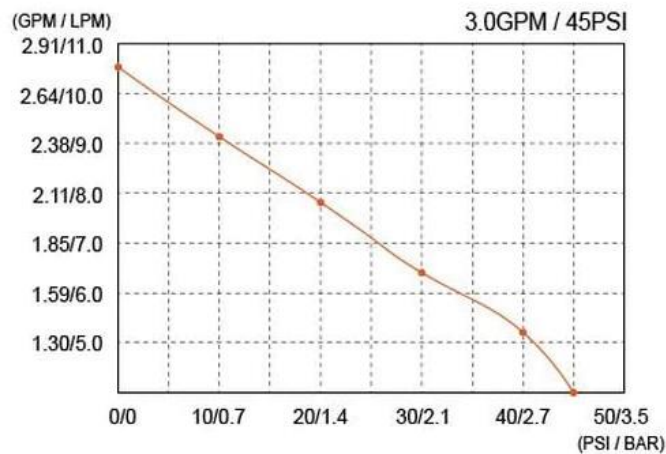


Figure 85: Pump characteristic curve

The pump (Figures 86 and 87) is a diaphragm pump with three chambers made with high quality materials, the maximum pressure can be adjusted with a screw and the pump automatically stops if the pressure exceeds the one which has been set, thanks to a pressure switch. The pump is self-priming and can run dry, thus it does not need to be placed in the lowest part of the circuit with water on one end but it can automatically pull the water from the tank.



Figure 86: New pump

This pump allows greater flow rate than the pump used before and has also a sufficient power to lift the water to the top of the machine still keeping an adequate flow rate to extract heat from the machine.

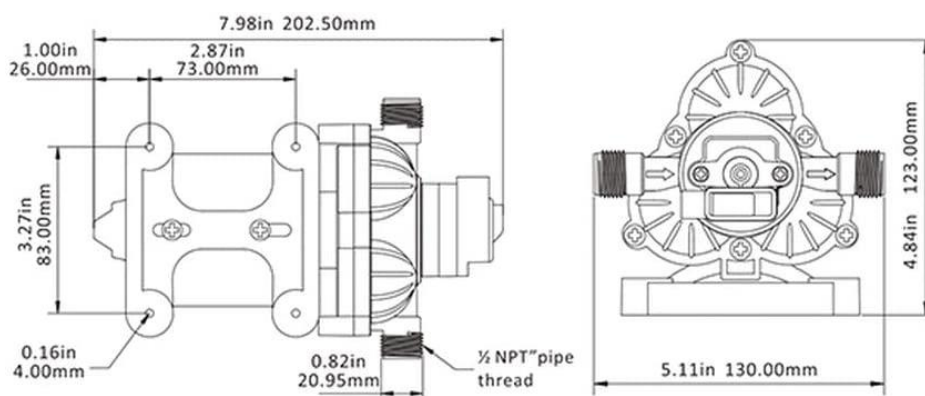


Figure 87: Dimensions of the pump

The pump has an overheating protection since its temperature might increase up to 100 °C with continuous use of the circuit. To prevent the overheat of the pump's motor in the working day two 5015 fans were placed on its sides. The fans were placed with additive manufactured supports mounted on an aluminum sheet on which also the pump was attached for better stability and vibrations damping, as shown in Figure 88. These fans also work at 12V and guarantee a satisfactory air flow rate for the job.



Figure 88: Pump structure with fans

The pump and fans are powered by a 12 V 100 W switching power supply, which can guarantee enough current for the pump to work properly.

To further increase the high temperature performances of the machine water-cooled heatsinks (Figure 89) on the brushless motors of the extruder and loader were installed. These heatsinks have an internal channel for water circulation with fins to increase conduction with water.



Figure 89: Motors water-cooled heatsink

Steppers motor indeed do not produce much heat due to joule losses and in many cases just the conduction with the structure they are installed on is enough to prevent overheating of the motors themselves. The motors of the delta platform for example are installed on the metal linear guides which

move the sliders and conduction with them ensure no overheating for the whole working day, even on heavy loads. The motors of the extruder and loader instead are only in contact with the extrusion unit, which instead of taking the heat produced from the motors provide some additional heat coming from the resistances. That is why often these motors used to get hot after few hours of working and I decided to enhance the cooling action on them with heatsinks, these were installed with Noctua thermal paste (Figure 90) to increase conductivity on the contact surface.



Figure 90: Thermal paste used

In Figure 91 the configuration of the heatsinks for the stepper motors is presented.

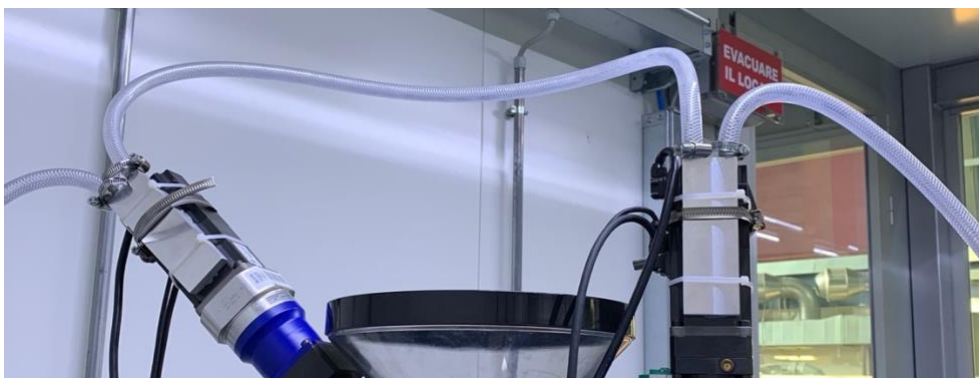


Figure 91: Heatsinks mounted on the motors

With the updated cooling system the machine is able to work with ABS (extrusion temperature 230 °C) for a complete working day without the cooling water increasing too much its temperature (maximum 36 °C in one day), read from the thermistor shown in Figure 92, and the control temperature reaching a steady state at 40 °C. It is not actual equilibrium since after few hours the temperature of the water increases slightly and the control temperature can increase by 1 or 2 °C, but never approaches 50 °C.



Figure 92: Tank temperature reading

The purpose of this improvement is mainly to have a more reliable machine, capable of printing for long time without damaging the sensitive parts due to overheat, it is also really useful for reaching higher temperatures needed for high performance thermoplastics such as ULTEM, PEEK and PEKK.

4.3 PLC tuning

Using the software GX Works from the MELSOFT suite I managed to change some thermal parameters on the temperature control unit, by communicating via USB with the PLC. In particular I increased the “loop disconnection detection judgment time” until no more alerts showed up

during normal heating of the three controlled zones and allowing direct setting of high temperatures from ambient ones.

With the improved cooling system I was also able to increase the working temperature range up to 410 °C, with a careful analysis through a thermal camera of the temperatures reached by different zones with increasing temperature of the chambers and by ensuring that the control temperature stays low. It is now possible to reach 390°C for more than 3 hours before the pistons zones reach a temperature higher than 55°C. This is mainly due to the water in the tank heating up to 39 °C, losing its cooling action since the gradient between the zone at about 50°C and the water gets too low for a considerable heat extraction. The useful working time at such high temperatures can be increased by changing the cooling water or, in the future, by implementing a chiller or refrigerator for the water in the tank. These improvements are respectively finalized to have an easier workflow and to have the possibility of printing high temperature plastics.

4.4 Heated bed

To fix heated bed and control it in closed loop I decided to use the a new resistance with embedded thermocouple, a desktop 3D printer motherboard, a Solid State Relay and the opensource software Marlin, which is able to handle a complete desktop 3D printer, including controlling the motors, temperature, reading of a G-code file, interpolation of the G-code points, auto-leveling with mesh generation of the build surface with a proximity sensor and many other tasks. For our purposes only the PID control on the heated bed surface and fan PWM control are useful and thus will be implemented. The marlin software was modified with the characteristics of the thermistor used, the maximum bed temperature of 250°C and adjusting the thermal protection timers since the heated bed is a thick plate of aluminum, shown in Figure 93, which takes some time to heat up. The maximum temperature set in Marlin is higher than what the new

resistance could achieve, but achievable with an even more powerful resistance or with preheating through IR lights.

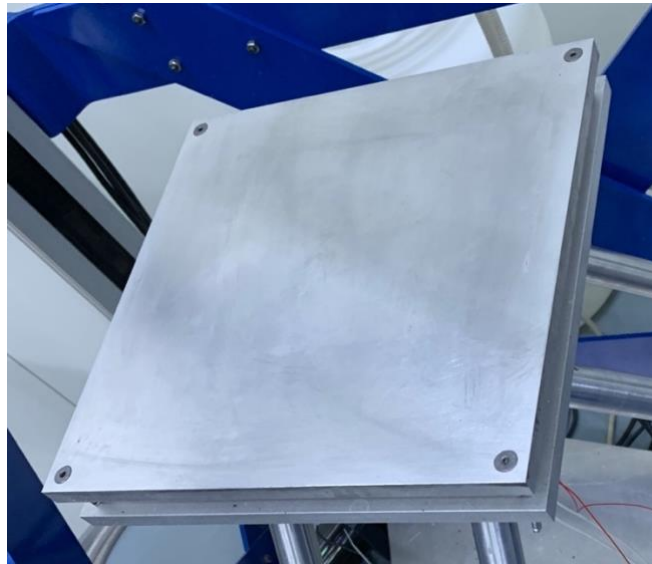


Figure 93: Cleaned build surface

The resistance chosen was a 200 W silicone rubber heating pad developed for FDM machines' heated build plate (Figure 94), the dimensions of the pad are 200x200mm and it has an embedded thermistor, model NTC 3950 100K, to measure the temperature at the base of the heated surface.



Figure 94: New resistance with thermistor

The measuring point is not the most appropriate since a difference in temperature will be always present between the bottom and the top of the build plate. By leaving the build plate at the set temperature the situation will be uniformed up to an adequate point. The resistance works at 220V AC, so a solid-state relay (Figure 95) will be used to control its behavior with the board powered at 12V. A solid state relay works similarly to an electromechanical relay but it does not have moving parts thus allowing higher switching frequency, for the relay chosen the switching time is lower than 10 ms.



Figure 95: Solid state relay (SSR)

The absence of moving parts also ensures a silent operation an increased lifetime, since no mechanical wear is present. It is composed by a triode for alternating current (TRIAC) which allow the opening or closing of the AC circuit when a control signal is respectively high or low. Thus it allows to control the AC line with the PWM signal coming from the board based on PID control on the temperature error. In Figure 96 the electrical schematic of a TRIAC is presented, it can conduct current in both direction when the gate is high, being thus ideal for AC circuit switching.

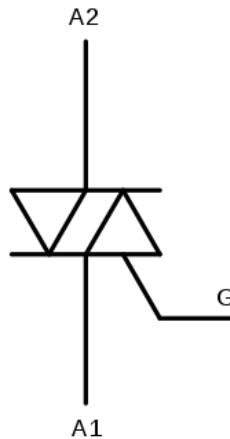


Figure 96: Electric representation of a TRIAC

In the SSR the coupling between the AC 220 V line and the 12 V line coming from the microcontroller is achieved in an optical way. The control voltage switches on a LED, which illuminates a photo-sensitive diode, the current of the diode is applied on the gate to switch the load. The optical coupling allows the control circuit to be electrically isolated from the load. The maximum voltage applicable to this specific SSR is 480 V with 40 A of current, more than what is needed for the bed, allowing a safe operation. The board chosen to control the bed and fan is an SKR V1.4 produced by BigTreeTech (Figure 97), it has a 32bit microcontroller and it is more than enough for the purposes, it is powered by the same switching power supply which is used for the pump. The board, as the Marlin software, is designed to handle a whole desktop additive manufacturing machine, but only the PWM control and analogic temperature reading are used in the EFeSTO machine setup.

In the new configuration it is possible to know at which temperature the bed is at every time instant and to control the temperature of the bed with accuracy and reliability. The bed can reach 145 °C with the resistance power but temperatures up to 200 °C can be reached by heating the bed with the infrared heater, presented in the Paragraph 4.7. The purpose of this improvement is to increase the first layer adhesion and reduce the tendency for warping in big prints with high shrinkage materials.

4.5 Pneumatic closure of the nozzle

The pneumatic closure of the nozzle was already configured from a software point of view and the mechanical components of the closure, such as the pin inside the nozzle, the arm and pneumatic actuator were already present. In the last years it was not used since the machine was not working properly but now it should be used since it guarantees a more clean and safe working on the machine. It is indeed possible to close the nozzle both when approaching the nozzle with the build surface, avoiding drops of material on the bed, but also when recharging the extrusion chamber, both during print or at the beginning of the working cycle.

The pneumatic shutter works by pushing a pin onto the inside of the nozzle, thus closing the hole from which the material should come out. The actuator only pushes the pin down, while, once the actuator is not exerting pressure on the pin, the pressure of the material pushes it up and opens the nozzle. In Figure 99 the schematic of the shutter control switch and actuator is presented.

To configure the shutter I used pneumatic tubes for compressed air and pneumatic connectors, linking the pneumatic switch with the compressed air outlet in the lab. Other two tubes were used to connect the switch with the two chambers of the pneumatic actuator.

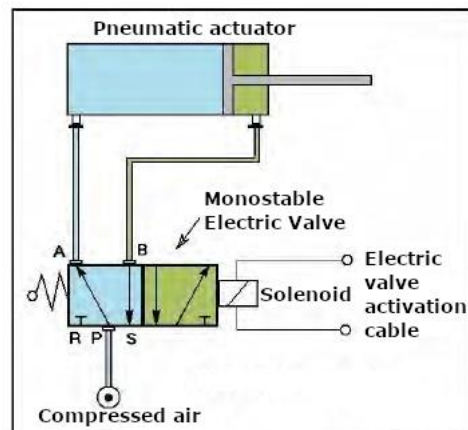


Figure 99: Schematic of the shutter control [49]

The nozzle present on the machine did not have the internal surface matching the angle of the pin, so the closure did not work properly when configured. The design of the new nozzle took that into account, by having a final internal angle of about 90° to match the one of the pin, as the original nozzles of the Babyplast machine.

4.6 Layer fan

As mentioned in the previous paragraph, one of the main solutions for problems related to an excess of heat flux through the piece is a layer fan, this was not present on the EFeSTO machine, leading to many overheating problems, such as poor bead stability and impossibility of making good overhangs and bridges as pointed out by G. Herve [56].

I chose a 12 V 5015 fan for cooling the layers, since it guarantees adequate flow rate and low consumption, at maximum power it spins at about 6500 rpm and draws 0.18 A. The technical drawing and appearance of the fan is presented in Figure 100.

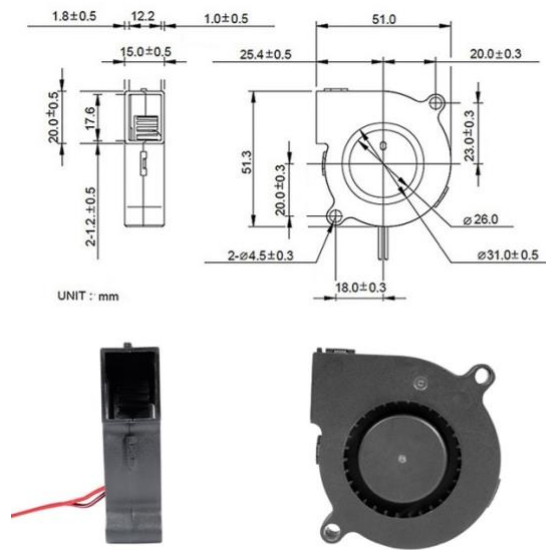


Figure 100: Dimensions and appearance of a 5015 fan

It is powered by the 12 V switching power supply and controlled through PWM by the Marlin Software on the board which also handles the bed. The water pump could be controlled by this board too but it is better to always run it at maximum power to ensure enough cooling rate of the sensitive parts. In most FDM additive manufacturing machines the duct to convey the air close to the nozzle tip is done with additive manufacturing technique in thermoplastics, but in this case this solution might gave problems. The duct has indeed to pass below the infrared lights, presented more in detail in the next paragraph, so if it was made from plastic the risk of melting it would have been high. For this reason, the duct is made with a copper tube with diameter 10 mm, which addresses the air right at the tip of the nozzle (Figure 102), with the fan away from any heated element to have cool air at the intake. On the intake side an additive manufactured joint has been designed and produced to connect the fan with the copper tube (Figure 101).



Figure 101: Fan and connection with copper tube



Figure 102: Copper fan duct

This improvement was introduced to increase and control the convection coefficient and thus cool faster the deposited layer in some geometries. Other than to make bridges and overhangs the layer fan is also useful when the time to deposit a layer is short and thus when depositing the next one it might still be too soft to maintain the desired geometry.

4.7 Infrared preheating for high temperature thermoplastics

High temperature thermoplastics, as explained in the previous paragraph, often need an enclosed chamber to be printed correctly. Since enclosing the build volume of this machine would have been difficult, due to the large volume and to the presence of sensitive parts that would be enclosed too, I decided to build an infrared heater to convey heat only where needed. The purpose of infrared preheating is to keep the previously deposited layers at a temperature close to the material glass transition temperature in order to have a better layer bonding and diffusion, resulting in higher tensile strength.

The heater is composed by three IR lamps, a reflector used to irradiate only the build plate and a separated controller which is able to reduce the power flowing to the lamps in a 230 V AC line. A model of the reflector is presented in Figure 103.

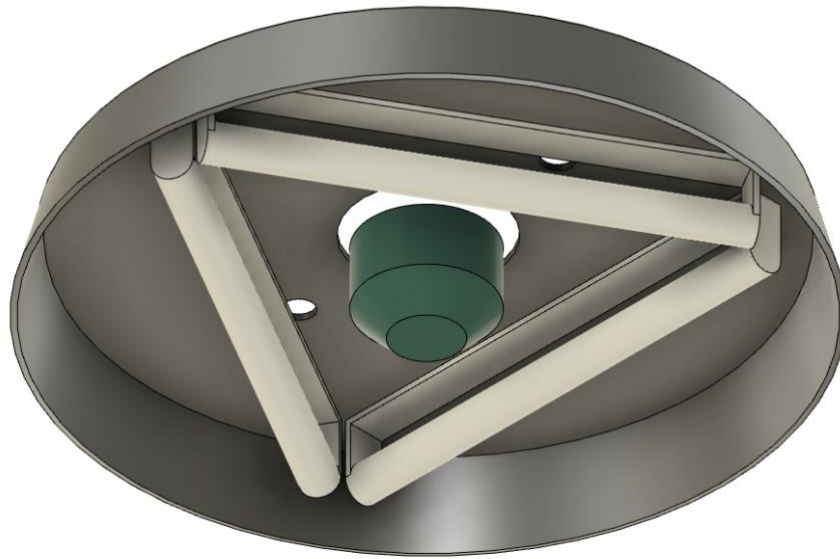


Figure 103: Model of the infrared heater

The reflector chosen has a circular cross section, with conical sides in order to reflect better the light on the piece, it has a base diameter of about 210 mm and its height is 30 mm, it is made of aluminum and is connected to the

machine frame using the holes of the two shafts which hold the extruder. It has a centered hole to make the nozzle unit pass through it, a hole for the copper tube for the air cooling and three holes for the cables of the lights. The lamps, presented in Figure 104, are from RS Pro, their dimensions are 118 mm in length and 10 mm in diameter, with R7S end style. Each one is 300 W and powered by 230 V AC, they are manufactured from doped quartz and convert virtually all the electrical power into heat, with minimal losses. The lamps heat the material mainly by radiation in the IR range and convection with air. The manufacturer ensures 5000 hours of useful life and that they are dimmer-able, perfectly matching the needs of the machine. Three lamp holders are obviously used, with R7S connection and made in metal and ceramics to avoid the risk of melting any material present in the reflector. The size of the lamp holders is carefully chosen in order not to exceed the height of the reflector.



Figure 104: IR lamp

The controller is based on Silicon Controlled Rectifier (SCR) technology and in particular it uses a TRIAC governed by a potentiometer, the exterior aspect is presented in Figure 105.

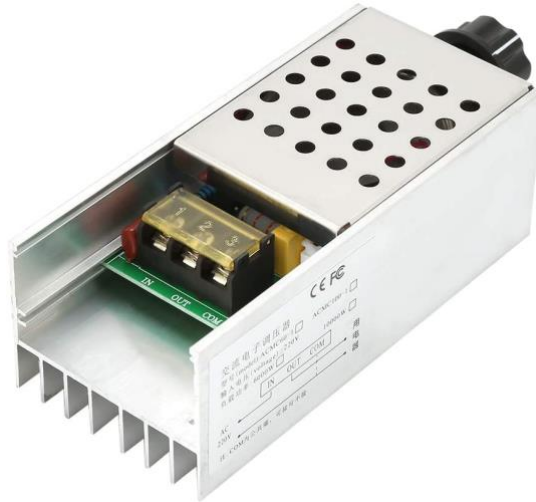


Figure 105: Lights controller

It is designed to sustain a continuous power of 3000 W and a peak one of 6000 W, since a large heatsink is present in contact with the TRIAC. The TRIAC used in the controller is a BTA41600B with an efficiency of about 90%. The TRIAC is insulated and can work at 600 V and 40 A, but limited in this controller for thermal management problems. The transmissible current is indeed decreasing rapidly to 0 A if the temperature of the case exceeds 75 °C as shown in Figure 106.

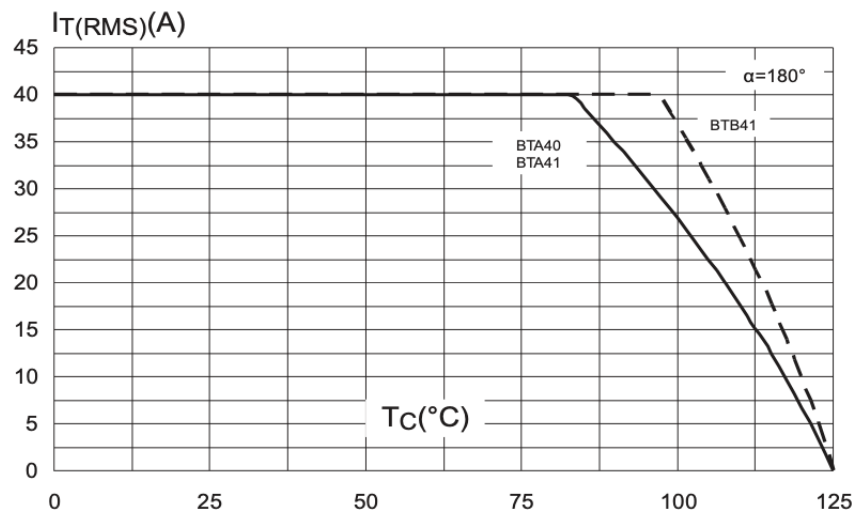


Figure 106: TRIAC behavior respect to case temperature [57]

The controller will be placed in a cool area on the frame of the machine, increasing the conduction possibilities.

In Figures 107 and 108 it is possible to see the reflector mounted on the machine and working.



Figure 107: IR heater side view



Figure 108: IR heater front view

4.8 Nozzle

As mentioned before the nozzle was also a critical part in EFeSTO, since its diameter was unknown and probably produced without the right tolerances, its internal geometry was not appropriate for the pneumatic shutter and was too short to be used with the infrared preheating, since it would have been just 1 mm longer than the height of the reflector, not allowing to see if the job was proceeding in an adequate manner in the first layers, the most critical ones.

The nozzles have been designed with orifice diameter of 0,6 mm or 0,4 mm; the other features are identical between the two.

In the design of the new nozzle I started from a drawing of the original injection molding nozzle from Babyplast, using the internal geometry present in the original nozzle to ensure compatibility with the closure of the nozzle. The thread and flange are also identical to the original nozzle for a precise mounting on the machine. The nozzle perpendicularity with the machine body is governed by the upper flange which strikes on the internal of the body, for this reason geometrical tolerances have been used on that surface as shown in Figure 109.

As shown in Figure 109 tolerances to ensure concentricity of the critical features have also been used. Since the pneumatic closure was designed to close a 2 mm hole and a longer nozzle was needed for the beforementioned reason, a 2 mm in diameter channel with length 13,2 mm was designed at the end of the conical section. The 2 mm channel also have the functionality of streamlining the flow and aligning it for the subsequent extrusion. This channel then reduces to 0,6 mm or 0,4 mm with a 120° angle, mainly chosen to simplify the production, although the fluid dynamics is not optimal.

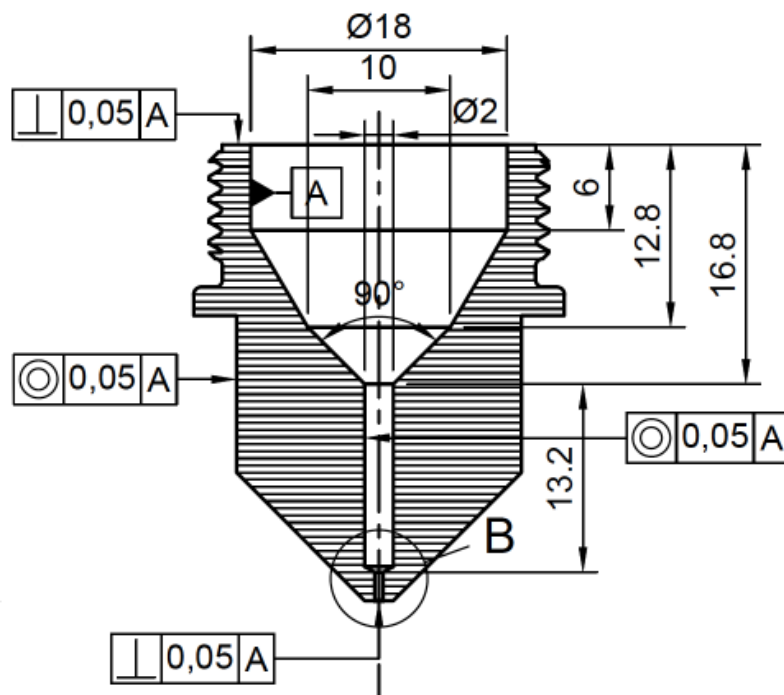


Figure 109: Technical drawing of the nozzle

The orifice has a circularity tolerance lower than 0,02 mm, ensuring a precise extrudate dimension and shape. The orifice channel has an L/D of 3,3 and 5 for the 0,6 mm and 0,4 mm diameter respectively.

The resultant nozzle has a length of 32 mm, ideal to see the first layers being deposited with the reflector mounted.

The nozzles have been produced by WatAJet s.r.l, starting from a bar of hardened and tempered steel 39NiCrMo3, with hardness 250 HB. They have been made on a milling-turning machine by turning, drilling, boring and milling. The 0,4 mm one has been processed also on an EDM machine to make the orifice, since the diameter is too small and L/D too large to be processed with their milling machine. In Figures 110 and 111 one of the produced nozzles is presented.



Figure 110: Nozzle tip view



Figure 111: Nozzle back view

The nozzle was modified to have a more coherent flow and a known extrudate diameter, with small uncertainty. It was also designed to implement the IR preheater and the pneumatic closure. In annex A the technical drawing of the nozzle is attached.

4.9 Summary of the modifications

Improvement	Purpose	Before	After
General improvements	Cleaner workspace and smoother workflow	Impossible to walk by the machine and really long startups and resets	Good workflow and easy to watch closely the machine working
Cooling System	Reliability and smoother workflow	Thermal problems of the sensitive parts even at low temperatures	High temperature printing possible
PLC Tuning	Smoother workflow and high temperature printing	Need to set temperature by steps to prevent errors and impossibility to go higher than 230 °C	High temperatures (up to 410 °C) can be reached by setting them directly
Heated bed	First layer adhesion and reduce warping	Impossible to control the bed temperature and to reach temperatures higher than 75 °C	Bed temperature can be controlled in closed loop up to 145 °C
Pneumatic Shutter	Smoother and safer workflow	Impossible to close the flow to the nozzle	The flow to the nozzle can be stopped thus preventing oozing
Layer Fan	Solve problems related to high heat flux	Impossible to control the cooling rate of the deposited filament	Possibility to control the convection cooling effect on the piece
IR preheater	Intralayer bonding and strength increase in HT plastics	Impossible to control the substrate temperature to increase layer bonding	In big layers prints possibility to heat the previous layers to increase bonding and reduce shrinkage
Nozzle	Increase printing precision and compatibility with other components	Difficult to define orifice size, not compatible with pneumatic closure and IR preheater	Precise and known orifice dimension, more coherent flow, compatibility with shutter and IR preheater

Table 4: Summary of the improvements

5 Experimental campaign

In this section the experimental campaign carried out with the improved EFeSTO machine with ULTEM material will be presented, including problems, solution and result obtained.

The possibility of printing high temperature material has been enabled by the modifications on the PLC and the improved cooling circuit, before these improvements the machine was not printing correctly neither PA nor ABS, it could only safely handle ceramic and metal printing, which, due to the binder low glass transition temperature, could be printed at temperatures lower than 180 °C.

In Figure 112 the final setup of the machine while printing a first layer is shown.

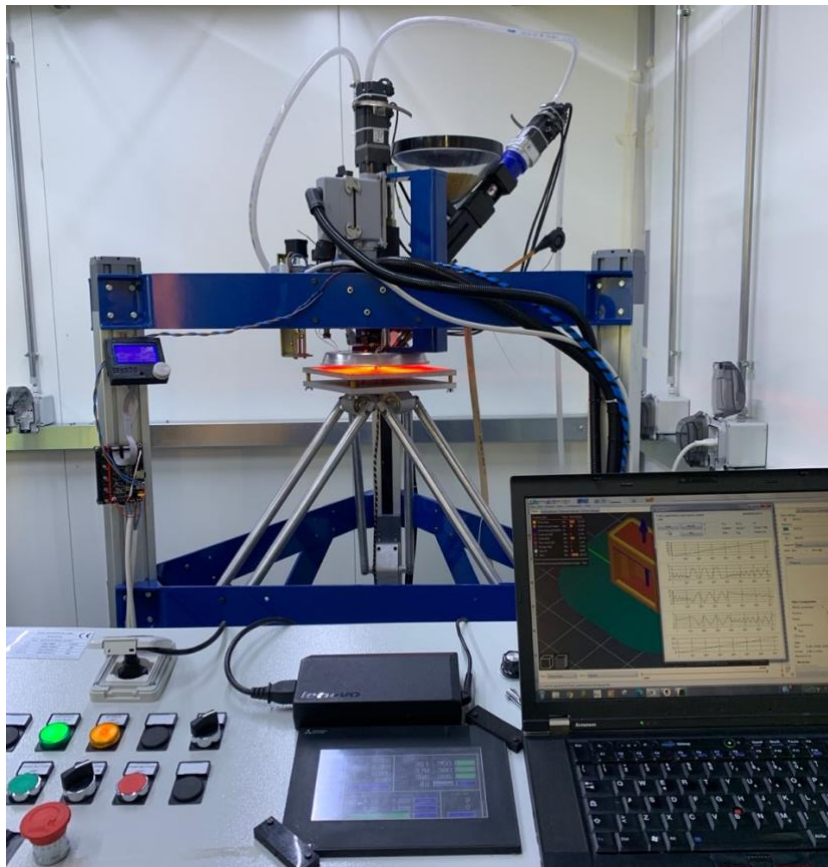


Figure 112: EFeSTO machine while printing the 1st layer of a sample

5.1 ULTEM

ULTEM is the commercial name given by the main producer Sabic to PEI, PolyEtherImide resin. PEI is an amorphous high performance polymer, which has the structure presented in Figure 113.

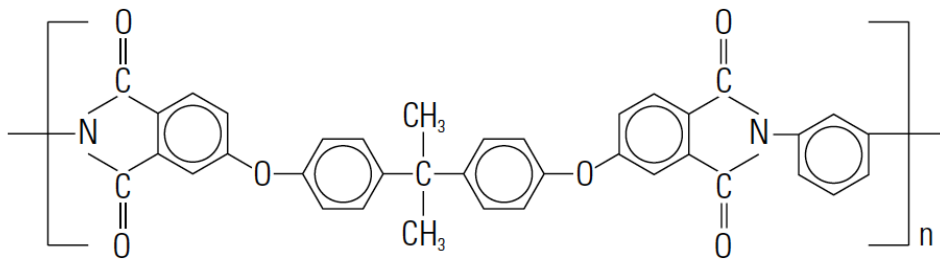


Figure 113: PEI molecular structure [58]

The key properties of PEI are:

- High long-term heat resistance with a glass transition temperature above 215 °C;
- Flame retardancy and low smoke burning evolution;
- Resistant to many chemicals such as hydrocarbons, automotive fluids, alcohols and aqueous solutions;
- High strength and modulus at ambient temperature and at elevated temperatures;
- Good dimensional stability with low creep sensitivity and low CTE;
- Compliancy with European and American food contact regulations;
- Stable dielectric constant and dissipation factor over a wide range of temperatures and frequencies.

Thanks to these outstanding properties in the field of thermoplastic ULTEM resin finds applications in many fields such as tableware, items for food preparations and storage, medical field, automotive field, telecommunications, aircrafts, electrical field and fluid handling field [58].

It is also a common material used to make direct Rapid Tools in production systems due to its high strength and high resistance in high temperature environments.

Its natural color is transparent amber brown and it is manufactured by polycondensation, shown in Figure 114, different types of this resin do exist depending on the application. The different resins in the PEI family are usually identified with a number and can differ in wear resistance, heat resistance, chemical resistance, strength, processability and some of them can be glass or carbon fiber reinforced.



Figure 114: ULTEM pellets

ULTEM resins can be welded with ultrasonic welding or assembled using adhesives such as epoxy glues. They can be painted and subjected to metallization with Physical Vapor Deposition, Plasma Enhanced Chemical Vapor Deposition or electroplating.

In this thesis I used the grade ULTEM 1000 from Sabic, which is the general-purpose resin, it is unreinforced, with exceptional high heat resistance,

strength and stiffness. It is inherently flame resistant according to UL94 V0 rating and has a good chemical resistance.

ULTEM 1000 has a density of 1,27 g/cm³, its conductivity is 0,22 W/(m°C), a linear CTE of about 5 10⁻⁵/°C in all directions and a specific heat capacity of about 2000 J/(kgK). The tensile stress can reach up to 110 MPa and the elastic modulus up to 3200 MPa according to ISO 527.

It tends to absorb water as all thermoplastics, but will only reach a 0,25% moisture content in 24 hours at room temperature of 23 °C. For extrusion and injection molding its moisture content has to be reduced to values lower than 0,02%, so drying of the material is mandatory.

In Annex B the complete datasheet of the chosen material is presented

5.2 Dryer

As for all thermoplastic the drying process is a key step before extrusion and injection molding to remove most of the moisture absorbed due to ambient exposure. Considerable moisture content might result in burns due to water boiling at extrusion temperature, voids in the extruded filaments and worse mechanical and physical properties.

To remove moisture I used the ARID dryer from 3Devo (Figure 115), which is a machine designed to dry polymers prior to filament extrusion.

It has a hopper to contain the material with a stirrer which moves the flakes to enhance the moisture removal on all the volume. Thanks to a resistance and a blower, while stirring the pellets, hot air at a given temperature is forced to flow through the material, heating the flakes and removing moisture.

For the ULTEM resin I followed a drying cycle of 16 hours at 120°C to remove moisture as much as possible and enhance properties of the extrudate.

After the drying cycle the material has been stored in enclosed jars or in the sealed hopper of the EFeSTO machine.



Figure 115: ARID drier by 3Devo

5.3 Materials for improving bed adhesion

A successful first layer is really important for the success of the building process, indeed bad first layer adhesion might result in warping but even detachment of the object from the build plate.

Every model has been sliced with a 10 mm brim in the first layer to increase the area of contact with the build surface and reduce the warping tendency. The brim is a structure composed by loops around the external perimeter of the first layer.

To improve adhesion of the first layer in addition to the brim, to make stresses due to shrinkage not give any strain, two different approaches were tried.

At first, I used Dimafix Spray, an adhesive engineered for improving adhesion of ABS on many build plate materials. It worked great in preventing warping on ABS samples printed at 230 °C with a bed temperature of 120 °C. In Figure 116 the Dimafix's adhesive power on ABS with respect to temperature is presented.

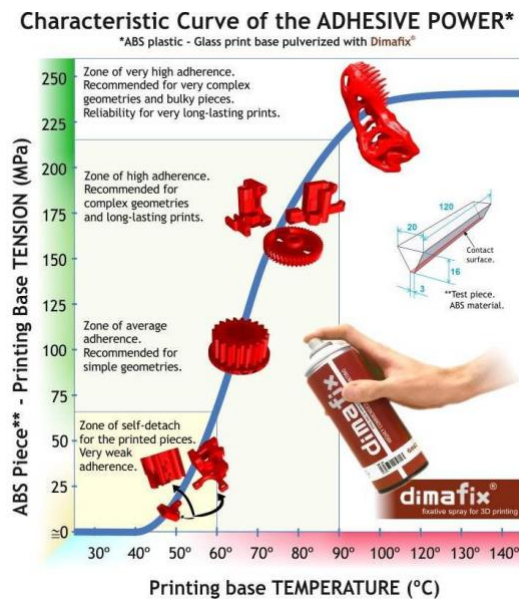


Figure 116: Dimafix characteristic curve

For ULTEM printing instead it has been noticed that it was not the most appropriate adhesive, since above 125 °C it started to degrade and lost its properties, thus preventing higher build plate temperatures. Printing ULTEM with bed temperature of 125 °C gave warping in some warpage prone geometries such as tensile tests but worked for compression tests. That is mainly due to high shrinkage stresses generated in long pieces rather than circular ones, in which the stresses are reduced and more uniform. Thermal stresses generated with ULTEM printing are higher in magnitude with respect to ABS due to the higher gradient from extrusion temperature (350-400 °C) to bed temperature (125°C). The Dimafix spray did not have enough adhesive force to retain the print on the build surface.

To solve the problem I used Magigoo HT (Figure 117), engineered for improving adhesion specifically for high temperature plastics such as PEEK, PEKK and PEI, which is sold in form of stick to be applied on the build surface.



Figure 117: Magigoo HT adhesive

This adhesive work in an adequate manner also for complex and elongated geometries, giving good bed adhesion for tensile tests with a bed temperature of 150 °C. The spreading on the build surface is harder than with the spray but once evenly distributed the object sticks to the bed even when high thermal stresses are present.

To improve the adhesion in addition to the beforementioned adhesives, a PEI sheet has been placed on the build plate, in order not to print on bare metal but on a plastic surface, to which the extruded filament is supposed to stick better.

5.4 Models designed for the campaign

The experimental campaign is intended to test the additive manufacturing quality and properties of the improved machine with a high temperature material which is not easily printed on many FDM machines, ULTEM.

To begin the experimental campaign some simple cubes and flat blocks have been designed (Figure 118 and Figure 119). These models are intended to find basic parameters which permit to print the material without

overloading the motors, burning the material and which guarantee an adequate layer bonding. These are used also to identify the printing speed, flow rate, layer height and others default printing parameters.

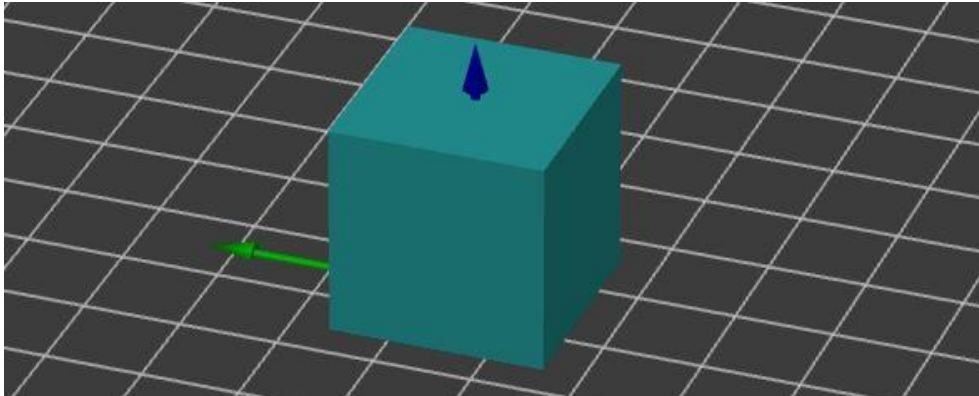


Figure 118: Simple cube model

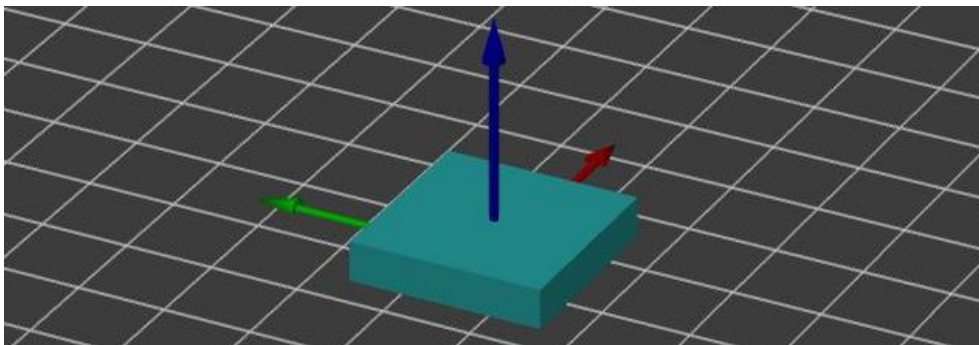


Figure 119: Flat block model

To test the mechanical properties tensile tests and compression test will be produced, with standard geometry and proportions but dimensions modified to be able to print them with one extruder chamber volume.

The tensile test is a dog bone specimen (Figure 120) with dimensions 100x16x4 mm (lxbxh) and with a neck section of 6x4 mm (bxh).

The compression test is a cylinder (Figure 121) which has an L/D ratio of 1,5 and a diameter of 17 mm.

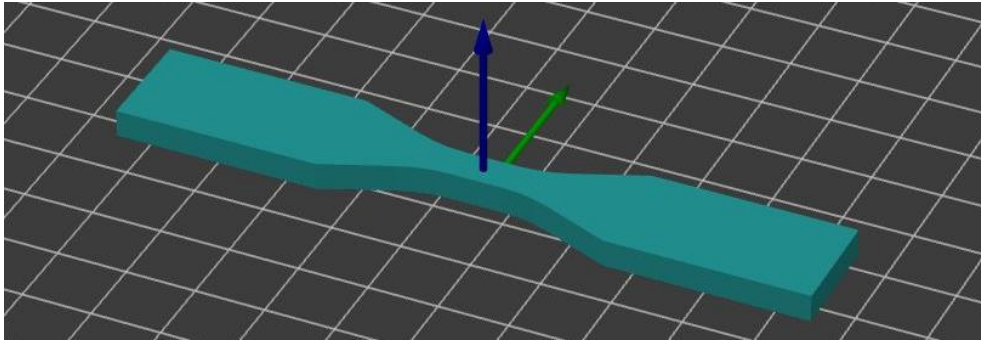


Figure 120: Tensile specimen model

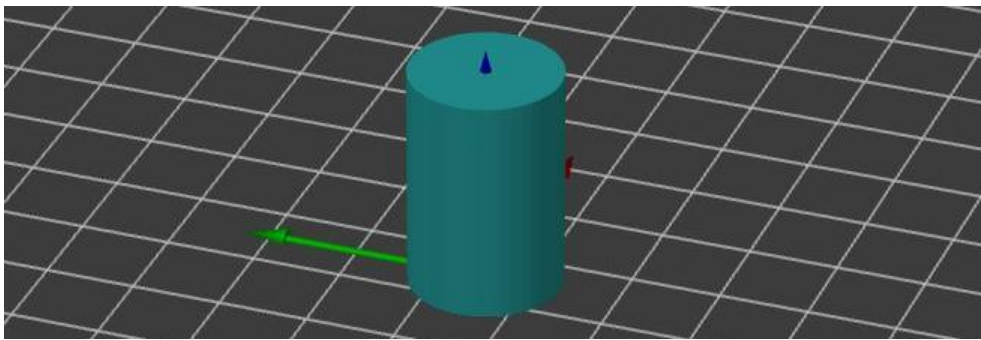


Figure 121: Compression specimen model

To test the printability of the material and quality achievable different test geometries have been designed: overhang test, bridge test, warping test, an engraved cube to test the surface quality and a test to highlight the staircase effect.

The overhang test (Figure 122) is a solid which has one surface with different overhang angles one after the other, it is divided in sections with a characteristic angle. The structure has been designed to see how angled the surface can be before failure in printing without supports. The angles present in the object are, from top to bottom, 10° - 30° - 45° - 60° from the vertical surface.

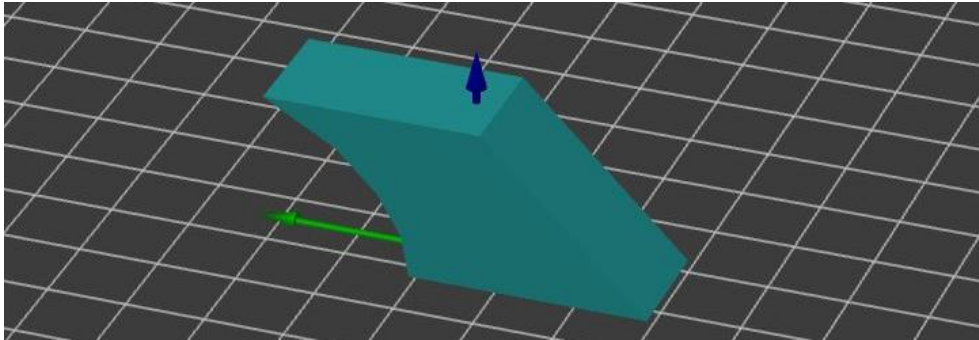


Figure 122: Overhang test model

The bridge test (Figure 123) is intended to highlight the bridging capabilities with the improved machine setup and the specific material. The structure has different bridge lengths at different heights to notice at which length the failure occurs. The bridge lengths are 3 mm, 10 mm and 15mm. In Figure 124 the sliced bridge feature is shown, it is possible to notice how the slicer understands the type of feature and makes parallel filaments in that area.

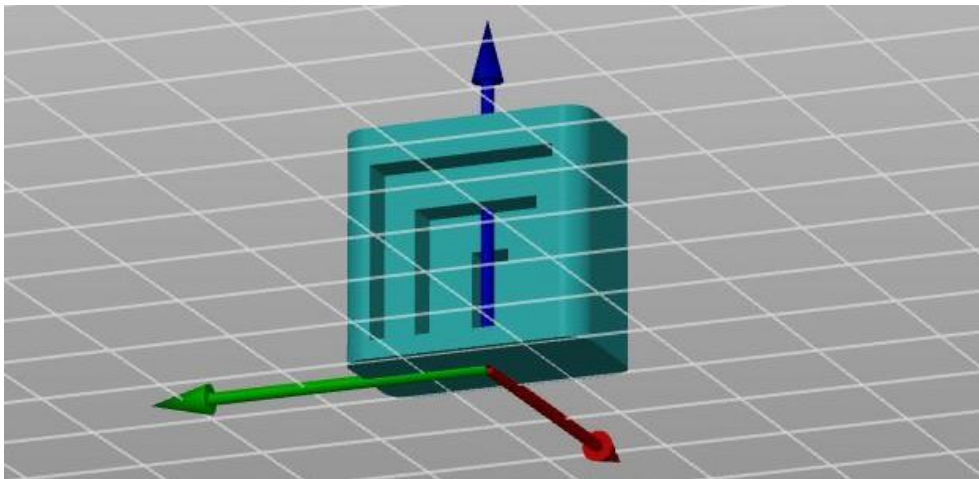


Figure 123: Bridge test model

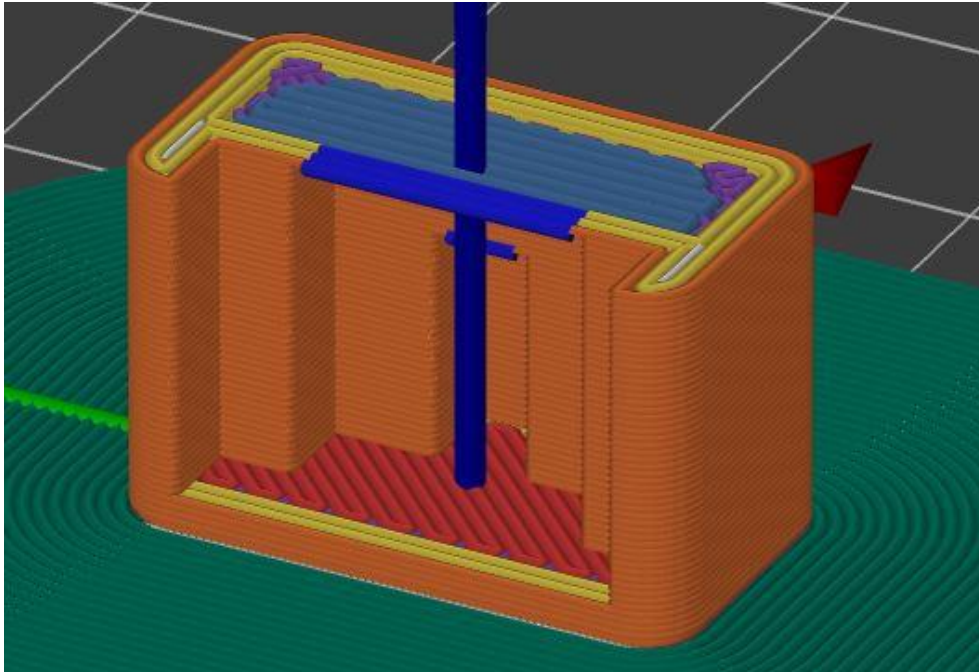


Figure 124: Bridge feature sliced

The engraved cube (Figure 125) has been designed to test the machine behavior with complex geometries. It features one engraved “M” letter on a surface, one “P” letter which protrudes from another surface and a surface with a hole in the center which enters in the body of the object.

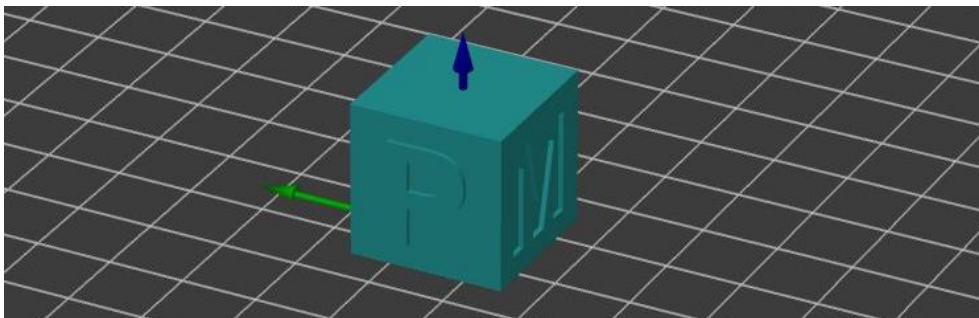


Figure 125: Engraved cube model

The staircase effect test (Figure 126) is intended to show how a different pattern will be generated by changing the surface angle, useful to understand the achievable quality for rapid tooling depending on the angle

of the mold. The angles present in this structure are 5° - 15° - 30° - 45° - 60° - 75° - 85° .

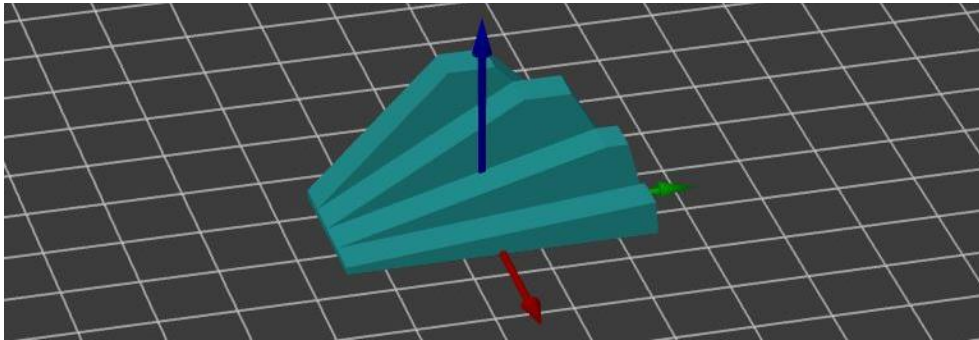


Figure 126: Staircase effect model

The warping test (Figure 127) is a flat rectangle with length of one side way larger than the other, this geometry being thin and long (70x15x1,5 mm) is prone to warping on the long side and will therefore be used to test the warping tendency of the material.

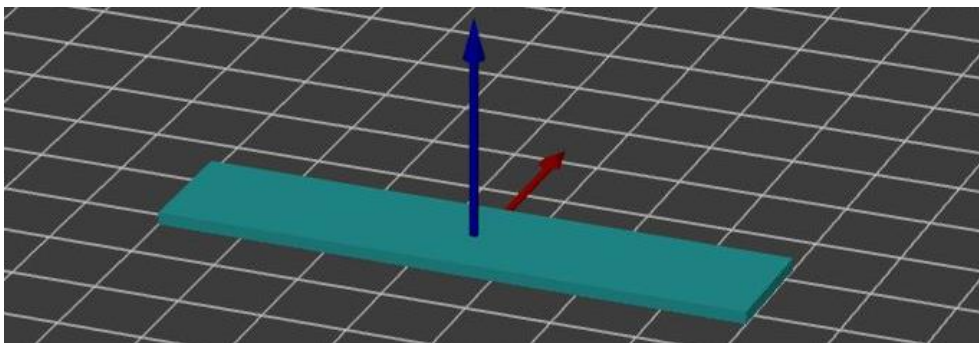


Figure 127: Warping test model

In Table 5 the purpose of each designed model is presented, along with the most significant variable affecting the behavior of the print.

Model designed	Goal	Variables
Compression Specimen	Test the compression mechanical properties, along with verifying the printability of a geometry with small layer area, prone to overheating.	Layer Fan, Body and Nozzle Temperatures
Tensile Specimen	Test the tensile mechanical properties of the additive manufactured material and their relationship with the preheating of the substrate.	IR power
Overhang Test	Test how much overhang angle can be printed with the EFeSTO machine.	Layer Fan
Bridge Test	Verify the maximum bridge length that the EFeSTO machine can perform.	Layer Fan
Engraved Cube	Verify the quality EFeSTO machine can achieve with complex geometries.	Layer Fan
Staircase Effect Test	Give a visual representation of the relationship between model angles and surface quality and roughness.	Layer Fan
Warping Test	Verify the warping tendency of the material with a prone-to-warping geometry.	Bed Temperature

Table 5: Designed models purpose and related variables

5.5 ABS trials with the improved EFeSTO machine

Once all the improvements had been installed and configured, I tried printing ABS material from LG Chem, which was easily available since it has already been object of another thesis which I closely followed [59].

The cooling system gave high reliability when printing ABS, giving the possibility to never worry about overheating in the whole working day.

The main problem encountered was an excess of heat flow through the piece with a body temperature of 230°C, which was the lowest temperature which gave flawless extrudability of the material, since for lower

temperatures the material viscosity was too high, resulting in overload of the motors.

In Figure 128, Figure 129 and Figure 130 some specimens printed with no fan is presented, showing how the substrate is affected by overheating problem and bad road stability and support, resulting in poor quality of the printed object.

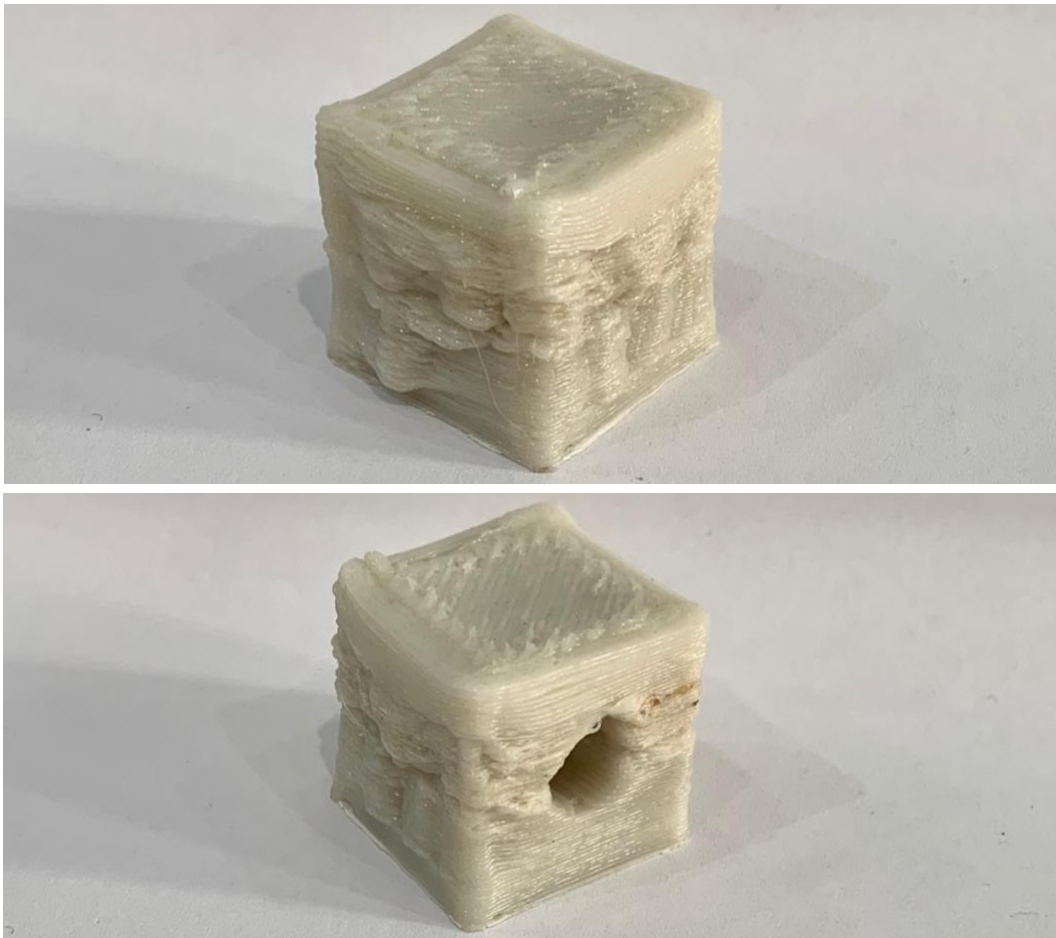


Figure 128: Overheated ABS engraved cube



Figure 129: Overheated ABS cube

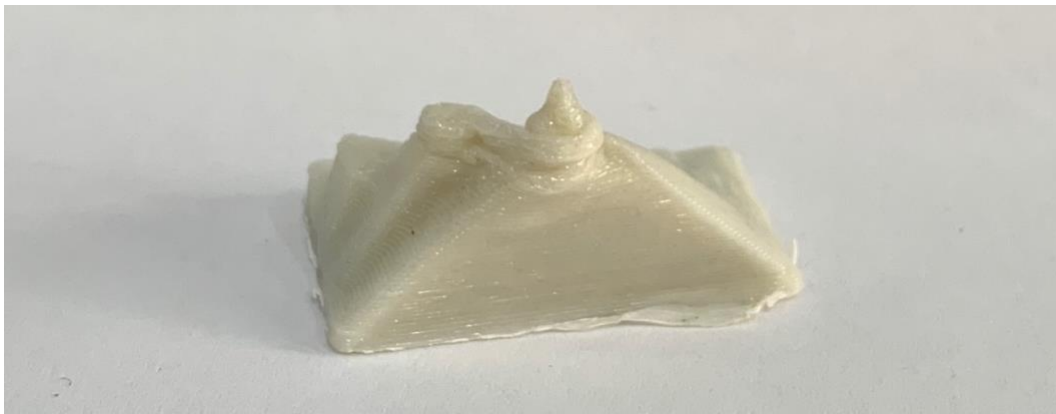


Figure 130: Overheated ABS staircase test

By running the layer fan at full power (100%) the quality of prints improves dramatically, since it basically solves all the overheating problems present in ABS printing at 230 °C extrusion temperature.

Overhang test and difficult geometries can be performed without any problem with the fan blowing at maximum speed, as shown in Figure 131, Figure 132 and Figure 133.

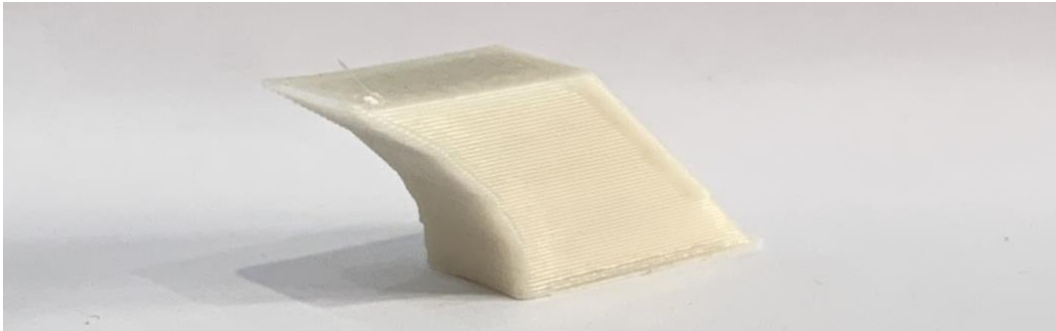


Figure 131: ABS overhang test with 100% fan speed

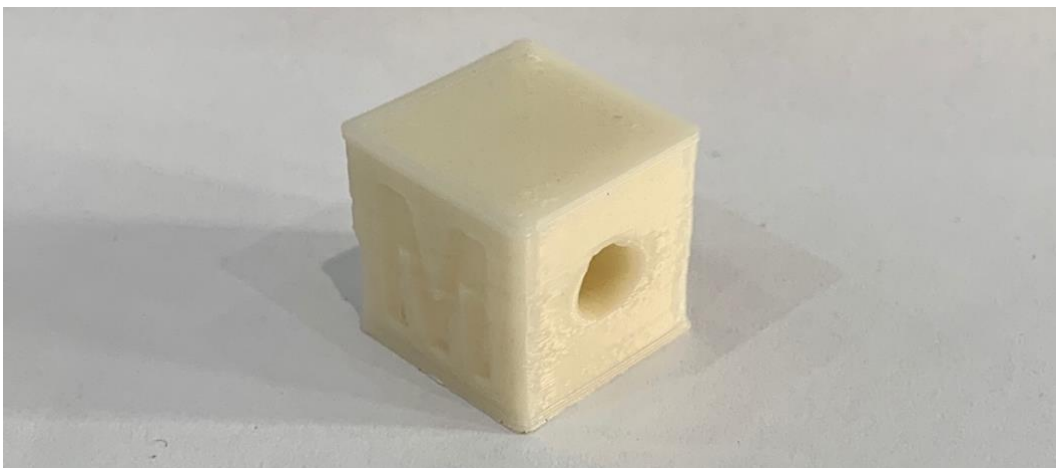


Figure 132: ABS engraved cube with 100% fan speed

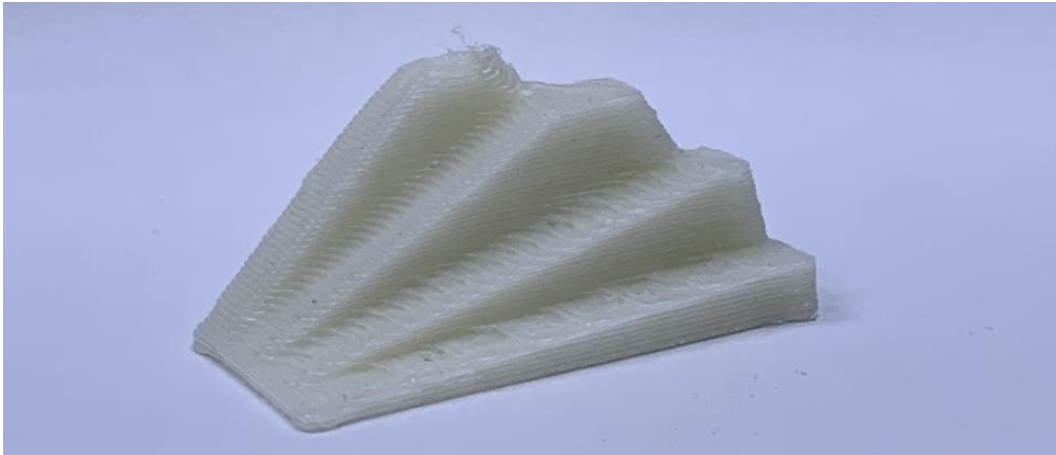


Figure 133: ABS staircase effect test with 100% fan speed

Since ABS has a low glass transition temperature, at about 100 °C, even with the fan at maximum speed, no signs of delamination are present.

The fan blowing cool air on the piece will surely reduce the layer bonding strength, therefore for tensile specimen (Figure 134) should be avoided.

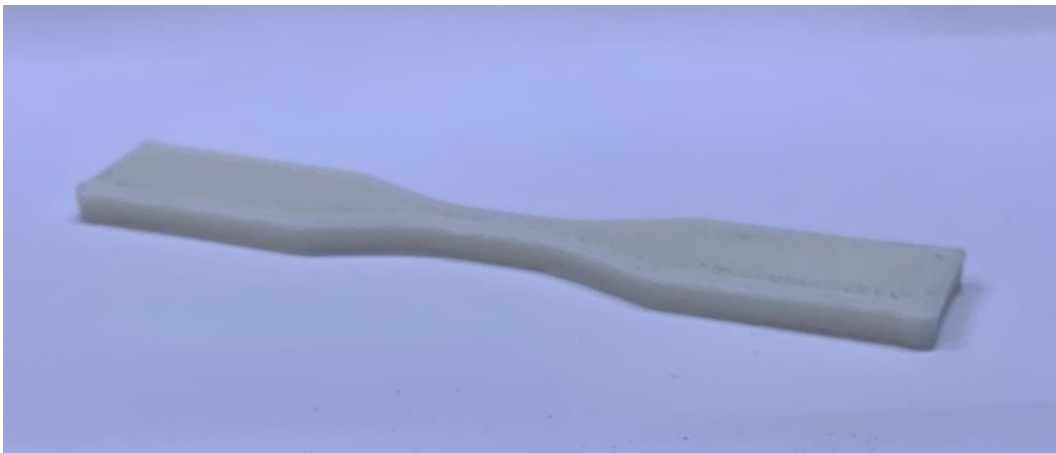


Figure 134: ABS tensile specimen

For compression specimens (Figure 135) a compromise between geometrical quality and strength should be reached by partializing the fan power.



Figure 135: ABS compression specimen

Therefore, in ABS printing many different designs can be produced without any problem by adjusting the fan speed at an adequate power for each geometry.

For ABS printing the IR preheater is not needed in small geometries as the ones presented before, since the substrate layer will always be at a temperature higher than T_g during the extrusion of the next one, resulting in good bonding between roads and layers.

These trials have been carried out to test the importance of the improvements made on different materials. It is needed to set the power of the fan and IR preheater according to the material problems shown in a particular geometry, by doing a first print without any external variable influencing the print. These results will be better explained in comparison with ULTEM ones in Paragraph 5.8.11.

5.6 Preliminary ULTEM trials

As I received the ULTEM pellets I tried extruding filament from the machine until the aspect and consistency was adequate. I started with the lowest temperature advised in the datasheet for injection molding, 345 °C for each thermal zone. The extruded filament was not good looking and the machine often gave overload problems since the viscosity at that temperature was too high. I raised up to 370 °C and the extruded filament started gaining the expected properties and consistency.

The temperature in the plasticization chamber has been set at 355 °C, which permits the plasticization with 1 Nm of torque from the motor, lower than the rated continuous value.

At this point I started printing the preliminary samples, cubes and flat boxes, varying different parameters to find some basic condition to proceed with the experimental campaign.

In the following table the different trials are reported with parameters used and a picture of the result obtained.


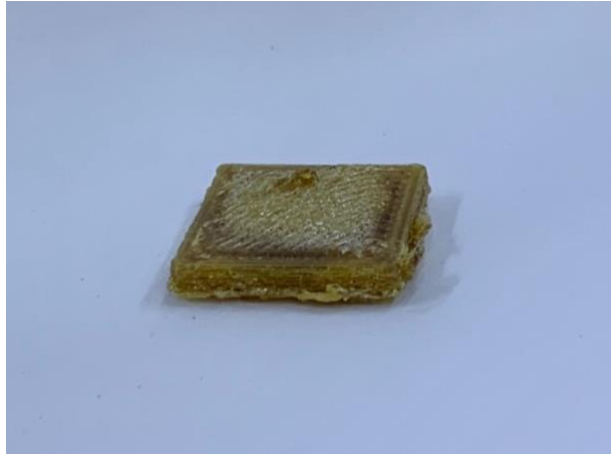
Some geometrical and kinematic variables have been fixed to simplify the problem, including layer height, line width and infill type.

The layer height has been set at 0,25 mm as a compromise between acceptable quality and time to print an object. The line width has been set as the nominal diameter of the nozzle at 0,6 mm. The infill type chosen is zig zag at 45° for the models printed with solid infill (100%) while a concentric infill has been chosen for the models with 20% infill, the ones who does not need to be mechanically tested.

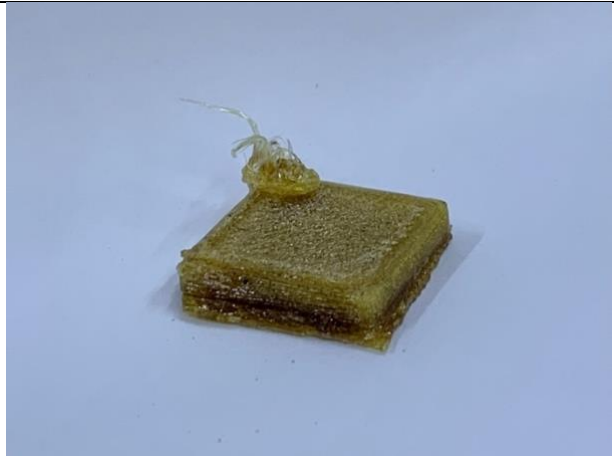
In Table 6 and Table 7 the parameters and pictures of the preliminary trials are presented.

Number	Geometry	Body Temp. [°C]	Nozzle Temp. [°C]	Bed Temp. [°C]	IR Power	Flow
1	Cube	365	365	140	75%	1.15
2	Flat Block	385	385	200	10%	1.15
3	Flat Block	375	375	220	50%	1.15
4	Flat Block	380	390	145	10%	1.05
5	Flat Block	380	385	150	10%	1.1
6	Cube	385	385	150	25%	1.1
7	Cube	380	385	150	0%	1.1
8	Tensile	380	385	150	25%	1.1

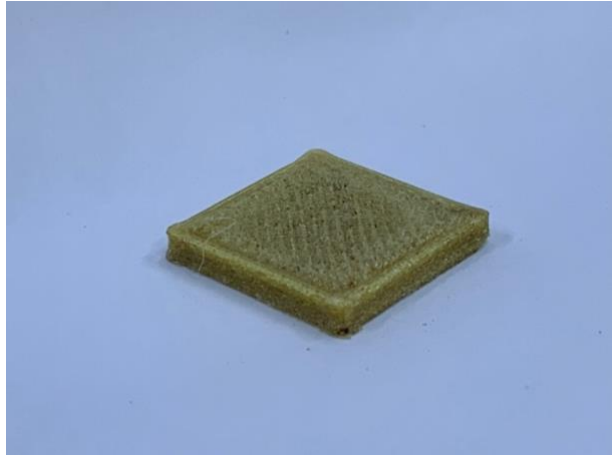
Table 6: Preliminary trails parameters

Number	Picture
1	
2	

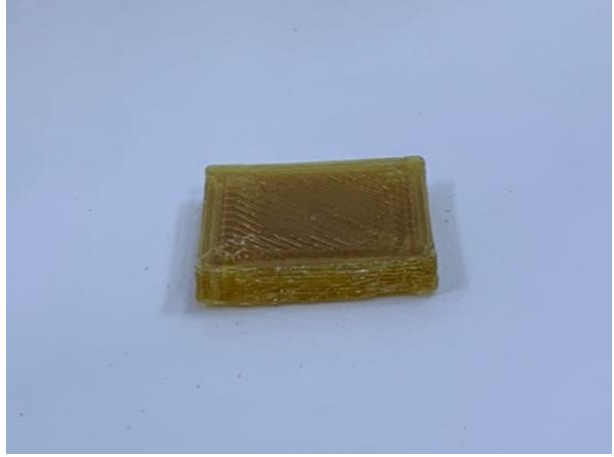
3



4



5



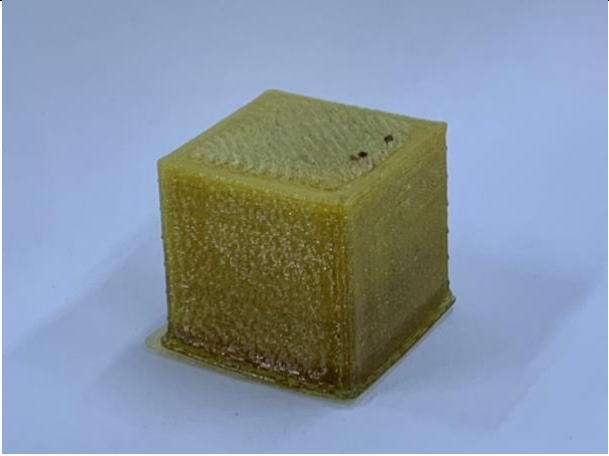


6	
7	
8	

Table 7: Preliminary trials aspect

After these trials some considerations can be drawn and basic parameters for printing ULTEM on the EFeSTO machine have been set.

The sample number 1 was completely burned, so I decided to reduce the infrared power. Sample number 2 show some signs of thermal degradation of the material, for this reason the next samples were printed with slightly lower body temperature.

Sample number 3 was partially burned due to excessive IR power, the print was proceeding with not adequate substrate stiffness since during the whole print the piece was probably at a higher temperature than ULTEM's glass transition temperature. Samples number 4 show that the flow was not adequate for a solid piece and was therefore increased. The flow of samples 5 through 9 seems adequate and will be fixed. Sample number 5 seems a good result for the flat solid block and therefore the settings will be just slightly modified from its conditions.

Samples number 6 and 7 can be regarded as successful prints, even if number 6 has some signs of material degradation, the situation improves with conditions of sample number 7. Sample number 8 seems adequate but has some sign of warping, since it was printed using Dimafix as adhesive, for this reason I moved to Magigoo.

From these first trials I also noticed that first layer speeds of 20 mm/s or 30 mm/s were too much to let the filament stick to the bed, it was instead dragged away by the nozzle. The first layer speed will therefore be set at 10 mm/s, resulting in adequate extrusion of the first layer.

During those trial it has also been noticed that turning on the IR lights during first layer increases the first layer adhesion and helps preventing warping, by keeping the first layer over the glass transition temperature it can absorb better the thermal stresses generated during its deposition in contact with the bed.

Once the infrared lights are turned off the whole layer cools more uniformly and results in less warping tendency.

The basic settings chosen for proceeding with the experimental campaign therefore are the ones presented in Table 8.

Parameter	Value
Plasticization Temperature	355 °C
Body Temperature	380 °C
Nozzle Temperature	385 °C
Bed Temperature	150 °C
Flow	1.1
1° Layer Speed	10 mm/s
Other Layers Speed	25 mm/s
1° Layer Height	0,4 mm
Other Layers Height	0,25 mm
Infrared Power 1° Layer	25%
Infrared Other Layers	0%
Fan Speed	0%
Line Width	0,6 mm
Number of Perimeters	3

Table 8: Default printing parameters

5.7 Design of experiments

In this paragraph the trials to be performed are presented. Each one is related to the variable which should affect to a larger extents the quality or properties of the sample, by keeping the other constants as presented in the basic parameters in Paragraph 5.6.

A factorial approach, by cross linking all the thermal variables for each test geometry, might have given more accurate results but for allocating time and resources in the best way I preferred to proceed in this way, eliminating the parameters which will not affect the tests in a considerable manner.

The variables chosen are related to the improvements made, among them the layer fan speed, the IR power and the printing temperatures.

Without the improved cooling circuit it would not be possible to operate these high temperatures due to excess of heat in the sensitive parts.

It has to be pointed out that the plasticization temperature is kept constant to the lowest value which guarantees a proper plasticization of the ULTEM material (355 °C), in order to reduce as much as possible the heat to be extracted by the cooling system. The plasticization temperature does not actually influence the printing process since the loading phase is done before starting the print. Once the material has been loaded in the body chambers it will tend to the extruder temperature, which will therefore affect the printing phase. It is indeed the extruder piston which pushes the material out of the nozzle by applying pressure on the whole volume of material in the chamber.

The best variable value is strictly related to the specific material which is printed, in fact diffusivity, glass transition temperature and other material related properties highly influence its behavior during additive manufacturing

In the following Tables each test with the most significative variable and its variation are presented.

Overhang test	1	2	3
Layer fan	0%	25%	50%

Table 9: Overhang test trials

The objective of the overhang test (Table 9) is to be able to perform the different angles in overhang without the structure collapsing.

Cube engraved	1	2	3
Layer fan	0%	25%	50%

Table 10: Engraved cube trials

The objective of the engraved cube test (Table 10) is to be able to make this complex geometry with the highest quality possible.

Bridge test	1	2	3
Layer fan %	0	25	50

Table 11: Bridge test trials

The objective of the bridge test (Table 11) is to notice how long the EFeSTO machine can bridge with this material and varying fan flow rate.

Compressi on specimen	1	2	3	4	5	6	7	8	9	10	11	12
Body Temp. [°C]	370	375	380	385	370	375	380	385	370	375	380	385
Nozzle Temp [°C]	375	380	385	390	375	380	385	390	375	380	385	390
Layer fan %	0	0	0	0	25	25	25	25	50	50	50	50

Table 12: Compression specimens trials

The objective of this test (Table 12) is to complete the geometry and correlate the compression properties, which will be mechanically tested, with the extrusion temperature and fan flow rate. Three trials for each condition will be performed to obtain average and standard deviation of the mechanical properties.

Tensile specimen	1	2	3
IR power %	0	25	50

Table 13: Tensile specimens trials

The purpose of this test (Table 13) is to evaluate the tensile strength of the material and elastic modulus and correlate them to a varying IR power, to evaluate how it affect the bonding between layers and roads. Three trials for each condition will be performed to obtain average and standard deviation.

Warping test	1	2	3
Bed Temp. [°C]	120	150	180

Table 14: Warping test trials

The purpose of the warping test (Table 14) is to highlight how much the specimen will warp at different bed temperatures with other conditions constant as defined in Paragraph 5.6. For all the specimens Magigoo HT adhesive will be used to maximize the adhesion with the build surface.

Staircase test	1	2	3
Layer fan %	0	25	50

Table 15: Staircase test trials

The staircase effect test (Table 15) is intended to show the relation between the model angles and the surface roughness to be obtained, the relation among the two is mainly driven by the layer height and nozzle dimensions, variable which are taken as fixed in this experimental campaign. The quality would improve by reducing the layer height. The geometry is a complex one since the area of the layers decreases a lot proceeding upwards, resulting in overheating problem as shown with ABS in Paragraph 5.5, for this reason I decided to investigate how the quality would improve increasing the fan speed and if some overheating is present also with ULTEM material.

5.8 Results

In this subsection the results of the experimental campaign will be presented, with focus on the causes of the results and explanation of the procedures and failed tests. The printing parameters have been kept constant as presented in Paragraph 5.6, changing only the most significant variable for each geometry as presented in Paragraph 5.7. The default variables are listed in Table 8.

5.8.1 Overhang Test

The overhang sample n. 1 with 0% fan (Figure 136) can be regarded as a successful print at all the different angles present in the test (up to 60°). On the top surface some slight signs of overheating are present but do not preclude the achievement of the results. This result is explicable thanks to the properties of the material, including diffusivity and glass transition temperature, and the ambient temperature surrounding the object. As the material was extruded it cooled down to a point where it had enough stiffness to sustain the overhang layer deposited upon it, guaranteeing enough layer adhesion. In ULTEM additive manufacturing the heat extracted by convection and conduction from the last deposited layer is considerable due to the high gradient between the extrusion temperature (385 °C) and the ambient and bed ones (respectively 24 °C and 150 °C). This result differs a lot from the ones obtained with ABS specimens.

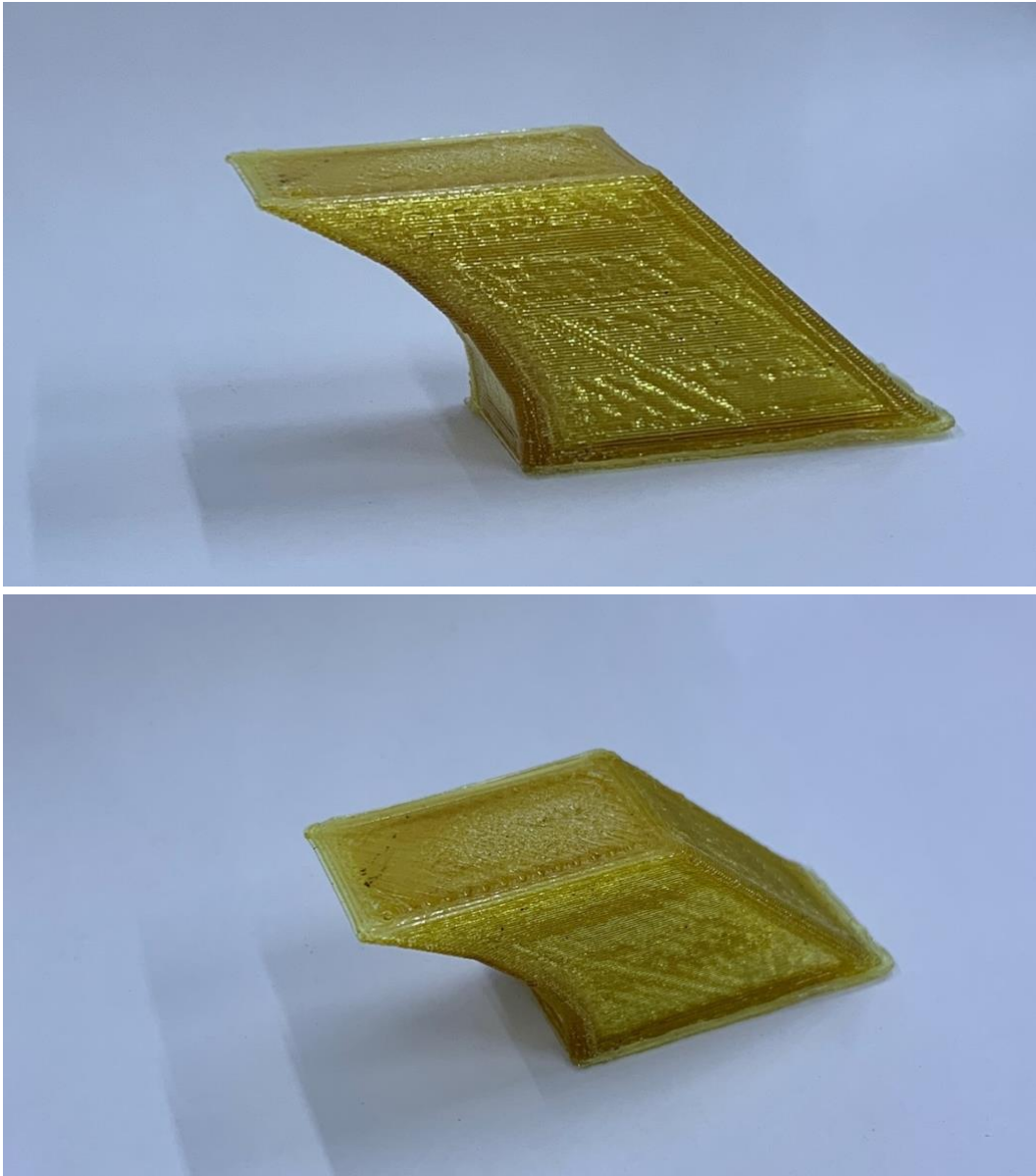


Figure 136: Overhang test 0% fan

The sample n. 2 with fan at 25% (Figure 137) resulted in a perfect object, with all the angles accomplished, no signs of delamination or overheating and excellent quality of the print and of the top surface.

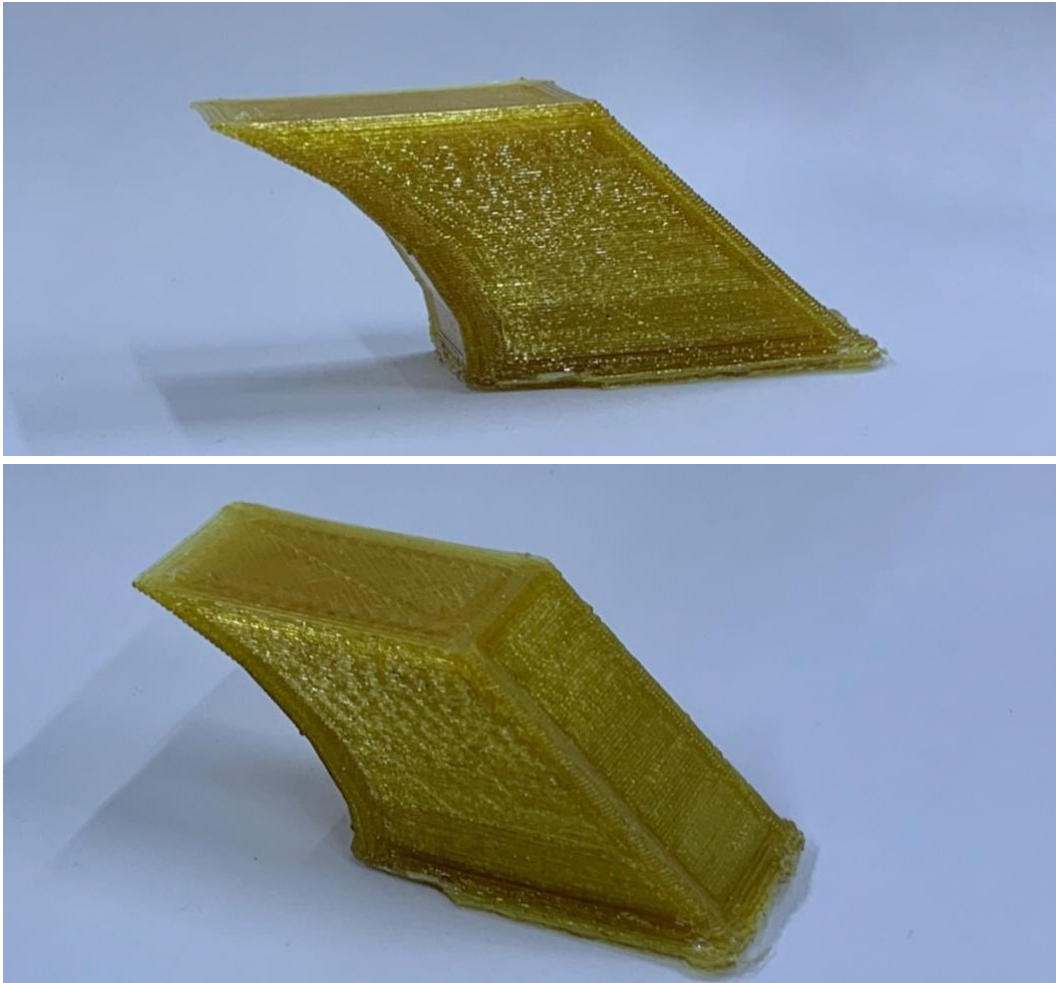


Figure 137: Overhang test 25% fan

Sample n. 3 with fan at 50% power (Figure 138) resulted in a failed print. The angles were pretty much achieved but strong delamination is present at the point that the piece was about to break in two distinct pieces when performing the zig zag top layer. This result is due to excessive cooling for respect to the one needed by the geometry and material combination. The previous deposited layer was brought at a temperature much lower than PEI's glass transition temperature before the next one was deposited upon it, resulting in really poor layer adhesion.

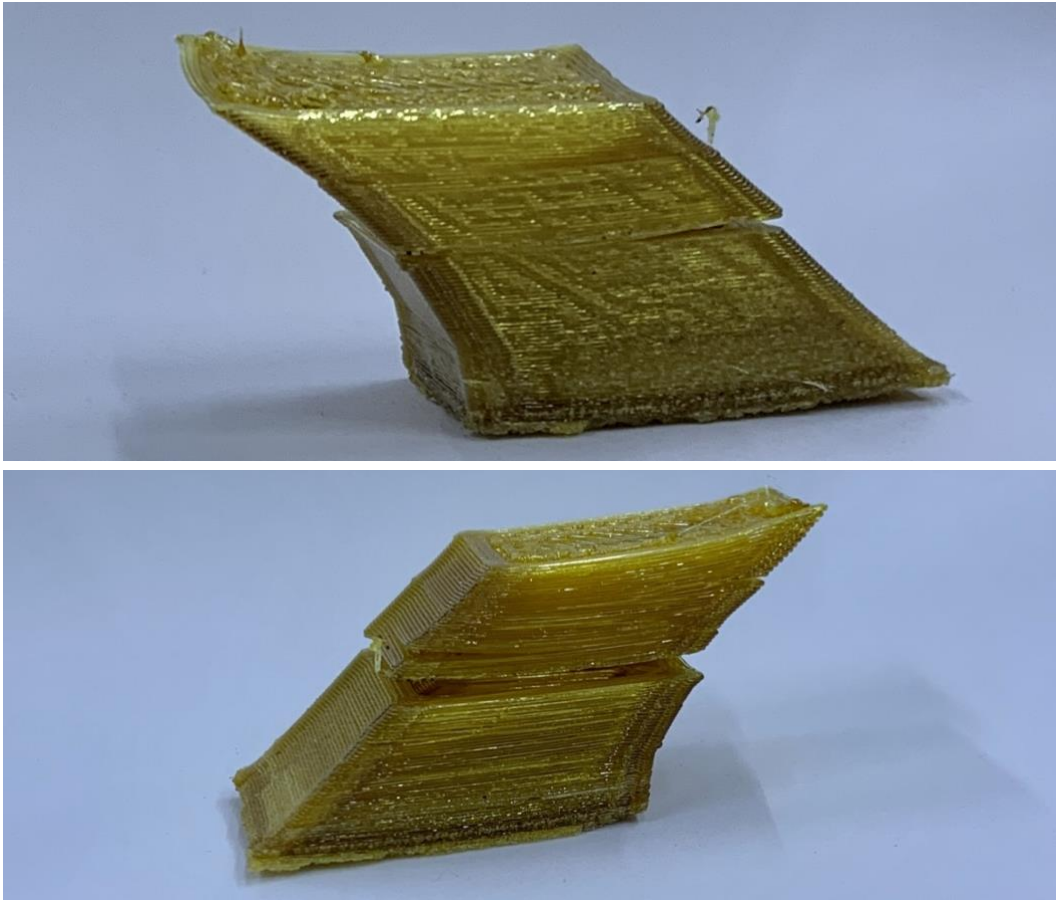


Figure 138: Overhang test 50% fan

In Table 16 the results of the overhang test are summarized, all the variables except the layer fan are kept constant as in Table 8.

Overhang test	1	2	3
Layer fan	0%	25%	50%
Accomplished	✓	✓	✗
Notes	Slight overheating	Perfect	Strong Delamination

Table 16: Overhang test results

5.8.2 Engraved Cube

The engraved cube n. 1 with fan switched off (Figure 139) shows some overheating both on the top surface and on some critical layers where the geometry is not perfectly respected and some drops of materials are present. Overall, the print can be considered successful but not flawless.

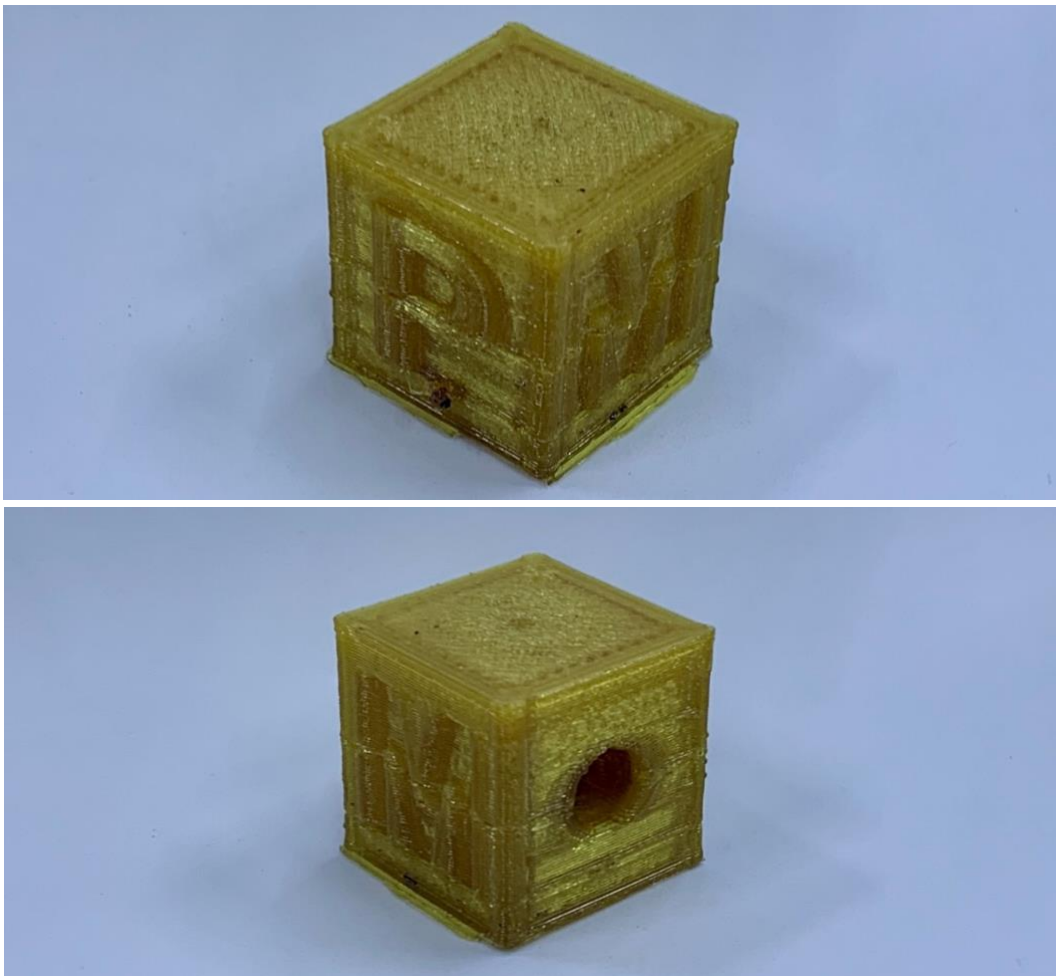


Figure 139: Engraved cube 0% fan

The sample n. 2 with 25% fan power (Figure 140) has been completed in a successful way, the geometry is respected in all the points, the letters are readable and no drops of material are present, the hole shows a good

circularity and the top surface is flawless. No signs of delamination are present and a good surface quality has been achieved.

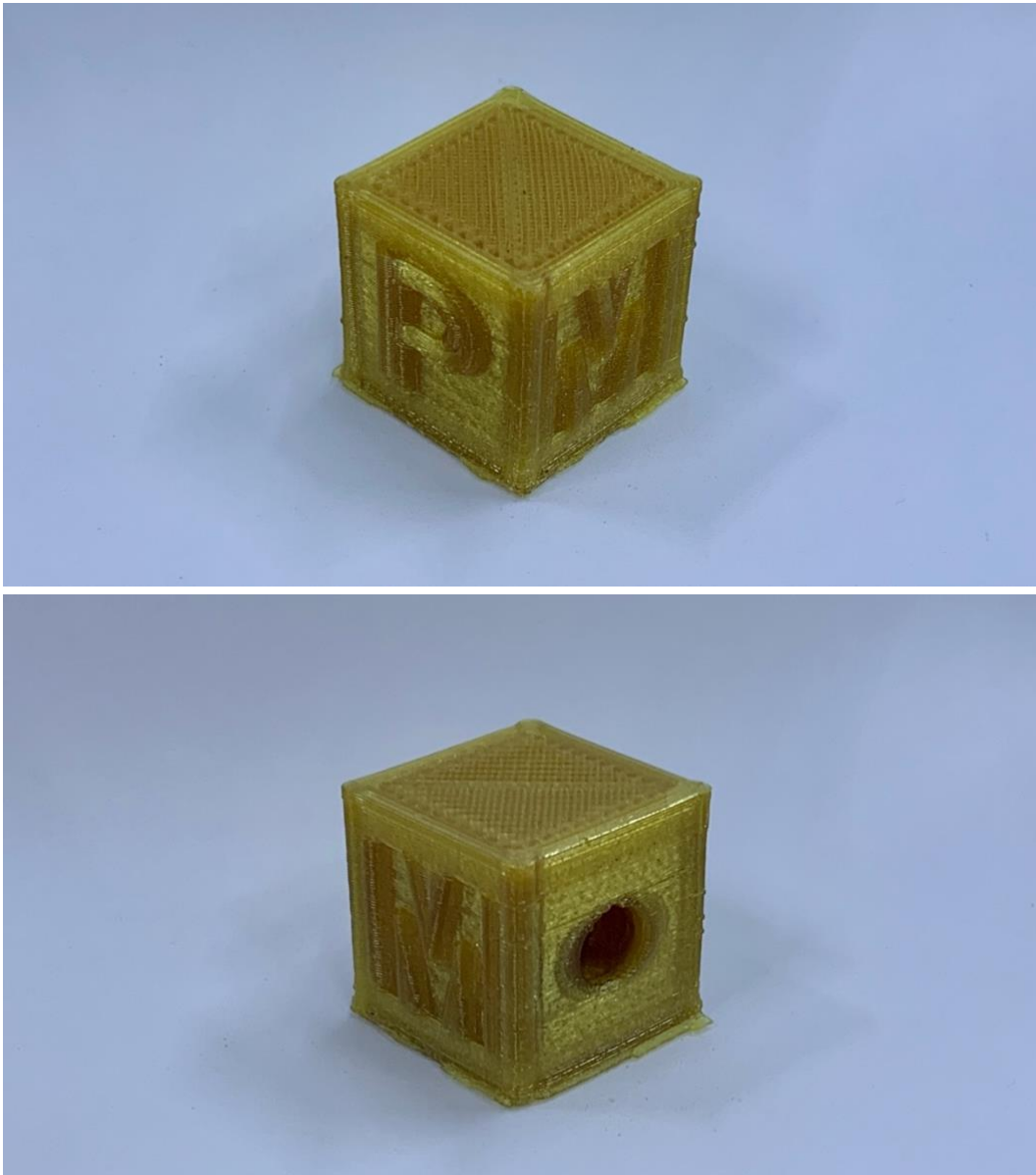


Figure 140: Engraved cube 25% fan

Sample n. 3 with fan at 50% (Figure 141) has to be considered a failed print since there is a strong delamination which was resulting in the piece being

broken in two distinct sections. The filament was anymore able to follow the geometry since the upper part was being moved by the nozzle and the print had to be stopped. In this case, as in the overhang sample, strong overcooling is present which does not guarantee adequate layer bonding. This result is strictly related to the geometry and material used.

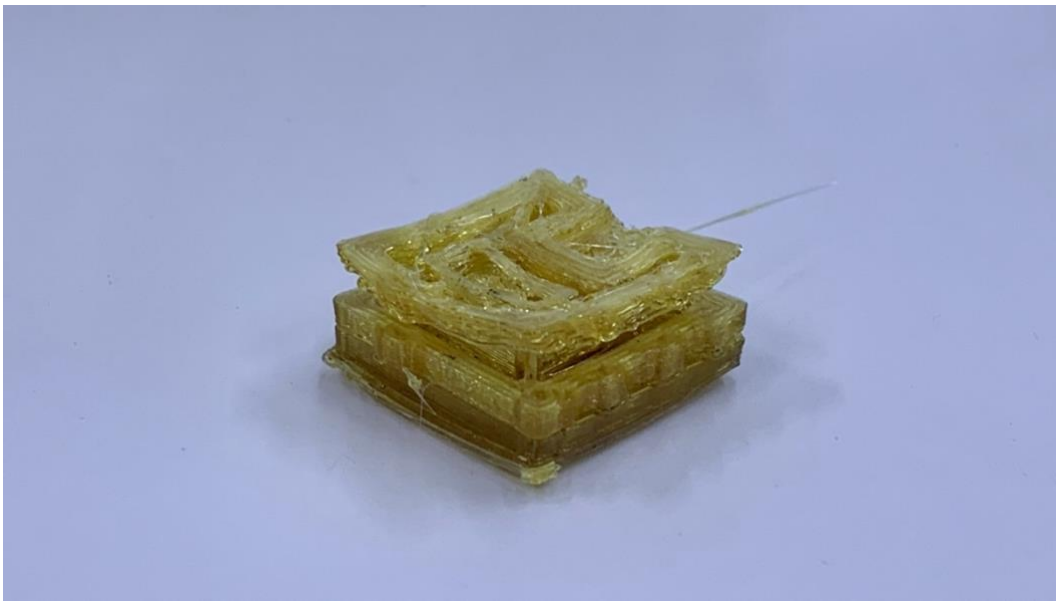


Figure 141: Engraved cube 50% fan

In Table 17 the results of the engraved cube test are presented, all the variables except the layer fan are kept constant as in Table 8.

Engraved cube	1	2	3
Layer fan	0%	25%	50%
Accomplished	✓	✓	✗
Notes	Slight overheating	Perfect	Strong Delamination

Table 17: Engraved cube results

5.8.3 Bridge Test

The bridge test n. 1 with layer fan off (Figure 142) has to be considered a failed print. Strong overheating is present on the whole print since the specimen is really small and the bridge features are all falling down in the center of the line, resulting in arcs. The longest bridge feature has also a road which curls and is completely detached from the structure.

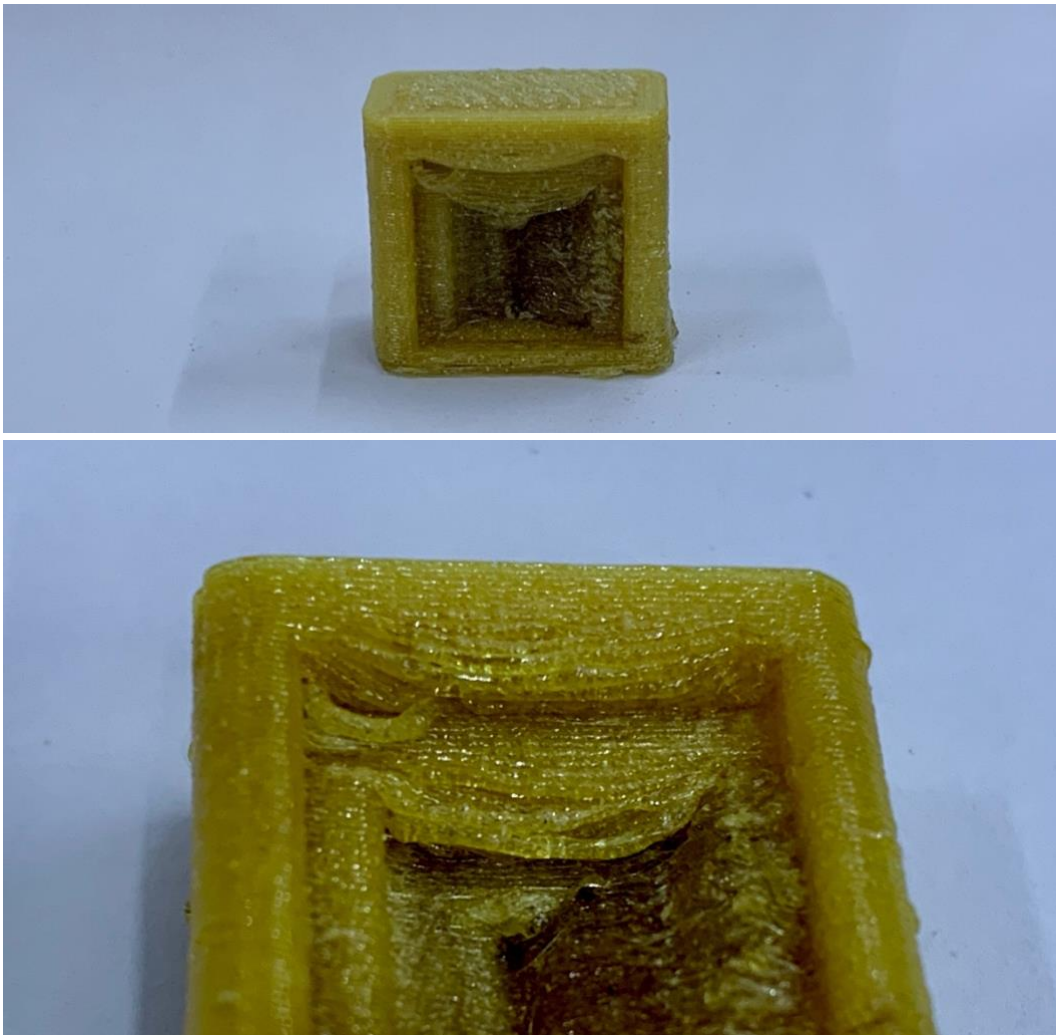


Figure 142: Bridge test 0% fan

The sample n. 2 with layer fan at 25% power (Figure 143) can be regarded as a successful print, the bridge features are adequately straight lines and overall no signs of overheating nor delamination are present. The quality of the bridge features could be improved by tuning better the slicer settings, but from a cooling point of view the condition seems adequate.

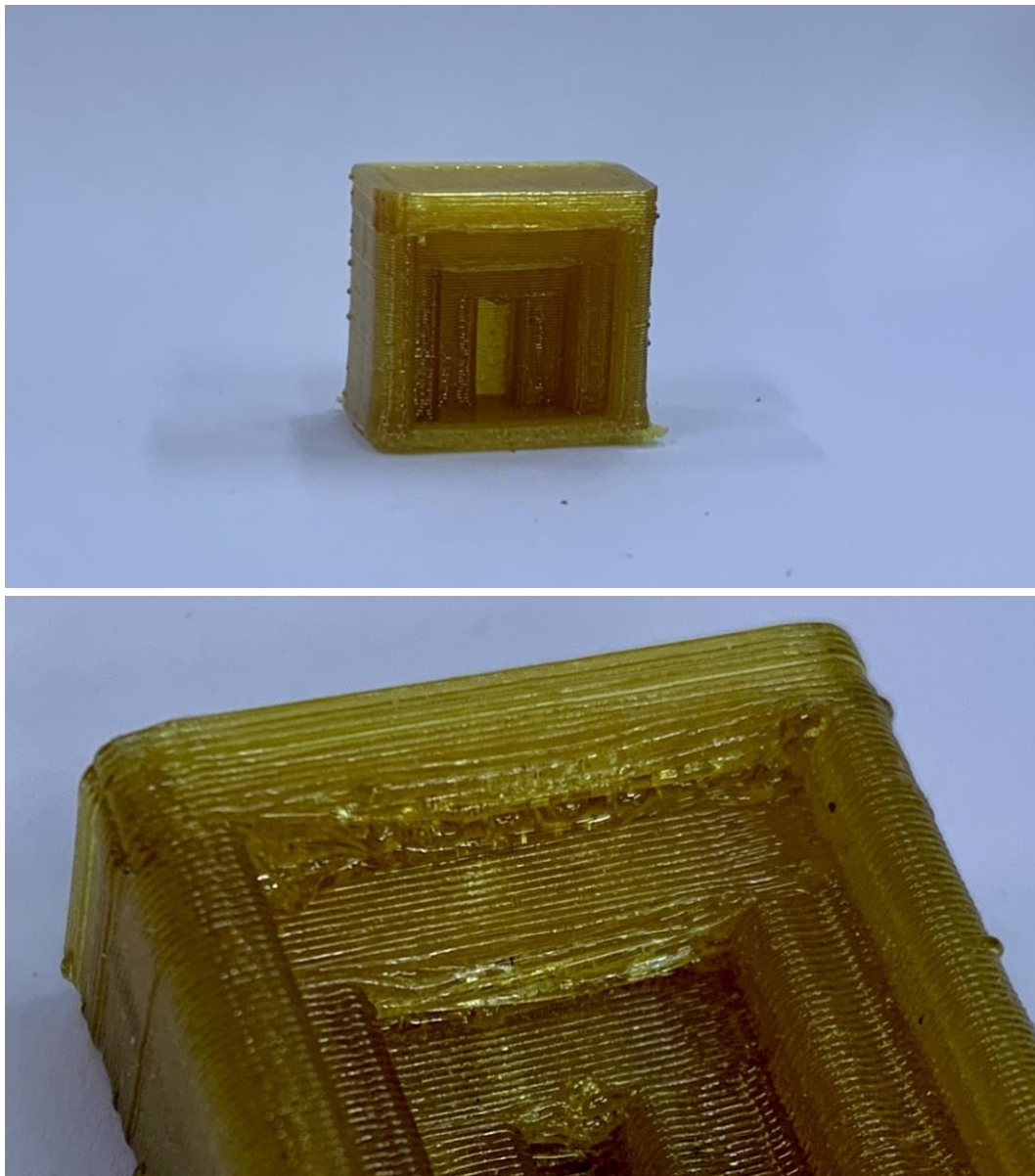


Figure 143: Bridge test 25% fan

Sample n. 3 with fan at 50% (Figure 144 and Figure 145) shows the bridge features better and straighter than sample n. 2, but in this case some slight delamination on the corners is present. Therefore, the condition of sample n. 2 is preferable.

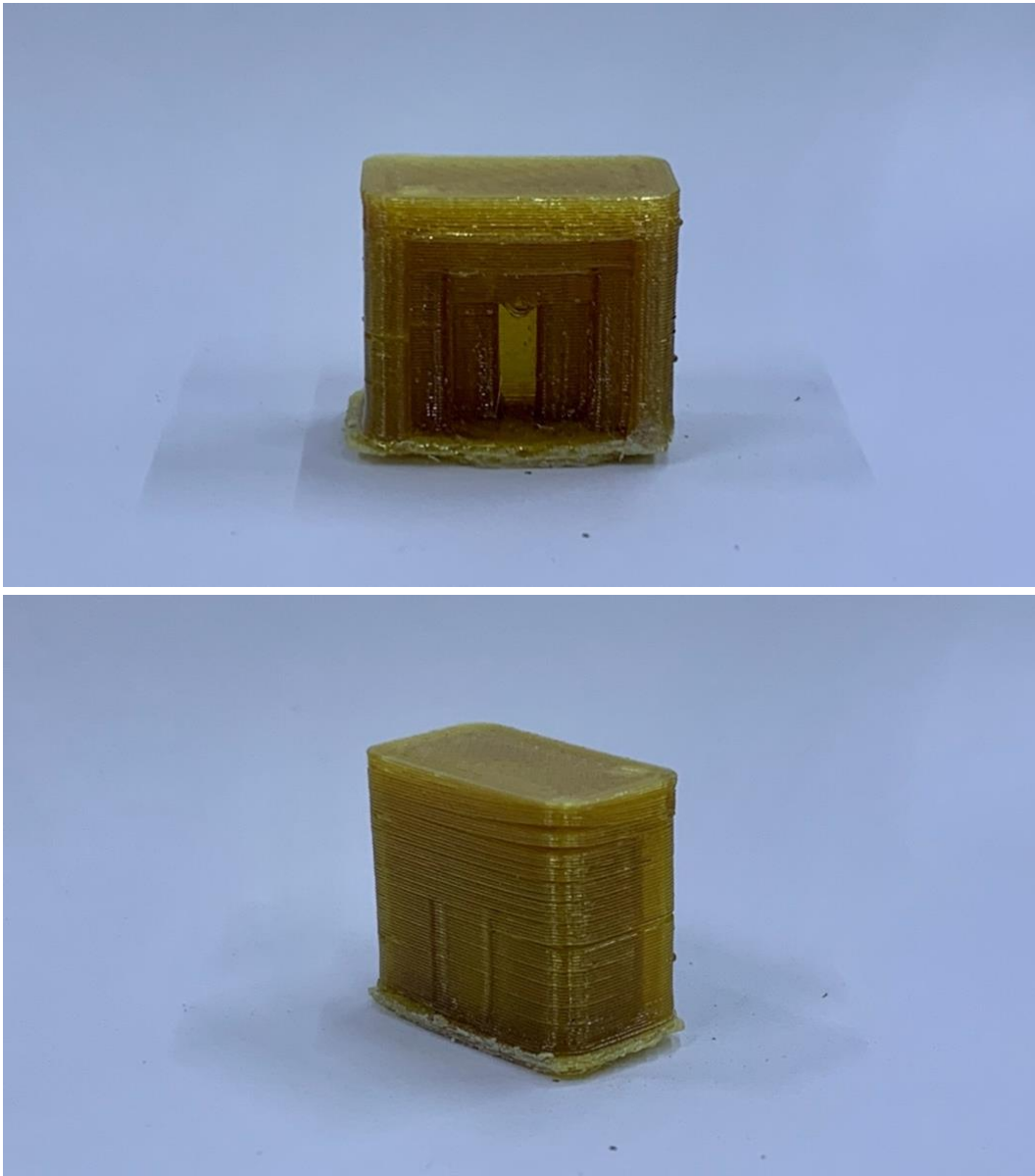


Figure 144: Bridge test 50% fan

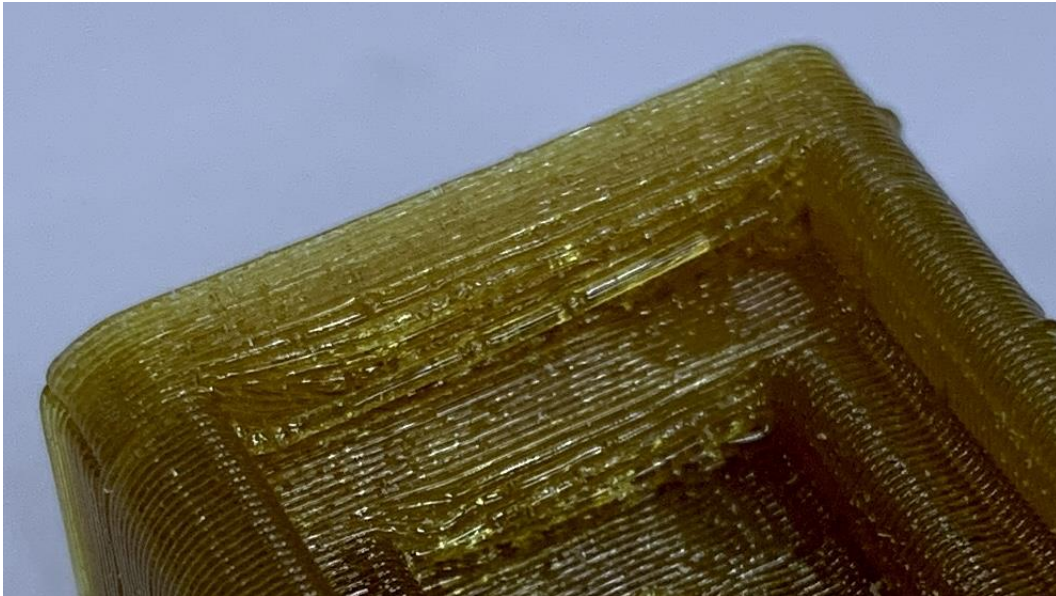


Figure 145: Bridge test 50% fan close up

In Table 18 the results of the bridge test are summarized, all the variables except the layer fan are kept constant as in Table 8.

Bridge test	1	2	3
Layer fan	0%	25%	50%
Accomplished	✘	✔	✔
Notes	Strong overheating	Adequate	Slight Delamination

Table 18: Bridge test results

5.8.4 Compression Specimen

For compression testing some cylindrical specimens have been produced with L/D ratio of 1,5. The successful printed specimens will be printed 3 times to test them and obtain mean and standard deviation of the mechanical properties. This geometry, even if looking simple, hides some problems due to the small area of each layer which makes these samples

prone to the overheating problem. As mentioned in the DOE the body temperature will always be kept 5 °C lower than the nozzle one.

Sample n. 1 with nozzle temperature of 375 and fan at 0% speed resulted in blockage of the machine due to high viscosity of the polymer and not enough power from the extruder motor. The result is show in Figure 146. The drop on top of the specimen is caused by the pneumatic closure of the nozzle which closes the orifice when an error occurs, pushing some material out of it in an uncontrolled manner.

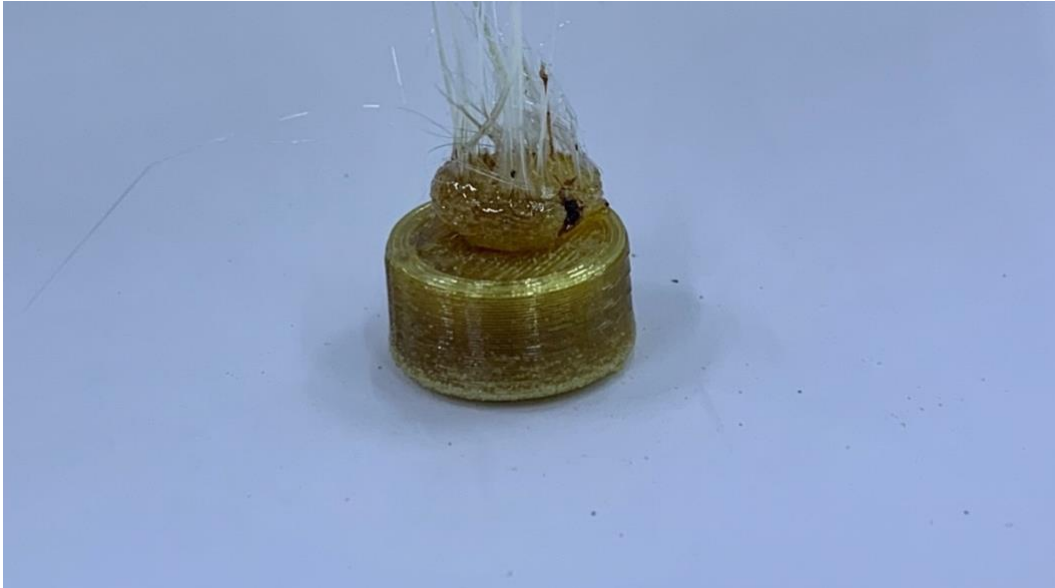


Figure 146: Compression specimen n. 1

Sample n. 2 with nozzle temperature of 380 °C and no fan (Figure 147) was produced in the correct manner, without blocking the machine neither problems post extrusion, even if some slight overheating on the top surface is present. Therefore, three samples are printed for testing.



Figure 147: Compression specimen n. 2

Sample number 3 with nozzle temperature of 385 °C and no fan shows signs of overheating problem, mainly related to the geometry. Indeed, the time to make a layer was shorter than other pieces in the experimental campaign and the piece did not have enough time to cool due to convection. Two trials for this condition were performed but both resulted in overheating problem which make the geometry different from the one of the cad file, resulting in non-testable parts, as shown in Figure 148.

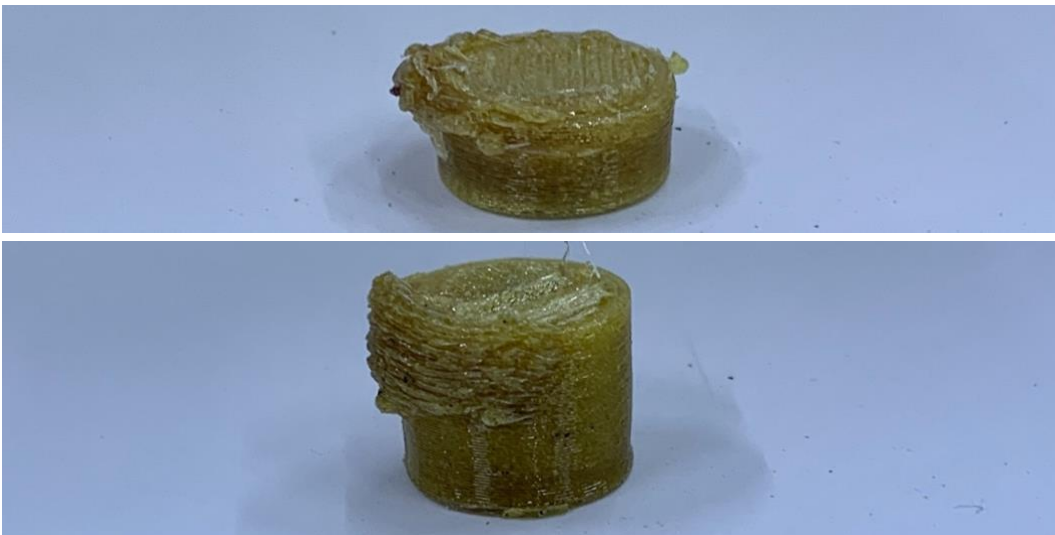


Figure 148: Compression specimen n. 3

Sample n. 4 with nozzle temperature of 390 °C and fan at 0% power (Figure 149) showed signs of material degradation inside the machine, due to a too high temperature in the extruder chamber and nozzle and too slow extrusion rate, which resulted in degraded material.



Figure 149: Compression specimen n. 4

Sample n. 5 with nozzle temperature of 375 °C and 25% fan speed blocked the machine due to overload, same condition happened with sample n. 1, since the fan speed does not affect the material prior to extrusion and the viscosity was too high. In Figure 150 the trial is shown.

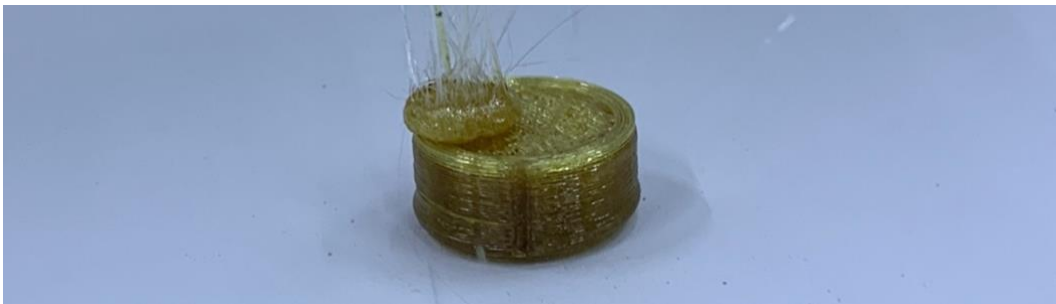


Figure 150: Compression specimen n. 5

Sample n. 6 with nozzle temperature of 380 °C and 25% layer fan speed was produced in a flawless manner, without any sign of overheating, material degradation nor delamination. The result is presented in Figure 151 .



Figure 151: Compression specimen n. 6

Sample n. 7 with nozzle temperature of 385 °C and 25% layer fan speed was produced with good shape and color, without any sign of overheating, material degradation nor delamination. The specimens prior to testing are presented in Figure 152 .



Figure 152: Compression specimen n. 7

Sample n. 8 with nozzle temperature of 390 °C and fan at 25% power (Figure 153) showed, as for sample n. 4, signs of material degradation inside the machine, even in this case changing the fan speed did not improve the situation since the thermal problem was in the extruder chamber.

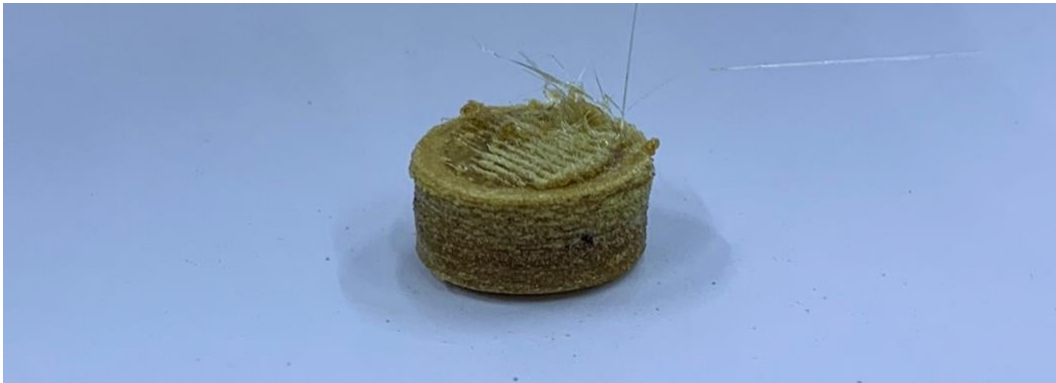


Figure 153: Compression specimen n. 8

Sample n. 9 with nozzle temperature of 375 °C and fan speed at 50% was not printed due to the high probability of machine overload, since both the previous trials at this temperature gave overload.

Sample n. 10 with nozzle temperature of 380 °C and layer fan speed at 50% resulted in delamination due to too cool substrate when depositing the next part. The process was thus interrupted. The result is shown in Figure 154.

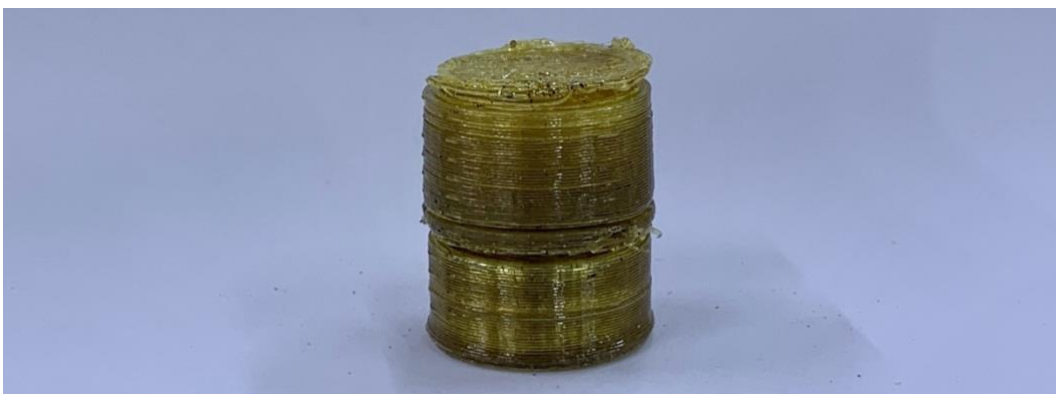


Figure 154: Compression specimen n. 10

Sample n. 11 with nozzle temperature of 385 °C and 50% layer fan power also resulted in a delaminated specimen, shown in Figure 155, which is not adequate for testing, therefore the printing phase was interrupted and no more specimens with this condition were printed.

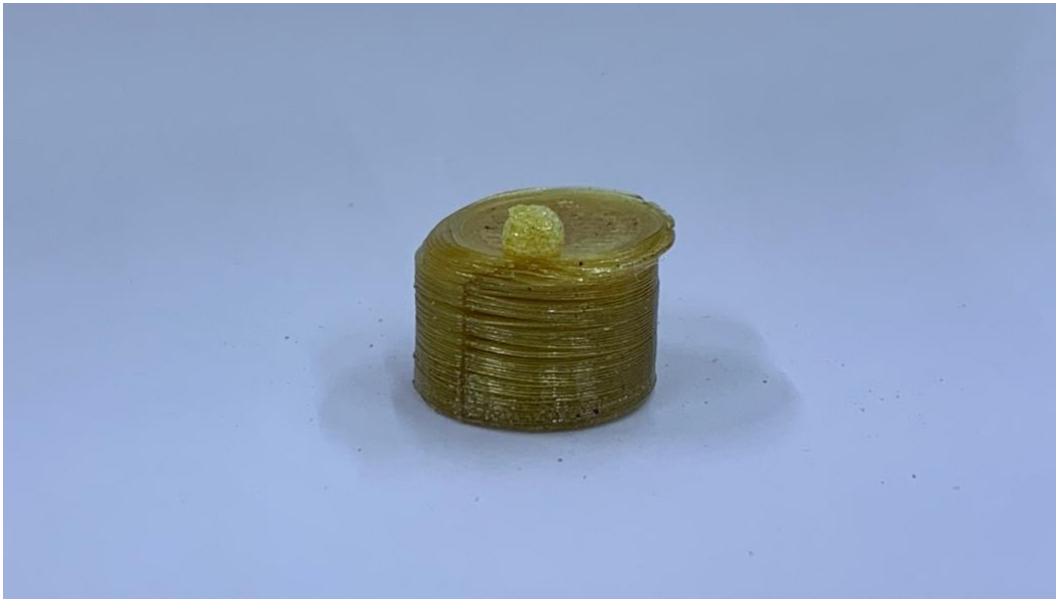


Figure 155: Compression specimen n. 11

Sample n. 12 with nozzle temperature of 390 °C and layer fan at 50% was not printed since both the previous trials at this temperature resulted in material degradation and increasing the fan speed would not have fixed this problem.

From the printing phase of the compression specimens, it is possible to notice how the temperature of 375 °C always gives machine blockage due to high viscosity of the ULTEM material in the extrusion temperature and not enough motor torque to extrude it. On the other hand a nozzle temperature of 390 °C always gives material degradation inside the machine, resulting in poor material properties and aspect once extruded.

The process window is therefore limited to a nozzle temperature of 380 °C-385 °C and the layer fan power contributes in giving overheating, perfect prints, or delamination. The three beforementioned problems are all related to the process and material state post extrusion, thus can be controlled by adjusting the layer fan speed.

In Table 19 the results obtained by printing compression specimens are summarized, all the variables except the layer fan and temperatures are kept constant as in Table 8.

Compressi on specimen	1	2	3	4	5	6	7	8	9	10	11	12
Body Temp. °C	370	375	380	385	370	375	380	385	370	375	380	385
Nozzle Temp °C	375	380	385	390	375	380	385	390	375	380	385	390
Layer fan %	0	0	0	0	25	25	25	25	50	50	50	50
Success	✘	✔	✘	✘	✘	✔	✔	✘	✘	✘	✘	✘
Notes	BL	GD	OV	DG	BL	GD	GD	DG	BL	DL	DL	DG

Table 19: Compression specimens printing phase results

Notes: BL=machine blockage/overload, GD= good piece, OV=overheating, DG=material degradation, DL=delamination

From the data in Table 19 it is possible to obtain a process window relating the fan speed and extrusion temperatures to the possibility of obtaining adequate pieces, as shown in Figure 156. The process window is not wide, therefore I expect the compression results not to vary a lot in the conditions

inside the process window. Many problems might occur if wrong process conditions are selected, as understood from the previous trials.

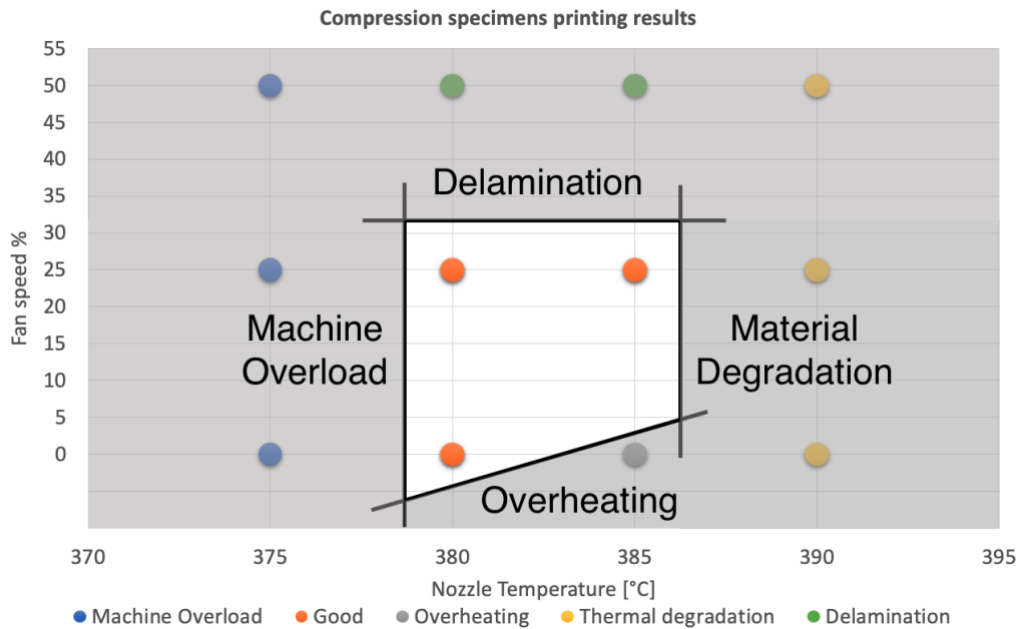


Figure 156: Temperature-Fan process window for cylinder specimen

5.8.5 Mechanical compression testing

The samples considered adequate were tested in compression, with a deformation rate of 2 mm/min on the MTS Alliance RF/150 machine, shown in Figure 157, equipped with an MTS extensimeter mounted on the specimen.



Figure 157: Compression test machine

The resulting shape after testing was usually the one presented in Figure 158, even if two specimens deformed in an unstable way, by inclining on one side.



Figure 158: Compression specimens after testing

The results gathered from the compression tests were analyzed and some conclusions can be obtained.

In Table 20 the results obtained from the tests are presented. The stress and strain value reported in Table 20 are the engineering ones, without considering the change in section due to compression.

Temperature [°C] – Fan [%]	380 - 0			380 - 25			385 - 25		
Specimen	1	2	3	1	2	3	1	2	3
Initial Speed [mm/min]	2	2	2	2	2	2	2	2	2
Removal Point [mm]	0,5	0,5	0,5	0,5	0,5	0,5	0,5	0,5	0,5
Secondary Speed [mm/min]	2	2	2	2	2	2	2	2	2
Diameter [mm]	17,5	17,8	17,8	17,5	17,4	17,5	17,4	17,4	17,4
Young's Modulus [MPa]	2723	2123	2641	2759	2854	2335	2668	2630	3016
Rp02 [MPa]	75	72	38	67	72	5	75	59	79
Rp1 [MPa]	99	89	62	97	103	87	103	91	104
Stress0.2 [MPa]	6	4	7	5	6	2	6	4	7
Stress1 [MPa]	29	21	28	27	29	15	28	22	32
Peak Stress [MPa]	160	143	141	167	165	158	168	162	163

Table 20: Compression test raw data

The samples n. 2 and 3 in the first condition were not considered since they deformed in an unstable way and the curves did not look correct. Probably due to overheating effects in the samples and on the top surface which did not allow a proper compression testing.

In Figure 159, Figure 160 and Figure 161 the True Stress-True Strain curves for the different condition tested are reported. In this case true stresses are used to be more accurate.

The True values take into account the increase in section during compression. The relation which links the engineering values and true values for compression is the following:

$$\sigma_{true} = \sigma_{eng}(1 - \varepsilon_{eng}) \quad \varepsilon_{true} = \ln(1 + \varepsilon_{eng})$$

The Matlab codes for obtaining the curves from comma separated values given by the tests are presented in Appendix C.

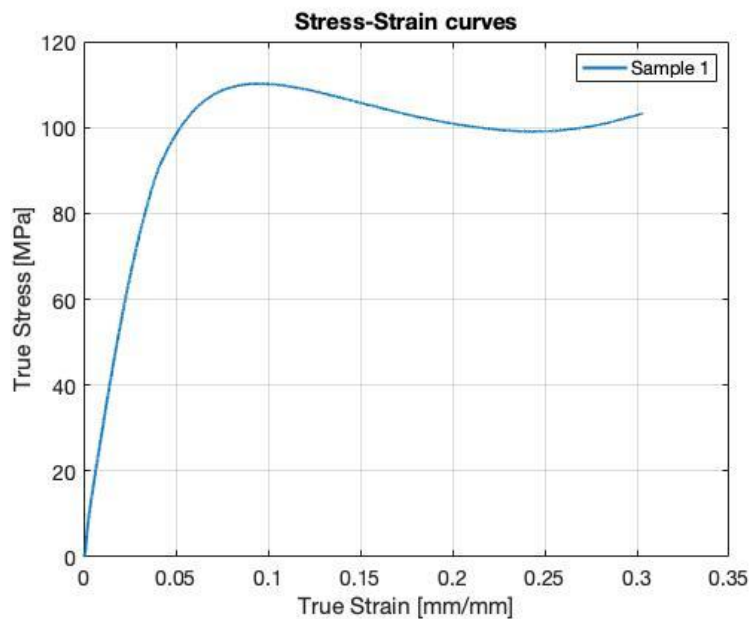


Figure 159: Stress-Strain curves Nozzle T. 380°C - Fan 0%

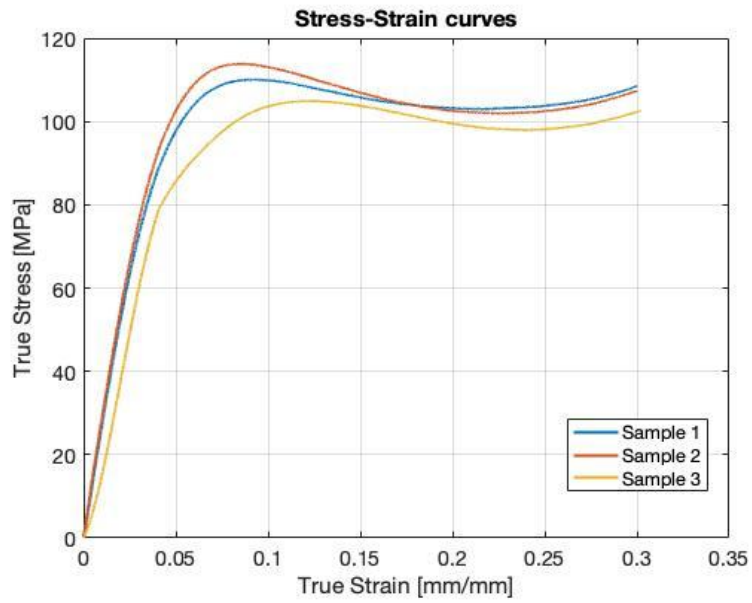


Figure 160: Stress-Strain curves Nozzle T. 380°C - Fan 25%

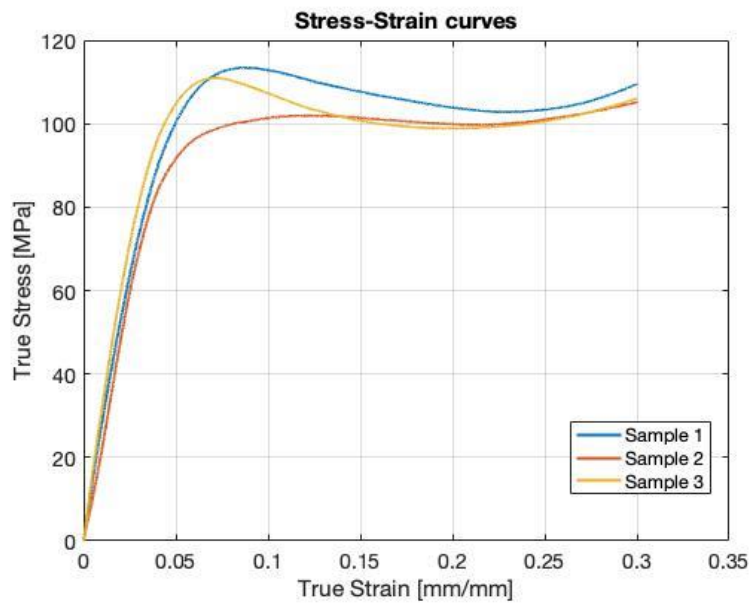


Figure 161: Stress-Strain curves Nozzle T. 385°C - Fan 25%

From the engineering values of stress and strain the mean and standard deviation of the Elastic modulus in compression have been computed. From the true stress the yielding compression stress mean and standard deviation have been computed, in order to be more conservative and accurate. In Table 21 the parameters of interest are summarized.

T. Nozzle 380-Fan 0%	Young's Modulus [MPa]	Yield stress [MPa]
Mean	2723,00	110,20
Std. Deviation	0,00	0,00
T. Nozzle 380-Fan 25%	Young's Modulus [MPa]	Yield stress [MPa]
Mean	2649,33	109,60
Std. Deviation	276,33	4,49
T. Nozzle 385-Fan 25%	Young's Modulus [MPa]	Yield stress [MPa]
Mean	2771,33	108,77
Std. Deviation	212,74	6,05

Table 21: Mean and standard deviation of the parameters of interest

The comparison between the key properties in different conditions are reported in Figure 162 and Figure 163.

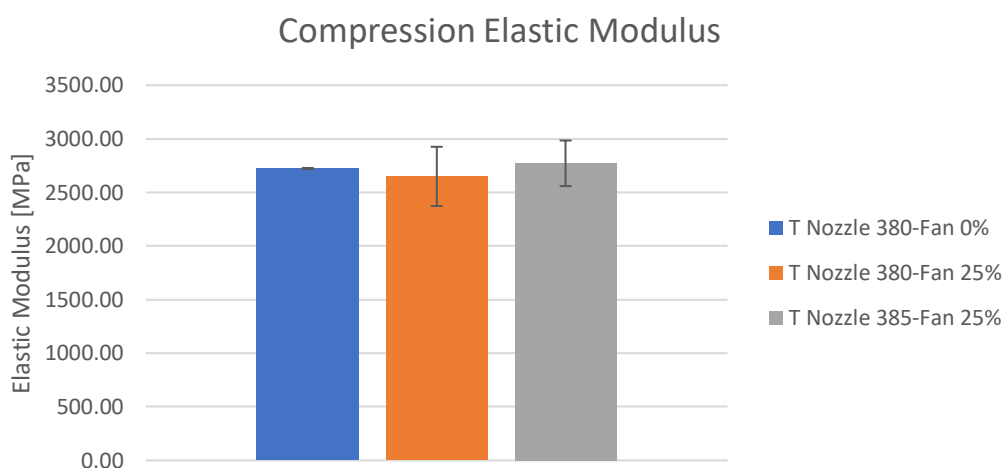


Figure 162: Compression elastic modulus comparison

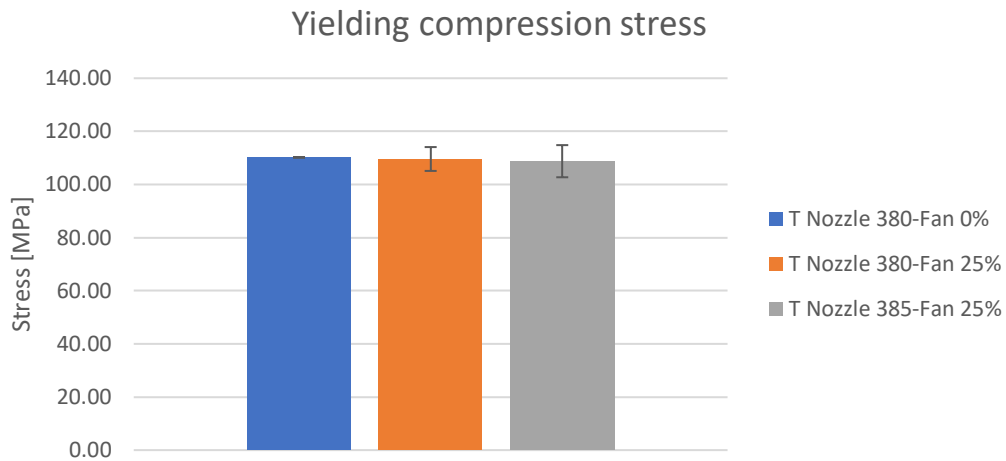


Figure 163: Yielding compression stress comparison

It is possible to notice that the parameters choice in the process window do not affect in a significant manner the results, since the process window is really tight. The condition with 0% fan speed, which presented slight overheating, is the one which often behaved in an incorrect way, leading to the elimination of two samples out of three, therefore should be avoided. From the Stress-Strain curves it can be seen that the conditions with 25% fan behave really similarly even if the one with 380 °C nozzle temperature seems more consistent. It is difficult to take conclusions on the best condition between the two with such a small number of samples. Overall, the additive manufactured material behaved in a good manner, with uniform deformation and no cracking, the average value of Yielding compression stress is about 109 MPa while the Compression Elastic Modulus is about 2700 MPa. These values are significant for an additive manufactured thermoplastic, confirming that ULTEM can be adopted in high stress conditions. Due to its high temperature resistance it can be considered an adequate material for Rapid Tooling.

5.8.6 Tensile Specimen

Three conditions have been evaluated for the tensile specimen, varying IR lights. For each condition 3 samples have been printed to obtain mean and standard deviation, in future works more samples for each condition should be printed for more reliable results.

The general aspect of the printed tensile test is reported in Figure 164. It can be noticed that the neck section, with nominal dimensions 6x4 mm, is really small and few roads and almost no zig zag infill are present in the area.

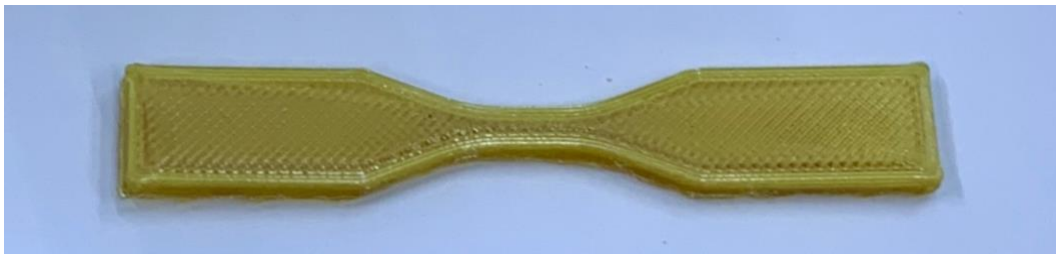


Figure 164: Tensile specimen geometry

The samples n. 1 with 0% IR power were built in a flawless way, resulting in a good geometry, color and general aspect, as shown in Figure 165.



Figure 165: Tensile specimens IR 0%

Samples n. 2 with 25% IR power also were produced without any problem or flaw, even if some slight change of color is present, as presented in Figure 166. Overall this condition does not affect printability in a significant manner.

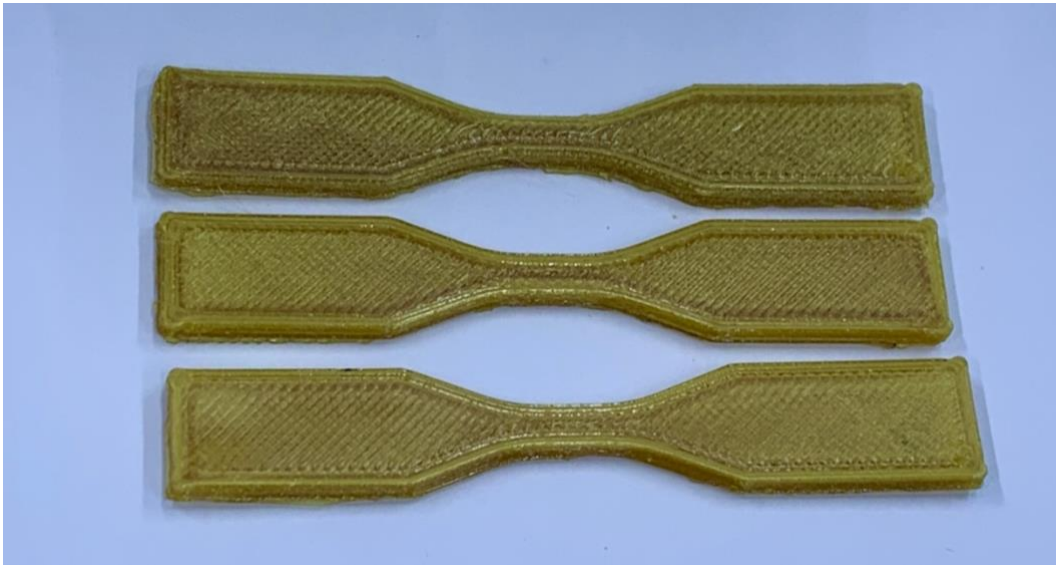


Figure 166: Tensile specimens IR 25%

Samples n. 3 with IR power of 50% (Figure 167) instead were damaged by a too high heat flux. The overheating problem is consistent and traces of material degradation are present. The geometry is not respected due to an exaggerated heat flux trough the piece which resulted in too high temperature of the substrate while the next layer was deposited. The piece was indeed still soft when the next layer was deposited and event when the print was completed, sign that all the material was at a temperature higher than its glass transition temperature when the building process was undergoing.



Figure 167: Tensile specimens IR 50%

The results of the printing phase are summarized in Table 22, all the variables except the IR power are kept constant as in Table 8.

Tensile specimen	1	2	3
IR power %	0	25	50
Accomplished	✓	✓	✗
Notes	Good looking	Adequate	Overheating

Table 22: Tensile specimens printing phase results

5.8.7 Mechanical tensile testing

All the printed tensile samples were mechanically tested according to ISO 527, with an extension rate of 1 mm/min. The samples were tested on the MTS Alliance RT/100 machine, shown in Figure 168, with an MTS extensometer mounted on the piece.



Figure 168: Tensile test machine

After testing the resulting fracture was fragile, usually on the neck but sometimes also at the beginning of the curvature radius. The usual fracture aspect is shown in Figure 169.



Figure 169: Tensile specimen fracture

Upon testing all the samples, the results obtained are presented in Table 23. The values in Table 23 for stresses and strains are the engineering ones while for the development of the curves the real stress and real strain have been computed, considering the reduction in section during tensile testing.

The relation which links the engineering values and true values for traction is the following:

$$\sigma_{true} = \sigma_{eng}(1 + \varepsilon_{eng}) \quad \varepsilon_{true} = \ln(1 + \varepsilon_{eng})$$

IR POWER	0%			25%			50%		
Specimen	1	2	3	1	2	3	1	2	3
Nominal Gage Length [mm]	8	8	8	8	8	8	8	8	8
Initial Speed [mm/min]	1	1	1	1	1	1	1	1	1
Removal Point [mm]	0,15	0,15	0,15	0,15	0,15	0,15	0,15	0,15	0,15
Secondary Speed [mm/min]	1	1	1	1	1	1	1	1	1
Thickness [mm]	3,8	3,8	3,8	3,8	3,8	3,8	3,8	3,8	3,8
Width [mm]	5,9	5,9	5,9	5,9	5,9	5,9	5,9	5,9	5,9
Young's Modulus [MPa]	3488	3330	3664	3358	3617	3244	2716	3151	3561
Rp02 [MPa]	56	54	52	50	57	58	40	47	56
Rp1 [MPa]	64	88	78	64	78	90	59	41	85
Stress0.2 [MPa]	7	7	7	7	7	7	6	6	7
Stress1 [MPa]	34	32	34	33	35	31	26	30	34
Peak Stress [MPa]	66	93	83	74	86	104	64	60	88
Strain At Break [%]	3	4	3,1	2,9	3,2	6,5	3,2	2,3	3,7
Stress At Break [MPa]	65	93	63	74	63	103	64	52	85
Peak load	1480	2091	1866	1666	1930	2337	1438	1336	1967

Table 23: Tensile test raw data

The first sample in condition IR 0% behaved in a particular manner during testing and was pulled two times, since during the first one it slipped, so its data have been neglected in the computation of mean and standard deviation and its curve was not reported.

The Matlab codes for obtaining the curves from comma separated values given by the tests are presented in Appendix C.

The stress-strain curves obtained are reported in Figure 170, Figure 171 and Figure 172.

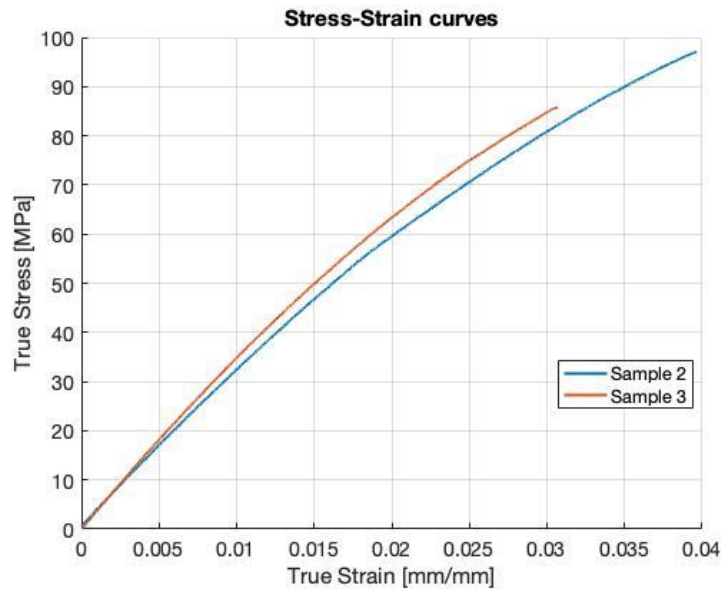


Figure 170: Stress-Strain curves for IR 0%

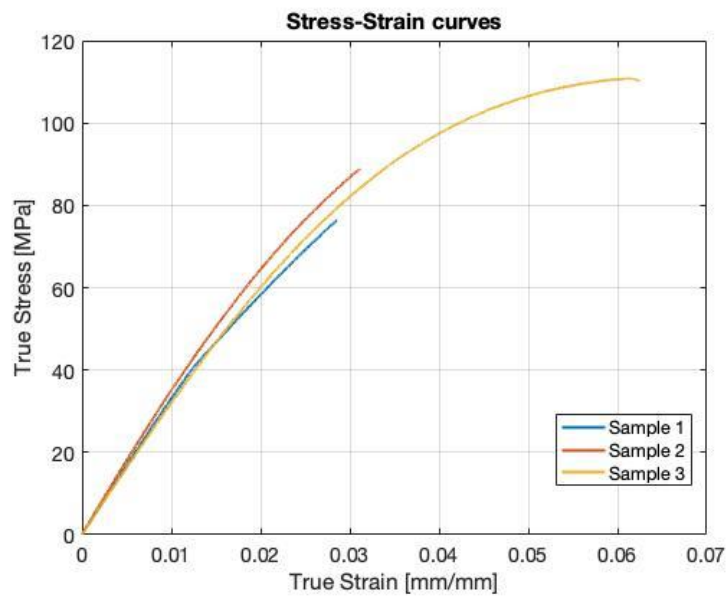


Figure 171: Stress-Strain curves for IR 25%

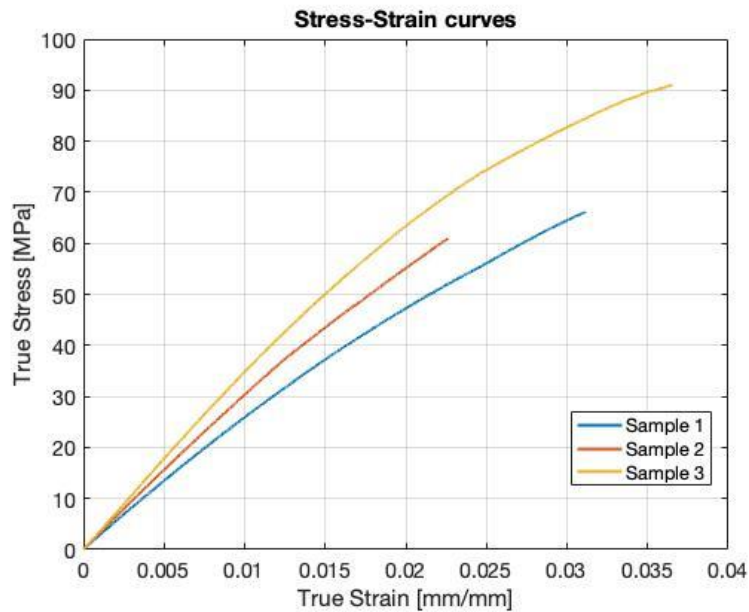


Figure 172: Stress-Strain curves for IR 50%

From the engineering values the mean and standard deviation for Young's Modulus, Peak Stress and Strain at Break have been computed at each different IR power, as reported in Table 24.

IR 0%	Young's Modulus [MPa]	Peak Stress [MPa]	Strain At Break [%]
Mean	3497,00	88,00	3,55
Std. Deviation	236,17	7,07	0,64
IR 25%	Young's Modulus [MPa]	Peak Stress [MPa]	Strain At Break [%]
Mean	3406,33	88,00	4,20
Std. Deviation	191,14	15,10	2,00
IR 50%	Young's Modulus [MPa]	Peak Stress [MPa]	Strain At Break [%]
Mean	3142,67	70,67	3,07
Std. Deviation	422,56	15,14	0,71

Table 24: Mean and standard deviation of the properties of interest

The comparison between important properties in the three conditions are reported in Figure 173, Figure 174 and Figure 175.

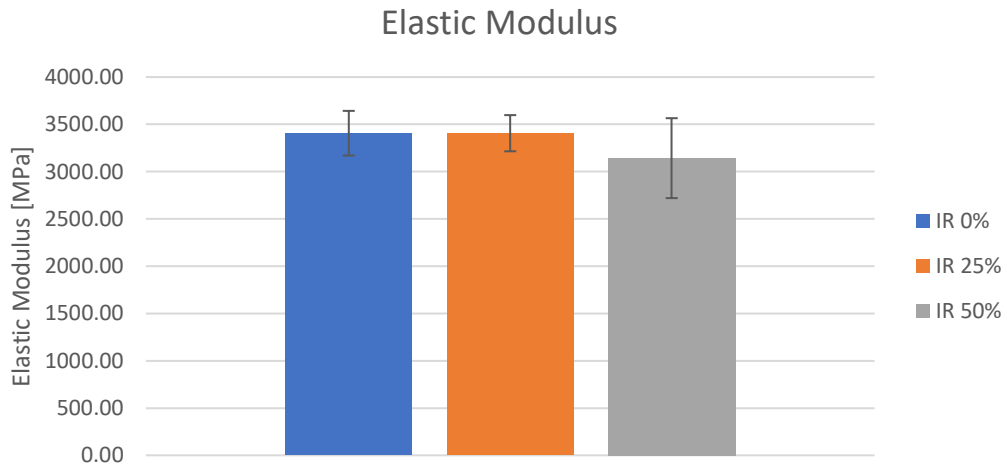


Figure 173: Tensile elastic modulus comparison

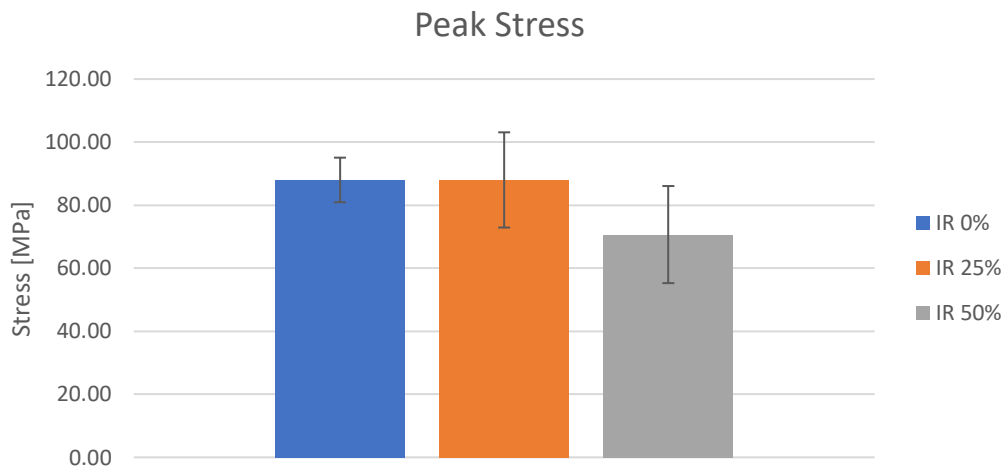


Figure 174: Peak tensile stress comparison

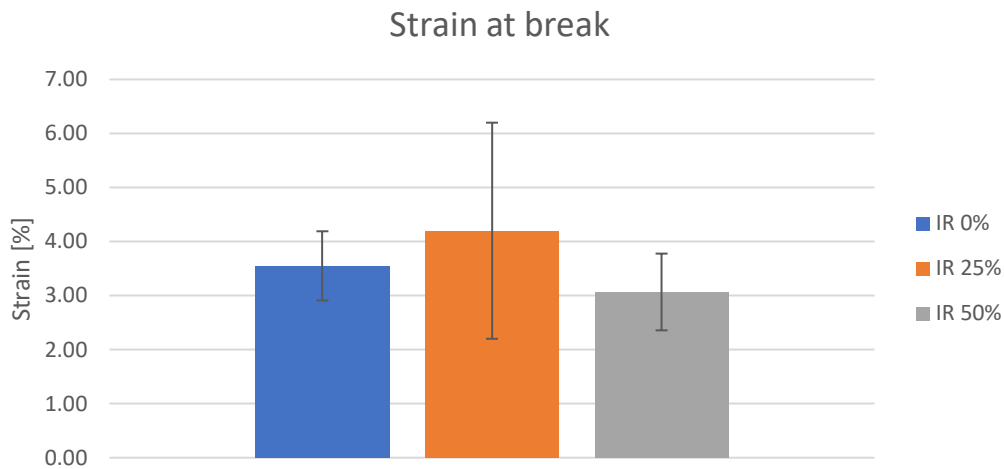


Figure 175: Strain at break comparison

From the analyzed data it can be seen how increasing the IR power the Elastic Modulus decrease, the strain at break increases up to the point of material degradation and the peak stress slightly increases but is not significantly modified up to material degradation. With only three samples per condition the conclusions cannot be considered accurate, in the future a wider study should be carried out.

Particular is the sample n. 3 with IR power 25%, from Table 23, it can be noticed that its characteristic parameters are really close to the ones present in the datasheet of the material for injected molded sample. It should be verified if this condition is repeatable by printing many more samples at 25% IR power.

The mechanical results of condition n. 3 with 50% IR power agrees with the qualitative considerations taken by looking at the samples. The material is degraded and loses strength, increases in dispersion of the results and reduces the stiffness of the specimens.

Overall the tensile mechanical properties of PEI thermoplastic are remarkable, with an achievable UTS of about 90 MPa and elastic modulus of about 3400 MPa. For respect to the ABS samples printed by J. Halo [59]

the strength is close to 3 times the one obtained by ABS specimens while the Elastic Modulus about 1,5 times the ABS one.

The dispersion of results is high, due to the many defects that additive manufacturing produces in the section. Porosity between roads is one of the most frequent defects which affect specimen's UTS, and the number of porosities can vary between different specimens. The relative dispersion in Young modulus is lower than the one in UTS, since this value is obtained in pure elastic field, while UTS is mainly characterized by the stochastic propagation of defects. Other uncontrollable variables might influence the results, such as moisture content of the material and ambient moisture content and temperature.

5.8.8 Warping Test

To evaluate in a repeatable and confrontable way the warping effect I decided to push the piece on one side and measure how much the other side lifts from a flat surface. All the tests are performed with a 10 mm brim around the object and the IR light switched on at 25% during first layer deposition.

The warping test n. 1 with bed temperature at 120 °C (Figure 176) shows consistent warping on the whole piece, which assumes a curved shape. The warping tendency began as the first layer was deposited and not the brim, neither the adhesive managed to keep it flat. As explained in Paragraph 2.5.3 warping effect is given by contraction of the first and subsequent layers as they cool down, while the top ones are still hotter and expanded. Since the layers are bonded together some thermal stresses arise which will eventually give deformation.

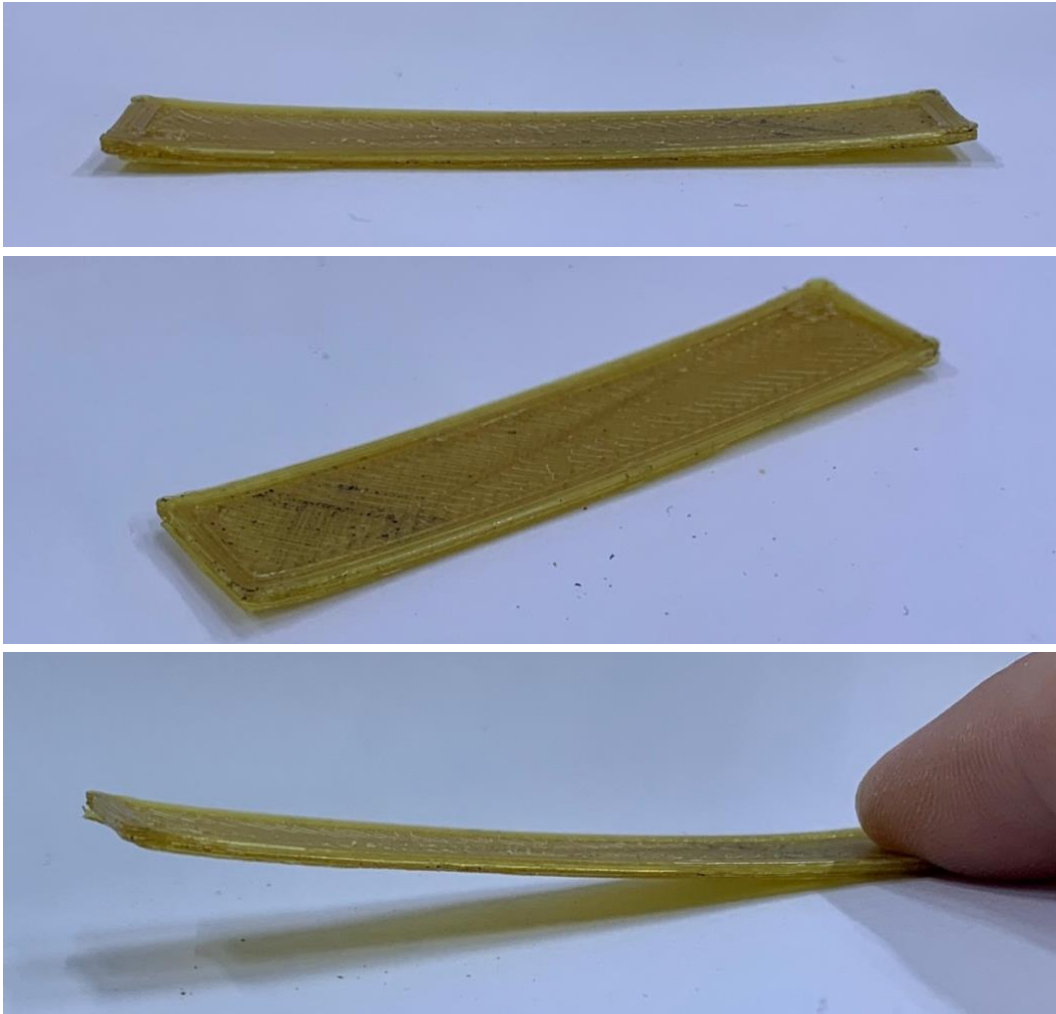


Figure 176: Warping test n. 1

In sample n. 2 with a bed temperature of 150 °C (Figure 177) the situation improves dramatically, with some slight warping only on the extreme sides of the piece, happened mainly as the piece was removed from the build surface due to residual stresses. During printing the adhesion was adequate and no warping occurred.

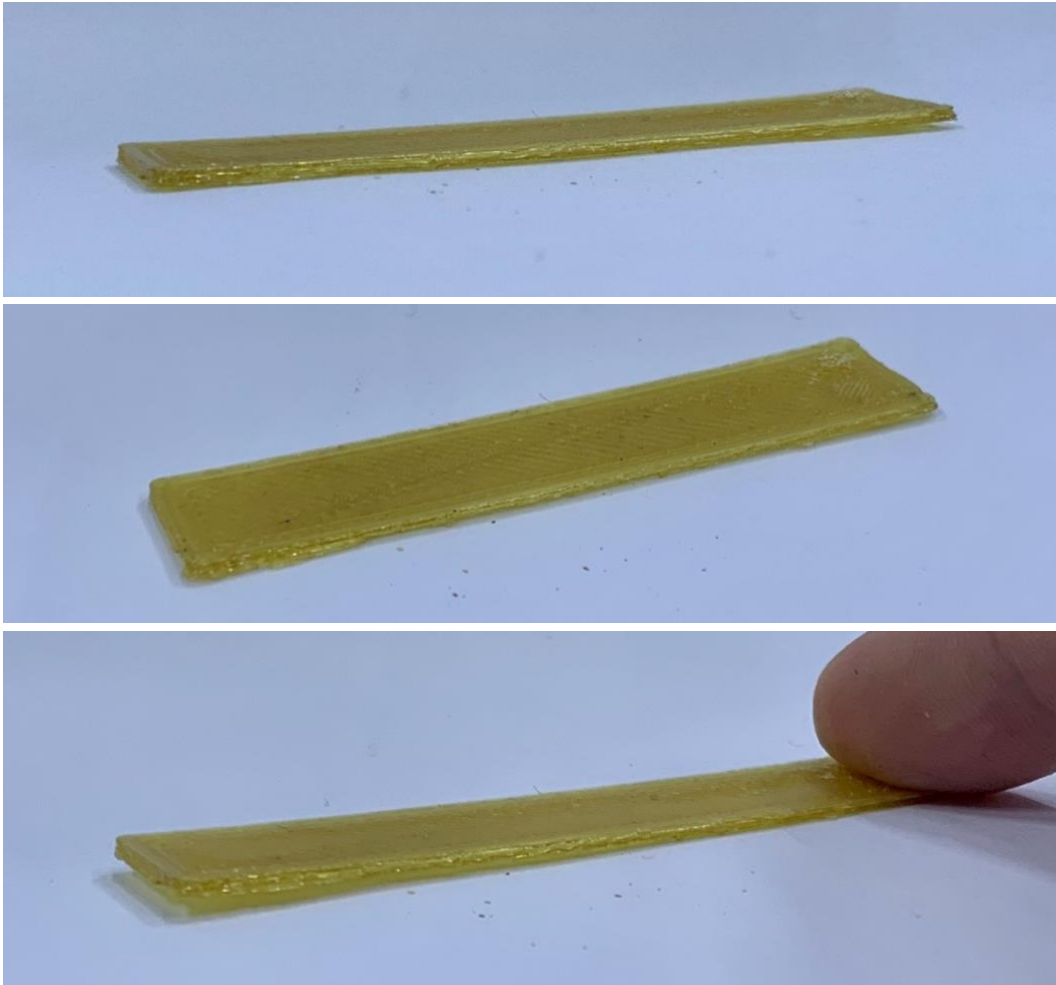


Figure 177: Warping test n. 2

Sample n. 3 with a bed temperature of 180 °C (Figure 178) stuck perfectly to the bed and no significant warping occurred neither upon removal from the build surface. The bed temperature of 180 °C was reached by preheating the build surface with IR lights before the print and during the first layer, after which they were turned off and the resistance of the bed managed to maintain that temperature for the whole printing time.

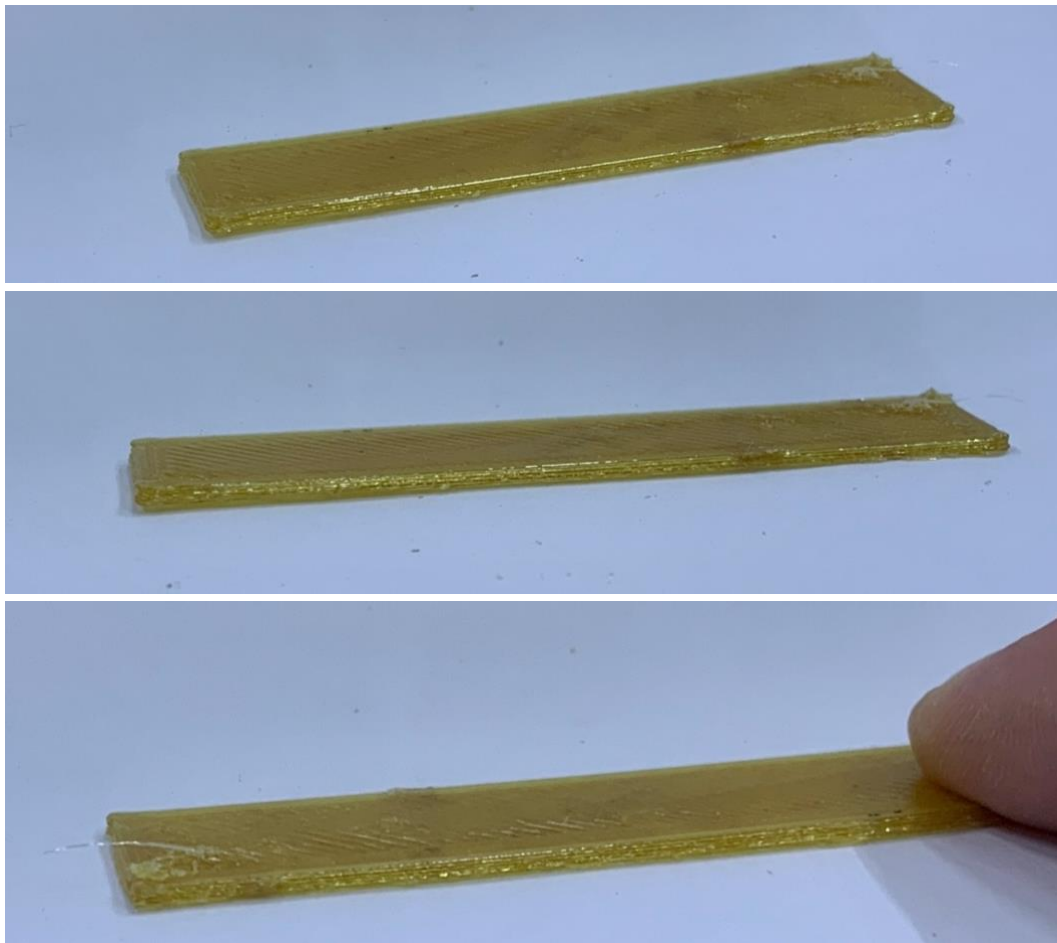


Figure 178: Warping test n. 3

In Table 25 the results of the warping test are summarized, all the variables except the bed temperature are kept constant as in Table 8.

Warping test	1	2	3
Bed Temp. °C	120	150	180
Accomplished	✘	✔	✔
Notes	Significant warping	Slight warping	No warping

Table 25: Warping test results

In Figure 179 the three samples side by side are presented, starting from the sample n.1 on the front and proceeding backwards.

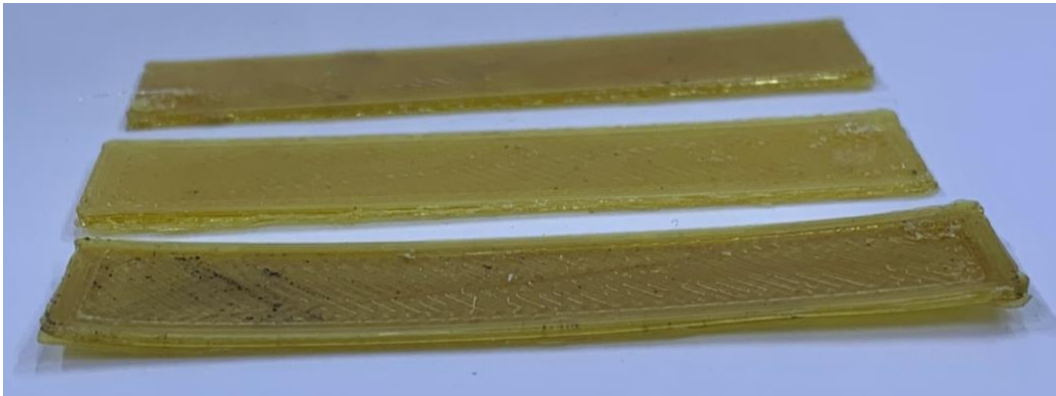


Figure 179: Warping tests comparison

5.8.9 Staircase Effect Test

The staircase effect sample n. 1 with no layer fan (Figure 180) showed some significant overheating in the smallest layers, due to not sufficient heat extraction by convection and conduction in the time needed to complete a layer. The geometry of the upper portion of the sample is completely modified due to the nozzle dragging the deposited material.



Figure 180: Staircase effect test 0% fan

The staircase effect sample n. 2 with 25% layer fan power (Figure 181) shows a correct completion of the geometry even if in some layers some slight delamination is present in one corner. The geometry is anyway successful and it is possible to notice the different surface roughness depending on the model angle. For the 5° angle the staircase effect is really important, while proceeding in steepness of the angle the quality improves dramatically.

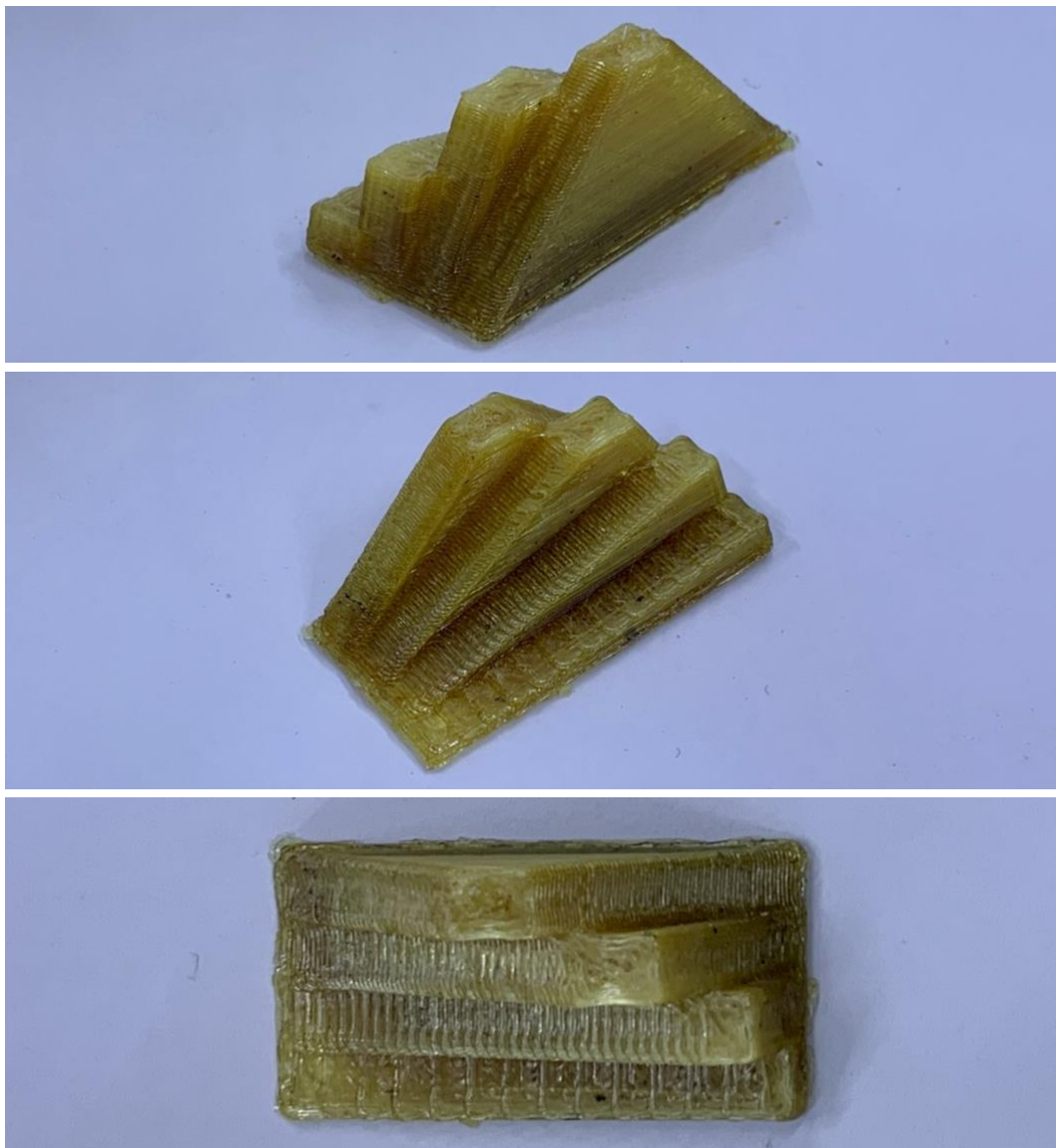


Figure 181: Staircase effect test 25% fan

The sample n. 3 with 50% layer fan power was not produced due to the high probability of delamination and the successful completion of the geometry with 25% fan speed. The tendency to delaminate was observed even in the staircase effect sample n. 2 and in the previous tests each geometry with 50% fan power delaminated, therefore this conclusion is straightforward. In Table 26 the results of the staircase effect test are reported, all the variables except the layer fan are kept constant as in Table 8.

Staircase test	1	2	3
Layer fan	0%	25%	50%
Accomplished	✘	✔	✘
Notes	Strong overheating	Adequate	Probable Delamination

Table 26: Staircase test result

5.8.10 Considerations on the results obtained

From the experimental campaign carried out some final conclusions about ULTEM printing with the EFeSTO machine can be drawn. Regarding the layer fan the optimum has been found to be at 25%, which permits to print in an adequate manner most of the geometries tested. For lower layer fan speeds the overheating problem might appear, while for higher ones delamination occurs.

Regarding the printing temperature the process window is tight, with good results only in the range of 380-385 °C nozzle temperature (Body temperature 5 °C lower), for lower temperatures the viscosity of the material is too high to be extruded by the brushless motor installed, resulting in machine overload. For higher temperatures instead material degradations happens inside the extruder chamber.

The IR lights can be used with power lower than 50%, resulting in overheating and material degradation if set higher. The IR preheating as

pointed out by A. Nycz et al. [45] is useful only if the substrate temperature falls below the glass transition temperature of the material, condition which probably does not occur with small samples as the one printed for this thesis. The IR preheating has been found to be effective if used during the first layer to improve bed adhesion and prevent warping.

The bed temperature has an important role in preventing warping, giving better results if it is set close to the material glass transition temperature, such to have a soft material in the first layer capable of absorbing stresses without excessive deformations.

The geometry of the specimen to be printed influences a lot the thermal parameters to be set, since depending on the area of each layer the time to complete a single layer might vary and thus the heat naturally dissipated by convection and conduction. For smaller layer area the tendency to the overheating problem increases. For increasing infill percentage the thermal inertia of the layer will increase thus increasing the overheating tendency. The mechanical properties of the material have been tested and the results are satisfactory, showing how ULTEM material is a high strength material able to withstand high loads for respect to many other thermoplastics. For this reason it can be of interest in application where a high mechanical resistance is required. Thanks to its high temperature resistance it can also be used for Rapid Tooling in injection molding.

5.8.11 Comparison with ABS results

The results obtained with ULTEM and ABS are very different for the same geometry and this can be explained by the two materials having different thermal parameters, as shown in Table 27. Attention has to be focused on the glass transition temperature and conductivity of the two materials.

	ABS	ULTEM
Extrusion temperature [°C]	230	385
Glass transition temperature [°C]	109	215
Specific heat capacity [J/(kgK)]	1600-2130	2000
Conductivity [W/(mK)]	0,128-0,187	0,22
Density [g/cm ³]	1,04-1,08	1,27

Table 27: ABS-ULTEM properties of interest

For the same geometry and fan speed ABS shows overheating in a much more important way with respect to ULTEM. In other terms, ABS requires a higher fan speed to avoid overheating, while ULTEM a lower fan speed to avoid delamination. For the overhang test ABS optimum has been found to be at 100% fan speed, with good geometry and no signs of delamination, while for ULTEM at fan speed 25%, with delamination present at just 50% fan speed.

These results can be explained from a thermal point of view. ABS has an extrusion temperature much lower than ULTEM and the ambient and bed temperature can be considered similar. Therefore, assuming a constant convection coefficient, the heat extracted by convection will be much higher in ULTEM printing since the gradient is higher. Usually even heat extraction by conduction will be higher with ULTEM material, but this effect is of secondary importance since the diffusivities of the two materials are similar. The extraction of heat results in lowering the temperature of the material and thus it will be easier for ULTEM to naturally reach a temperature close to the glass transition temperature, where overheating problems disappear and some stiffness is present. By using the fan at the same power ULTEM will therefore easily go below the glass transition temperature resulting in delamination, while ABS would require more power to do so. To explain better this reasoning a simple model has been

developed using the lumped system model, after verifying that the Biot Number is lower than 0,1. To compute the Biot Number a value of convection coefficient of 20 W/m²K [60] has been used. Therefore:

$$Bi = \frac{hL}{k}$$

With h convection coefficient, L characteristic length of the heat transfer and k conductivity of the material. The Biot number is different for ULTEM and ABS since they have a slightly different value of conductivity, for ABS the lower value reported in Table 27 will be used. The characteristic length of the problem is taken as the layer height since it is usually defined as the ratio between the volume and the area exchanging heat. Therefore $Bi_{ABS}=0,039$ while $Bi_{ULTEM}=0,023$, since both are lower than 0,1 the lumped system model can be used.

The body under analysis have been assumed to be a small section of deposited road, and attention will be focused on its temperature profile during the time to complete the layer. That's because, assuming a geometry with constant profile for each layer, after the time to complete the layer the nozzle will deposit another small section of road above the one under analysis. The temperature of the road under analysis is important to determine good bonding, overheating or delamination when the next small section at the extrusion temperature is deposited above it.

Thanks to the lumped system model the whole deposited filament section can be considered at the same temperature, without temperature gradients in the volume.

The model is developed by using Newton's Convection Law and the relation between internal energy and temperature.

$$q'' = \frac{\dot{Q}}{A} = h(T_s - T_\infty)$$

With q'' being the heat flux per unit of area A, h the convection coefficient and T_s and T_∞ the temperatures respectively of the surface and of the fluid. And:

$$\frac{dU}{dt} = c_p m \frac{dT}{dt}$$

With U being the internal energy, m the mass of the object, c_p the specific heat capacity and T the temperature.

By applying the first law of thermodynamics it's possible to obtain:

$$\frac{dU}{dt} = -\dot{Q}$$

The rate of heat transfer \dot{Q} can be written thanks to the Newton's Law, resulting in:

$$\begin{aligned} \frac{dT(t)}{dt} &= \frac{1}{c_p m} \frac{dU}{dt} = -\dot{Q} \\ \frac{dT(t)}{dt} &= -\frac{hA}{c_p m} (T_s(t) - T_\infty) = -\frac{1}{\tau} \Delta T(t) \text{ with } \tau = \frac{c_p m}{hA} \\ \frac{dT(t)}{dt} &= \frac{d\Delta T(t)}{dt} = -\frac{1}{\tau} \Delta T(t) \end{aligned}$$

The solution of the differential equation, by integrating from the initial condition at $t = 0$ is:

$$\Delta T(t) = \Delta T(0) e^{-t/\tau}$$

By explicating the temperatures in $\Delta T(t)$ and $\Delta T(0)$:

$$T_s(t) = T_\infty + (T_s(0) - T_\infty) e^{-t/\tau}$$

So the temperature difference between the deposited road of material and the environment decays exponentially as a function of time.

In first approximation the time constant τ can be considered constant between ABS and ULTEM, since the specific heat capacity is similar, the convection coefficient for the same conditions might be considered similar and mass and area of the external surface for the same object are equal.

Therefore the driving force for cooling is mainly given by the difference $T(0) - T_\infty$, which is the temperature difference between the extrusion one and the ambient one.

The temperature behavior in time is similar in the two materials, the temperatures of interest are the extrusion, glass transition and ambient temperature, as shown in Figure 182.

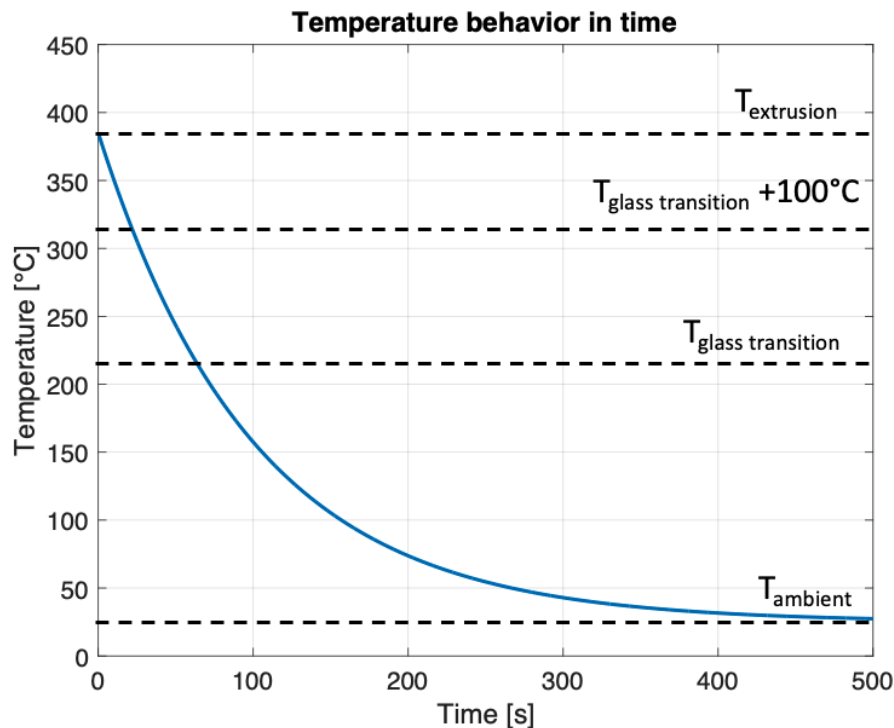


Figure 182: Temperature behavior in time

At $t=0$ for both the materials:

$$T(0) = T_{\infty} + (T_s(0) - T_{\infty})e^{-0/\tau} = T_{extrusion}$$

Which will be 230 °C for ABS and 385 °C for ULTEM. As pointed out by N. Turner et al. [28] and E. L. Gilmer et al. [61] for extrusion temperatures close to $T_g^* = T_g + 100 \text{ }^{\circ}\text{C}$, there is the best diffusion and bonding among different roads and layers, but this depends also by the cooling effects on the deposited filaments.

After a certain t^* both the materials will reach the glass transition temperature, so $T(t^*) = T_g$, with T_g lower than $T_{extrusion}$.

$$T_s(t^*) = T_{\infty} + (T_{extrusion} - T_{\infty})e^{-t^*/\tau} = T_g$$

By subtracting the two equations it's possible to obtain:

$$T_{extrusion} - T_g = T_{\infty} + (T_{extrusion} - T_{\infty})e^{-0/\tau} - (T_{\infty} + (T_{extrusion} - T_{\infty})e^{-t^*/\tau})$$

That after some simplifications will result in:

$$T_{extrusion} - T_g = (T_{extrusion} - T_\infty)(1 - e^{-t^*/\tau})$$

And therefore:

$$e^{-t^*/\tau} = 1 - \frac{T_{extrusion} - T_g}{T_{extrusion} - T_\infty}$$

$$-t^*/\tau = \ln \left(1 - \frac{T_{extrusion} - T_g}{T_{extrusion} - T_\infty} \right)$$

Considering a unitary τ :

$$t^* = -\ln \left(1 - \frac{T_{extrusion} - T_g}{T_{extrusion} - T_\infty} \right)$$

or:

$$t^* = -\ln (1 - \xi)$$

With $\xi = \frac{T_{extrusion} - T_g}{T_{extrusion} - T_\infty}$.

With this equation it is possible to interpret better how long does it take for the temperature to reach T_g , this time is proportional to t^* . If for one material t^* is higher, the material is more prone to overheating for the same geometry, in which the time to complete a layer is the same.

For ULTEM $\xi = 0,47$ and $t^*=0,64$, while for ABS $\xi = 0,59$ and $t^*=0,89$, which have a t^* 39% higher than ULTEM's one.

In other words if, in the time to complete one layer, the temperature stays consistently above T_g the material will be subjected to the overheating problem, while if its temperature falls below T_g it is probable that delamination will occur. Slightly over and around T_g there is the zone of good bonding, since when the next filament section is deposited upon the one under analysis the temperature of the latter will rise to some extent, as shown by B. D. Vogt et al. [23] (more details in Paragraph 2.5.2).

The parameter $\xi = \frac{T_{extrusion} - T_g}{T_{extrusion} - T_\infty}$ is significant in this model, since it is the ratio between the ΔT proportional to the heat to be extracted and the driving force for cooling by convection. If the numerator is high the heat to be extracted to reach good bonding condition will be higher, if it is low the

heat to be extracted will be lower, and thus it will be easier, in natural cooling by convection, for delamination to occur, since it will be more probable to go to temperatures lower than T_g . If the denominator is low overheating is more prone to occur, while if it is high delamination will probably occur since a lot of heat is extracted in natural convective cooling. From the last equation it also is possible to draw a qualitative graph (Figure 183) relating the t^* and the variable ξ . This graph will have an exponential trend and will provide different values of t^* for different $\frac{T_{extrusion}-T_g}{T_{extrusion}-T_\infty}$, which depend on the material used, extrusion conditions and ambient temperature.

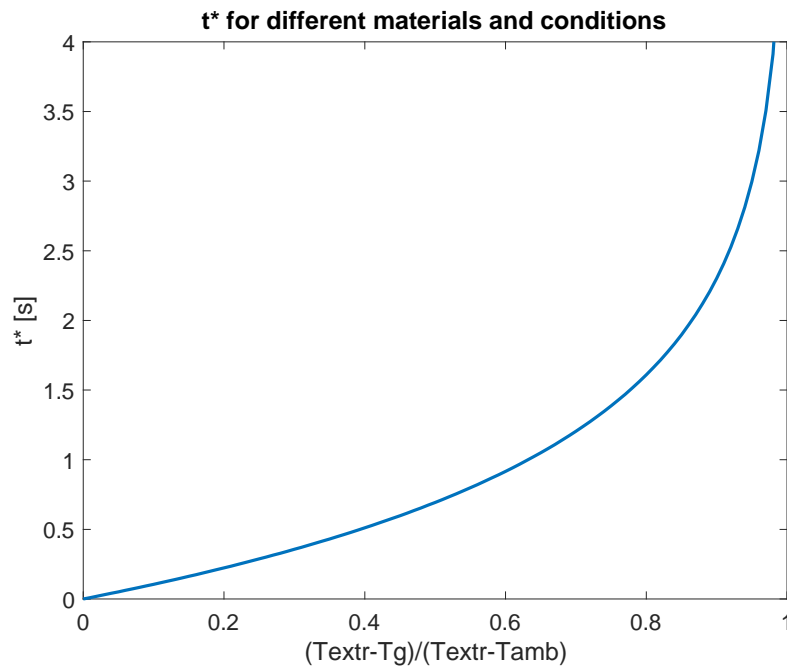


Figure 183: t^* for different materials and extrusion conditions

For one material the extrusion, glass transition and ambient temperatures will be constant, giving a constant $\frac{T_{extrusion}-T_g}{T_{extrusion}-T_\infty}$. The time to complete a layer in a given geometry defines an experimental point, by comparing it to t^* obtained by the following equation it is possible to qualitatively understand

if the condition is prone to overheating, delamination or will give good results.

$$t^* = -\tau \cdot \ln\left(1 - \frac{T_{extrusion} - T_g}{T_{extrusion} - T_\infty}\right) \text{ with } \tau = \frac{c_p m}{hA}$$

The overheating problem will happen if the experimental point lies significantly below the t^* line, delamination instead if the experimental point lies above. Close to the t^* line the adequate conditions lie, for which it is possible to have good bonding between layers without delamination and overheating occurring. From Figure 184 (in which times are qualitative, since τ is considered unitary), it is possible to notice that for ABS the experimental layer times giving overheating are higher than for ULTEM, thus for the same geometry with same layer time the ABS specimen will be more prone to the overheating problem.

For example, if a geometry has a layer time positioned at a qualitative time of 0,7 in Figure 184, it will be in good bonding condition for ULTEM, since it is close to t^* , but overheating condition for ABS, since it would be not enough to reach temperature for good bonding.

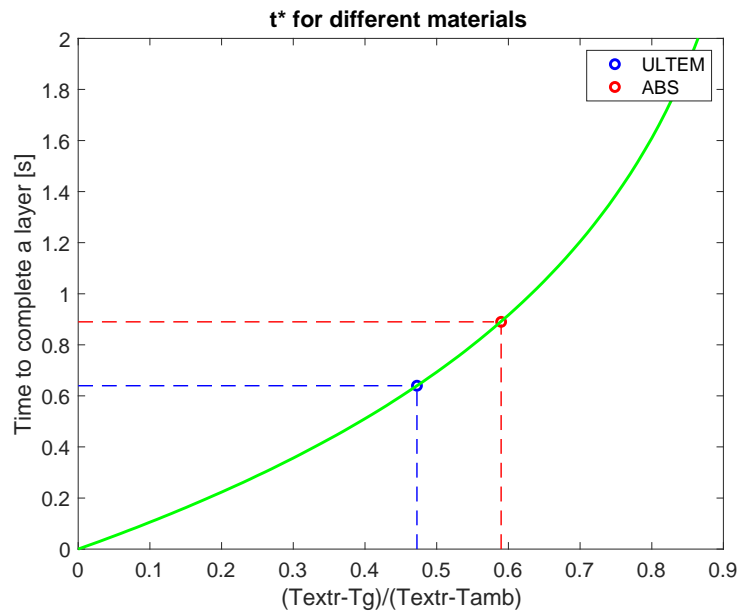


Figure 184: Overheating and delamination tendency ABS and ULTEM

6 Conclusions

This work was able to reach the desired results, by using a scientific and accurate procedure with focus on the process. The aim of this thesis was indeed to improve the machine in order to print with better quality and reliability and to test the printability of difficult materials such as ULTEM. I started by investigating the problems of the machine, found solutions for these flaws and then verified the solutions with an experimental campaign. This thesis is divided in four parts, all of them related and organized with logical links, the previous section is indeed useful and important for the next one. In the first part the scientific background both for the specific machine technology and for the thermal problems in the process of EAM has been gathered and organized. In the second part an in-depth study of the machine characteristics, limits and problems has been carried out. In the third section the improvements, to solve the problems present on the machine, are presented and explained. Lastly an experimental campaign has been carried out to verify how the improvements on the machine would affect the quality and strength of the produced parts.

The improvements carried out started from a complete upgrade of the cooling system and heated bed, the installation of a layer fan, proceeded with the installation of an infrared preheater, configuration of the pneumatic nozzle closure, PLC parameter modifications and ended by designing new nozzles for the machine. The improvements affected many aspects of the machine, from reliability and functionality to the thermal conditions. At the beginning of this thesis the EFeSTO machine was not able to properly print any material, while after the improvements carried out it is able to print even the most challenging materials, such as ULTEM pellets, with high quality and adequate properties.

The experimental campaign showed how in EAM the thermal conditions after extrusion can completely modify the results in terms of quality. The thermal conditions should be controlled according to the geometry and

material to be printed, as understood from the differences between ABS and ULTEM results in different objects to be produced.

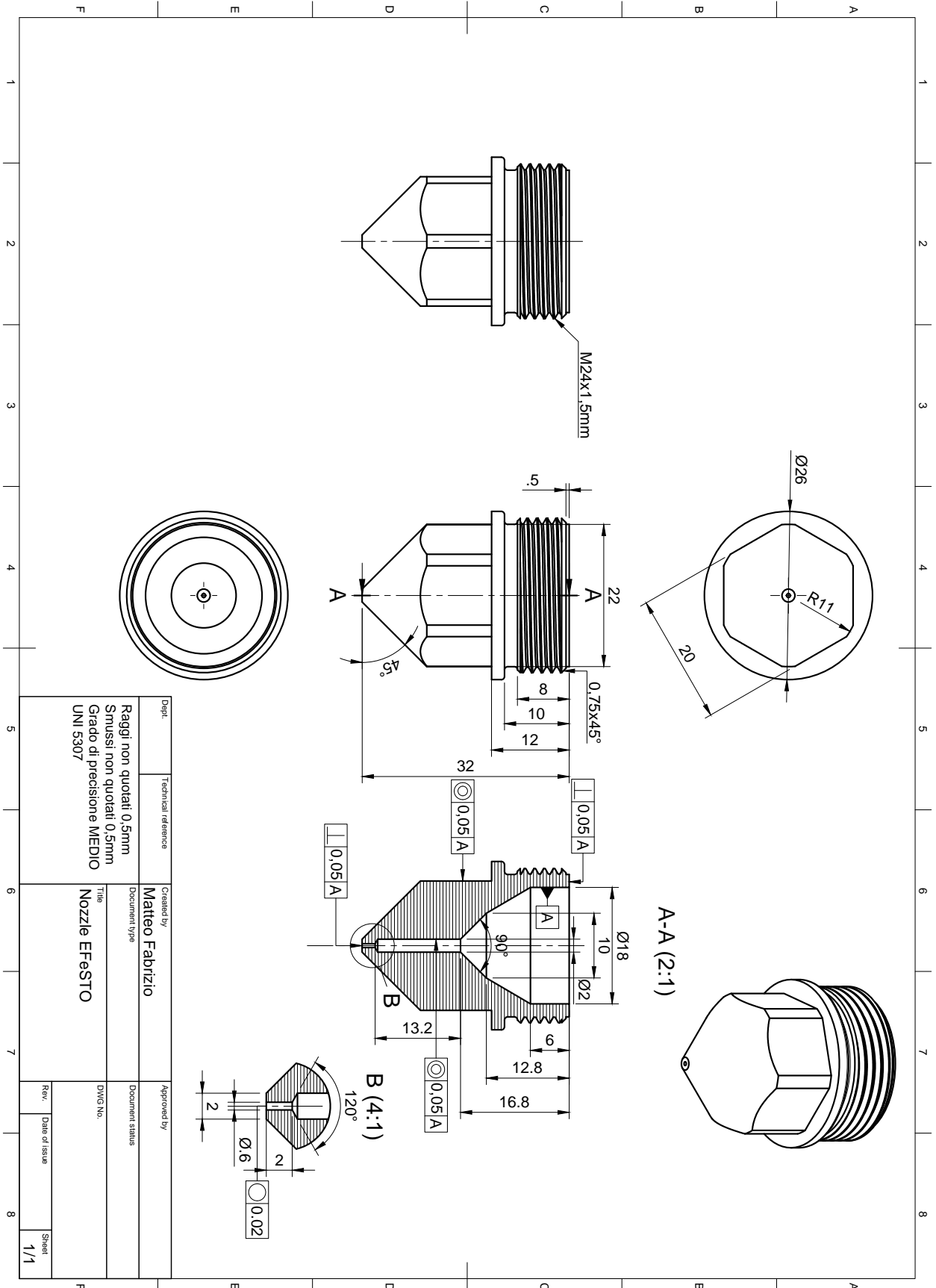
ULTEM material is not well characterized and not often used in additive manufacturing literature. No researches so far have been developed about ULTEM printing from pellets, therefore this work can be a starting point for future investigations on this specific material, which has some interesting applications, such as high resistance components and Rapid Tools.

It was possible to develop a process window in terms of printing temperatures and layer fan speed, with 380 – 385 °C nozzle temperature (body 5°C lower) and layer fan at a power of about 25% to achieve the best results in terms of quality and good mechanical properties. Lower extrusion temperatures resulted in machine overload, higher ones in material degradation. For fan speed power higher or lower than 25%, respectively delamination or overheating problems occurred. The bed temperature affects in a significant manner the warping tendency of the material, with best results for a bed temperature of 180 °C, close to the material glass transition temperature. From the IR preheater trials it was possible to understand that close to 50% power the material started to degrade and overheat, for lower power the results do not change in a dramatical manner, further studies should be carried out on this aspect. The preheater on the other hand increased in a significant way the adhesion of the first layer. The results in terms of mechanical properties are adequate for an additive manufacturing machine printing ULTEM material, but a wider and complete study should be carried out in the future, to achieve more consistent and reliable results.

In the future other improvements on the machine could be implemented, such as a chiller for the cooling water, in order to print for longer time high temperature materials, and improvements on the chamber recharge feature, to print bigger objects without issues.

Appendix A

Nozzle technical drawing



Dept:	Technical reference	Created by	Approved by
		Matteo Fabrizio	
Raggi non quotati 0,5mm Smussi non quotati 0,5mm Grado di precisione MEDIO UNI 5307		Document type	Document status
		Nozzle EFESTO	
DWG No.		Rev.	Date of issue
		Sheet	1/1

Appendix B

ULTEM 1000 Datasheet



ULTEM™ RESIN 1000

DESCRIPTION

ULTEM 1000 Resin is an unreinforced amorphous polyetherimide (PEI) resin that may offer a high glass transition temperature (Tg) of 217°C. Features are excellent mechanical, electrical and dimensional properties up to high temperatures. The material may offer very good chemical resistance for an amorphous material and is inherently flame retardant offering UL94 V0 and 5V ratings and aerospace FAR 25.853 compliance. The material is RoHS compliant and the natural, uncolored, material is halogen free according to standards IEC 61249-2-2.1, IPC 4101E and JEDEC JS709B. For colored variants compliance needs to be checked case by case. The base material is transparent amber colored but is also available in custom colors - transparent and opaque.

GENERAL INFORMATION	
Features	Flame Retardant, Transparent, Chemical Resistance, Good Processability, Hydrolytic Stability, Low Creep Sensitivity, Low Smoke and Toxicity, Good dimensional stability, High Heat Resistance, High Stiffness, High Strength, Amorphous, Good metal adhesion, Low Shrinkage, Good Mechanicals in Broad Temperature Range, High electric breakdown strength (BDS), UV-C Resistance, Radiation Resistance (gamma, x-ray), Metallizable, Transparent to Microwave radiation and near IR
Fillers	Unreinforced
Polymer Types	Polyetherimide (PEI)
Processing Techniques	Additive manufacturing, Extrusion Blow Molding, Film Extrusion, Injection Molding, Profile Extrusion, Extrusion, Extrusion compounding, Compression molding, Injection compression molding, Foam Extrusion
Regional Availability	Europe, Asia, Americas
INDUSTRY	SUB INDUSTRY
Automotive	Heavy Truck, Automotive Interiors, Bus, Automotive Under the Hood
Building and Construction	Outdoor, Lawn and Landscape
Consumer	Ophthalmics, Sport/Leisure, Personal Accessory, Home Appliances, Personal Recreation, Commercial Appliance, Recreational Vehicle
Electrical and Electronics	Electrical Devices and Displays, Lighting, Electrical Components and Infrastructure
Hydrocarbon and Energy	Fossil, Electric Vehicle, Wind Energy, Energy Storage
Industrial	Defense, Semiconductors, Textile, Servomotor, Electronic Material Handling, Industrial Material Handling, Composite
Mass Transportation	Aircraft Interiors, Specialty Vehicles, Rail
Packaging	Rigid Packaging, Consumer Packaging

TYPICAL PROPERTY VALUES

Revision 20210812

PROPERTIES	TYPICAL VALUES	UNITS	TEST METHODS
MECHANICAL ⁽¹⁾			
Tensile Stress, yield, 50 mm/min	110	MPa	ISO 527
Tensile Strain, yield, 50 mm/min	6	%	ISO 527
Tensile Strain, break, 50 mm/min	50	%	ISO 527
Tensile Modulus, 1 mm/min	3200	MPa	ISO 527
Flexural Stress, yield, 2 mm/min	160	MPa	ISO 178
Flexural Modulus, 2 mm/min	3300	MPa	ISO 178
Ball Indentation Hardness, H358/30	140	MPa	ISO 2039-1
Hardness, Rockwell M	106	-	ISO 2039-2
Tensile Stress, yld, Type I, 50 mm/min	115	MPa	ASTM D638

© 2021 Copyright by SABIC. All rights reserved

CHEMISTRY THAT MATTERS™

PROPERTIES	TYPICAL VALUES	UNITS	TEST METHODS
Tensile Strain, yld, Type I, 50 mm/min	7	%	ASTM D638
Tensile Strain, brk, Type I, 50 mm/min	60	%	ASTM D638
Tensile Stress, yld, Type I, 5 mm/min	110	MPa	ASTM D638
Tensile Strain, yld, Type I, 5 mm/min	7	%	ASTM D638
Tensile Strain, brk, Type I, 5 mm/min	60	%	ASTM D638
Tensile Modulus, 5 mm/min	3350	MPa	ASTM D638
Flexural Stress, yld, 1.3 mm/min, 50 mm span	165	MPa	ASTM D790
Flexural Modulus, 1.3 mm/min, 50 mm span	3200	MPa	ASTM D790
Flexural Stress, yld, 2.6 mm/min, 100 mm span	160	MPa	ASTM D790
Flexural Modulus, 2.6 mm/min, 100 mm span	3400	MPa	ASTM D790
Hardness, Rockwell M	109	-	ASTM D785
Taber Abrasion, CS-17, 1 kg	10	mg/1000cy	ASTM D1044
IMPACT ⁽¹⁾			
Izod Impact, unnotched 80°10°4 +23°C	NB	kJ/m ²	ISO 180/1U
Izod Impact, unnotched 80°10°4 -30°C	NB	kJ/m ²	ISO 180/1U
Izod Impact, notched 80°10°4 +23°C	6	kJ/m ²	ISO 180/1A
Izod Impact, notched 80°10°4 -30°C	6	kJ/m ²	ISO 180/1A
Charpy 23°C, V-notch Edgew 80°10°4 sp=62mm	4	kJ/m ²	ISO 179/1eA
Charpy -30°C, V-notch Edgew 80°10°4 sp=62mm	4	kJ/m ²	ISO 179/1eA
Izod Impact, unnotched, 23°C	1800	J/m	ASTM D4812
Izod Impact, unnotched, -30°C	1540	J/m	ASTM D4812
Izod Impact, notched, 23°C	53	J/m	ASTM D256
Izod Impact, notched, -30°C	50	J/m	ASTM D256
Izod Impact, Reverse Notched, 3.2 mm	1335	J/m	ASTM D256
Gardner, 23°C	36	J	ASTM D3029
THERMAL ⁽¹⁾			
HDT/Bf, 0.45 MPa Flatw 80°10°4 sp=64mm	209	°C	ISO 75/Bf
HDT/ Af, 1.8 MPa Flatw 80°10°4 sp=64mm	192	°C	ISO 75/ Af
Vicat Softening Temp, Rate A/50	215	°C	ISO 306
Vicat Softening Temp, Rate B/50	211	°C	ISO 306
Vicat Softening Temp, Rate B/120	212	°C	ISO 306
CTE, -20°C to 150°C, flow	5.2E-05	1/°C	ISO 11359-2
CTE, -20°C to 150°C, xflow	5.2E-05	1/°C	ISO 11359-2
Ball Pressure Test, 125°C +/- 2°C	PASS	-	IEC 60695-10-2
Thermal Conductivity	0.22	W/m-°C	ISO 8302
HDT, 0.45 MPa, 6.4 mm, unannealed	210	°C	ASTM D648
HDT, 1.82 MPa, 6.4 mm, unannealed	201	°C	ASTM D648
HDT, 0.45 MPa, 3.2 mm, unannealed	207	°C	ASTM D648
HDT, 1.82 MPa, 3.2mm, unannealed	190	°C	ASTM D648
Vicat Softening Temp, Rate B/50	211	°C	ASTM D1525
CTE, -20°C to 150°C, flow	5.6E-05	1/°C	ASTM E831
CTE, -20°C to 150°C, xflow	5.4E-05	1/°C	ASTM E831
Thermal Conductivity	0.22	W/m-°C	ASTM C177
Relative Temp Index, Elec ⁽²⁾	170	°C	UL 746B
Relative Temp Index, Mech w/impact ⁽²⁾	170	°C	UL 746B

PROPERTIES	TYPICAL VALUES	UNITS	TEST METHODS
Relative Temp Index, Mech w/o impact ⁽²⁾	170	°C	UL 746B
PHYSICAL ⁽¹⁾			
Density	1.27	g/cm ³	ISO 1183
Moisture Absorption, (23°C/50% RH/24hrs)	0.2	%	ISO 62-4
Moisture Absorption, (23°C/50% RH/Equilibrium)	0.7	%	ISO 62-4
Water Absorption, (23°C/24hrs)	0.25	%	ISO 62-1
Water Absorption, (23°C/saturated)	1.25	%	ISO 62-1
Melt Volume Rate, MVR at 360°C/5.0 kg	13	cm ³ /10 min	ISO 1133
Specific Gravity	1.27	-	ASTM D792
Water Absorption, (23°C/24hrs)	0.25	%	ASTM D570
Water Absorption, (23°C/Saturated)	1.25	%	ASTM D570
Melt Flow Rate, 337°C/6.6 kgf	9	g/10 min	ASTM D1238
Poisson's Ratio	0.36	-	ASTM E132
Mold Shrinkage, flow, 3.2 mm ⁽³⁾	0.5 – 0.7	%	SABIC method
Mold Shrinkage, xflow, 3.2 mm ⁽³⁾	0.5 – 0.7	%	SABIC method
ELECTRICAL ⁽¹⁾			
Volume Resistivity	1.E+15	Ω.cm	IEC 60093
Surface Resistivity, ROA	>1.E+15	Ω	IEC 60093
Dielectric Strength, in oil, 0.8 mm	33	kV/mm	IEC 60243-1
Dielectric Strength, in oil, 1.6 mm	25	kV/mm	IEC 60243-1
Dielectric Strength, in oil, 3.2 mm	16	kV/mm	IEC 60243-1
Relative Permittivity, 1 MHz	2.9	-	IEC 60250
Dissipation Factor, 1 MHz	0.006	-	IEC 60250
Relative Permittivity, 50/60 Hz	2.9	-	IEC 60250
Dissipation Factor, 50/60 Hz	0.0005	-	IEC 60250
Dielectric Constant ⁽⁴⁾			
at 1.1 GHz	3.01	-	-
at 5 GHz	3.02	-	-
at 10 GHz	3.02	-	-
Dissipation Factor ⁽⁴⁾			
at 1.1 GHz	0.0012	-	-
at 5 GHz	0.0024	-	-
at 10 GHz	0.0027	-	-
Comparative Tracking Index ⁽⁵⁾	150	V	IEC 60112
Comparative Tracking Index, M ⁽⁵⁾	100	V	IEC 60112
Volume Resistivity	1.E+17	Ω.cm	ASTM D257
Dielectric Strength, in air, 1.6 mm	32.7	kV/mm	ASTM D149
Dielectric Strength, in oil, 1.6 mm	28.0	kV/mm	ASTM D149
Dielectric Strength, in oil, 3.2 mm	19.7	kV/mm	ASTM D149
Relative Permittivity, 100 Hz	3.15	-	ASTM D150
Dissipation Factor, 100 Hz	0.0015	-	ASTM D150
Relative Permittivity, 1 kHz	3.15	-	ASTM D150
Dissipation Factor, 1 kHz	0.0012	-	ASTM D150
Comparative Tracking Index (UL) [PLC] ⁽²⁾	4	PLC Code	UL 746A
Hot-Wire Ignition (HWI), PLC 1 ⁽²⁾	≥3	mm	UL 746A



PROPERTIES	TYPICAL VALUES	UNITS	TEST METHODS
Hot-Wire Ignition (HWI), PLC 2 ⁽²⁾	≥0.75	mm	UL 746A
High Amp Arc Ignition (HAI), PLC 3 ⁽²⁾	≥3	mm	UL 746A
High Amp Arc Ignition (HAI), PLC 4 ⁽²⁾	≥0.75	mm	UL 746A
High Voltage Arc Track Rate (PLC) ⁽²⁾	2	PLC Code	UL 746A
Arc Resistance, Tungsten (PLC) ⁽²⁾	5	PLC Code	ASTM D495
FLAME CHARACTERISTICS ⁽²⁾			
UL Yellow Card Link	E121562-101048254	-	-
UL Recognized, 94-5VA Flame Class Rating	≥3	mm	UL 94
UL Recognized, 94V-0 Flame Class Rating	≥0.75	mm	UL 94
UL Recognized, 94V-2 Flame Class Rating	≥0.4	mm	UL 94
UV-light, water exposure/immersion	F2	-	UL 746C
Oxygen Index (LOI)	47	%	ASTM D2863
Oxygen Index (LOI)	47	%	ISO 4589
Glow Wire Flammability Index 960°C, passes at ⁽⁵⁾	3.2	mm	IEC 60695-2-12
NBS Smoke Density, Flaming, Ds 4 min	0.7	-	ASTM E662
INJECTION MOLDING ⁽⁶⁾			
Drying Temperature	150	°C	
Drying Time	4 – 6	Hrs	
Drying Time (Cumulative)	24	Hrs	
Maximum Moisture Content	0.02	%	
Melt Temperature	350 – 410	°C	
Nozzle Temperature	345 – 405	°C	
Front - Zone 3 Temperature	345 – 415	°C	
Middle - Zone 2 Temperature	340 – 405	°C	
Rear - Zone 1 Temperature	330 – 400	°C	
Mold Temperature	135 – 180	°C	
Back Pressure	0.3 – 0.7	MPa	
Screw speed (Circumferential speed)	0.2 – 0.3	m/s	
Shot to Cylinder Size	40 – 60	%	
Vent Depth	0.025 – 0.076	mm	
EXTRUSION BLOW MOLDING			
Drying Temperature	140 – 150	°C	
Drying Time	4 – 6	Hrs	
Drying Time (Cumulative)	24	Hrs	
Maximum Moisture Content	0.01 – 0.02	%	
Melt Temperature (Parison)	320 – 355	°C	
Barrel - Zone 1 Temperature	325 – 350	°C	
Barrel - Zone 2 Temperature	330 – 355	°C	
Barrel - Zone 3 Temperature	330 – 355	°C	
Barrel - Zone 4 Temperature	330 – 355	°C	
Adapter - Zone 5 Temperature	330 – 355	°C	
Head - Zone 6 - Top Temperature	330 – 355	°C	
Head - Zone 7 - Bottom Temperature	330 – 355	°C	
Screw Speed	10 – 70	rpm	
Mold Temperature	65 – 175	°C	



PROPERTIES	TYPICAL VALUE [‡]	UNITS	TEST METHODS
Die Temperature	325 – 355	°C	

- (1) The information stated on Technical Datasheets should be used as indicative only for material selection purposes and not be utilized as specification or used for part or tool design.
- (2) UL Ratings shown on the technical datasheet might not cover the full range of thicknesses and colors. For details, please see the UL Yellow Card.
- (3) Measurements made from laboratory test coupon. Actual shrinkage may vary outside of range due to differences in processing conditions, equipment, part geometry and tool design. It is recommended that mold shrinkage studies be performed with surrogate or legacy tooling prior to cutting tools for new molded article.
- (4) Based on SPDR testing technique on dry as molded specimens.
- (5) Value shown here is based on internal measurement.
- (6) Injection Molding parameters are only mentioned as general guidelines. These may not apply or may need adjustment in specific situations such as low shot sizes, large part molding, thin wall molding and gas-assist molding.

DISCLAIMER

Any sale by SABIC, its subsidiaries and affiliates (each a "seller"), is made exclusively under seller's standard conditions of sale (available upon request) unless agreed otherwise in writing and signed on behalf of the seller. While the information contained herein is given in good faith, SELLER MAKES NO WARRANTY, EXPRESS OR IMPLIED, INCLUDING MERCHANTABILITY AND NON-INFRINGEMENT OF INTELLECTUAL PROPERTY, NOR ASSUMES ANY LIABILITY, DIRECT OR INDIRECT, WITH RESPECT TO THE PERFORMANCE, SUITABILITY OR FITNESS FOR INTENDED USE OR PURPOSE OF THESE PRODUCTS IN ANY APPLICATION. Each customer must determine the suitability of seller materials for the customer's particular use through appropriate testing and analysis. No statement by seller concerning a possible use of any product, service or design is intended, or should be construed, to grant any license under any patent or other intellectual property right.

Appendix C

Stress-Strain curves - Matlab code Compression test

```

clear all
close all
clc

data1(:, :)=readtable('1-1');
for i=1:length(data1.Stress_MPa_)-1

condition(i)=(data1.Stress_MPa_(i)>=abs(data1.Stress_MPa_(i+1)+0.5
));
end

index=find(condition==1);
if length(index)>=1
    index=index(1);
    data2(index:end, :)=[];
end

index2=find(data1.Extension_mm_<=0|data1.Stress_MPa_<=0);
if length(index2)>=1
    index2=index2(end);
    data1(1:index2, :)=[];
end

time1=data1.Time_s_;
displacement1=data1.Extension_mm_;
force1=data1.Load_kN_; %kN
strain1=data1.Strain_./100;
stress1=data1.Stress_MPa_; %MPa
truestress1=stress1.*(1-strain1);
truestrain1=log(1+strain1);

%%

data2(:, :)=readtable('1-2');
for i=1:length(data2.Stress_MPa_)-1

condition(i)=(data2.Stress_MPa_(i)>=abs(data2.Stress_MPa_(i+1)+0.5
));
end

index=find(condition==1);
if length(index)>=1
    index=index(1);
    data2(index:end, :)=[];
end

index2=find(data2.Extension_mm_<=0|data2.Stress_MPa_<=0);
if length(index2)>=1

```

```

        index2=index2(end);
        data2(1:index2,:)=[];
end
time2=data2.Time_s_;
displacement2=data2.Extension_mm_;
force2=data2.Load_kN_; %kN
strain2=data2.Strain___./100;
stress2=data2.Stress_MPa_; %MPa
truestress2=stress2.*(1-strain2);
truestrain2=log(1+strain2);

%%

data3(:,:)=readtable('1-3');
for i=1:length(data3.Stress_MPa_)-1

condition(i)=(data3.Stress_MPa_(i)>=abs(data3.Stress_MPa_(i+1)+0.5
));
end

index=find(condition==1);
if length(index)>=1
    index=index(1);
    data2(index:end,:)=[];
end

index2=find(data3.Extension_mm_<=0|data3.Stress_MPa_<=0);
if length(index2)>=1
    index2=index2(end);
    data3(1:index2,:)=[];
end
time3=data3.Time_s_;
displacement3=data3.Extension_mm_;
force3=data3.Load_kN_; %kN
strain3=data3.Strain___./100;
stress3=data3.Stress_MPa_; %MPa
truestress3=stress3.*(1-strain3);
truestrain3=log(1+strain3);

figure
plot(truestrain1,truestress1,'LineWidth',2)
set(gcf,'color','white')
set(gca,'fontsize',14)
xlabel('True Strain [mm/mm]')
ylabel('True Stress [MPa]')
title('Stress-Strain curves')
grid on
hold on
plot(truestrain2,truestress2,'LineWidth',2)
hold on
plot(truestrain3,truestress3,'LineWidth',2)

```

```
legend('Sample 1','Sample 2','Sample 3')
```

Stress-Strain curves - Matlab code Tensile test

```
clear all
close all
clc
% 1mm/min
data1(:, :)=readtable('Test-3-1');
for i=1:length(data1.Stress_MPa_)-1

condition(i)=(data1.Stress_MPa_(i)>=abs(data1.Stress_MPa_(i+1)+0.5
));
end

index=find(condition==1);
index=index(1);
data1(index:end, :)=[];

index2=find(data1.Extension_mm_<=0|data1.Stress_MPa_<=0);
if length(index2)>=1
    index2=index2(end);
    data1(1:index2, :)=[];
end

time1=data1.Time_s_;
displacement1=data1.Extension_mm_;
force1=data1.Load_kN_; %kN
strain1=data1.Strain_mm_mm_;
stress1=data1.Stress_MPa_; %MPa
truestress1=stress1.*(1+strain1);
truestrain1=log(1+strain1);

%%

data2(:, :)=readtable('Test-3-2');
for i=1:length(data2.Stress_MPa_)-1

condition(i)=(data2.Stress_MPa_(i)>=abs(data2.Stress_MPa_(i+1)+0.5
));
end

index=find(condition==1);
index=index(1);
data2(index:end, :)=[];

index2=find(data2.Extension_mm_<=0|data2.Stress_MPa_<=0);
if length(index2)>=1
    index2=index2(end);
    data2(1:index2, :)=[];
end

time2=data2.Time_s_;
```



```

displacement2=data2.Extension_mm_;
force2=data2.Load_kN; %kN
strain2=data2.Strain_mm_mm_;
stress2=data2.Stress_MPa; %MPa
truestress2=stress2.*(1+strain2);
truestrain2=log(1+strain2);

%%

data3(:,:)=readtable('Test-3-3');
for i=1:length(data3.Stress_MPa_)-1

condition(i)=(data3.Stress_MPa_(i)>=abs(data3.Stress_MPa_(i+1)+0.5
));
end

index=find(condition==1);
index=index(1);
data3(index:end,:)=[];

index2=find(data3.Extension_mm_<=0|data3.Stress_MPa_<=0);
if length(index2)>=1
    index2=index2(end);
    data3(1:index2,:)=[];
end

time3=data3.Time_s_;
displacement3=data3.Extension_mm_;
force3=data3.Load_kN; %kN
strain3=data3.Strain_mm_mm_;
stress3=data3.Stress_MPa; %MPa
truestress3=stress3.*(1+strain3);
truestrain3=log(1+strain3);

%%

figure
plot(truestrain1,truestress1,'LineWidth',2)
set(gcf,'color','white')
set(gca,'fontsize',14)
xlabel('True Strain [mm/mm]')
ylabel('True Stress [MPa]')
title('Stress-Strain curves')
grid on
hold on
plot(truestrain2,truestress2,'LineWidth',2)
hold on
plot(truestrain3,truestress3,'LineWidth',2)
legend('Sample 1','Sample 2','Sample 3')

```

References

- [1] Tanisha Pereira, John V Kennedy, Johan Potgieter, A comparison of traditional manufacturing vs additive manufacturing, the best method for the job, *Procedia Manufacturing*, Volume 30, 2019, Pages 11-18.
- [2] Wei Gao, Yunbo Zhang, Devarajan Ramanujan, Karthik Ramani, Yong Chen, Christopher B. Williams, Charlie C.L. Wang, Yung C. Shin, Song Zhang, Pablo D. Zavattieri, The status, challenges, and future of additive manufacturing in engineering, *Computer-Aided Design*, Volume 69, 2015, Pages 65-89.
- [3] Wang, L., Gardner, D.J. Contribution of printing parameters to the interfacial strength of polylactic acid (PLA) in material extrusion additive manufacturing. *Prog Addit Manuf* 3, 165–171 (2018).
- [4] www.astm.org/COMMIT/F42_AMStandardsStructureAndPrimer.pdf
- [5] <https://make.3dexperience.3ds.com/processes/3D-printing>
- [6] <https://www.polyplastics.com/en/support/mold/outline/>
- [7] Kale, Prachi & Darade, Pradip & Sahu, Ramnarayan. (2021). A literature review on injection moulding process based on runner system and process variables A literature review on injection moulding process based on runner system and process variables. *IOP Conference Series: Materials Science and Engineering*. 1017. 10.1088/1757-899X/1017/1/012031.
- [8] T. Gutowski, *Injection Molding*.
- [9] Gurjeet Singh, Ajay Verma, A Brief Review on injection moulding manufacturing process, *Materials Today: Proceedings*, Volume 4, Issue 2, Part A, 2017, Pages 1423-1433.
- [10] F. R. Eirich, C. E. Beyer, R. S. Spencer, *Rheology*, Volume 3, Academic Press, New York and London, 1960, Pages 505-551
- [11] H. Saechtling, *Manuale delle materie plastiche, tecniche Nuove*, 1988, Pages 60-89.
- [12] <https://www.mech4study.com/2017/04/extrusion-process-working-types-application-advantages-and-disadvantages.html>

- [13] Xinjian Duan, Terry Sheppard, Simulation and control of microstructure evolution during hot extrusion of hard aluminum alloys, *Materials Science and Engineering: A*, Volume 351, Issues 1–2, 2003, Pages 282-292.
- [14] <https://engineeringproductdesign.com/knowledge-base/metal-extrusion/>
- [15] Bacalhau, José & Cunha, Túlio & Afonso, Conrado. (2017). Effect of Ni content on the Hardenability of a Bainitic Steel for Plastics Processing.
- [16] Chris Rauwendaal, *Polymer Extrusion 5E*, Hanser, Pages 16-17
- [17] F. R. Eirich, W. L. Gore, J. M. McKelvey, *Rheology*, Volume 3, Academic Press, New York and London, 1960, Pages 589-631.
- [18] F. R. Eirich, E. B. Bagley, H. P. Schreiber, *Rheology*, Volume 5, Academic Press, New York and London, 1960, Pages 93-124.
- [19] J. Goff, T. Whelan, *The Dynisco Extrusion Processors Handbook*
- [20] F. R. Eirich, D. H. Kaelble, *Rheology*, Volume 5, Academic Press, New York and London, 1960, Pages 223-243.
- [21] Fontainhas, Ana & Fernandes, Célio & Nóbrega, J. (2019). Injection moulding simulation using OpenFOAM.
- [22] Elkholy, A., Rouby, M. & Kempers, R. Characterization of the anisotropic thermal conductivity of additively manufactured components by fused filament fabrication. *Prog Addit Manuf* 4, 497–515 (2019).
- [23] Bryan D. Vogt, Fang Peng, Emily Weinheimer, and Miko Cakmak, *FDM from a polymer processing perspective: challenges and opportunities*, Department of Polymer Engineering, University of Akron
- [24] S.F. Costa, F.M. Duarte & J.A. Covas (2015) Thermal conditions affecting heat transfer in FDM/FFE: a contribution towards the numerical modelling of the process, *Virtual and Physical Prototyping*, 10:1, 35-46,
- [25] Duty, Chad E., Ajinjeru, Christine, Kishore, Vidya, Compton, Brett, Hmeidat, Nadim, Chen, Xun, Liu, Peng, Hassen, Ahmed A., Lindahl, John

- M., and Kunc, Vlastimil. A VISCOELASTIC MODEL FOR EVALUATING EXTRUSION-BASED PRINT CONDITIONS. United States: N. p., 2017.
- [26] El Moumen, A., Tarfaoui, M. & Lafdi, K. Modelling of the temperature and residual stress fields during 3D printing of polymer composites. *Int J Adv Manuf Technol* 104, 1661–1676 (2019).
- [27] Choi, Y. Kim, C. , Jeong, H. and Youn, J. (2016) Influence of Bed Temperature on Heat Shrinkage Shape Error in FDM Additive Manufacturing of the ABS-Engineering Plastic. *World Journal of Engineering and Technology*, 4, 186-192.
- [28] N. Turner, B., Strong, R. and A. Gold, S. (2014), "A review of melt extrusion additive manufacturing processes: I. Process design and modeling", *Rapid Prototyping Journal*, Vol. 20 No. 3, pp. 192-204.
- [29] Yongnian Yan, Renji Zhang, Guodong Hong, Xiaomeng Yuan, Research on the bonding of material paths in melted extrusion modeling, *Materials & Design*, Volume 21, Issue 2, 2000, Pages 93-99.
- [30] Krishna P. Motaparti, Gregory Taylor, Ming C. Leu, K. Chandrashekhara, James Castle, Mike Matlack, Effects of build parameters on compression properties for ULTEM 9085 parts by fused deposition modeling.
- [31] Wang, L., Gardner, D.J. Contribution of printing parameters to the interfacial strength of polylactic acid (PLA) in material extrusion additive manufacturing. *Prog Addit Manuf* 3, 165–171 (2018).
- [32] J.E. Seppala, S. Hoon Han, K.E. Hillgartner, C.S. Davis, K.B. Migler, Weld formation during material extrusion additive manufacturing, *Soft Matter* 13 (2017), Pages 6761–6769.
- [33] Chuncheng Yang, Xiaoyong Tian, Dichen Li, Yi Cao, Feng Zhao, Changquan Shi, Influence of thermal processing conditions in 3D printing on the crystallinity and mechanical properties of PEEK material, *Journal of Materials Processing Technology*, Volume 248, 2017, Pages 1-7.
- [34] <https://www.simplify3d.com/support/print-quality-troubleshooting/>

- [35] <https://www.raise3d.com/academy/when-and-how-to-use-3d-printed-support-structures/>
- [36] <https://www.simplify3d.com/software/release-notes/version-4-0-0/>
- [37] Chad Duty, Christine Ajinjeru, Vidya Kishore, Brett Compton, Nadim Hmeidat, Xun Chen, Peng Liu, Ahmed Arabi Hassen, John Lindahl, Vlastimil Kunc, What makes a material printable? A viscoelastic model for extrusion-based 3D printing of polymers, *Journal of Manufacturing Processes*, Volume 35, 2018, Pages 526-537.
- [38] <https://www.aniwaa.com/buyers-guide/3d-printers/best-peek-3d-printer-pei-ultem/>
- [39] <https://www.roboze.com/it/stampanti-3d/argo-350.html>
- [40] <https://www.3dwasp.com/stampante-3d-peek/>
- [41] <https://www.stratasys.com/it/3d-printers/fortus-450mc>
- [42] Callie Zawaski, Christopher Williams, Design of a low-cost, high-temperature inverted build environment to enable desktop-scale additive manufacturing of performance polymers, *Additive Manufacturing*, Volume 33, 2020.
- [43] Pu Han, Alireza Tofangchi, Anagh Deshpande, Sihan Zhang, Keng Hsu, An approach to improve interface healing in FFF-3D printed Ultem 1010 using laser pre-deposition heating, *Procedia Manufacturing*, Volume 34, 2019, Pages 672-677.
- [44] Vidya Kishore, Christine Ajinjeru, Andrzej Nycz, Brian Post, John Lindahl, Vlastimil Kunc, Chad Duty, Infrared preheating to improve interlayer strength of big area additive manufacturing (BAAM) components, *Additive Manufacturing*, Volume 14, 2017, Pages 7-12.
- [45] Andrzej Nycz, Vidya Kishore, John Lindahl, Chad Duty, Charles Carnal, Vlastimil Kunc, Controlling substrate temperature with infrared heating to improve mechanical properties of large-scale printed parts, *Additive Manufacturing*, Volume 33, 2020.

- [46] Charles B. Sweeney, Micah J. Green, Mohammad Saed, Microwave-induced localized heating of CNT filled polymer composites for enhanced inter-bead diffusive bonding of fused filament fabricated part, Texas tech university system, 2020
- [47] Darshan Ravoori, Hardikkumar Prajapati, Viswajit Talluru, Ashfaq Adnan, Ankur Jain, Nozzle-integrated pre-deposition and post-deposition heating of previously deposited layers in polymer extrusion based additive manufacturing, *Additive Manufacturing*, Volume 28, 2019, Pages 719-726.
- [48] Hermes Gibertia, Matteo Strano and Massimiliano Annoni, An innovative machine for Fused Deposition Modeling of metals and advanced ceramics.
- [49] Thesis: Alessandro Marseglia, Prof. Ing. Hermes Giberti, Progetto e Sviluppo di una Testa di Iniezione MIM applicata ad una Stampante 3D
- [50] Massimiliano Annoni, Hermes Giberti, Matteo Strano, Feasibility Study of an Extrusion-based Direct Metal Additive Manufacturing Technique, *Procedia Manufacturing*, Volume 5, 2016, Pages 916–927.
- [51] Hermes Giberti, Luca Sbaglia and Marco Silvestri, Mechatronic Design for an Extrusion-Based Additive Manufacturing Machine, *Machines* 2017, 5, 29
- [52] Thesis: Luca Sbaglia, Gianni Royer Carfagni, Marco Silvestri, Design and development of an additive manufacturing prototype
- [53] Thesis: Marco Parabiaghi, prof. Ing. Hermes Giberti, Pianificazione di traiettorie di deposizione per una stampante 3d innovativa a 3 g.d.l. a portata di estrusione costante
- [54] Mitsubishi Electric, MELSEC-Q Temperature Control Module User's Manual
- [55] Mitsubishi Electric, MELSERVO-JE Servo Amplifier Instruction Manual
- [56] Thesis: Guillaume Herve, Matteo Strano, Kedarnath Rane, Extrusion-based AM of Ceramic Materials for Biomedical Applications

- [57] ST Microelectronics, BTA40, BTA41, BTB41 Datasheet
- [58] GE Engineering Thermoplastics, ULTEM PEI Resin Product Guide
- [59] Thesis: Jurgen Halo, Matteo Strano, Sustainable Additive Manufacturing: Mechanical Response Of 3D Printed Recycled Abs, 2021
- [60] Daniele Farioli, Matteo Strano, Francesco Briatico Vangosa, Veronica Geraldine Zaragoza, Andrea Aicardi, Rapid tooling for injection molding inserts, ESAFORM 2021
- [61] Eric L. Gilmer, David Anderegg, John M. Gardner, Godfrey Sauti, Emilie J. Siochi, Steven H. McKnight, David A. Dillard, Claire McIlroy, Michael J. Bortner, Temperature, diffusion, and stress modeling in filament extrusion additive manufacturing of polyetherimide: An examination of the influence of processing parameters and importance of modeling assumptions, Additive Manufacturing, Volume 48, Part A, 2021.